Integrating glacier dynamics into hydrological modelling

A climate change impact assessment of the data-scarce headwaters of the Tarim River, Central Asia

Thesis submitted for the degree of

Doctor of Philosophy at University College London

Michel S. J. Wortmann

Department of Geography,
University College London (UCL),
Gower Street,
London WC1E 6BT,
United Kingdom

in cooperation with:
Potsdam Institute for Climate Impact Research (PIK),
Telegraphenberg A62,
14473 Potsdam,
Germany

July, 2017

Declaration

I, Michel Samuel Johannes Wortmann confirm that the work presented in this thesis is my own. Where information has been derived from other sources, I confirm that this has been indicated in the thesis.

Potsdam, July 31, 2017

Abstract

This thesis addresses the complexities of conducting hydrological climate change impact assessments in mountainous, highly glacierised catchments by developing and validating a glacier dynamics module for the hydrological model SWIM. It provides the first integrated climate change impact assessment for the five headwaters of the Tarim River, NW China/Kyrgyzstan, Central Asia, overcoming the region's severe data-scarcity.

The region's heterogeneity and limited data availability is characterised, with a focus on the quality of precipitation datasets. After using the original SWIM model for an analysis of observed glacial lake outburst floods and highlighting the model's insufficiencies for long-term assessments, a new glacier dynamics model of intermediate complexity is developed, bridging catchment and glacier scales. This new model implements all major glacier processes, including ice movement, avalanching, sublimation and sub-debris melting. It is validated in one of the data-scarce Tarim River headwater catchments as well as the data-abundant Upper Rhone catchment, Switzerland. The model is then implemented in all five Tarim headwaters and calibrated to discharge, glacier hypsometry and mass balance, using an automatic multi-objective approach. The model provides a correction of the high mountain precipitation, a driving variable shown to be highly uncertain. It is then used to assess three IPCC climate change scenarios for the 21st century using an ensemble of eight global and one regional climate model. Impacts on glacier area and volume as well as discharge are explored, including their climate model and calibration parameter uncertainties.

Results show current catchment precipitation to be 1.4–4.3 times greater than observation datasets suggest, a finding in-line with climate model simulations and remote sensing based datasets. Under a generally warmer and wetter climate, glacier cover is expected to recede and discharge may experience large increases as a consequence, especially in the near future. Uncertainties are large, however, mainly owing to climate model variability.

Impact statement

Understanding the responses of rivers to changes in the global and regional climate is vital to ensure domestic and agricultural freshwater supplies as well as to protect communities from devastating floods. Water practitioners and researchers rely on long-term observations of hydrometeorological variables (such as river discharge, precipitation or temperature) to create computer models of river basins. These models are vital in understanding and predicting the response of freshwater resources to climate and other environmental changes. The quality and accuracy of such models largely depend on the availability and density of such observations but also on our understanding of the hydrological system.

In mountainous regions, the density of hydrometeorological observations is commonly low while the factors that control hydrological process as well as the processes themselves are diverse in space in time. For example, the high altitudes lead to the occurrence of glaciers and large spatial variations in precipitation. This has long challenged the accurate assessment of freshwater resources in glacierised catchments leading to inadequate planning and consequent environmental problems downstream. This is especially true in arid and semi-arid regions of the world, such as Central Asia, where people and plants are crucially dependent on surface water originating from mountainous and glacier-covered river basins.

The research presented in this thesis improves the way individual glaciers are represented in hydrological models of large, data-scarce regions. It uses such a model to update current estimates of annual mean precipitation of five highly glacierised catchments in Central Asia (the headwaters of the Tarim River, NW China/Kyrghyzstan) and to assess the expected changes in river discharge and glacier cover over the 21st century. The thesis enhances our understanding of the case study catchments by reducing the uncertainties inherent in predicting future river discharge. Parts of the thesis have already been published in peer-reviewed scientific journals that highlight these academic contributions (see page 243).

The impact of the thesis is both of academic and operational nature. It enables an accurate inclusion of glaciers in hydrological assessments over large, data-scarce catchments employing a number of ensemble simulations for model calibration and uncertainty assessment. The methods that are developed will benefit hydrological and glaciological researchers interested in these specific as well as other high altitude glacierised catchments. At the operational level, the results of the climate change impact assessment provide inputs to a basin-scale decision support system (DSS) that is used to advise local stakeholders and the creation of a river basin management plan by the regional authority.

Contents

Acknowledgements

This thesis has been an immense endeavour for me, both enriching and rewarding as well as challenging and at times frustrating. It would have not been possible without the many friends and colleagues who believed in my abilities to complete it and I will be forever grateful to them for supporting me through this. I especially thank my supervisor at PIK, Valentina Krysanova, for giving me the opportunity to work in the Sumario Project, for putting her confidence in me and for pushing me to be pragmatic. Equally important has been Julian Thompson's supervisory support at UCL. I am grateful for his encouragement and suggestions as well as his relentless understanding for my other commitments outside of the PhD work.

I also thank my project partners for their guidance. I am grateful to Tobias Bolch (University of Zurich) for giving me the professional advice in publishing and necessary background in glaciology. I thank him also for giving me the chance to accompany him and his colleagues on a glaciological fieldtrip to the Aksu catchment, which gave me a "feel" for the region. I acknowledge the colleagues that enabled the work by sifting through dusty data archives and providing local insights, such as Azamat Osmonov (Central Asian Institute of Geosciences, Bishkek), Jiang Tong (Chinese Meteorological Administration, Beijing) and numerous colleagues from the Xinjiang Institute of Ecology and Geography in Urumqi. The BMBF, who funded the project, is also acknowledged (grant number: 01LL0918J). I also very much appreciated working with my colleagues and fellow PhD candidates at PIK, in no particular order, Stefan Liersch, Valentin Aich, Anastassi Stefanova, Tobias Conradt, Tobias Vetter, Julia Reinhardt, Samuel Fournet, Judith Stagl, Hagen Koch, Anastasia Lobanova, Michael Roers, Shaochun Huang and Fred Hattermann. They proved invaluable in learning and growing and gave me a sense of belonging.

Finally, I am grateful to my girlfriend Laure Cesari, my daughter Matilda, my parents as well as many of my friends and family for supporting me along the way and putting up with my excuses when my PhD demanded my time.

Thank you. Rakhmat. Danke.

Glossary

ANOVA analysis of variance
An analysis to decompose variance between multiple ensemble factors, such as climate model, model parameters etc. (Bosshard et al., 2013; Vetter et al., 2015).. 229

APHRODITE Asian Precipitation Highly Resolved Observational Data Integration Towards the Evaluation of Water Resources
is a quality assured precipitation dataset for various Asian domains compiled from a dense gauge network (Yatagai et al., 2012).. 23, 76, 77, 79, 80, 111, 112, 183, 211

CCLM COSMO Climate Limited-area Model
A regional climate model that was used to produce high climate (scenario) data as part of the Sumario Project.. 79

CMA Chinese Meteorological Administration
The national weather and climate agency of China (also partners in the SuMaRiO project).. 19, 25, 103, 104, 111

CMIP Climate Model Intercomparison Project
A research project coordinating the standardised creation of climate scenarios using general circulation models (GCMs).. 19, 23, 67, 68, 211, 229

DDF degree-day factor
An empirical parameter used to relate daily mean surface temperature above a certain threshold (usually 0 °C) to glacier ablation or only melting. It is given in $\mathrm{mm\,K^{-1}\,d^{-1}}$. 51, 52, 62

DEM Digital Elevation Model
A grid-based representation of topography, often constructed using satellite or air-born sensors.. 50, 60, 94, 113, 134, 180

DPD direct precipitation dataset as define in Section 3.3.1.. 79

DSS decision support system
A computer-based application to synthesis research results and make them relevant to stakeholders and decision makers of a natural system, e.g. a catchment. See Jonoski (2006).. 34

ELA Equilibrium Line Altitude
The altitude above see level, at which glacier ablation and accumulation are approximately equal, often close to the firn line.. 141

GCM general circulation model
A computer model that simulates the 3D atmosphere of the entire Earth as well as relevant oceanographic and land processes.. 15, 17, 21, 48, 60, 67–69, 211, 232

glacier '[H]ard, thick and compact ice mass on land that forms through the recrystallization of snow and moves forward under its own weight.' (Dobhal, 2011, p. 376). 42

GLIMS Global Ice Measurment from Space Project
A global inventory of glacier area primarily from satellites (Kargel et al., 2014).. 22, 42, 43, 63, 113

GLOF Glacier Lake Outburst Flood
A river flood produced by the rapid discharging of an ice or moraine-dammed lake caused by a dam failure or the uplifting of the ice dam by floatation (Iturrizaga, 2011). GLOFs from ice-dammed lakes are also frequently called jökulhlaups after the Icelandic word for the phenomenon.. 34, 36, 40, 100–102, 107, 108, 132, 235, 236

GPCC Global Precipitation Climatology Centre
provides a monthly precipitation dataset and is operated by the German Weather Service. Described in Section 3.3.1.. 79

GPM Global Precipitation Measurement
is described in more detail in Section 3.3.1.. 79, 81

HAR High Asia Refined analysis
is a high resolution (10km and 30km) climate model analysis run of the High Asia region, further described in Section 3.3.1.. 79, 81

HRU hydrological response unit. 60

HWSD Harmonized World Soil Database
The database contains global soil information from many national soil databases, which were merged and adjusted for coherence. See FAO et al. (2011). 25, 105

IDW inverse distance weighted interpolation
An interpolation method, which weights the nearest data points by the inverse of their distances.. 112, 183, 190

IPCC Intergovernmental Panel on Climate Change
An international organisation to coordinate the global efforts to research and address climate change. Central output are seven-yearly assessment reports, e.g. IPCC (2007).. 17, 67

LIA Little Ice Age
A climatic cold period in the middle of the 19th century, in which most glaciers were more extensive then at present.. 95

MODIS Moderate Resolution Imaging Spectroradiometer
A multi-spectral earth observation sensor on board the NASA Terra (launched in 1999) and Aqua (launched in 2002) satellites. Since the launch the sensor has provided data on the state of the biophysical environment of the Earth at a resolution of 500m and a return time of 2-3 days.. 19, 25, 42, 103, 104

MPD model-based precipitation dataset as defined in Section 3.3.1.. 79

NSE Nash-Sutcliffe Efficiency
A measure of hydrological modelling performance indicating the discrepancy between simulations and observations. It ranges from 1 (identical) to -infinity, while 0 indicates that the observation mean is as a predictor as the simulations (Nash and Sutcliffe, 1970).. 58, 116, 151, 158, 235, 237

permafrost Soil and rock with permanently (at least 2 years) frozen water (Shur et al., 2011).. 42

PIK Potsdam Institute for Climate Impact Research (in German *Potsdam Institute für Klimafolgenforschung*)
An independent research institute in Potsdam, Germany focusing on the impacts of climate change as well as mitigation and adaptation strategies.. 17, 37, 39, 59, 102, 211

RCM regional climate model
A computer model that simulates the 3D atmosphere of a (mostly rectangular) region and related land/sea processes. It takes output from GCMs as boundary conditions.. 21, 30, 68, 69, 211, 217, 232, 240

RCP Represenative Concentration Pathways
The latest climate change scenarios defined by the fifth assessment report of the Intergovernmental Panel on Climate Change (IPCC) that are based and named after the values of radiative forcing in the year 2100 (i.e. RCP2.6, RCP4.5, RCP6.0, RCP8.5).. 23, 68, 69, 210

SPD satellite-based precipitation dataset as define in Section 3.3.1.. 79

SuMaRiO Sustainable Management of River Oases in the Tarim Basin
An interdisciplinary research project financed by the German Federal Ministry of Education and Research (BMBF).. 15, 39, 40, 94, 211, 240

SWAT Soil Water Assessment Tool
A widely used, semi-distributed hydrological model first developed by Arnold et al. (1993).. 57, 59, 60

SWIM Soil and Water Integrated Model
A semi-distributed hydrological model developed by the hydrological modelling group at PIK. More details are provided in Section 2.8.. 18, 19, 22, 25, 32, 37, 40, 41, 59–62, 103–105, 107, 113, 116, 179, 233

SWIM-G SWIM-Glacier dynamics
The glacio-hydrological version of SWIM developed and validated in Chapter 5.. 20, 28, 133, 173, 175, 176, 180–182, 208, 212

WATCH Water and Global Change project
The Water and Global Change project produced a consistent reanalysis climate dataset with all variable relevant for hydrological modelling (Weedon et al., 2011).. 23, 76, 77, 81, 111, 112, 183, 211

WGMS World Glacier Monitoring Service
A global archive of glacier fluctuation data administered by the Department of Geography at the University of Zürich under the auspices of the UNEP, UNESCO and WMO.. 93

List of Tables

List of Figures

Chapter 1

Introduction

1.1 Introduction

Agriculture, the economy, hydropower and people's health depend on the availability of freshwater found in rivers in all regions of the world (Hazell and Wood, 2008; IPCC, 2014a). This precious resource is subject to constant change depending on weather and climate, but also on the anthropogenic demands placed on it. Knowing the direction and degree of change in the future – be it tomorrow, in the next season or over the next decades – is fundamental to all societies, yet uncertainties are large and there is an array of influencing factors (Jiménez Cisneros et al., 2014). This is especially true for Asia's mountainous and glacierised regions, where populations highly depend on meltwater during dry seasons and drought years (Bolch, 2017; Immerzeel et al., 2010; Lutz et al., 2014; Miller et al., 2012). Figure 1.1 (by Pritchard, 2017) illustrates this dependence on the basis of meltwater and precipitation contributions in dry years to reservoirs in High Mountain Asia (High Asia). Glacier net meltwater contributions of 50–100% are common in arid catchments, such as those of the Indus River, the Aral Sea or the Tarim River, which is the focuses of this thesis.

Computer-based hydrological models are commonly applied to aid water managers and planners to assess present resources and future changes, taking account of changes in climate as well as environmental and socioeconmic factors (Bronstert, 2005). A

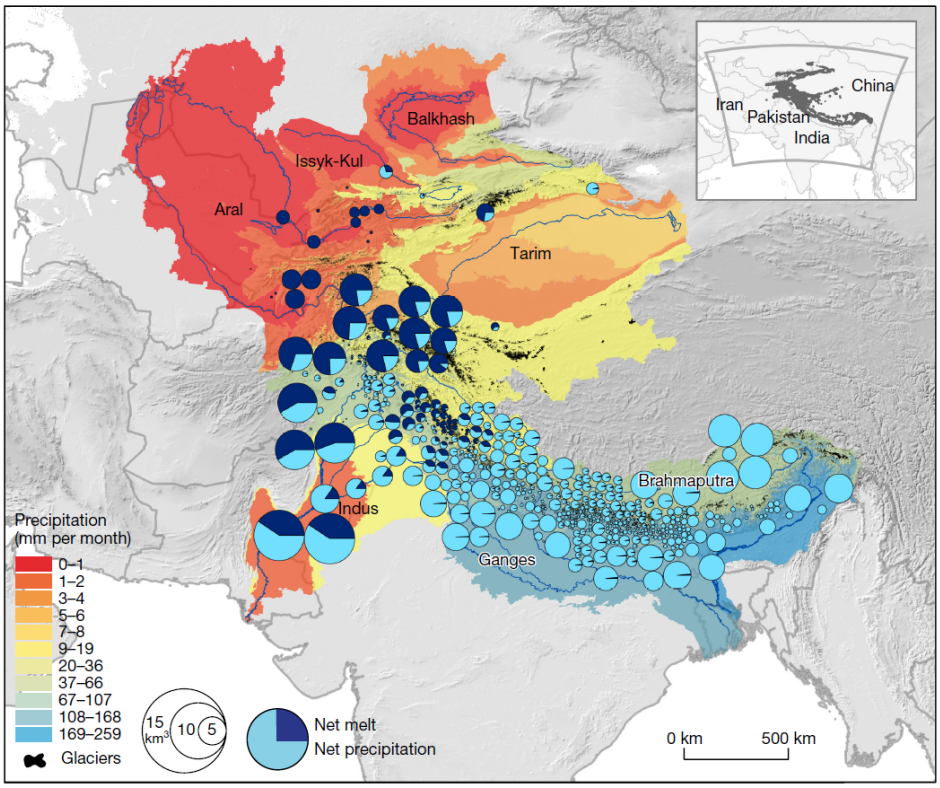

Figure 1.1: Monthly precipitation (background colors), net glacier meltwater and net precipitation contributions to planned and installed dams in drought years across High Asia. By Pritchard (2017, p. 173).

hydrological model is defined by Klemeš (1986, p. 14) as 'a mathematical model aimed at synthesising a (continuous) record of some hydrological variable Y, for a period T, from available and concurrent records of other variables X, Z...'. It provides a decision support tool to stakeholders of a river basin that integrates all important drivers (e.g. meteorological observations, land cover, abstractions etc.) and processes (e.g. snow and glacier melt, infiltration, overland flow etc.). For example, hydrological models are used to predict flood events, water availability for the next growing season or to assess the impacts of climate change. Computer models are most commonly a collection of files containing commands of the computer language that suits the scale of the model and make up a computer programme capable of reading input data, processing it and writing results out again. They contain numerical implementations of the equations that together define the model. One such model is the Soil and Water Integrated Model (SWIM) (Hattermann et al., 2005; Krysanova et al., 1998), a process-based model of intermediate complexity that is the focus of this thesis and was developed for climate

change impact assessments of medium to large-scale catchments (as further described in Section 1.3).

In mountainous catchments, the need for hydrological tools has only partially been met by highly localised, loosely integrated and empirical models (Blöschl, 2006; Peel and Blöschl, 2011; Sivapalan, 2003). The complex and heterogeneous hydrology is combined with inaccessibility and a scarce network of observations, which is limiting our process understanding and long-term data availability, especially for precipitation (Barry, 2008; Peel and Blöschl, 2011). Part of this complex mountain hydrology are glaciers, defined by Dobhal (2011, p. 376) as 'a hard, thick and compact ice mass on land that forms through the recrystallization of [accumulated] snow and moves forward under its own weight'. Hydrologists have developed numerous models for many mountainous and glacierised catchments, so-called glacio-hydrological models. However, few of them fully integrate glacier processes into a general and transferable hydrological simulation tool. Mountainous catchments are plagued with data scarcity and have received disproportionate scientific attention (Blöschl, 2006; Bolch et al., 2012b), despite their importance as water towers. For example, poor precipitation measurements are known to underestimate glacier accumulation by factors of 2-10 (Immerzeel et al., 2015). This has hampered model implementation as well as the advancement of process understanding (Berry et al., 2006).

These problems culminate in the catchment of the Tarim River (Xinjiang Uighur Autonomous Region, NW China and Kyrgyzstan), an arid region highly dependent on glacier meltwater generated in its high-elevation headwaters (Figure 1.1, Liu and Chen, 2006; Tao et al., 2011; Thevs, 2011). The surrounding highly glacierised mountain ranges – the Tian Shan, East Pamir, Kunlun Shan and Karakoram – are poorly gauged and researched. They are difficult to access for field studies due to the extreme altitudes (1400–8611 m asl) and steep terrain. Yet they are the source of the rivers flowing through the inhabited fringes of the Taklamakan Desert, where the livelihoods of approx. 9 million people and an expanding cotton industry depend on irrigation water (Feike et al., 2015; Wang et al., 2010). Water resource planning is thus important to local, regional and national stakeholders, but the means to do so have been constrained by data-scarcity as well as insufficiently integrated and robust models.

In the Tarim River basin, integrated assessment tools (e.g. hydrological models or entire decision support system (DSS)) are needed for the following purposes: *a*) to assess impacts of and plan agricultural management (such as water allocation and irrigation practices; Feike et al., 2015; Thevs, 2011; Wang et al., 2010), *b*) to investigate flood processes and to inform infrastructural development (of e.g. dams, flood defences, irrigation channels; Glazirin, 2010; Hewitt and Liu, 2010; Shen et al., 2007), and *c*) to assess future changes of water availability under climate change for *a* (climate change impact assessments, Duethmann et al., 2016; Rumbaur et al., 2015). This thesis addresses the last two of these tasks focusing on the mountainous headwaters of the Tarim River, while the results are also relevant to the first task that is concerned with the inhabited lowlands.

There is a need for a robust climate change impact assessment because the agriculture in the water-scarce lowlands is highly dependent on the glacierised headwaters and has developed in response to observed changes in the past. Increases in discharge of the principle headwater, the Aksu River, have already been observed (Liu et al., 2006b; Wang et al., 2008) and have been attributed to both increases in precipitation and temperature (Duethmann et al., 2015; Pieczonka and Bolch, 2015). A second problem observed in the headwaters of the Tarim River are Glacier Lake Outburst Floods (GLOFs), catastrophic flood events that occur in response to glacial changes (Hewitt and Liu, 2010; Krysanova et al., 2015a; Zhang, 1992). Most prominently, the Merzbacher Lake in the Aksu headwaters produces reoccurring GLOFs that have shown great variability and have proven destructive to downstream infrastructure (Glazirin, 2010; Liu and Fukushima, 1999).

The following sections outline how this thesis addresses the above problems for the Tarim River headwaters and more generally for similar catchments. The aims and objectives are given in Section 1.2, the research design and constraints are described in Section 1.3 and an overview of the thesis structure is provided in Section 1.4.

1.2 Aims and objectives

As a consequence of the above defined problems, the overall aim of this thesis is:

To increase the confidence of hydrological climate change impact assessments in glacierised catchments by overcoming data scarcity and through model improvement, with a particular focus on the headwaters of the Tarim River.

In order to achieve this aim, the following set of research questions are addressed. They are broadly divided into three groups, reflecting the research topics and the order in which they are undertaken in this thesis.

1. Data scarcity

   (a) What is the quality and uncertainty of the available regional precipitation datasets?

   (b) How can the glacio-hydrological model inform the correction of precipitation data by using inverse modelling, as previously tested in other high mountain catchments?

   (c) What is the simulated catchment precipitation and how does it compare to other precipitation datasets?

Since accurate precipitation data is important to the calibration of a hydrological model, available datasets are assessed and compared. Discrepancies in this as well as other model setup and driving data have to be overcome by novel correction approaches. An improved model in combination with glaciological information will be used to provide a corrected precipitation that is consistent with both the hydrology and glaciology.

2. Model improvement

   (a) How well does the standard SWIM model code as described by Huang et al. (2010, 2013b) perform in a highly glacierised catchment compared to discharge observations without accounting for glaciological observations?

   (b) How can a hydrological catchment model aid the analysis and detection of glacial lake outburst floods in discharge timeseries of mountainous catchments?

   (c) How can the SWIM model be improved to account for all major glacier processes, especially ice dynamics?

   (d) How well does the improved model reproduce hydrological and glaciological observations over the reference period 1971–2000 in the data-scarce Tarim headwaters?

The semi-distributed hydrological model SWIM will be implemented and calibrated to one highly glacierised headwater (the Aksu River) of the Tarim River and used to investigate the impact of the Merzbacher Lake GLOFs, while shortcomings in the original model are described. The model is extended by a glacier dynamics module to represent glaciological changes on the catchment scale and their impacts on river discharge. The module is validated in a 'data-abundant' (the Upper Rhone) and a 'data-scarce' (the Upper Aksu) catchment. The improved model is then implemented and calibrated to all five headwater catchments of the Tarim River in an ensemble approach that allows the evaluation of parameter uncertainties.

3. Climate change impact assessment

(a) What are the projected impacts on river discharge of the Tarim headwaters considering three IPCC climate change scenarios simulated by an ensemble of climate models in three periods of the 21st century with regards to the reference period 1971–2000?

(b) How will the glacier cover (area and volume) change under these climate projections?

(c) What are the uncertainties of the discharge and glacier cover projections induced by the climate model ensemble and the calibration parameters and how do both sources compare to the scenario uncertainty?

The calibrated model of the Tarim headwaters will be used to assess three climate scenarios of the 21st century as simulated by an ensemble of eight global and one regional climate models. Potential future changes to river discharge and glacier cover (area and volume) will be evaluated including the evolution of the parameter, climate model and scenario uncertainties.

1.3 Research design

In the discipline of hydrology, a common methodology has emerged for implementing and improving hydrological models, and by that contributing to the knowledge of a catchment or testing and validating new methods of the modelling process. Refsgaard (1997) describes the steps of this methodology in what he calls 'the modelling protocol'.

This is broadly followed in this thesis with some variations and constraints, as illustrated in Figure 1.2. The input data used in each step are also indicated.

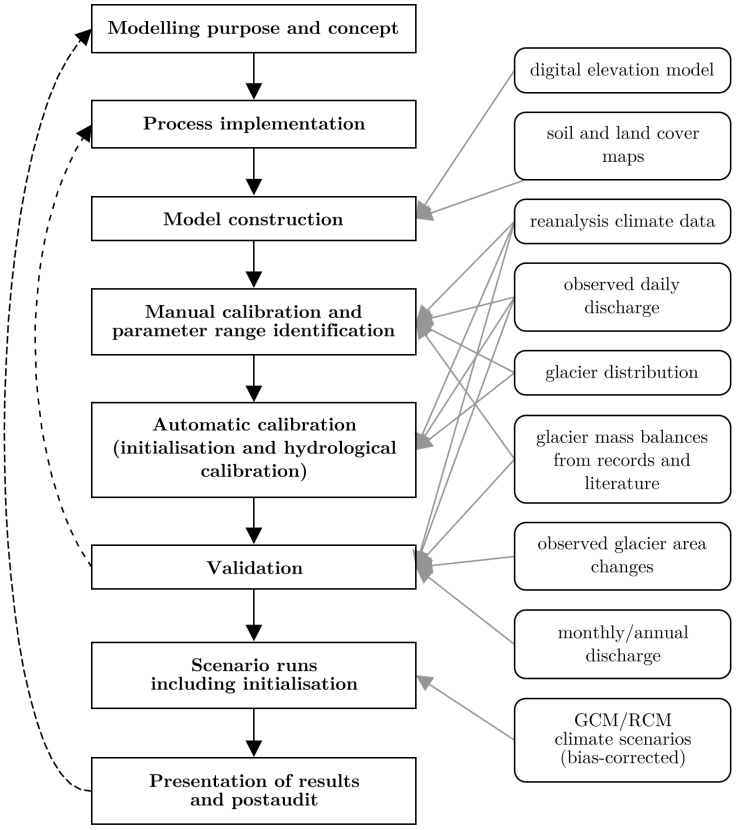

Figure 1.2: The modelling protocol (as proposed by Refsgaard, 1997) with the main input data (on the right in round boxes) adapted to the workflow of this thesis and the final aim of conducting a climate change impact assessment. The dashed arrows on the left indicate the revaluation of previous steps.

All modelling work should start with a purpose definition clearly describing the research question and a conceptualisation of the hydrological system to be modelled. According to the modelling protocol of Refsgaard (1997), the next step is the choice of a model code and if no suitable one exists, a new code needs to be developed. The work conducted here was constrained in its model choice as it was conducted within the regional hydrological modelling group at Potsdam Institute for Climate Impact Research (PIK) that focuses on the development of SWIM (a detailed description of the model is given in Section 2.8). The objective of the research position was to advance the capabilities of SWIM in glacierised catchments, which had previously only been simulated using a simple linear reservoir approach.

Once the model code is chosen or, as is the case here, newly developed, the model needs to be implemented (or constructed) for a particular modelling domain (e.g. a catchment). This includes the preprocessing of all input data that is not time-resolved to form the spatial structure of the model (Beven, 2006b; Ross and Tara, 1993). In most cases, the driving data also needs to be specially prepared to fit the format the model requires, such as transforming variable units or interpolating the variables to the model structure.

The next steps deal with the adjustment of the model to the independent observations. The model parameters are calibrated to maximise the defined performance criteria, for example reducing the errors between observed and simulated discharge (Gupta et al., 2006; Nash and Sutcliffe, 1970). Another set of observations is used to compare with the simulations to validate the model, while the performance between calibration and validation should be comparable (Refsgaard, 1997).

Once validated the model is used for its original purpose, i.e. the simulation of the hydrological variables in question under different driving conditions. Depending on the previously defined research question, this may be a forecast or hypothetical change in meteorological conditions or land use patterns. This is often the stage where other research results are used to test their influence on the hydrological cycle, such as climate change scenarios simulated by global or regional climate models as is done here. The results are subsequently presented to stakeholders or published (Hattermann et al., 2014; Refsgaard et al., 2014).

In practice the modelling protocol is very much a circular process, as the dashed arrows in Figure 1.2 suggest. Model validations may fail, new data become available and possibly invalidate previous results or the results lead to modified research questions. In such cases, the previous steps need to be reviewed and the protocol repeated.

The majority of this work was carried out as part of a government-funded research project, which had a great influence on the research design. It is therefore briefly described below.

1.3.1 The SuMaRiO project

The research position at PIK, in which the PhD was carried out, was funded by an interdisciplinary research project financed by the German Federal Ministry of Education and Research (BMBF), with the title Sustainable Management of River Oases in the Tarim Basin (SuMaRiO). The project was divided into 5 work blocks dealing with 1) scenario and data management, 2) regional climate change and discharge of the Tarim tributaries, 3) sustainable land use management, 4) ecosystem services and functions and 5) socio-economic assessment of ecosystem services and implementation tools.

Together with the hydrology group from the German Institute for Geosciences (GFZ) and the glaciology group from the Technical University of Dresden (TUD), the PIK working group was part of Work Block 2, examining the glaciological, hydrological and climatological changes over the 21st century in the headwater region of the Tarim River. This defined the main study region of this thesis.

The 5-year project started in March 2011 involving 17 German working groups from 12 universities and research institutes. Although originally conceived to be co-funded for as many Chinese partners, the project failed to receive funding from the Chinese Academy of Science (CAS), rendering the cooperation between the groups financially uneven. This made the data acquisition a complicated and lengthy process, occupying nearly the first 2 years of the project. The main research findings of the project were eventually published by Rumbaur et al. (2015).

1.4 Structure of the thesis

The structure of the thesis broadly follows the modelling protocol presented in the previous section. In Chapter 2, the fundamental principles and concepts are explored which this thesis builds upon with reference to the existing literature. The role of glaciers in the hydrological cycle is discussed, the existing modelling approaches as well as climate change impact assessments in mountainous regions. It is followed by a thorough site description of the main catchments of investigation in Chapter 3. This includes a presentation of the scarce database with a focus on precipitation datasets of the region and an analysis of trends in climate and river discharge.

Chapter 4 introduces the initial model implementation without changes to the model code. It demonstrates how this implementation can be used to analyse the effects of the reoccurring GLOFs of the Upper Aksu catchment. The central part of the thesis is presented in Chapter 5: The development of a glacier dynamics module for SWIM is described with a validation in the data-abundant Upper Rhone catchment and the data-scarce Upper Aksu catchment. Chapter 6 describes the implementation of the improved model to the five headwater catchments of the Tarim River, including a precipitation correction as well as calibration and validation results for river discharge and glacier changes.

The climate change impact assessment of the Tarim headwaters is presented in Chapter 7, including hydrological and glaciological changes under three climate change scenarios. This part of the thesis represents the main contribution to the SuMaRiO project. Finally, Chapter 8 summarises the main research findings for each research question and concludes with recommendations for further research.

Chapter 2

Glaciers in the hydrological cycle under climate change

2.1 Introduction

This chapter introduces the principles and concepts this thesis is based on, with reference to the relevant literature. Its purpose is to provide the background for the problems and research questions addressed in this thesis. Sections 2.2 and 2.3 introduce the reader to glacial and other cryospheric water resources and examines their changes under climate change, defining the basic terms and concepts used in the following sections. The way these water resources are conceptualised in cryospheric and hydrological models is shown in Section 2.4. The next chapters discuss the current approaches used to model the glacier mass balance and snow melt (Section 2.5) as well as glacier dynamics (Section 2.6). Section 2.7 provides an analysis of hydrological modelling, including a model classification and focusing on the cryospheric processes represented in these models. It is followed by a detailed description of the Soil and Water Integrated Model (SWIM), the model improved in this thesis, in Section 2.8. Section 2.9 discusses models that combine both the glaciological and hydrological modelling approaches, so-called glacio-hydrological models. Section 2.10 introduces the practice of climate change impact assessments using hydrological models with a particular focus on mountainous and data-scarce regions.

2.2 Glacier and other cryospheric water resources

The cryosphere can be defined as 'all frozen water and soil on the surface of the Earth' (Bamber and Payne, 2004, p. 1), this includes ice sheets, sea ice, snow, glacier, permafrost and frozen surface water. In hydrological research and for the purpose of this thesis, this definition can be narrowed to the frozen water that may produce river discharge when subject to melting (Willis, 2006). More specifically, it includes those components that are part of and influence the water balance of a river catchment and need to be taken into account when predicting river discharge. This excludes ice sheets and sea ice as their melt water typically discharges directly into the sea. In the remainder of this thesis, cryosphere refers to these components only and with a particular focus on glaciers.

These hydrologically active components of the cryosphere are the Earth's second largest freshwater reserves accessible to human civilisations (after groundwater). A first global assessment of snow and ice resources was compiled in the 1980s by Kotlyakov and colleagues (Kotljakov, 1997; Kotlyakov and Dreyner, 1985) and later refined with the emergence of global earth observation satellites, such as the Moderate Resolution Imaging Spectroradiometer (MODIS) on board the Terra and Aqua satellites for snow mapping (Hall et al., 2002) and the Global Ice Measurment from Space Project (GLIMS) project for glaciers (Kargel et al., 2014). Table 2.1 provides the water equivalent of available freshwater of glaciers, permafrost and seasonal snow, highlighting the importance these cryospheric freshwater storages have relative to other global reserves (i.e. without ice sheets and polar glaciers) (Barry and Gan, 2011; Jones, 1997). However, the storage is not as important a measure as its output flux, i.e. the melt water that produces river discharge (Oki, 2006).

A large proportion of the world population is dependent upon rivers fed by glacier, snow and permafrost meltwater. Figure 2.1 shows major rivers and their basins that receive significant contributions to their annual discharge from meltwater. They are predominantly located in Asia (Yangtze River, Ganges River, Indus River, Yellow River, Mekong River, Brahmaputra River, Lena River) but also in North America (Mississippi River, Colorado River, Mackanzie River) and Europe (Danube River, River Rhine, Rhone River). These basins are home to large populations; approximately 1.3 billion

Table 2.1: Cryospheric water reserves outside of the polar regions. Groundwater, lakes and rivers shown for comparison.

Freshwater storage	Area	Ice volume	Water equivalent
	10^6 km^2	10^3 km^3	km^3
Mountain glaciers	0.74[a]	156 – 176[b]	143–161
Permafrost	22.79[a]	114 – 365[a]	104–365
Seasonal snow	3.75 – 46.57[a]	0.16 – 2.00[a]	0.14–1.83
Groundwater			8200[c+]
Lakes and rivers			101.7[c]

a) Barry and Gan (2011)

b) Radić and Hock (2010)

c) Jones (1997)

* without ice sheets and polar glaciers

+ large uncertainties exists in estimates of total volume and accessibility

people in Asia, 100 million people in Europe, 76 million people in North America and 16 million in South America (Kaser et al., 2010; Revenga, 2003). Combined this comprises a quarter of the world population that at least in part depends on glacial and snow meltwater.

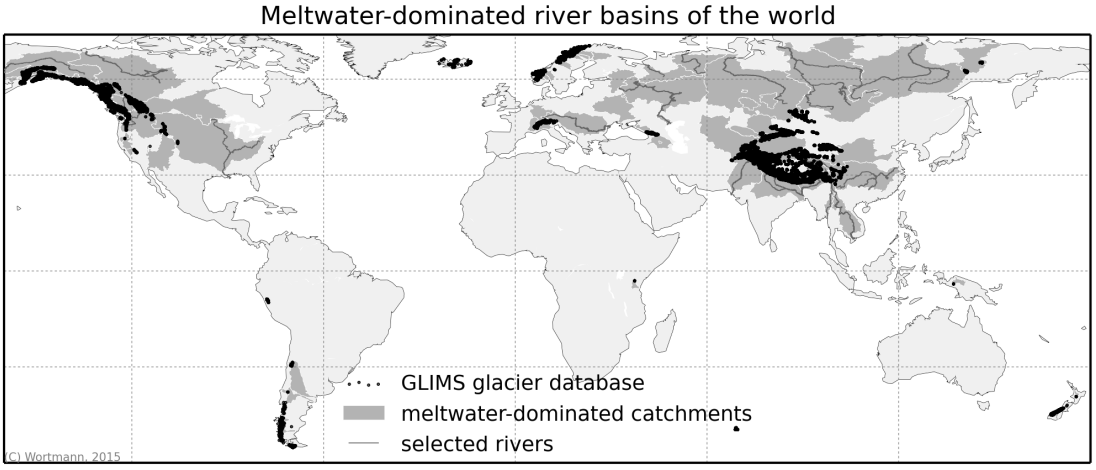

Figure 2.1: Selected catchments with significant contributions of glacier and/or snow meltwater (*Major River Basins of the World / Global Runoff Data Centre* 2007). Glaciers from the GLIMS database (Kargel et al., 2014) outside of the polar regions are marked.

Cryospheric freshwater is highly unevenly distributed in space and time: in space because glaciers, snow and permafrost occur in high-latitude and high-altitude regions; and in time because they are highly dependent upon seasonally as well as diurnally changing temperatures. As a consequence, meltwater-dominated rivers have a high amplitude in discharge with a pronounced peak in the melt season and sustained low flows during the cold season. Figure 2.2 shows an example of a meltwater-dominated flow regime, day of year mean values are given for river discharge, temperature and precipitation over the highly glacierised Yarkant catchment in the NW Karakoram mountains. The dependence on meltwater is demonstrated by the high correlation of discharge with temperatures above 0 °C, rather than with precipitation.

2.3 Uncertain changes under climate change

CO_2 concentrations in the Earth's atmosphere have increased from pre-industrial levels of 280ppm to 390ppm in 2010, a development that has lead to an increase in global mean surface temperature of 0.76 °C ± 0.18 °C through the greenhouse effect (Hengeveld, 2006; Houghton et al., 1996; Houghton et al., 2001; Solomon et al., 2007; Stocker et al., 2014). The global cryosphere is especially vulnerable to rises in temperature due changes in melting and snow formation (Barry, 2005; Barry and Gan, 2011; Shrestha, 2011).

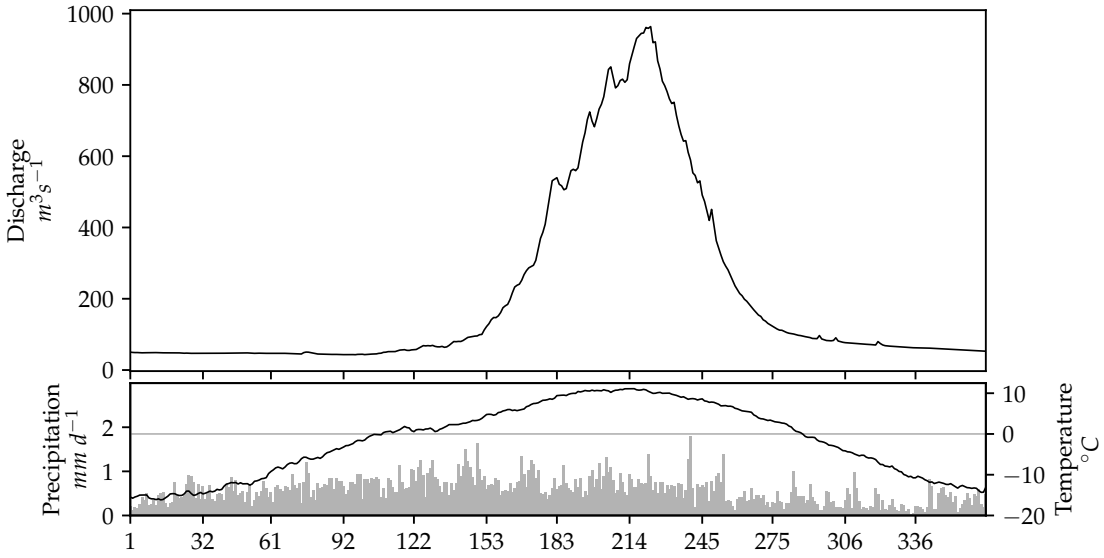

Figure 2.2: Day of year flow regime of the Yarkant River at Kaqun station, NW Karakoram, China. 90% of the catchment is located above 3000 m asl with a glacier coverage of 12%.

While the impacts of a warming climate have become ever more certain for the water cycle, terrestrial and maritime ecosystems and humans over the past decades, changes in the cryosphere have been studied disproportionately and proven with higher uncertainties (Barry and Gan, 2011; Slaymaker and Kelly, 2007; Stocker et al., 2014). The principle questions that are driving the research and that are of global concern are as follows: *a*) How much sea level rise is attributable to mountain glacier recession? *b*) If glacier ice is shrinking under higher temperatures, what are the consequences for downstream communities in terms of the initial increase in discharge, the timing of peak flow and the subsequent lower flow compared to steady-state conditions? *c*) How strong is the effect of changes in snow coverage on the Earth's radiation budget? Will it exasperate climate change through the positive feedback of a reduced albedo with reduced snow cover? *d*) How much is permafrost changing under higher temperatures and how much methane will be released as a consequence, leading to additional Greenhouse Gas (GHG) concentrations and a positive feedback loop?

The remoteness and hostility of cold and high altitude regions makes the cryosphere difficult to appreciate, let alone study and monitor (Barry, 2005, 2006; Blöschl, 2006). This has hampered efforts to decrease uncertainties and improve the understanding of processes and future changes in the quest of answering these questions. In general, cryospheric systems (both outside and in the polar regions) are in decline as higher temperatures have led to enhanced melting (Stocker et al., 2014). For example, mountain glaciers have experienced a significant decline since systematic measurements of area and mass balance began in the 1940s, as Figure 2.3 illustrates. Global mass balances range from -150–$-580\,\mathrm{mm\,weq.\,a^{-1}}$ since then, with a strong ice loss in the 1940-50s, a weak to moderate decline in the 1960-70s and the strongest since the early 1980s (Dyurgerov and Meier, 2004; Shrestha, 2011; Zemp et al., 2009). Regional changes vary widely and most assessments of future changes are conducted on a subregional scale (Radić and Hock, 2010; Radić et al., 2013). An overview of changes in the main glacierised regions is given in Table 2.2. As is evident, he changes have been regionally and highly heterogeneous, often leading to investigations with high uncertainties.

Observed changes in the global snow cover are driven both by rising temperatures and changes in precipitation patterns: The former leads to a shorter snow duration

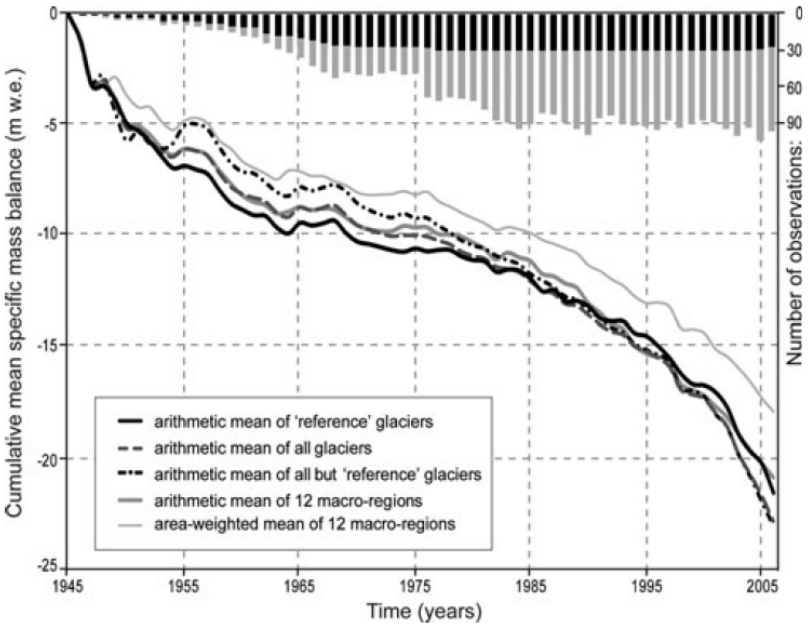

Figure 2.3: Global glacier mass changes since the 1940s according to the World Glacier Monitoring Service (WGMS) by Zemp et al. (2009). Five different ways of calculating the means are given and the number of available observations per year is shown on the inverted right axis.

and affects the snow to total precipitation ratio (Barry, 2005; Bulygina et al., 2009). The latter mainly influences snow depth and snow cover distributions, while increases in total precipitation fail to counteract the snow cover duration (Stewart, 2009). The global snow-covered area in spring has shrunk by about 10% (Barry and Gan, 2011). For the northern hemisphere, Dye (2002) find a shift of the maximum snow cover extent from February to January and a notable decline in spring snow cover since 1972 with a shortening of the snow season at a rate of 3–5 days per decade. While confirming those results for the northern hemisphere, other studies highlight changes in snow cover distribution with constant or even increases in snow depth during the winter months (Bulygina et al., 2009; Robinson and Frei, 2000). This trend is likely to continue in the 21st century as large-scale climate change assessments show: Lawrence and Slater (2009) predict a shortening of the northern hemisphere snow season by 14 ± 7 days in spring and 20 ± 9 days in autumn under the IPCC SRES A1B scenario.

Changes to snow cover duration affect the discharge regime of snowmelt-dominated rivers by producing earlier spring peaks. This shift has already been observed in discharge observations in the western United States (Regonda et al., 2005;

Table 2.2: Observed and predicted regional changes of glacier area and volume.

Region	Observed change in 20th century	Projected change in 21st century	References
Himalaya–Karakoram	Himalayan glaciers are thinning at 0.3–1 m a^{-1}, sings of positive mass balances in the Karakoram since 1980s	Glacier area will decrease by 35% by 2050 with a discharge peak expected between 2030-70 at 150–170% of the initial flow.	Bolch et al. (2012a)
Central Asia	10–40% area loss in last half of 20th centuary, mass balances vary beetween $-570--170$ mm weq. a^{-1}	Glacier area change of up to 70–86% until 2100 in Kyrgyzstan	Sorg et al. (2012)
Alps	Averaged cumulative mean specific mass balance of 30 Swiss glaciers of -20 m weq , with rapid ice loss since the 1980s also found for the Italian Alps; 50% area lost in 1850-2000	75% of area lost by 2050 in the Swiss Alps, 80-100% glacier area loss with a temperature increase of 3–5 °C	Haeberli and Hohmann (2008), Huss et al. (2010b), and Zemp et al. (2006)
North America	51% of glacier volume lost in British Columbia (1800-2005); 10-25% shrinkage of glacier area in BC and Alberta in 1985-2005		Bolch et al. (2010) and Koch et al. (2009)
Andes and Tropics	Mean mass balance of $-1200--600$ mm weq. a^{-1} in tropical Andes; 12% of ice loss since early 1980s in Patagonia; in Papua, Indonesia, 78% of ice lost since 19th centuary; Mt. Kilimanjaro, Tanzania has lost 85% since 1912		Klein and Kincaid (2006), Rabatel et al. (2013), and Thompson et al. (2009)

Stewart et al., 2005) with significant changes of 5–15 days especially in snowmelt dominated catchments with relatively low elevations. Contrary to the intuitive presumption that a warmer climate will lead to a more intense melting season (higher snowmelt rates and greater meltwater discharge peaks, e.g. Molini et al., 2011), recent findings by Musselman et al. (2017) suggest the opposite to be true. An earlier snowmelt season is likely to occur under less intense solar radiation (i.e. May to early June versus March to April) and thus at lower melt rates, as observations and model simulations from western North America have shown. Although a shift towards more rain-driven catchments does not necessarily lead to lower annual discharge, a shorter snow cover

together with higher temperatures also leads to greater evaporation losses and thus a net reduction in river discharge (Berghuijs et al., 2014).

Changes in permafrost are still the most uncertain, but a general trend of permafrost degradation has been detected (Lawrence et al., 2008). Large-scale landscape changes have provided the first evidence of thawing, collapsing houses and pipelines previously anchored on permafrost, but also high-latitude shorelines are receding and are more prone to coastal erosion (Rowland et al., 2010). As soil temperature is highly dependent on the snow cover, predictions of future changes are associated with high uncertainties. Slater and Lawrence (2013) assess past and future permafrost changes in the northern hemisphere modelled by an array of general circulation models (GCMs) and find large uncertainty ranges depending on the models' structural weaknesses to represent subsurface processes and the spread of possible future climates. They find an average shrinkage of permafrost extent with warming temperatures of $1.67 \pm 0.7 \times 10^6\,\mathrm{km}^2$ per degree Celsius change, which would confine the permafrost area to the Canadian Achipelago, the Russian Arctic coast and the east Siberian uplands under the most severe RCP8.5 climate change scenario by the end of the 21st century.

In summary, the evidence of a decline in the land components of the global cryosphere has been growing in the past century and the consequences influence a large share of an ever growing world population. Due to the inaccessible and thus uninhabited environment of cryospheric freshwater resources, systematic monitoring has been and will be infeasible in most regions. This has prevented accurate quantifications and predictions of changes in the terrestrial cryosphere and its impact on river hydrology, leading to high uncertainties in most assessments. The concepts and models to assess future changes are examined in the next sections.

2.4 Conceptualisation of snow and glaciers in the hydrological cycle

The cryospheric components of the hydrological cycle represent buffers, accumulating water in the cold season and discharging water in the warmer periods. They can thus be represented in terms of their storage and in- and out-flux within the hydrological

cycle. The concept graph given in Figure 2.4 shows how the cryospheric components have traditionally been included in hydrological research (e.g. Lindström et al., 1997; Oki and Kanae, 2006; Willis, 2011). The snow pack, the glacier and permafrost are the storage components, with the first two components exchanging mass through snow turning into ice and the latter receives mass through rain or melt water infiltration. Other mass exchanges exist such as rainfall on snow and ice, river seepage into permafrost (omitted in Figure 2.4 for clarity), but they play a negligible role in the cryospheric-hydrological system. Snow accumulation is typically taken as the part of precipitation falling while the temperature is below 0 °C or a parametrised snowfall temperature. Other accumulation processes such as avalanching, wind redistribution and rain freezing are strongly dependent on the topography and are typically negligible factors (Cuffey and Paterson, 2010).

The range of models implementing this or parts of this conceptualisation is large and can be broadly divided by their focus and purpose: a) models focusing on the land ice mass balance (i.e. glaciers) and its runoff and b) models focusing on the hydrology of a river catchment with or without snow and permafrost. In the following, this spectrum of models is reviewed beginning with the approaches of glacier and snow melt modelling, glacier dynamics modelling and permafrost modelling. Then the modelling of the small

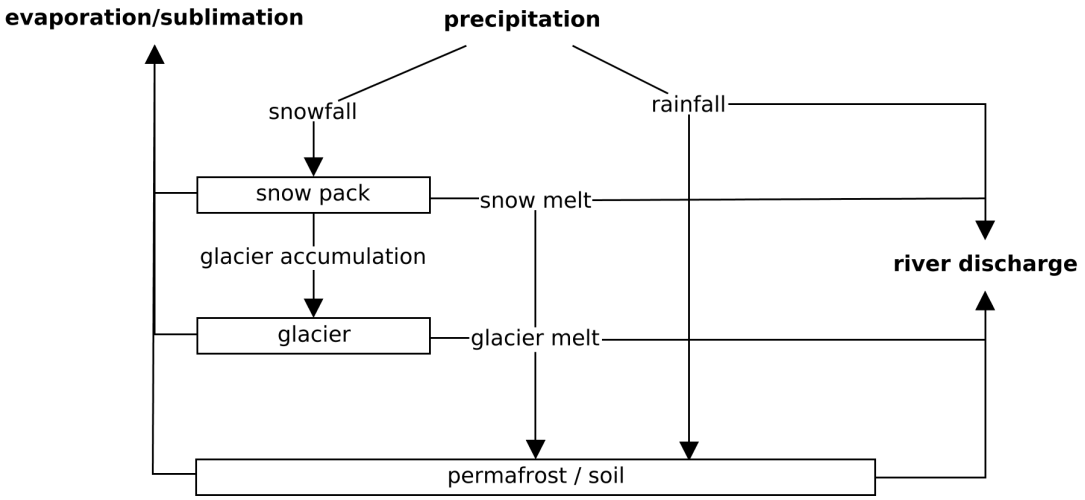

Figure 2.4: Schematic representation of the cryospheric components in the hydrological cycle.

scale glacier hydrology is described and concluded with the combination of glacier and hydrological models (so called glacio-hydrological modelling).

2.5 Glacier mass balance and snow melt modelling

Two glacier and snow melt modelling approaches have emerged and are distinct in their physicality and input data requirements: a) the energy balance model and b) the degree-day model (Greuell and Genthon, 2004; Hock, 2005). Ice dynamics are calculated separately with varying degrees of complexity and physicality as discussed in the next section. The two mass-balance modelling approaches will be described below.

The energy balance approach involves measuring or estimating all energy components at the glacier or snow surface that are available for melting. This includes net radiation as well as turbulent heat fluxes (latent and sensible heat from air and rain). As these components are difficult to measure for a large area, they have to be interpolated from scarce point measurements (e.g. Hock and Holmgren, 2005). Net radiation is the sum of the incoming short-wave radiation multiplied by the albedo plus the diffuse long-wave radiation. The albedo varies greatly on glaciers both over time and space, as does irradiation in complex terrain (Grenfell, 2011). This has required the development of various approximations and makes this approach highly input data intensive. Hock (2005) provides an extensive review of the developed approaches to overcome these requirements, mainly covering the use of a Digital Elevation Model (DEM) with empirical relationships.

Due to these data requirements, only a few models have been developed that implement this approach. Various point studies have pioneered this approach (Hock and Holmgren, 1996; Oerlemans, 2000) but only over some summer days or several years at most. Distributed approaches are rare and only for single glaciers: Klok and Oerlemans (2002) implemented an energy and mass balance model on the Morteratschgletscher in Switzerland making use of an extensive *in-situ* measurement network gathered over two years. They are able to accurately simulate the energy and mass balance components, and by that, melt rates and simple climate sensitivities. Hock and Holmgren (2005) provide a similar study for a glacier in northern Sweden and conclude that energy bal-

ance models are useful despite the large data requirements where diurnal discharge is of interest and for a more robust assessment of glacier melt under climate change. As most longer-term studies have to rely on fewer observed parameters, this approach remains prohibitively data intensive leading to the more empirical approach of the degree-day factor.

The Degree-Day or Temperature-Index approach to snow and ice melt modelling exploits the high correlation of temperature with the turbulent heat fluxes that in turn determine melting (Hock, 2003; Ohmura, 2001). An empirical factor is used to relate the daily mean temperature above 0 °C to the accumulated ice melt, commonly called the degree-day factor (DDF) ($\mathrm{mm\,K^{-1}\,d^{-1}}$). Compromising physicality by using an empirical factor, the approach benefits from the, in most cases, readily available temperature observations. It lumps all components of the surface energy balance into a single factor that is site-specific and needs to be calibrated. The empirical description of complex meteorological conditions also raises questions of the validity under climate change, which can potentially change the factors of the energy balance equation and consequently the DDF (Merz et al., 2011).

Numerous models have implemented the degree-day approach mainly for snow melt simulations in river catchments (e.g. Fontaine et al., 2002; Kuchment and Gelfan, 1996). Most applications show a good model performance at the daily time step, while hourly simulations perform less well. Typical DDFs are between 2–5 $\mathrm{mm\,K^{-1}\,d^{-1}}$. The method also dominates glacier melt simulations (e.g. Braithwaite and Zhang, 2000; Konz and Seibert, 2010), but with generally higher factors in the range of 4–15 $\mathrm{mm\,K^{-1}\,d^{-1}}$ due to the lower albedo of glaciers. Due to the spatial dependency of the DDF, combined approaches have been developed to vary the factor with other parameters influencing the surface energy budget over space and/or time. Quick and Pipes (1977) used the temperature range, Dunn and Colohan (1999) used the slope and aspect, while Kane and Gieck (1997) estimated the albedo and used radiation to differ the melt factor.

Another important factor influencing the degree-day melt factor is debris and dust on ice and snow (Bozhinskiy et al., 1986; Nakawo and Rana, 1999; Nicholson and Benn, 2006). DDFs typically decrease with increasing debris cover in a hyperbolic

function: The lower albedo of a thin dust or debris cover first leads to enhanced melting up to a thickness of 1–3 cm, thereafter the debris insulates the ice and leads to strongly decreasing DDFs. Figure 2.5 shows this decreasing melt with debris thickness using observations from four glaciers. A debris thickness of 15–20 cm cuts the melt factor by one half of the clean ice melting. This negative exponential relationship has been used in glacier mass balance models to simulate ice melt on highly glacier covered in the Tian Shan (Hagg et al., 2008; Juen et al., 2014).

2.6 Glacier dynamics modelling

Glacier dynamics models are strongly influenced by the study of ice sheet dynamics, as accumulation, ice dynamics and ablation processes are transferable, whereas the primary purpose has been the investigation of the mass-balance and its contribution to sea level rise (Bamber and Payne, 2004). Glacier dynamics comprises the lateral movement and deformation of ice due to gravity including all internal stress and strain processes initiated by gravity (Jiskoot, 2011a). Flow velocities are of the magnitude of several 100 m a^{-1}, while outlet glaciers terminating in a water body flow one magnitude

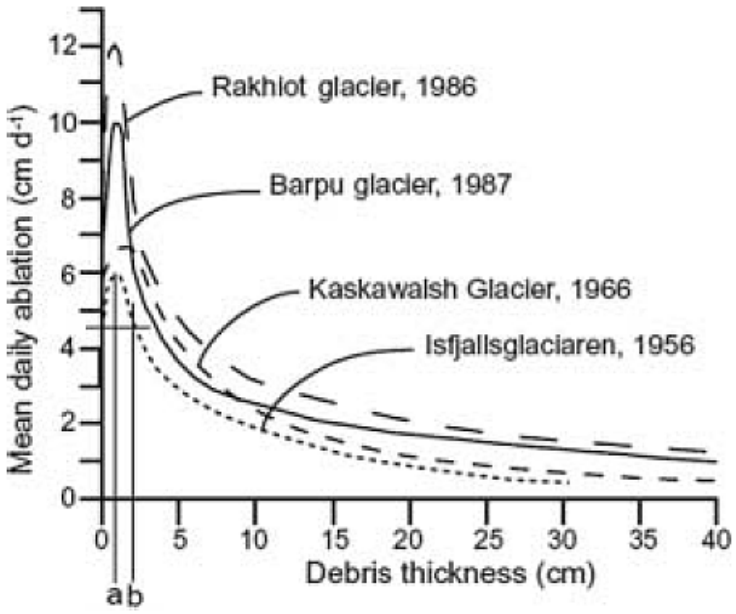

Figure 2.5: Subdebris melt factors under an increasing supraglacial debris layer from measurements at four glaciers. Melt increases up to (a) and has lower than clean ice values from (b). Reproduced from Nicholson and Benn (2006) and Mattson (1993).

faster (Cuffey and Paterson, 2010). This redistribution leads to typical residence times of 10-1000 years, inversely correlated with annual accumulation rates.

Ice flow is decomposed into several processes with varying degrees of importance for modelling purposes:

a) Creep: By far the most dominant process is ice creep, i.e. the flow or downwasting of ice under its own weight (Lambiel et al., 2011). Like any viscous material, ice moves downslope once its weight overcomes the gravitational driving stress at the glacier base (basal shear stress). While it is difficult to measure and varies significantly between regions and individual glaciers, existing studies find a global average of 10^5 Pa (Cuffey and Paterson, 2010). The traditional and widely used approach to modelling creep is given by Glen's Flow Law, an experimental relationship of basal shear stress and ice flow using a factor and an exponent to approximate ice viscosity (Glen, 1955, 1958; Immerzeel et al., 2011; Marshall et al., 2011; Pattyn, 2002).

b) Basal sliding: If the weight of the ice column at the glacier base sufficiently reduces the pressure melting point (also known as warm-based glaciers), ice melts and forms a film of water between ice and the basal material, i.e. sediments and bedrock. This wet layer leads ice to slip off the glacier bed accelerating flow velocities significantly (Kumar, 2011). Weertman's Sliding Law (Weertman, 1969) has become the dominant approach to modelling this sliding process as a function of bed roughness, bed water supply, ice thickness and temperature (Immerzeel et al., 2011; Naz et al., 2014; Oerlemans, 2008). Implementing and validating this approach in isolation, however, has been difficult as all driving factors can not be measured and rely on approximations.

c) Non-steady surging: Through the commonly complex terrain and glacier bed material, the combination of the above two processes and less important flow components (such as longitudinal stress and soft bed deformation) leads to internal stress and strain fields that are not readily transferred to ice motion but accumulate instead. This quasi-cyclic behaviour leads to a highly non-steady, non-linear flow component known as surging (Jiskoot, 2011b). Surge-type glaciers exhibit long periods (10s-100s years) of depressed flow (build-up phase) followed by a much shorter period (1-15 years) of rapid flow (surge phase). After the surge phase the glacier experiences rapid depletion with a thick debris cover developing as a consequence (Clarke et al., 1986). Although only 1%

of glaciers are known and classified as surge-type glaciers, they have an impact on the glacier distribution in lower elevations. Modelling or predicting these events has been difficult and only attempted for single glaciers as the mechanisms involved vary strongly (Clarke, 1987; Tangborn, 2013).

Two modelling principles implementing the above processes are found depending on scale and underlying observational data: a) analytical, semi-empirical models and b) numerical 'full Stokes' models. The first class entails a wide spectrum of mostly lumped but also fully-distributed models that approximate and calibrate unknown and/or unobservable variables. They are making use of observations to calibrate and validate other model results (Huss et al., 2010a; Marshall et al., 2011). Marshall et al. (2011) implemented a simple glacier mass-balance model for several glacierised river basins in Western Canada to assess the long-term changes evolution of glacier meltwater. Mass-balance changes and ice flow are computed for 100-m elevation bands using an adaptation of Glen's Flow Law. The glacier volume is initialised and calibrated using a rheology term to approximated total basin-wide ice volumes. A more empirical treatment of ice dynamics was developed by Huss et al. (2010a). They propose a glacier specific empirical function that is derived from several past observed glacier outlines, the δh-parametrisation. This function is then transferred to a larger glacier group or subcatchments, as Duethmann et al. (2013) have shown.

Models of the second class, numerical or also called 'full Stokes' models because their results are based on solving the full set of Navier-Stokes finite difference equations for ice motion are rare for glaciers (Pimentel and Flowers, 2011). The finite difference approximation of ice flow only yields marginally better results than process-based analytical approaches and gains in accuracy often do not exceed the error of observations, while computing power is in most cases several magnitudes higher and exponentially increasing with grid resolution (Huss et al., 2010a). They are therefore mainly applied to ice sheets with resolutions of several kilometres or individual glaciers with resolutions of 10s of meters. For example, Pattyn et al. (2012) employed a finite difference ice sheet model of Antarctica at a resolution of 12 km. On the other end of the scale, Hubbard et al. (1998) used a three-dimensional finite difference model at a resolution of 70m to model the ice flow of the Haut Glacier d'Arolla, Switzerland.

Further development of glacier dynamics models has been mainly limited by observations and computational power with most model implementations having to balance the scale of investigation or the resolution to the available driving and validation data. As computational power, however, has rapidly increased and driving datasets have become more widely available, so have the glacier dynamics models shifted to more regional applications with higher resolutions. One such example is provided by Clarke et al. (2015), who are modelling all glaciers of Western Canada using a fully-distributed glacier dynamics model with a grid resolution of 200m. Their model is initialised over a 1900 year period to reproduce observed glacier distributions and then used to simulate 21st century glacier changes, predicting glaciers to recede to the maritime fringe of the continent. Their work has been pioneering the large-scale application of fully-distributed glacier dynamics models (Vieli, 2015).

2.7 Hydrological modelling

The use of mathematical models to simulate the hydrological cycle (or parts thereof) has a long and rich history in the hydrological sciences starting as early as the 19th century (Singh and Frevert, 2002). Although they only consisted of a few equations for mostly single components until the 1960s, their development was already driven by similar needs, such as flood forecasting and the design of roads, sewers and drainage systems. Since then, the complexity, range of use and scales has widened significantly to river basin management, water resource management, flood prediction and climate change impact assessments (Klemeš, 1986; Praskievicz and Chang, 2009; Singh and Woolhiser, 2002; Young, 2002). This development was also driven by the greater availability of driving data and computing power, leading to a gradual integration of more processes and larger catchments, as the development of the MIKE SHE model has shown, for example (Refsgaard et al., 2010).

Models are broadly distinguished by their process representation (empirical, conceptual to physically-based), spatial disaggregation (lumped to distributed) and system representation (deterministic and stochastic) (Pechlivanidis et al., 2011; Refsgaard, 1997). Models that include a probabilistic element to represent the inherent uncertainties of the system are described to have a stochastic system representation (e.g. Lee et al., 2001).

The vast majority of models, however, have a deterministic representation where one set of inputs generally has a unique and repeatable set of outputs. The spatial disaggregation of models has evolved from singular representations of a catchment (all input and outputs are averages over the model domain) to subbasin and grid-spaced representations, as illustrated in Figure 2.6. The choice between these disaggregation schemes depends on the modelling purpose and the available input data. Similarly, the representation of processes has evolved from empirical, 'black-box' or conceptual approaches to more physics-based descriptions of processes. A detailed classification including a list of existing models can be found in Singh and Woolhiser (2002). Three examples relevant to the scope of this thesis are described below.

For mountainous and cold regions there are several prominent examples that exemplify the range the different process and spatial representations. The Hydrological Simulation Model (HBV) was designed as a conceptual and spatially lumped model, which has seen numerous applications in snow-dominated catchments mostly in Sweden (Lindström et al., 1997). The model domain was later divided into elevation zones to better account for snow melt with elevation (Ferguson, 1999). Although it parametrises most processes and receives spatially averaged inputs, it yields very good results when compared to observations. For example, it was applied in five small mountainous catch-

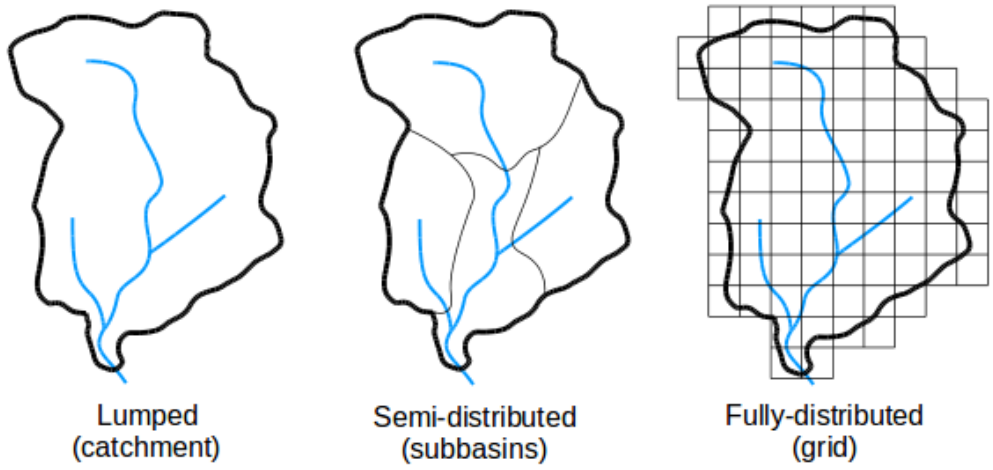

Figure 2.6: The three most common spatial disaggregation schemes of hydrological models. Computational units are given in brackets. Others exist but are less frequently used.

ments in Switzerland by Braun and Renner (1992), who achieve good correlations with observations (R^2 of 0.66–0.92) after manual calibration.

The Soil Water Assessment Tool (SWAT) represents a conceptual model of intermediate complexity that calculates the water balance for many internal subbasins and routes the river water to the basin outlet (Arnold et al., 1998). The model has seen numerous modifications and applications to mainly larger catchments investigating the effects of land-use changes, pollution, irrigation or wetlands amongst others (Krysanova et al., 2015a). The model used and modified in this thesis is also a variant of SWAT and will be reviewed in detail in the next section.

As mentioned above, there is a gradual shift to more physically-based models where data exist to drive them. The SHE model (System d'Hydrologic Européan) has been a prominent pioneer of this development; from an European research initiative in the 1980s, it has become the most widely used fully-distributed, physically-based hydrological model and was commercialised as MIKE SHE/MIKE 11 (Abbott et al., 1986a,b; Refsgaard et al., 2010). It has been used in a range of applications including snow melt modelling (Bøggild et al., 1999; Keilholz et al., 2015; McMichael et al., 2006; Thompson et al., 2013). Its modular algorithm structure has enabled a great deal of flexibility to, for example, ignore certain processes or couple the model with other models of the proprietary MIKE model suite (Refsgaard et al., 2010). For example, Thompson et al. (2009) use MIKE SHE to assess climate change impacts in a coastal wetland in SE England and couple it with the hydraulic model MIKE 11. The necessity for detailed and mostly distributed driving data has presented a major hurdle to the wider use and better results than some conceptual models, especially in data scarce catchments.

With the increase in the number of model codes and structures, a modelling methodology has emerged since the 1970s. A typical modelling protocol is given by Refsgaard (1997). It includes the purpose definition, the conceptualisation of the hydrological system to be modelled and the subsequent code selection and/or development. The more contentious parts of the protocol relate to the implementation and evaluation of the model compared to observed field conditions. Typically, a model is calibrated by

adjusting the model's parameters so that the simulated variable (predominantly river discharge) compares well with one set of observations. Another set of observations that is not used in the calibration is subsequently compared with simulations to validate the model. The validation observations may be of the same variable but in a different period or location, or an entirely different variable. The model's performance is expressed by an objective function that can be optimised by either varying the parameters manually or by changing them according to an optimisation algorithm (Gupta et al., 2006).

A common objective function to assess the efficiency of discharge simulations is the ratio of the simulation's residual variance and the observation's variance (Bosshard et al., 2013; Hattermann et al., 2005; Kane and Gieck, 1997). Nash and Sutcliffe (1970) established the following efficiency measure, the Nash-Sutcliffe Efficiency (NSE), incorporating this ratio:

$$NSE = 1 - \frac{\sum(Q_o - Q_m)^2}{\sum(Q_o - \overline{Q_o})^2} \tag{2.1}$$

where Q_o and Q_m are the observed and modelled discharges. The NSE ranges from -infinity to 1, with 1 denoting a perfect model fit and 0 indicating that the model is as good as the mean value in predicting discharge. Other objective functions and combinations have also been used depending on the model, calibration variable and purpose of the study, such as the correlation coefficient, the root mean squared error or the logarithmic NSE (Krause et al., 2005).

Since the emergence of spatially distributed models and the related increase in the number of model parameters, criticism of this methodology was mainly directed at the possibility of reaching the same results (model performance) with different parameter sets, a characteristic called equifinality (Beven, 1989, 2006a). That means that there are many right results for the wrong reasons, making it impossible to identify the parameters that produce the right results for the right reasons. Hence, the fact that some parameters are strongly correlated is seen as a redundancy or overcomplexity of the model (Schoups et al., 2008). To minimise this possibility, Refsgaard (1997) recommend that a) parameters should be closely associated to measurable field conditions, b) that their ranges should be set to tight, physically possible bounds and c) that the

number of parameters should be kept as low as possible or reduced by keeping their relative difference constant over space and only varying them by a single global parameter. Parameter sets that represent the right results for the wrong reasons can also be eliminated by internal validation, i.e. ensuring that intermediate variables are within reasonable bounds over space and time.

While the greater availability of environmental data over the last decade has contributed to more rigorous validation of some, well-gauged catchments, the above issues remain a great hindrance to more robust model implementations in data-scarce conditions, as mostly found in cold and mountainous catchments. In this regard, Klemeš (1990) argued that 'modelling of mountain hydrology [is] the ultimate challenge', an assessment that still stands after two decades. Strasser and Kunstmann (2013) point to the traditional challenges in modelling mountainous catchments, including accessibility, the representativeness of sparse data over highly heterogeneous terrain and the scale dependence of model input and output. Although more physically-based, process-integrated and spatially-distributed approaches have been developed, their uncertainties remain high and can in most cases only be assessed through sensitivity analyses of the most sensitive parameters. However, the increased availability of remote sensing and regional climate model reanalysis datasets has given hydrological models new constraints (Rast et al., 2014). Integrating the heterogeneity over space, time and processes requires the use of an integrated model that keeps data requirements to a minimum while maximising the opportunities for model validation.

2.8 The Soil and Water Integrated Model (SWIM)

SWIM is described as a process-based, ecohydrological model (Krysanova et al., 1998). It was developed out of the water quality model MATSALU (Krysanova et al., 1989) and the semi-distributed rainfall-runoff model SWAT (Arnold et al., 1993) at the Potsdam Institute for Climate Impact Research (PIK) predominantly for long-term climate change impact and vulnerability assessments for medium to large river basins. Its first application was to the Czech and NE German Elbe River that experienced drastic climate and land-use changes since the 1990s (Hattermann et al., 2004; Krysanova et al., 1999, 2015b).

It has since been developed into a fully integrated ecohydrological model encompassing a number of hydrological and water management processes for both water availability and water quality assessments and has been applied to a wide range of catchments. For example, Hattermann et al. (2011) and Huang et al. (2010) used SWIM to simulate potential impacts of climate and landuse changes in the five largest German river basins. Liersch et al. (2012) and Aich et al. (2014) assessed climate change impacts in the Niger basin, West Africa and Koch et al. (2013) shows the integrated assessment of reservoirs for the upper part of the basin. Vetter et al. (2015) compare climate change impacts of the Rhine, Upper Niger and Upper Yellow rivers simulated using an ensemble of GCMs to drive SWIM and the other hydrological models VIC and HBV. Most recently, SWIM was part of a global intercomparison study of 12 medium to large river basins assessed by nine hydrological models (Krysanova and Hattermann, 2017).

SWIM is a semi-distributed hydrological model with the three-level disaggregation of the catchment, subbasins and hydrotopes inside the subbasins (also known as hydrological response unit (HRU)), as illustrated by Figure 2.7. The latter is defined by unique combinations of land cover and soil type within one subbasins. This may be further divided by including elevation bands, which is important for snow and ice melt processes. First, all water components are calculated for each hydrotope and lateral flows are aggregated at the subbasin level. The accumulated subbasin river flow is routed along the river network to the catchment outlet. Spatial input data includes a DEM needed for the subbasin delineation and parametrisation, land cover and soil maps with an associated soil database. Daily precipitation, temperature (mean, maximum, minimum), relative humidity and solar radiation are interpolated to the subbasin centroids to drive the model at the daily time step.

SWIM has adopted most hydrological processes from SWAT, but was extend by several processes. Figure 2.8 shows the processes considered and their relation. The model considers four volumes for each hydrotope: the soil surface, the root or unsaturated zone (divided into 3–10 soil layers in accordance with the soil database) and the shallow and deep aquifers. At the soil surface, surface runoff is calculated by a modified curve number method (Arnold et al., 1990). It is described as a non-linear function of precipitation and snow, depending on the current soil water content, soil type and land

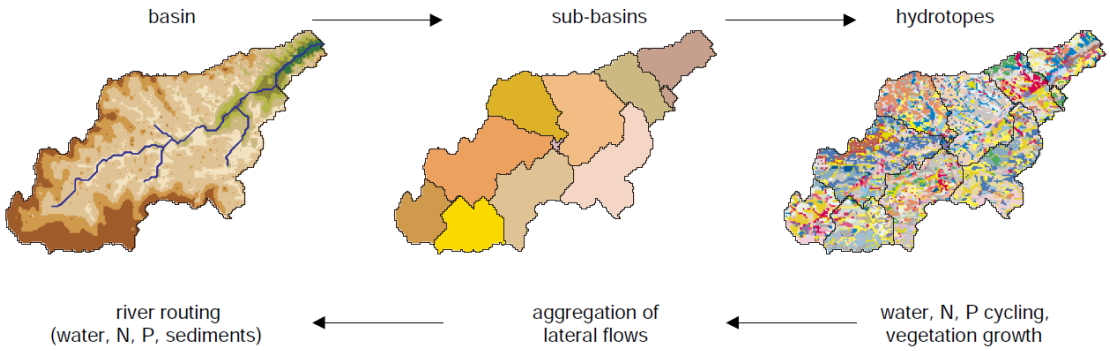

Figure 2.7: The spatial disaggregation of SWIM and processes considered at each level. Reproduced from Krysanova and Wechsung (2000).

cover type. Potential evapotranspiration is calculated by the Priestley–Taylor method (Priestley and Taylor, 1972) which is used to evaluate actual evapotranspiration depending on the soil water, leaf area index and root depth (Ritchie, 1998). The remaining water infiltrates into the soil column. Lateral flow in the individual soil layers occurs when field capacity is exceeded after percolation. Return flow to the stream is calculated based on the method described in (Smedema et al., 2004). Percolation into the shallow aquifer is subject to the delay time function proposed by (Sangrey et al., 1984). Finally, water exchanges (discharge and groundwater) between subbasins are calculated according to the Muskingum routing method (Maidment, 1993).

SWIM has an extended snow module and a rudimentary representation of glaciers as implemented by Huang et al. (2013b). As the accumulation and melting of snow is a principle driver of glacial change, the processes are important for mountainous catchments and most relevant for this thesis. The snow and glacier module is thus described in more detail below.

2.8.1 The snow and glacier module

An extended degree-day method is used to simulate snow melt in SWIM (Huang et al., 2013a; Huang et al., 2013b). It includes a continuous description of ice and water content in the snowpack as well as refreezing and metamorphism according to the approach of Gelfan et al. (2004). This relies on accurate mean daily temperature, which is highly elevation dependent. 100 m elevation contours are used to further split hydrotopes to allow for a better spatially explicit representation of snow melt.

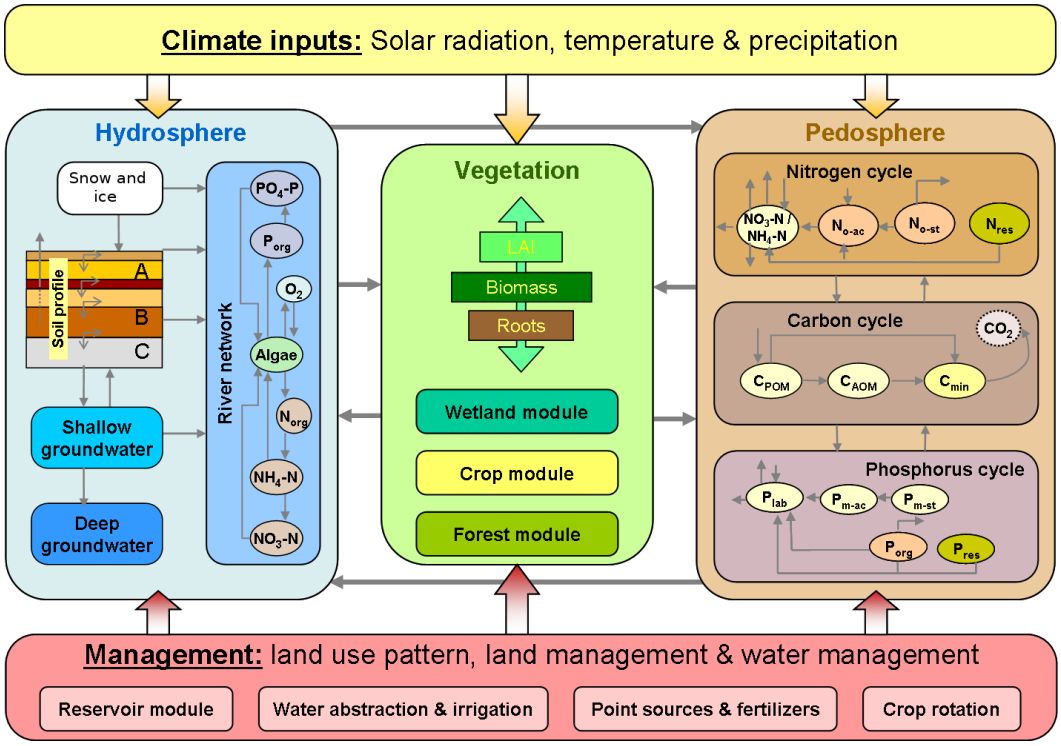

Figure 2.8: Conceptual representation of the SWIM model code, adapted from Krysanova and Wechsung (2000).

Mean subbasin temperatures are corrected to the mean hydrotope elevations by lapse rates, according to:

$$T_h = T_s + \gamma \cdot (Z_h - Z_s) \tag{2.2}$$

where T_h and T_s are hydrotope and subbasin temperature in °C, Z_h and Z_s are hydrotope and subbasin elevation in m, respectively, and γ is the lapse rate that is subject to calibration. The lapse rate γ varies between $-0.3\,°\mathrm{C}\,100\mathrm{m}^{-1}$ for humid condition and up to $-0.9\,°\mathrm{C}\,100\mathrm{m}^{-1}$ for dry conditions.

Precipitation falls as snow if $T < T_s$. Snow melt M_s is calculated by the degree-day method that has proven to be the most reliable method where accurate information on energy fluxes is unavailable (Hock, 2005). Snow melt is calculated by the DDF ddf_s $\mathrm{mm\,K^{-1}\,d^{-1}}$ as described by the following equation:

$$M_s = \begin{cases} \delta_s(T - T_m), & T > T_m \text{ and } H_s > 0 \\ 0, & H_s = 0 \text{ or } T \leq T_m \end{cases} \tag{2.3}$$

The temperature thresholds T_m and T_s can be adjusted around the freezing point of 0 °C during calibration.

A simple linear reservoir approach is used to simulate glaciers. The snowpack left at the end of the melting season (defined as September 30th in the northern hemisphere) is becomes glacier ice. It is then subject to the same Degree-Day melting approach when snow-free, but with a different melt factor. An initial ice cover is defined for each hydrotopes using glacier data such as GLIMS (Kargel et al., 2014). Glacier dynamics and more complex melt regimes are remain unaccounted, as shown in Section 4.7. The improvement of this simple glacier representation is the topic of Chapter 5.

2.9 Glacio-hydrological models

The hydrological response of glacier melt using hydrological models has been investigated and used in practice since the late 1960s (Hock and Jansson, 2006). These first models mainly consisted of multiple regression functions and were developed out of the need to provide weekly to seasonal forecasts for hydroelectric power plants. Their implementation mainly involved the identification of highly correlating meteorological variables with observed discharge, explaining the observed variability. This type of model, however, is inherently non-transferable and loses its predictive power as those simple correlations change. This led to the inclusion of glaciers in hydrological models.

Similarly to the development of hydrological models as described above, glacio-hydrological models follow the theoretical development from conceptual, empirical and spatially-lumped approaches to more physically-based and distributed ones. Table 2.3 lists a selection of prominent glacio-hydrological models that reflect the range of existing integrated glacier and hydrological models. The first conceptual glacio-hydrological models such as the UBC or the HBV-ETH models represent glaciers as large prescribed volumes of initial snow cover, distributed as fractional cover over the elevation zones or hypsometry. This has the advantage of lumping potentially large glacier areas, but preserving their sensitivity to melt via the elevation distribution. However, it ignores all other terrain related factors influencing melt and does not allow for the lateral movement of ice over the terrain (although Huss et al. (2008) try to incorporate this through

empirical relationships). While this may not affect model performance on short time scales, it restricts the models transferability, physical basis and application over longer time scales and climate change studies (Naz et al., 2014).

The other group of glacio-hydrological models have fully-distributed representations of space, i.e. all processes are calculated for each cell in the domains grid. Grid resolutions range from 25m (Huss et al., 2010c) to 500m (Immerzeel et al., 2014) and are constrained by the DEM and model runtime or computing power. In most cases, they also adopt more physically-based approaches, although many processes have the same description as the lumped/semi-distributed models, mostly depending on available observations. A main difference is their ability to represent ice movement due to their higher resolutions. Naz et al. (2014), for example, implemented a two-dimensional ice creep and basal slip model at a 300m resolution for a glacierised catchment in Western Canada with an area of 422 km^2. Similarly but with a more empirical ablation routine, Immerzeel et al. (2013) assess climate change impacts of two Himalayan glacier catchments, the one of the Baltoro glacier with a size of 1415 km^2 and the Langtang catchment with a size of 360 km^2. Both models used a spatial resolution of 90m.

Although much progress has been made in integrating the disciplines of glaciology and hydrology in fully integrated glaciohydrological models, several unresolved issues remain. They can be loosely divided into issues of a) integration and b) scale:

a) *Integration.* Most existing glaciohydrological models use simple representations of the remaining catchment hydrology, as it remains a less important factor in small, highly glacierised catchments. However, there is often some distance between the glacierised part of a catchment and the locations where water becomes a socioeconomic and ecological resource. These are also the locations where long-term hydrological observations exist for model calibration. As these factors increase with catchment size, more accurate and physically-based approaches of the diverse landscape hydrology is needed. This is particularly important in long-term climate impact studies where an accurate description of glacier evolution and catchment hydrology is needed to ensure reasonable results with drastic changes. For example, glacier shrinkage exposes more

Table 2.3: A selection of glaciohydrological models, their spatial representation and glacier processes.

Name	Description	Scales	Mass-balance approach	Ice dynamics	References
UBC	Conceptual rainfall-runoff model for snow-dominated catchments	Semi-distributed, based on elevation zones	Degree-day		Quick and Pipes (1977) and Singh and Kumar (1997)
HBV-ETH	Highly emperical, mostly lumped conceptual model, but also distributed applications	Lumped and semi-distributed, snow and glacierised basins	Degree-day factor, varied via sinus curve with upper and lower boundaries		Braun and Renner (1992) and Hagg et al. (2007)
WASA	Conceptual, process-oriented, for semi-arid catchments	Semi-distributed, based on HRUs and elevation zones	Degree-Day factor varied with sinus curve		Duethmann et al. (2013)
TOPKAPI	Physically-orientated with various empirical components with many calibration terms	Fully-distributed	Degree-Day with irradiation component	Changes in glacier distribution are prescribed	Finger et al. (2011) and Immerzeel et al. (2014)
GERM	Distributed mass-balance, ETa and runoff routing model	Fully-distributed, mostly DEM resolution adopted (≈25–200 m)	Degree-day factor varied by potential direct solar radiation	Glacier surface updated annually with empirical parametrisation of ice thickness changes	Huss et al. (2008, 2010c)
DHSVM	Physically-based, for partially glacierised catchments	Gridded 100–300 m, applied to 422 km^2 Bow river basin	Energy balance, but DDF in initialisation	Shallow ice approximation, vertically integrated, initialised over 1000 years	Dickerson-Lange and Mitchell (2014) and Naz et al. (2014)

area to only hydrological processes, while precipitation increase promotes glacier growth but also more runoff in lower-laying areas of the catchment.

b) *Scale.* So far fully integrated, physically-based models have only been used for relatively small catchments (a few 100s to a few 1000s of square kilometre in size). This is mainly due to their fully-distributed nature and the related grid discretisation. In most cases, these models include a computationally intensive, two-dimensional finite-difference approach to ice flow. The grid resolution is dictated by the complex terrain or the smallest glacier area that is intended to be represented, which puts the maximum grid size to several 100s of meters. Lutz et al. (2014) use 500m as the largest found in literature. While these resolutions are necessary for the representation of glacier processes, they are unnecessary for hydrological processes in larger catchments considering the sparse observation data available. Also, model runtimes increase drastically with finer resolutions, larger catchments and numerical finite-difference calculation.

2.10 Climate change scenario assessments of mountainous catchments

Investigating the potential impact of future changes of the climate on a river catchment typically involves a) the definition, calibration and validation of a hydrological model driven by observed climate data of a reference period, b) the definition and construction of climate change scenarios as well as c) running the model with the perturbed climate and comparing the results with the reference run or 'baseline' (Arnell, 1999). The underlying assumption of this approach is a static hydrological system but a dynamic climate. Only the driving variables change in the scenario period, but the modelled system along with all parameter configurations remains unchanged. It is intended to show only the response to the climatic signal without any system internal changes such as land use changes or other anthropogenic factors. While this is desirable in theory, parameter stability is not always guaranteed as driving variables change (Merz et al., 2011). More general, physical representations of processes are preferred over conceptual approaches as they are typically more stable over time and driving variable ranges.

The second step of this standard approach has been centralised in coordinated scenario definitions by the Intergovernmental Panel on Climate Change (IPCC) (IPCC, 2014b) and climate scenario production Climate Model Intercomparison Project (CMIP) using GCMs (Taylor et al., 2011). This has allowed comparable assessments across disciplines and regions, eliminating the potentially time-consuming definition and simulation of climate change scenarios. However, the accuracy and resolution of the latest GCM results is still not good enough for smaller model domains. Hence, alternatives to using GCM results directly include the delta-change method, by which the observed climate is perturbed by the signals of the GCM results, and simply changing the observed climate by benchmark signals (e.g. $+1-2$K temperature change or $\pm 10-20\%$ precipitation change).

In the latest assessment report (AR5), the IPCC defines four future scenarios, based on ranges of future greenhouse gas concentrations and their associated global radiative forcing by the end of the 21st century, as Figure 2.9 illustrates. The associated change in global mean temperature is given in Table 2.4.

This methodology has been used in a great number of hydrological impact assessments over the past two decades or so with models of all scales (see numerous examples in Bronstert, 2006 and Krysanova and White, 2015). For example, Lobanova et al. (2016) used the SWIM model to assess potential future changes to hydropower production in the 80×10^3 km^2 Tagus basin, Spain/Portugal under two scenarios realised by five GCM. In a large scale assessment, Gosling et al. (2010) simulate global water resources with a 0.5°-grid hydrological model for four temperature change scenarios and 21 GCMs.

Although GCMs perform reasonably well at the global scale, they often fail to adequately represent regional and local climates, either due to their spatial resolution or

Table 2.4: Changes in global mean temperature [K] with respect to the reference period 1986–2005 in two future periods according to the CMIP5 simulations including the (5–95%) ranges. Adapted from Collins et al. (2013).

	RCP2.6	RCP4.5	RCP6.0	RCP8.5
2046–2065	1.0 (0.4, 1.6)	1.4 (0.9, 2.0)	1.3 (0.8, 1.8)	2.0 (1.4, 2.6)
2081–2100	1.0 (0.3, 1.7)	1.8 (1.1, 2.6)	2.2 (1.4, 3.1)	3.7 (2.6, 4.8)

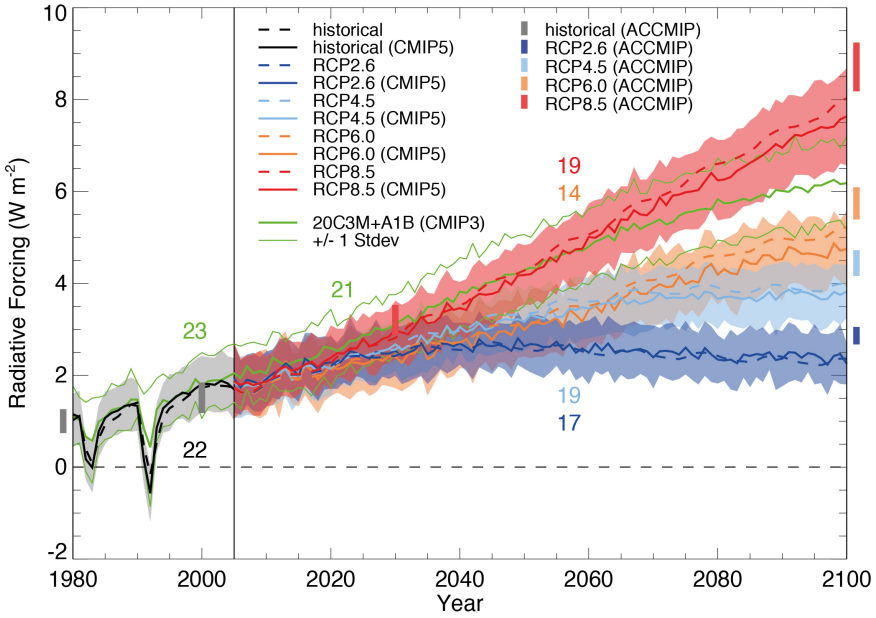

Figure 2.9: Global mean radiative forcing for the four RCPs over the 21st century including the reference period 1980–2005. Dashed lines show the initial scenario design pathways and the solid lines show the CMIP5 multi-model mean with error ranges. Reproduced from Collins et al. (2013).

due to coarse process implementation, e.g. cloud formation (Hawkins and Sutton, 2009) or the inclusion of aerosols (Rosenfeld et al., 2014). This is especially true in mountainous regions, as steep and variable terrain produces highly localised and vertically stratified climates (Maussion et al., 2014). For this reason, global climate change simulations are regularly downscaled to regional scales using regional climate models (RCMs). These spatially confined models use the GCM model output as their boundary conditions and simulate the regional climate at resolutions of 0.1–1.0°. Similar to the CMIP project, regional climate modelling efforts have been coordinated by the CORDEX initiative, a global agreement on modelling domains, model tuning approaches and a common delivery platform (Giorgi and Gutowski, 2015). The individual subproject provide a collection of standardised regional climate scenarios for seven domains, such as Europe, East Asia, Africa and others.

Climate change impact assessments of mountainous catchments are challenged by complex physical conditions and data availability. Complex hydrological processes such as snow and glacier melt paired with data scarcity require catchment models to compromise physical for more empirical representations using more time-constant parameters

(Wagener et al., 2004). This has been shown to lead to large uncertainty ranges under future climates (Gurtz et al., 2003; Merz et al., 2011; Moussa et al., 2007). Climate change projections from GCMs as well as RCMs are shown to introduce the largest share of uncertainty (Hawkins and Sutton, 2009; Thompson et al., 2013; Vetter et al., 2015), but also the large regional variations in projected changes and the corresponding response of mountainous and glacierised catchments is highly uncertain. For example, Horton et al. (2006) investigate the uncertainty introduced by RCMs in several Alpine catchments and show that the uncertainty range of the different models overlaps with the results of two emission scenarios. Mountainous regions are especially susceptible to climate model uncertainties as orographic processes are implemented to various degrees in those models and are highly scale dependent. Many elevation dependent processes have not been fully understood, but evidence suggests enhanced warming with higher elevations, a phenomenon termed 'elevation dependent warming' (MRIEDWWG, 2015).

The other major source of uncertainty stems from a lack of understanding of present-day conditions that is reflected in the glaciological and hydrological impact models (Immerzeel et al., 2014; Ragettli et al., 2013). As mentioned in the previous section, most comprehensive assessments either have a coarse process representation (Duethmann et al., 2016; Immerzeel et al., 2010; Kaser et al., 2010) or are confined to smaller catchments (Fatichi et al., 2015; Immerzeel et al., 2013). A notable example that is trying to address this gap is given by Lutz et al. (2014), who assessed climate change impacts of the major headwaters of the Karakoram-Himalaya region investigating two RCPs and four GCMs using a fully distributed glaciohydrological model at a 1km resolution. Although they are projecting moderate and robust increases in discharge, the GCM uncertainties are of similar magnitudes to the changes and ice dynamics are neglected. Reductions in those uncertainties will likely depend on advances of regional climate models as well as their application especially for mountainous regions, such as Maussion et al. (2014).

Chapter 3

The Tarim River headwaters and the limited data availability

3.1 Introduction

In large parts of China, climate change as well as rapid land use change induced by the expansion of agricultural land have put increasing pressure on water resources (Piao et al., 2010). This development is of specific importance to the semi-arid and arid areas of north and north-western China where irrigation water is inherently scarce (Thomas, 2008). The headwaters of China's largest endoheric river system, the Tarim River, are the focus region of this thesis. This chapter provides on overview of the region's climatology, glaciology and hydrology (Sections 3.2 to 3.5), focusing on data availability and reviewing the datasets used in the subsequent chapters. Chapter 4 and Chapter 5 also include shorter, more specific site descriptions for the modelling domains they are concerned with. Apart from providing the site description for the thesis, this chapter also answers the following research question: What is the quality and uncertainty of the available regional precipitation datasets? The analysis of this question is important for the model implementation and precipitation correction in Chapter 6. The model-based precipitation estimations presented there will be compared to the findings in this chapter.

3.2 The Tarim River headwater catchments

The Tarim River has one of the largest endorheic (inland) catchments of the world with a topographical catchment size of about 800 000 km^2 and a mainstream length of 600–800 km depending on discharge and water abstractions. As the catchment encompasses the Taklamakan Desert and various salt lakes, the hydrologically active catchment is less than half the area. The river is fed by three large tributaries with their confluence at the northern edge of the desert; the Aksu River originating in the central Tien Shan to the north, the Hotan River originating in the Kunlun Shan to the south and the Yarkant River originating in the Karakoram and the eastern Pamirs as shown in Figure 3.1 (Tao et al., 2011). As the desert climate in the lower parts of these tributaries produces virtually no river runoff (except for rare extreme rain events; annual potential evapotranspiration exceeds precipitation by a factor of 30–50), the vast majority of river discharge is generated in the mountainous and glacierised headwaters. This study focuses on the five catchments of the gauging stations that are situated at the boundary of the Taklamakan Desert, i.e. before river abstractions and significant transmission losses occur (Figure 3.1 and Table 3.1).

The Tarim headwaters suffer from severe data scarcity due to the high-altitude, heterogeneous terrain, the associated inaccessibility and a very sparse population. Most of the catchment area is used by semi-nomadic cattle farmers that retreat to lower altitudes during the harsh winter months; small settlements or military posts are rare exceptions. Long-term meteorological stations are therefore extremely difficult to maintain and are scarce. Moreover, the mountain climate exhibits strong vertical gradients (e.g. temperature stratification and orographic precipitation), leading to microclimates and short correlation distances (Beniston, 2006). The few meteorological stations are disproportionately located in valley or low-altitude locations (or worst still, at the edge of the Taklamakan desert). This introduces a low-altitude bias in the climate data, which leads especially to underestimations of precipitation, making some form of correction and extrapolation necessary (Immerzeel et al., 2012). The variability between precipitation datasets is analysed in Section 3.3.1.

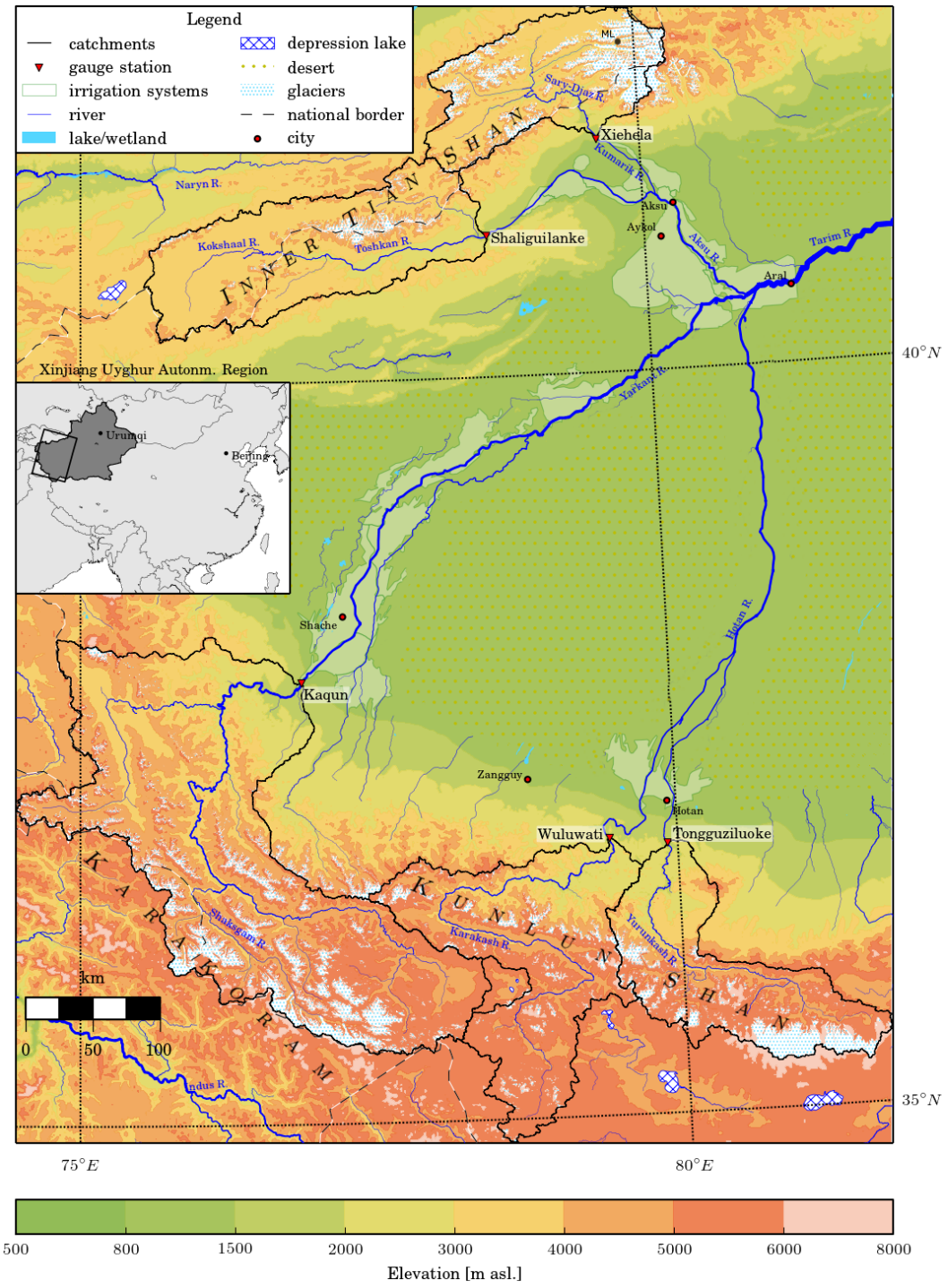

Figure 3.1: Map of the five headwater catchments that supply the vast majority of discharge to the Tarim River including the large agricultural areas downstream. The location of the Merzbacher Lake in the Aksu catchment is marked with ML.

Table 3.1: Basin statistics sorted by headwater stations and stations in the oases. The five headwater catchments that this thesis focuses on are shown in Figure 3.1. Mean discharge is given for summer months (June, July, August (JJA)) and winter months (December, January, February (DJF)) based on available data in 1960–1989. Glacier cover is inferred from glacier outlines in 2009/10 by Bolch et al. (2012b). The discharge data is described in more detail in Section 3.5.

	ID-Name	River	Drainage area km^2	Station altitude m asl	Discharge JJA $m^3 s^{-1}$	Discharge DJF $m^3 s^{-1}$	Glacier cover %
Headwaters							
Aksu	S01-Xiehela	Kumarik	12989.3	1484	406.6	27.9	19.8
	S04	Sary-Djaz	1924.1	2697	85.6	8.3	15.4
	S05	Kolju	799.2	2668	29.1	2.5	21.8
	S06	Ak-Shirak	2229.2	2811	34.1	1.6	6.8
	S15	Inylchek	1073.6	3401			54.7
	S16-Merzbacher L.	Inylchek	316.4	2742			56.8
	S02-Shaliguilanke	Toshkan	18408.3	1889	208.1	15.9	4.3
Hotan	S07-Wuluwati	Karakash	20600.5	1880	200.5	14.1	7.5
	S08-Tongguziluoke	Yurunkash	14889.5	1638	223.3	9	22.8
Yarkant	S10-Kaqun	Yarkant	46759.1	1451	578.7	51.5	10.3
Oases							
Aksu	S03-Xidaqiao	Aksu	35610.2	1085	317.7	27.9	
Hotan	S09-Xiaota	Hotan	52954.6	1026	127.7	0	
Tarim	S11-Arla	Tarim	184567.5	1010	375.7	66	

3.3 Climate

The climate of the headwaters is highly continental with a strong seasonality governed by the Westerlies (Aizen et al., 1995; Maussion et al., 2014). The regional climate is visualised by the High Asia Refined dataset by Maussion et al. (2014), as shown in Figure 3.2. The mountain ranges at the south and north western edges of the Tarim basin act as large climatic barriers in the highly continental region, producing the vast Taklamakan Desert in its centre. In the headwaters, the high-elevation topography has a significant impact on the meteorology, reducing the effects of the continentality and giving rise to microclimates. Lower pressure and temperatures lead to more cloudiness and precipitation, reducing the amplitudes of daily and annual meteorological variability as a result. Thus, high elevations harvest the Western air masses arriving from the Atlantic Ocean.

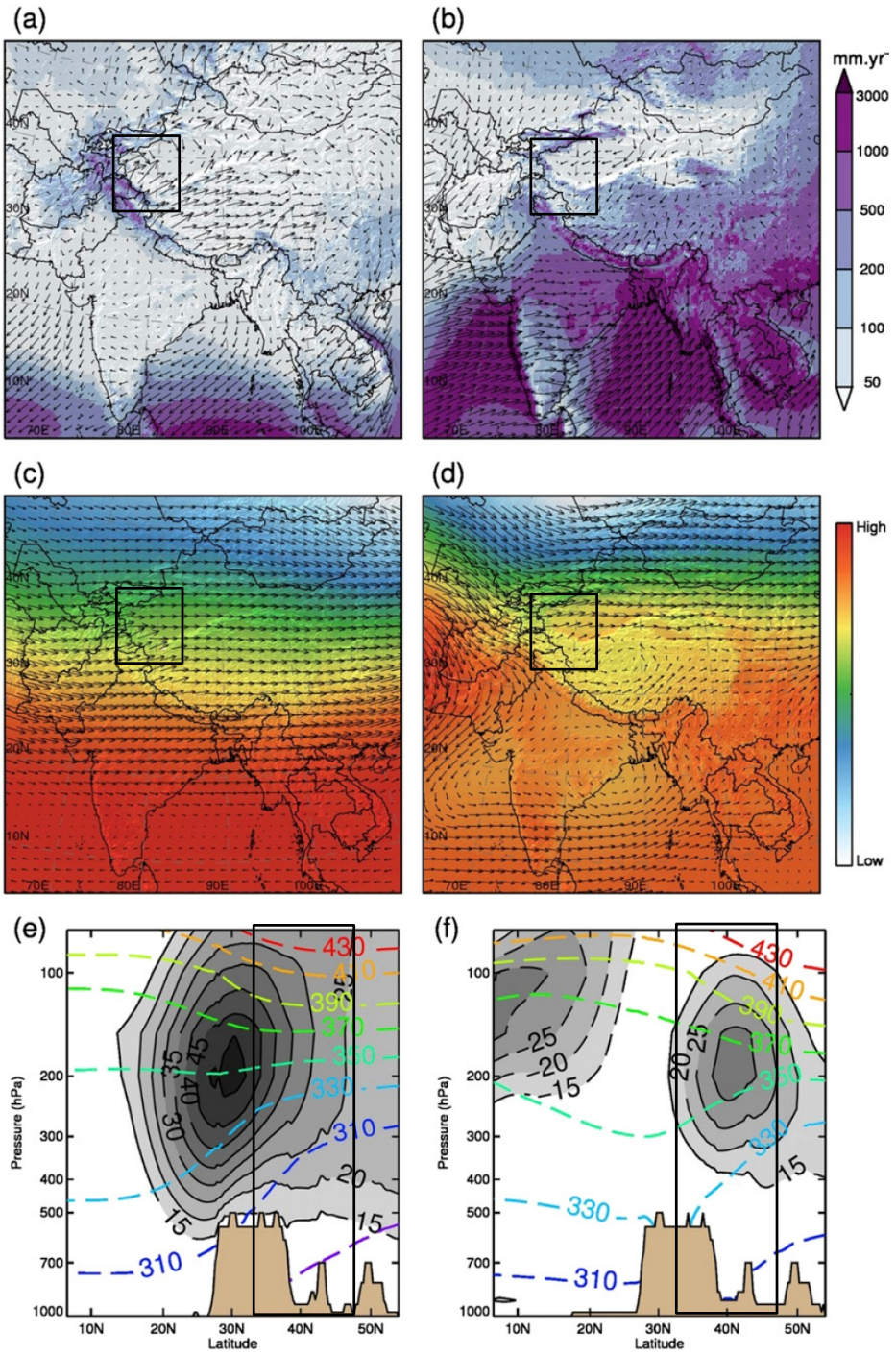

Figure 3.2: Winter (DJF, on the left) and summer (JJA, on the right) mean values of the High Asia Refined 30m dataset for the period 2001–2011, adapted from Maussion et al. (2014). (a,b) Precipitation [mm a^{-1}] with 10-m wind directions. (c,d) Geopotential height and horizontal wind directions at the 500-hPa level. High and low values of the geopotential height are in winter (low: 5.24 km; high: 5.89 km) and summer (low: 5.67 km; high: 5.90 km). (e,f) Horizontal wind speed [m s^{-1}] (grey shades) and potential temperature [K] (colored dashed lines) at the 90°-longitudinal transect. Rectangels indicate the approximate extent of Figure 3.1.

The limited meteorological stations that exist testify a great heterogeneity and strongly seasonal climate regime as shown in Figure 3.3 and Figure 3.4. Mean summer (winter) temperatures fall between 3–10 °C (−19–−15 °C), as provided by the WATCH dataset. About 75% of precipitation falls between the months of April and September, winters are mostly dry and lower valley elevations remain snow free despite freezing temperatures. The Tian Shan station located just outside of the Aksu catchment in Kyrgyzstan at 3614 m asl provides a rare and long-term account of the high elevation climate since the 1930s (albeit inconsistencies introduced by a replacement and a move in 1997 to 3660 m asl). Figure 3.5 shows this record for the period 1961–2013 with mean temperatures of −6.2 °C and annual precipitation of 320 mm a^{-1}. No direct meteorological records exist from the Hotan catchment and only a single meteorological station exists in the Yarkant catchment (Tao et al., 2011), but inaccessible due to China's data-sharing policy. The regional reanalysis dataset APHRODITE (Yatagai et al., 2012) assimilates the Chinese meteorological records on a 0.25° grid (described in more detail in the next section). It indicates annual total precipitation of 220–300 mm a^{-1} in

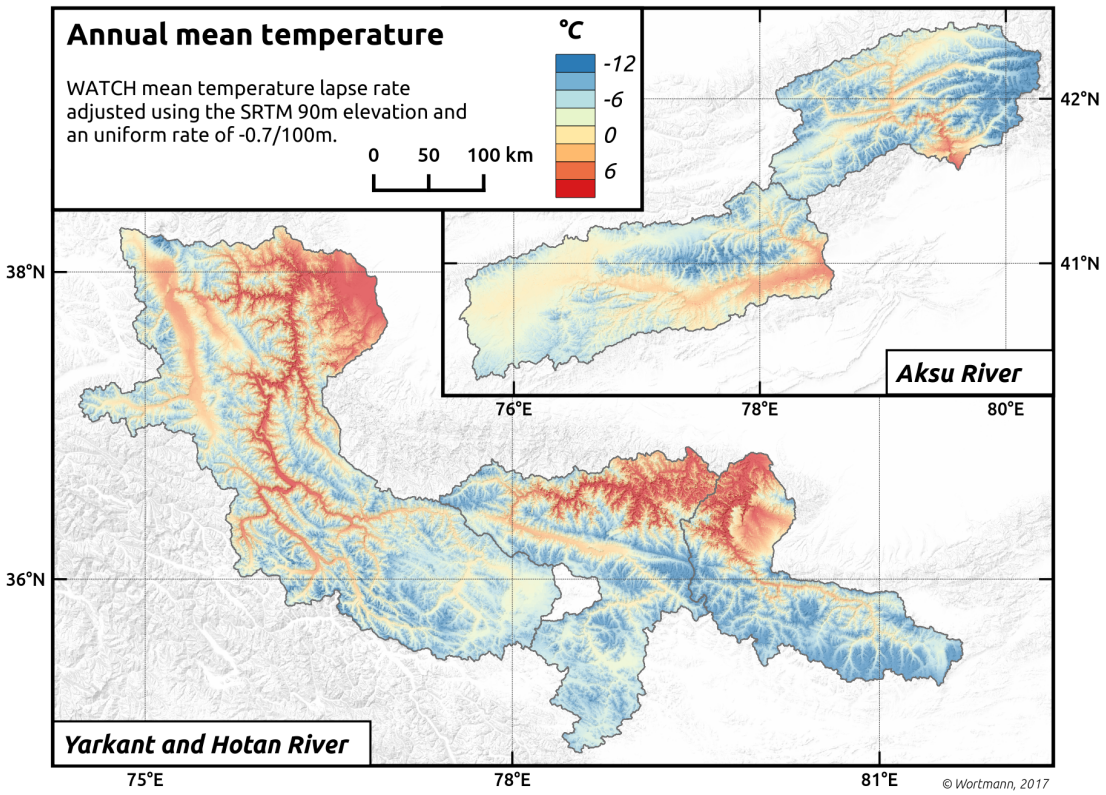

Figure 3.3: Annual mean temperature of the WATCH dataset lapse rate adjusted to the 90m SRTM elevations.

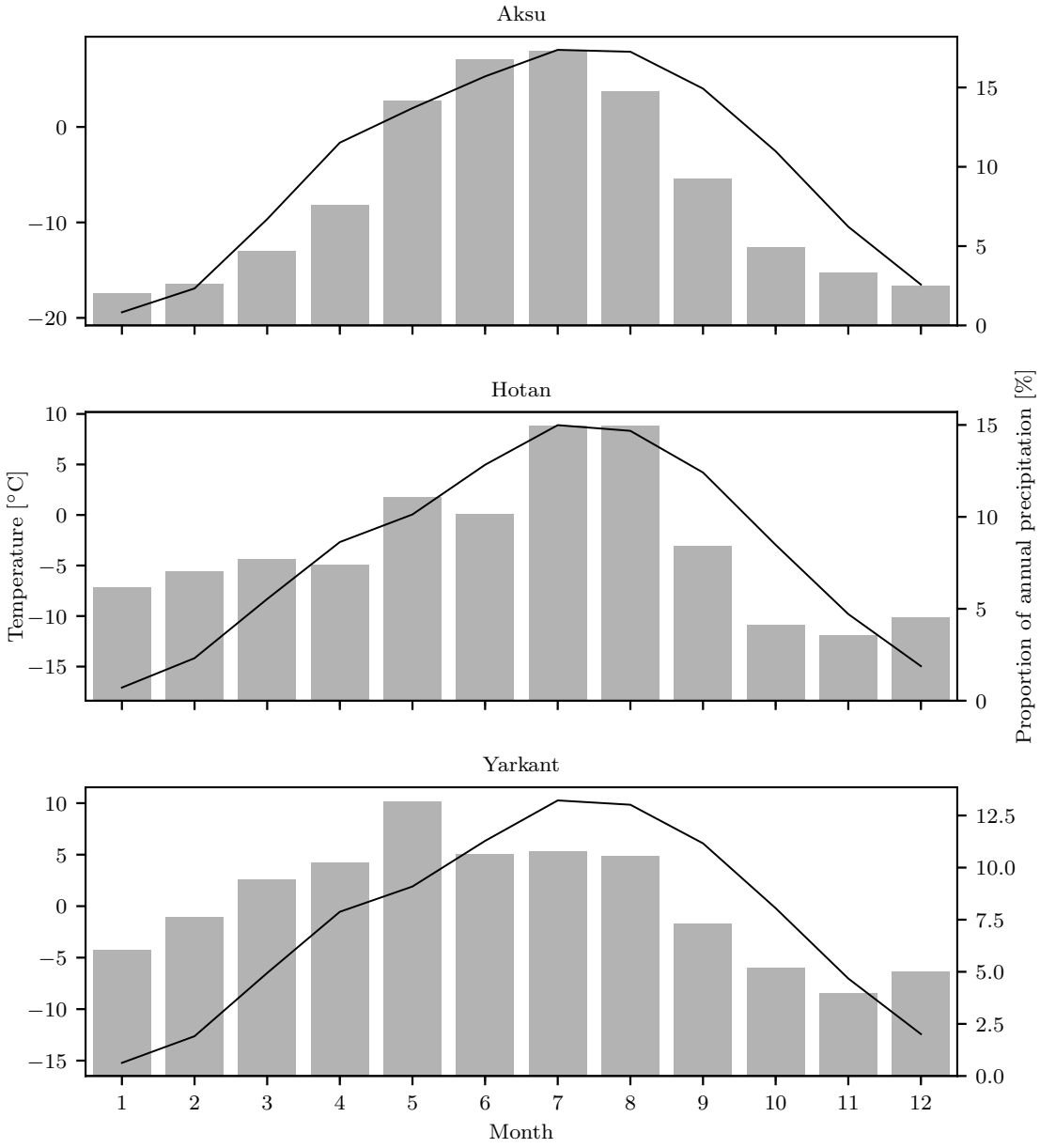

Figure 3.4: Temperature (line) and precipitation (bars) regime in the three Tarim headwater regions for the period 1961–2000. Temperature is lapse rate adjusted from the WATCH dataset. Precipitation proportions are from the APHRODITE dataset, for annual total precipitation see Section 3.3.2.

the Aksu catchments and 60–100 mm a^{-1} in the Hotan and Yarkant catchments. An in depth analysis of precipitation datasets is provided in the next two sections.

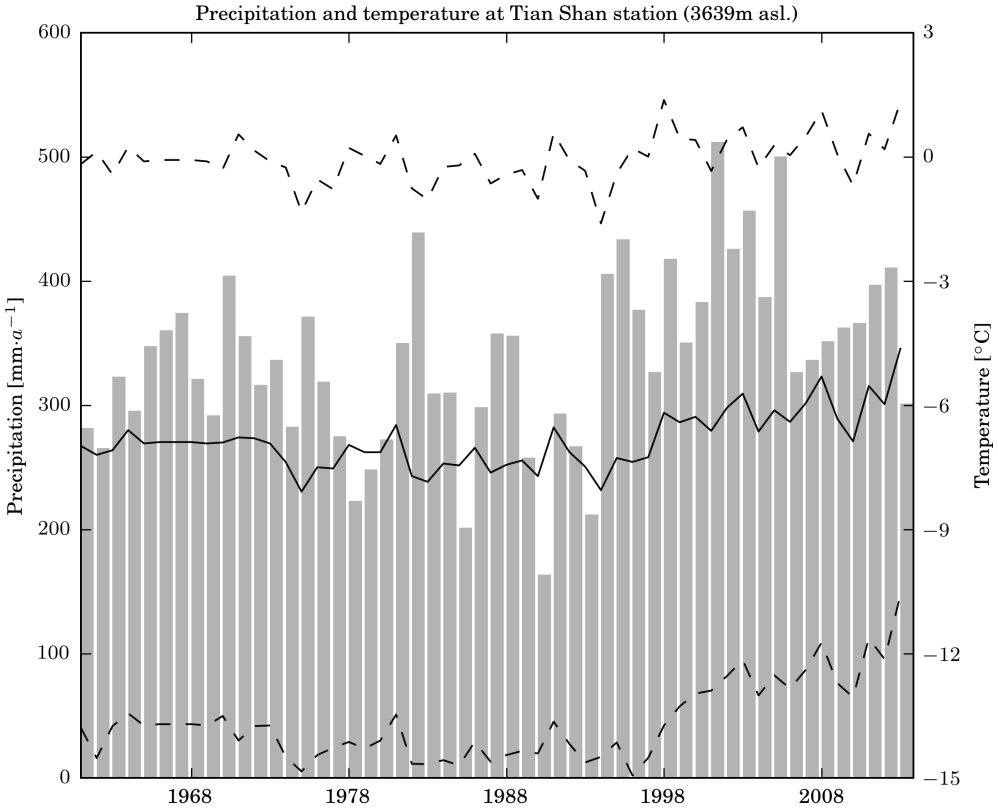

Figure 3.5: Total annual precipitation (bars, left axis) and annual averages of daily minimum, mean and maximum temperature (lines, right axis) as measured at the high-altitude Tian Shan station, in the Akshirak massif. The station was moved in the 1997 to 3660 m asl.

3.3.1 Available precipitation datasets

Six precipitation datasets covering all five catchments were selected to analyse the variability of precipitation in the region (Table 3.2). They may be broadly distinguished

Table 3.2: Selected precipitation datasets with temporal coverage, resolution and boundary conditions.

Name	Coverage	Resolution	Boundary conditions
APHRODITE	1951–2007	0.25°/0.5°	point observations
GPCC	1901–2010	0.5°	point observations
TMPA/GPM	1998–pres.	0.25°/0.1°	RADAR data from multiple satellites
ERA-Interim	1979–pres.	0.5°	Satellite and point observations
CCLM	1959–2001	0.44°	ERA-40
HAR	2001–2014	10 km/30 km	GFS-FNL

by the manner they assimilate observations and produce distributed precipitation fields. The APHRODITE and Global Precipitation Climatology Centre (GPCC) datasets use direct precipitation ground observations and are thus referred to as direct precipitation datasets (DPDs). The satellite-based datasets TMPA (TRMM Multi-satellite Precipitation Analysis, version 7) and the Global Precipitation Measurement (GPM) data as well as the ERA-Interim (ECMWF re-analysis) reanalysis dataset assimilate mainly indirect observations from space (radiance, sea surface temperature) and some ground-based datasets. They are referred to as satellite-based precipitation datasets (SPDs). ERA-Interim falls into this category because it is mainly driven by indirect satellite measurements and does not assimilate direct precipitation observations. A third category includes the COSMO Climate Limited-area Model (CCLM)) and the High Asia Refined analysis (HAR) datasets that are results of regional climate models. They only use global climate model results as boundary conditions. They are referred to as model-based precipitation datasets (MPDs).

The APHRODITE dataset

The APHRODITE dataset is a gridded, daily precipitation interpolation of the densest gauge network in Asia (Yatagai et al., 2012) and is thus considered the best available precipitation data available for the region. A Sheremap-type interpolation scheme was employed to construct daily 0.25° and 0.5° precipitation fields, considering dominant wind exposition and monthly varying correlation distances. While it is the best data available, the underlying station density is still extremely poor as illustrated in Figure 3.6. The Hotan catchments are devoid of any meteorological stations with the closest stations located at the edge of the Taklamakan desert (see also Tao et al., 2011). Similarly, the Yarkant catchment has only one station within the catchment boundary with most surrounding stations at significantly lower-laying locations. The Karakoram range in the south-west of the catchment is particularly remote from any stations.

Despite its drawbacks, it is the best dataset available for longer-term hydrological modelling, as it covers more than 5 decades and has a high correlation with observed discharge (in comparison e.g. to the MPD). The other datasets are used to highlight the large range of uncertainties and to compare different types of observations. The

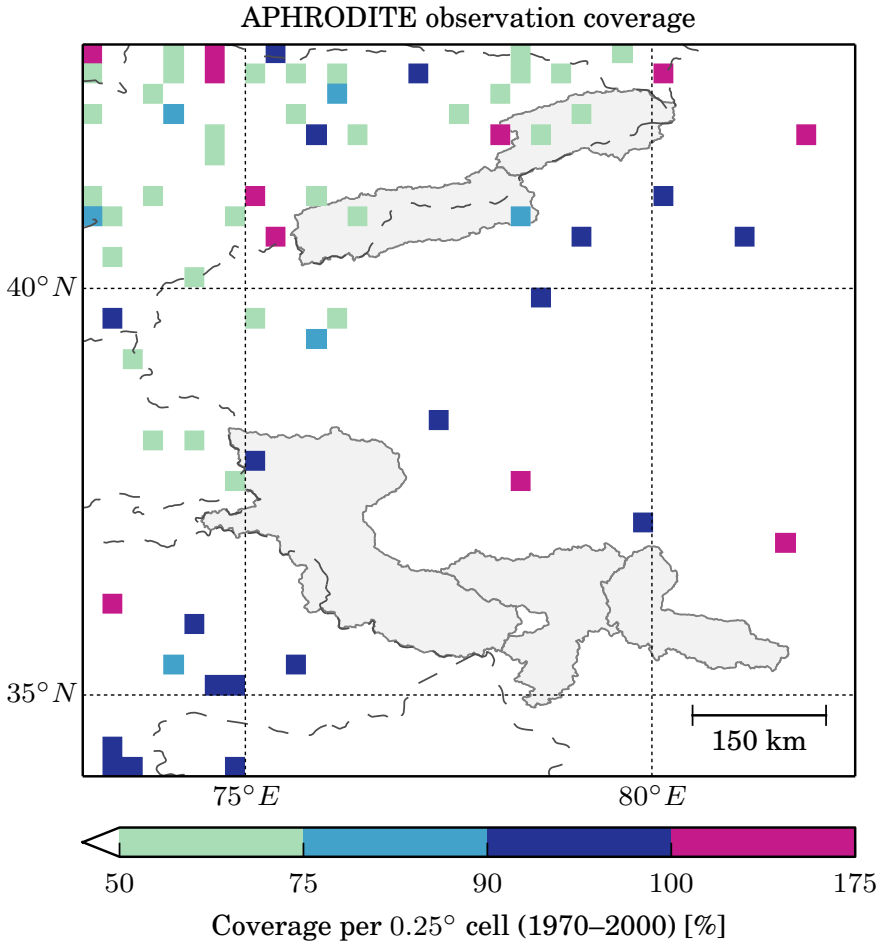

Figure 3.6: Precipitation observations in the Tarim headwaters as assimilated into the APHRODITE dataset given as percent of days with observations in the period 1970–2000 in each grid cell. Cells with more than 100% indicate multiple, simultaneous observations. Catchment outlines (grey shaded areas) and country boundaries (dashed lines) are shown for reference. Refer to Figure 3.1 for elevations.

comparison is focused on annual mean precipitation as it summarises gauging biases well in a highly seasonal climate and because the annual timestep is most relevant to glacier accumulation. The model used to correct the APHRODITE dataset is operating at a daily resolution, but most results will also be given at annual means to make it comparable to the precipitation dataset analysis.

Other precipitation datasets

The GPCC precipitation dataset is a global, monthly interpolation of 70 000 long-term meteorological observations at a resolution of 0.5° covering the period 1901–2013

(Schneider et al., 2015). It is similar to APHRODITE in its interpolation method and error correction but has a less dense observation network in Asia, e.g. only climate reference stations in China. It is considered here, as it presents an authoritative global dataset often used in reanalysis products (e.g. WATCH), fully aware of its limitations for daily hydrological modelling. The ERA-Interim is a reanalysis dataset with a resolution of about 0.7° on a reduced Gaussian grid (i.e. thinned towards the pole) (Dee et al., 2011). The reanalysis assimilates various sources observations (through four-dimensional variational assimilation) – mainly satellite-based, ocean buoy and some land-based temperature observations, but it does not take up precipitation records except for a limited set of snow observations. It represents a sophisticated global product that is increasingly being used as a climate reference as the driver for regional downscaling (e.g. Panitz et al., 2014).

Two satellite-based datasets are analysed. The TMPA (3B42 V7), which is a combined precipitation product of the Tropical Rainfall Measurement Mission (TRMM) fleet, and a high-resolution, research-level product (3IMERGM) mainly derived from the GPM fleet. While space-borne precipitation observations provide homogeneous spatial coverage and are improving in quality and resolution, they have the disadvantage of relatively recent temporal coverages (TMPA since 1998, GPM since 2014), limiting their scope for climatic analyses. The TMPA dataset combines data from TRMM Combined Instrument (TCI), TRMM Microwave Imager (TMI) and the Advanced Microwave Sounding Unit (AMSU), amongst others, using current calibration algorithms, that also assimilate monthly totals from the GPCC dataset (Liu and Liu, 2015). It covers the latitudes up to 50° N–S at a resolution of 0.25°. The global GPM-derived dataset is the result of an algorithm intended to calibrate and interpolate many satellite measurements as well as precipitation gauge analyses, taking advantage of the new and greatly enhanced spatial resolution of 0.1° of the GPM satellite fleet (Huffman et al., 2014). It is used here, although there is only two years of data available, because of its state of the art resolution and focus on all types of precipitation. It is best placed to explore spatial differences in precipitation, especially at high elevations in years to come.

Results from two regional climate models are compared here, the CCLM and the WRF (Weather Research and Forecasting) used to produce the HAR dataset.

CCLM (COSMO model in Climate Mode) is a non-hydrostatic regional climate model based on the primitive hydro-thermodynamical equations (Rockel et al., 2008; Steppeler et al., 2003). Atmospheric variables are computed on a rotated grid with a 0.44° resolution for the CORDEX East Asia domain. Boundary conditions for the large scale circulation are taken from the global ERA-40 reanalysis dataset (Uppala et al., 2005). The HAR dataset was generated using the Advanced Research Weather Research and Forecasting model (WRF-ARW; Skamarock, 2004) at a 10km grid over the Tibetan Plateau and a 30km for all of high mountain Asia (nested modelling approach) for the period 2000–2014 (Maussion et al., 2014). It receives its boundary condition from the Global Forecasting System (GFS) operational model global tropospheric analyses.

3.3.2 Discrepancies between precipitation datasets

Mean annual precipitation varies widely between the selected datasets in both space and time. The discrepancies are evident in catchment mean values (Table 3.3), mean annual and monthly values (Figures 3.7 and 3.10) as well as horizontal and vertical distributions of precipitation (Figure 3.9). Some datasets refer to different periods than the 1971–2000 (reference period); these periods are clearly indicated in the figures, where they are shown together. Although care must be taken when comparing values of different periods, the annual variability is below the differences between most of the precipitation datasets (Figure 3.7).

In the Aksu catchments (Xiehela and Shaliguilanke), the DPD show mean annual values of 230–320 $\mathrm{mm\,a^{-1}}$, while ERA-Interim and CCLM are higher at 486–838 $\mathrm{mm\,a^{-1}}$ over the reference period. These differences are also reflected in much higher summer precipitation for ERA-interim and CCLM compared to the DPD and higher precipitation at higher altitudes for HAR, ERA-interim and CCLM (Figure 3.9). Although slightly lower, the DPD are in line with observations from the single high-altitude Tian Shan meteorological station (3600m asl.), ranging between 200–400 $\mathrm{mm\,a^{-1}}$. However, the altitude dependence is only vaguely visible with most of the Tian Shan showing values between 200–300 $\mathrm{mm\,a^{-1}}$. At similar resolutions, ERA-Interim, HAR and CCLM show much higher values especially at the north eastern fringe of the Xiehela catchment.

Table 3.3: Catchment mean annual precipitation, standard deviation of mean annual precipitation over the catchment area and runoff coefficients for datasets with overlap of discharge data (1971-1987). Mean and standard deviations over 1971–2000 unless otherwise stated.

		Aksu		Hotan		Yarkant
		Xiehela	Shalig.	Wuluwati	Tong.	Kaqun
APHRODITE		314	230	98	62	113
	σ	63	20	28	11	24
GPCC		320	238	63	44	111
	σ	90	25	27	3	39
TMPA (1998–2015)		390	300	147	148	211
	σ	83	26	38	44	54
ERA-Interim (1979–2000)		838	486	566	572	566
	σ	123	80	137	138	195
CCLM		617	482	548	567	609
	σ	150	160	167	160	134
HAR (2001–2014)		1213	894	276	439	463
	σ	499	253	137	232	388

In the Hotan and Yarkant catchments, catchment mean values of the DPD are in the range of 44–113 $\mathrm{mm\,a^{-1}}$, values similar to the Taklamakan Desert. As was shown in Figure 3.6, there are no meteorological stations in the Hotan catchments (Wuluwati and Tongguziluoke) and only one in the north of the Yarkant catchment. The region's typical summer precipitation peak is not evident in the Wuluwati and Kaqun catchments, while there is virtually no precipitation recorded between October and March in the Tongguziluoke catchment. This leads to the conclusion that the DPD are strongly biased by the observations in the desert with annual mean values below 100 $\mathrm{mm\,a^{-1}}$ in the Hotan and around 100–150 $\mathrm{mm\,a^{-1}}$ in the Yarkant catchment. The SPD and MPD, on the other hand, have mean values of 147–609 $\mathrm{mm\,a^{-1}}$ and show a greater correlation with the major mountain ranges in the region. The high resolution GPM and HAR datasets show the heterogeneities in precipitation well. For example in the HAR dataset, the strong differences between the north of the Yarkant catchment and the much wetter Karakoram range in the south are striking. This elevational dependence in precipitation over the catchments is barely noticeable in the DPD (Figure 3.9).

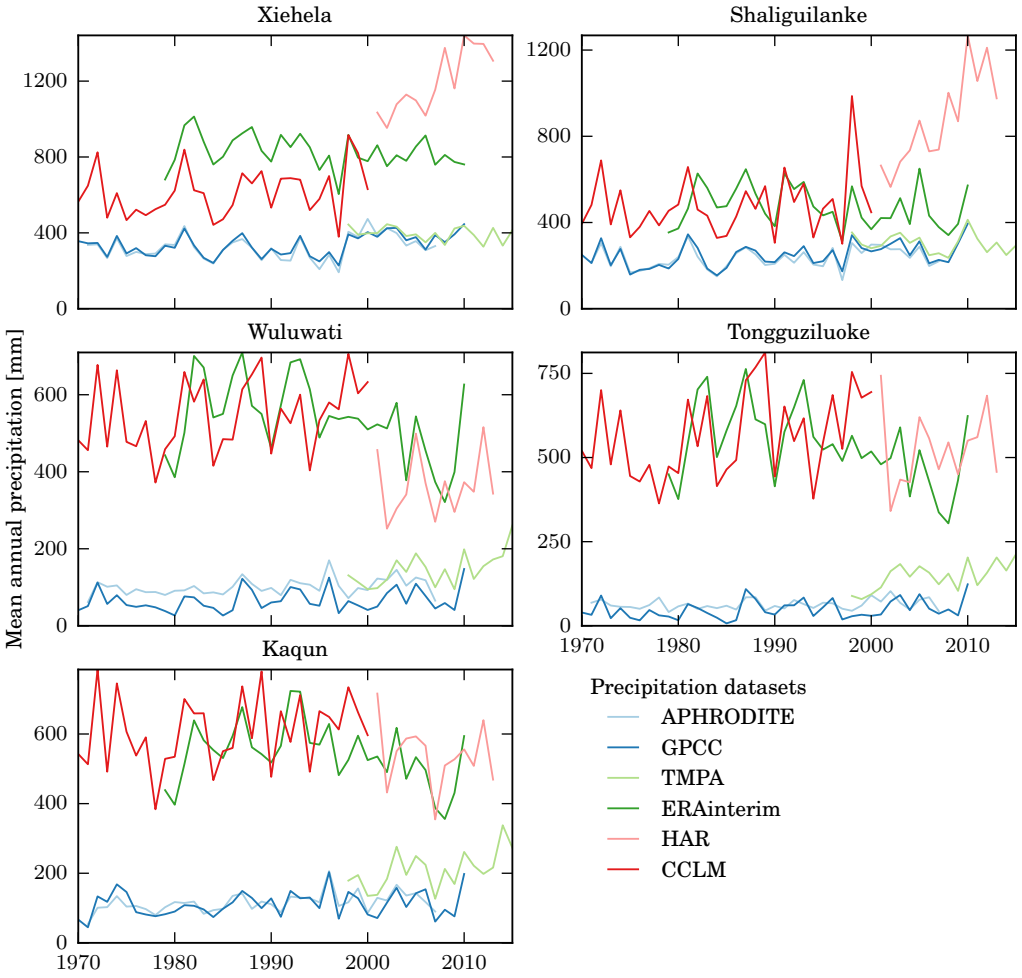

Figure 3.7: Annual mean precipitation for the selected datasets (1971–2015). The top two plots are the Aksu catchments, the Hotan (middle) and the Yarkant catchment at the bottom. Note the varying vertical scales.

A first order indication of precipitation underestimation is also provided by runoff coefficients, the ratio of catchment discharge to precipitation. For four of the five catchments, runoff coefficients are greater than 1 with precipitation from the DPD (Table 3.4). The Hotan and Yarkant catchments have exceptionally high coefficients up to 3.9. Runoff ratios for the ERA-Interim and CCLM precipitation, on the other hand, are much lower at 0.19–0.60. Coefficients vary roughly with glacier cover (as given in Table 3.1 and further described in Section 3.4) and aridity. The highly glacierised catchments Xiehela and Tongguziluoke show significantly higher values than their neighbouring less glacierised catchments, Shaliguilanke and Wuluwati.

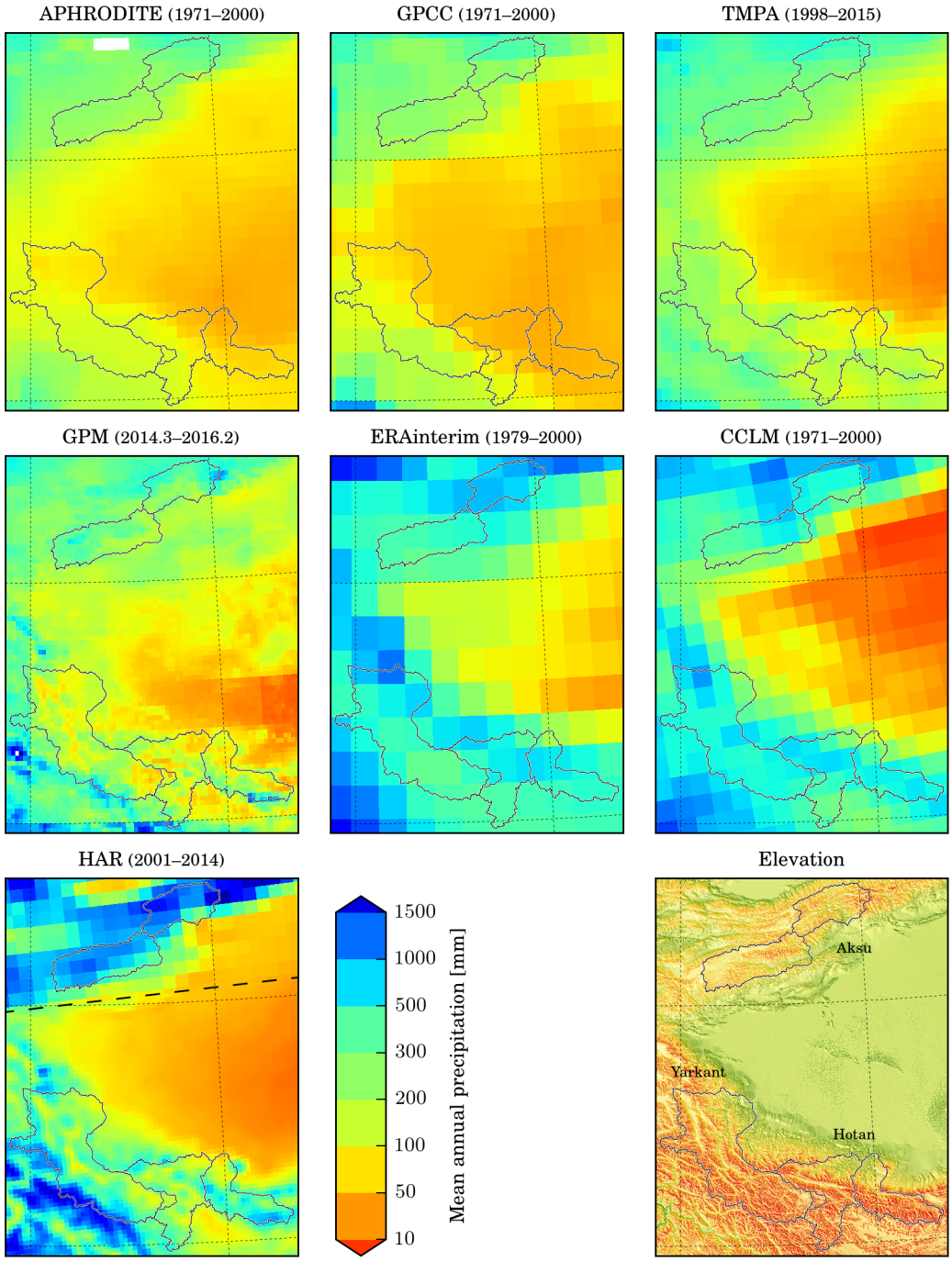

Figure 3.8: Mean annual precipitation for the selected datasets over the periods stated in the title. The APHRIDITE, GPCC and CCLM datasets all refer to the reference period 1971–2000. All datasets are shown at their original resolution but in UTM projection. Elevation from the SRTMv3 DEM for reference. The horizontal line in the HAR dataset indicates the boundary of the 10km-resolution domain; the northern part is the 30km-resolution domain.

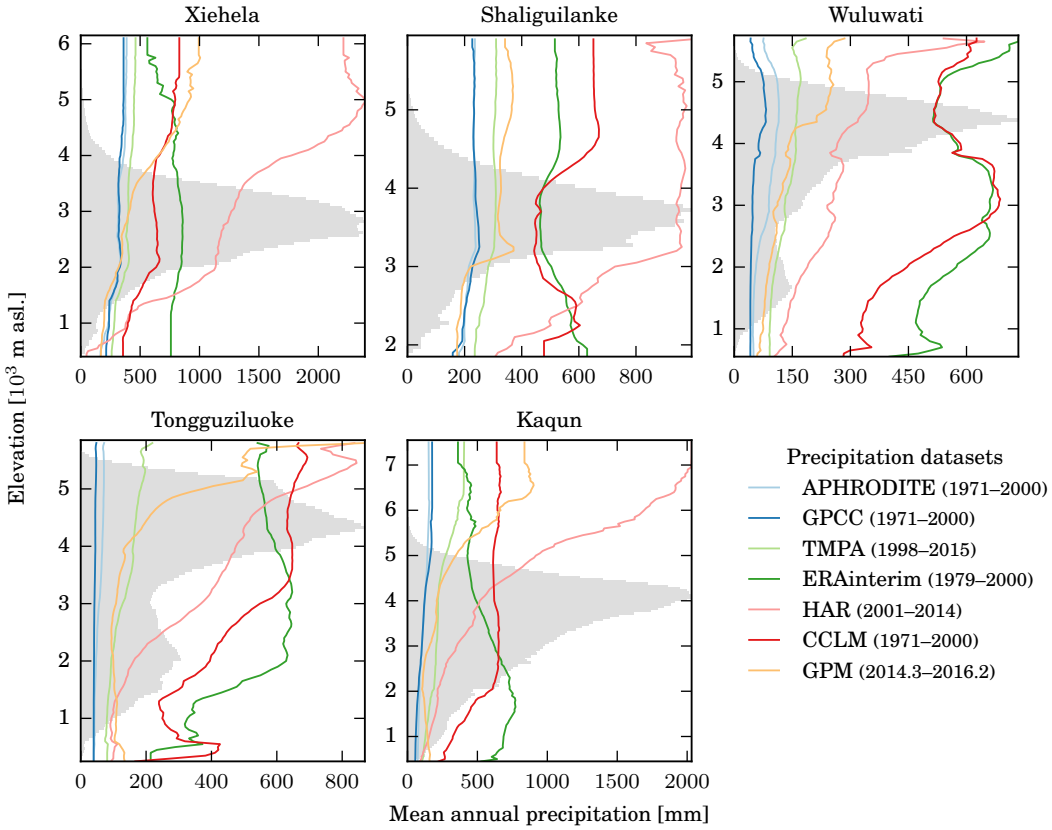

Figure 3.9: Mean annual precipitation (1971–2000, unless otherwise stated) hypsometries over the five headwater catchments. 50m elevation intervals sampled from the original values at a 90m resolution.

The extensive glacier cover of the catchments has the potential to alter runoff without a change in precipitation; negative mass balances drive the ratio up and vice versa, but only within the limits of reasonable mass balance assumptions. Simultaneously, mountainous catchments generally exhibit high runoff coefficients, as shallow soils and steep slopes favour fast surface runoff and low temperatures coupled with sparse vegetation

Table 3.4: Runoff coefficients for the datasets with overlap with discharge observations (1971–1987). The discharge data is described in Section 3.5.

	Aksu		Hotan		Yarkant
	Xiehela	Shalig.	Wuluwati	Tong.	Kaqun
APHRODITE	1.10	0.62	1.26	2.51	1.38
GPCC	1.08	0.61	1.99	3.87	1.39
ERA-Interim	0.43	0.30	0.19	0.26	0.25
CCLM	0.60	0.31	0.22	0.29	0.25

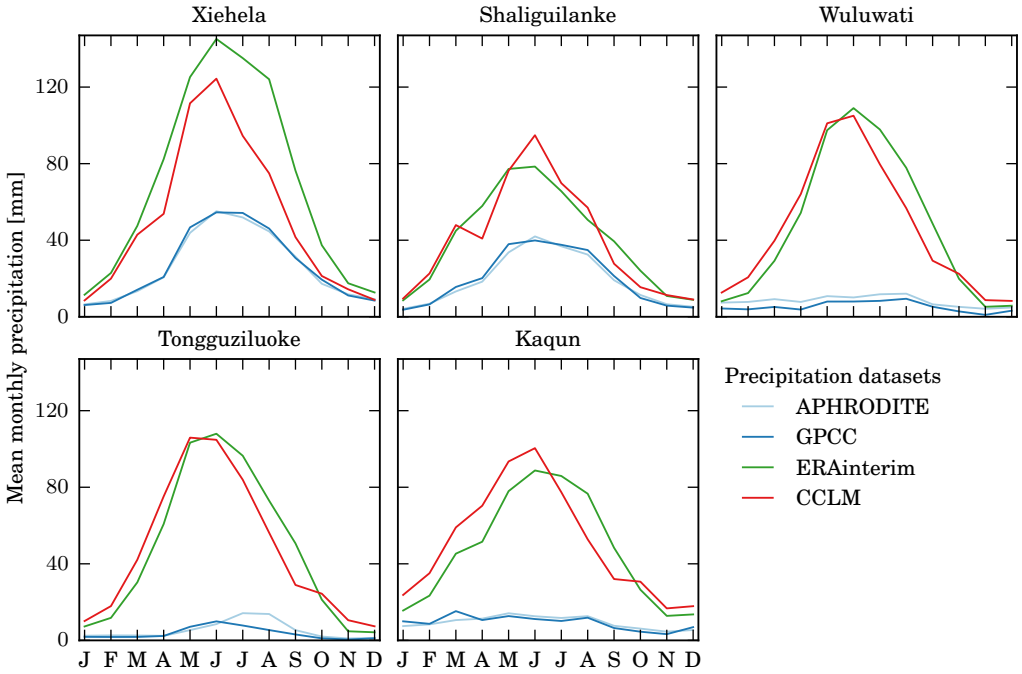

Figure 3.10: Mean monthly precipitation for the datasets with long-term coverage between 1971–2000. Aksu catchments (Xiehela and Shaliguilanke), the Hotan (Wuluwati and Tongguziluoke) and the Yarkant catchment (Kaqun). Note the varying vertical scales.

keep evapotranspiration down Barry, 2008. However, in the Tarim headwaters this is counterbalanced by an arid to hyper-arid climate. Numerous high-altitude salt water (endorheic) lakes are close to the catchments on the Tibetan Plateau and in the western central Tien Shan (see Figure 3.1), providing evidence for evaporation-driven water cycles. These opposing conditions and largely unknown mass balances in the Yarkant and Hotan catchment make it hard to estimate reasonable runoff coefficients. Even when considering for the region atypically large negative mass balances (i.e. -500–$-600\,\mathrm{mm\,weq.\,a^{-1}}$), coefficients greater than 1 are improbable and would signal a significant alteration of the glacier and catchment hydrology.

The comparison of the six precipitation datasets allows the following general conclusions for the Tarim headwater catchments: a) The SPD and MPD give significantly higher values than the DPD (catchment means 3–4 times higher, locally up to 12 times). b) The mountain ranges are not well reproduced by the DPD, especially where the closest meteorological stations are at the desert fringes. c) The DPD do not capture the heterogeneity and elevation dependence of precipitation in the catchment as it is,

for example, measured by the satellite-based datasets or modelled by the MPD. d) All datasets vary significantly from each other especially in the elevation distribution, with the exception of the strong similarity between the DPD. To reconcile these differences into a consistent and for modelling purposes useful precipitation dataset, the daily APHRODITE dataset is corrected in Chapter 6. Despite its weaknesses at higher elevations, it is the only daily dataset available for many decades, it has the greatest meteorological station density and it shows a strong correlation with the observed discharge, in comparison to the climate model-based datasets. The findings of the above comparison are used to constrain the precipitation correction with the help of a glaciohydrological model, as described in Chapter 6.

3.3.3 Trends in temperature and precipitation

The trends in temperature, precipitation and river discharge over the past 50 years of the Aksu River, the most important tributary to the Tarim River, have been widely discussed (Krysanova et al., 2015a; Wang et al., 2008; Xu et al., 2010c) as well as trends in the wider Tarim basin (Tao et al., 2011). The observed climate in Xinjiang has experienced a trend towards warmer and wetter conditions since the 1970s (Shi et al., 2006). Statistically significant increasing trends were found for temperature and precipitation over nearly the entire Tarim catchment (at 1% significance level), as shown by Figure 3.11 reproduced from Tao et al. (2011). Temperatures have risen at a rate of 0.23 °C per decade, while precipitation at a rate of 5.2 mm or 7.4 % per decade (linear trend over 1961–2008). Since these trends are mainly based on observations from the mountain-desert transitional zone with mean annual precipitation between 50–100 $\mathrm{mm\,a^{-1}}$, relative changes are drastic. Due to the poor observation density in the mountainous headwaters and especially the Hotan and Yarkant catchments, however, those results must be interpreted with caution.

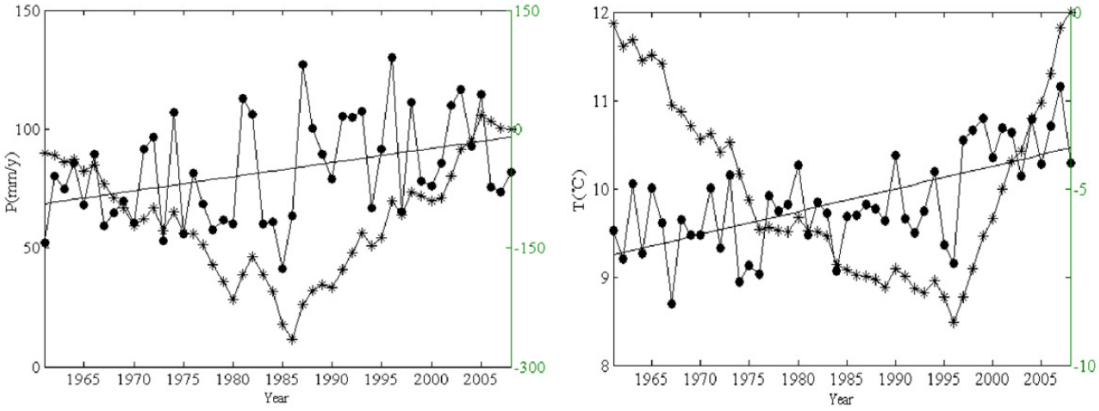

Figure 3.11: Change in precipitation (left) and temperature in the Tarim basin over the past 5 decades as analysed by Tao et al. (2011). The dotted line line is the variable with a trend line, the asterisked line is the cumulative sum of annual residuals from the mean value.

3.4 Glaciology

The mountain ranges surrounding the Taklamakan Desert comprise steep, high-altitude terrain that has given rise to an extensive glacier cover accounting for significant proportions of the catchment areas (Table 3.1, Figure 3.12). The mean elevation of the Aksu catchments is 3500 m asl and includes the highest peak of the Tian Shan, the Jengish Chokuso (Pik Pobedy in Russian or Tömür in Uyghur) at 7439 m asl. The two catchments cover a total glacier area of 3354.7 km^2 (in $\approx$ 2010), including the largest glacier of the range, the South Inylchek Glacier (Osmonov et al., 2013; Pieczonka and Bolch, 2015). A unique glaciological feature of the Aksu headwaters is the ice-dammed Merzbacher Lake between the South and North Inylchek glaciers sending near-annually reoccurring subglacial outburst floods (jökulhlaups) downstream (Glazirin, 2010 and further described in Chapter 4). The glaciers here are mainly temperate, polythermal (both warm and cold-based) and nourished by summer accumulation (Pieczonka et al., 2013).

The two catchments of the Hotan River span the northwestern edge of the Tibetan Plateau at a mean elevation of 4695 m asl, including the Liushi Shan at 7167 m asl, the highest summit of the Kunlun Shan range. Glaciers cover some 5883 km^2 ($\approx$ 2010) and are mostly cold-based at very high altitudes (Bolch et al., 2012b; Shangguan et al., 2007). Accumulation mainly occurs during the summer months. The Yarkant headwater catchment has an average elevation of 4425 m asl with the Karakoram in the south, includ-

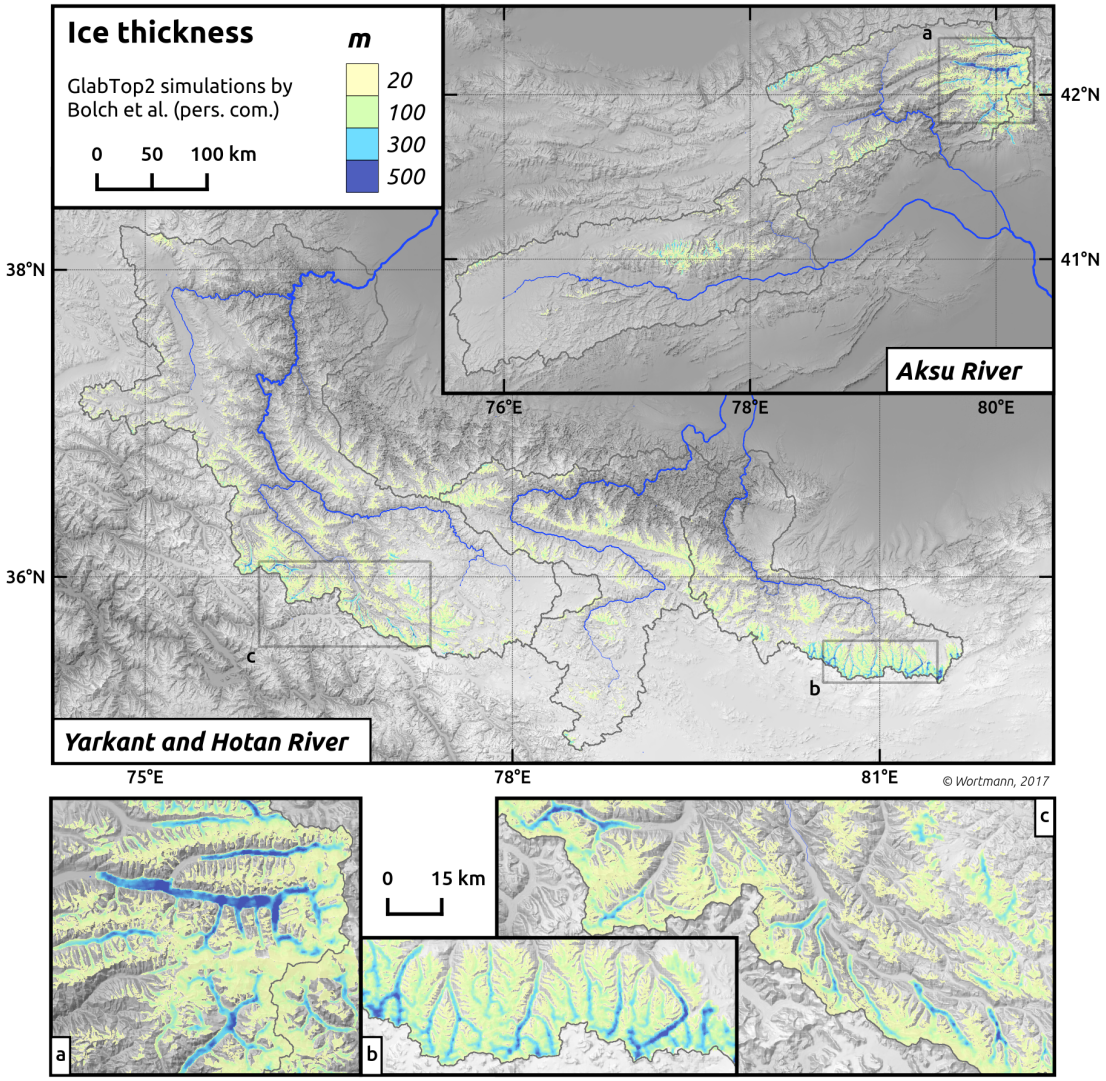

Figure 3.12: Observed glacier extents (≈ 2008) and thickness estimates based on the GlabTop2 model in the five Tarim River headwaters by Bolch et al. (personal communication). The major glacier massifs are shown in detail: a) the Khan-Tengri massif with the South Inylchek glacier in the center, b) the northern slopes of the West Kunlun Shan icecap and c) the NE slopes of the Karakoram including the K2 mountain and the Shaksgam valley.

ing the K2 at 8614 m asl, and the East Pamir in the north. A total glacier area of 5609 km^2 (≈ 2010) is found within the catchment at extremely high and steep altitudes (Frey et al., 2014). Similar to the Hotan catchment, glaciers are mainly cold based but see some accumulation also in winter.

Many glaciers of the region have a significant debris cover (supraglacial moraines) (Hagg et al., 2008; Scherler et al., 2011; Yao et al., 2014). Debris is typically concentrated

at the terminus of large valley glaciers and decreases in thickness uphill. Figure 3.13 shows two examples of the large-scale distribution of such debris covers in the Aksu catchment. The debris not only hinders the identification of glacier outlines using satellite imagery, it also affects the energy balance, mainly suppressing melt rates due to a shielding effect (Nicholson and Benn, 2006; Östrem, 1959). Systematic observations of debris on glaciers are unavailable for the region, but studies on individual glaciers have been conducted. Hagg et al. (2008) investigated the moraine extent of the South Inylchek glacier and conducted ablation measurements. They confirmed the exponential decreasing relationship of melt with debris thickness (the Östrem curve, Östrem 1959) with a correlation of 0.94 on debris covers up to 35 cm. Yao et al. (2014) and Juen et al. (2014) reported an extensive debris cover on the Koxkar Glacier with a thickness of more than 3 m at the terminus. A more description of processes and modelling approaches is provided in Chapter 5, where a dynamic debris evolution is incorporated into the glacio-hydrological model.

3.4.1 Glaciological trends

Insights into the glaciological trends of the region are sparse since systematic and long-term glaciological studies are rare. The earliest glaciological investigations in the Chinese part of the Tarim headwaters started in the 1950s and 1960s and slightly earlier in the Tian Shan by research teams of the USSR (Ding et al., 2006). In situ observations, topographic maps and aerial photographs provided the basis for the first analyses, often of specific glaciers, leading to the compilation of the Chinese Glacier Inventory (CGI, Shangguan et al. 2007). Only since the advent of the satellite era have larger glacierised regions been studied systematically, enabling area and mass change assessments that are representative for entire river catchments (e.g. Bolch et al., 2017; Gardelle et al., 2013).

Glacier area and mass balance studies relevant to the three Tarim River headwater regions are summarised in Tables 3.5 and 3.6. The Aksu catchment has again received most research attention, in particular over longer time scales. This is in part driven by the better accessibility of the Tian Shan. Glacier terminus elevations are much lower (2800–3500m asl) than in the Hotan and Yarkant catchments (4000–5000m asl) and are close to larger settlements. The Karakoram and Kunlun Shan ranges on the, other hand,

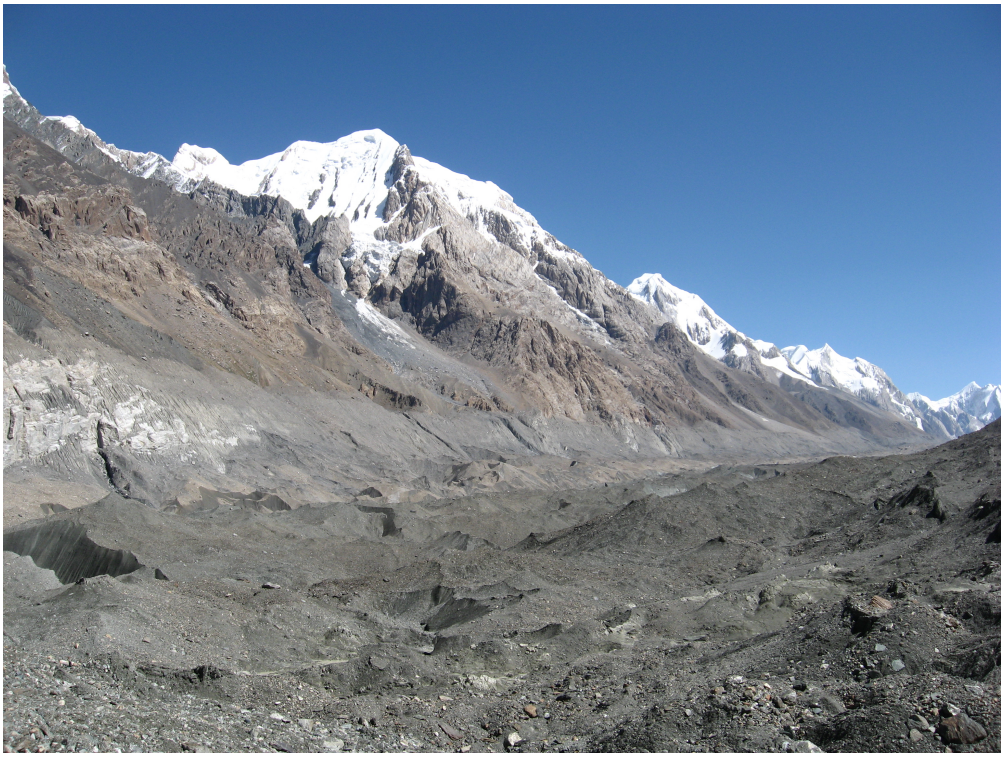

Figure 3.13: The debris-covered terminus of the Kaindy glacier to the southeast of the South Inylcheck Glacier (top) and proglacial moraines with meltwater lakes in the Akshirak massif (bottom) in the Aksu headwater. The pictures were taken by the author in late August 2012.

Table 3.5: Glacier area change studies within or close to the catchments of the three Tarim tributaries over different investigation domains and periods.

Source	Domain	Period	Area change %
Aksu			
Pieczonka and Bolch (2015)	Aksu catchment	1975–2008	-3.6±4.9
	Akshirak	1975–2008	-8.9±4.9
Osmonov et al. (2013)	Kyrgyz Aksu	1990–2010	-3.7±2.7
Aizen et al. (2006)	Akshirak	1943–1977	-4.2
		1977–2003	-8.7
Kutuzov et al. (2009)	Terskey–Alatoo	1965–2003	-12.6
Hotan			
Shangguan et al. (2007)	W Kunlun Shan	1970–2001	–0.4
Yao et al. (2012)	Yurungkax catchment	1970–2001	-0.27
Yarkant			
Shangguan et al. (2006)	East Pamirs	1966–1999	–7.9
	NW Karakoram	1968–1999	-4.1
Yao et al. (2012)	Muztagh Ata group	1965–2001	-1.05

are surrounded by the mighty and largely unpopulated Tibetan Plateau and the Taklamakan Desert with high-altitude approaches. Close to the Aksu catchment lies one of only a few reference glaciers of the World Glacier Monitoring Service (WGMS) the Karabat Kak glacier (Zemp et al., 2009) with more than 40 years of mass balance observations. Several glacier area investigations reach as far back as the 1940s (Aizen et al., 2006). In contrast, there are hardly any regular in-situ observations for the Hotan and Yarkant catchments (≈3 times the glacier area) with the exceptions of some terminus variations (Shangguan et al., 2007) and a short mass balance measurement campaign at a single glacier (Muztagh Ata glacier in 2005–2010, Yao et al. 2012). All other studies rely on space-born observations.

Glaciers in the Aksu catchment (often referred to as the central Tian Shan) have generally experienced area retreat and mass loss at least over the past 50 years or so, although at a slower rate than other regions of the Tian Shan (Farinotti et al., 2015; Pieczonka and Bolch, 2015). The long-term in-situ timeseries of the aforemen-

Table 3.6: Glacier mass balance studies within or close to the catchments of the three Tarim tributaries over different investigation domains and periods. Domain definitions may vary slightly between the studies.

Source	Domain	Period	Mass balance m weq. a^{-1}
Aksu			
Pieczonka and Bolch (2015)	Xiehela catchment	1975–2000	-0.35±0.34
	Akshirak	1975–2000	-0.51±0.36
Aizen et al. (2006)	Akshirak	1943–1977	-0.24±0.12
		1977–2003	-0.69±0.37
Farinotti et al. (2015)	Central Tian Shan	2003–2009	-0.06±0.31
Hotan			
Kääb et al. (2015)	W Kunlun Shan	2003–2008	+0.05±0.07
Gardner et al. (2013)	W Kunlun Shan	2003–2008	+0.17±0.15
Neckel et al. (2014)	W Kunlun Shan	2004–2009	+0.04±0.29
Yarkant			
Gardelle et al. (2012)	Central Karakoram	2000–2008	+0.11±0.22
Gardelle et al. (2013)	E Karakoram	2000–2010	+0.11±0.14
	W Karakoram	2000–2008	+0.09±0.18
Yao et al. (2012)	Muztagh Ata glacier	2005–2010	+0.25
Kääb et al. (2015)	Karakoram	2003–2009	-0.10±0.06
Gardner et al. (2013)	Karakoram	2003–2009	-0.12±0.15

tioned Karabat Kak glacier (Figure 3.14) testifies this with a mean mass balance of 0.49 m weq. a^{-1} over the period 1960–1998. Since this is only from a single glacier, extrapolation of this mass balance over an entire region is associated with large uncertainties. A recent study, also conducted with the Sustainable Management of River Oases in the Tarim Basin (SuMaRiO) project, has provided invaluable insights into area and mass changes over the entire Aksu catchment using recently unclassified satellite imagery from the 1970s (Pieczonka and Bolch, 2015). Glacier area changes between 1975–2008 were investigated using two multi-spectral image pairs (see Table 3.5). More importantly, glacier surface elevations were assessed from a stereo-pair of KH9-Hexagon imagery from 1975 and compared to the SRTM Digital Elevation Model (DEM) in 2000 (see Table 3.6 and Figure 3.15). Results showed heterogeneous glacier mass and

area loss over the catchment, but the average mass balance of $0.35 \pm 0.34\,\mathrm{m\,weq.\,a^{-1}}$ (1975–2000) is comparable to global values and is used in the core chapters of this thesis (Chapters 5 and 6). Area shrinkage is comparatively low at $-0.11 \pm 0.15\,\%\,\mathrm{a^{-1}}$ (1975–2008). This study also identified several surge-type glaciers, i.e. glacier that have recently experienced a rapid advances. The relatively high uncertainty ranges are mainly caused by vertical accuracies of terrain datasets, extensive englacial glacier cover, but the results are largely in-line with related studies (Farinotti et al., 2015; Osmonov et al., 2013; Pieczonka et al., 2013).

The Kunlun Shan and the Karakoram are vast glacierised regions with complex climatic and topographical features making the extrapolation from neighbouring regions difficult (Hewitt, 2011; Liu, 2011). Although early observations and studies suggest a general receding trend since the Little Ice Age (LIA) (Hewitt, 2011; Hewitt and Liu, 2010), they are mainly based on single field campaigns and geomorphological observations. Over more recent decades, area change assessments based on satellite imagery indicate moderate rates of shrinkage, but also signs of individual advancing glaciers (Table 3.5). Few mass balance studies have been conducted for the region and those

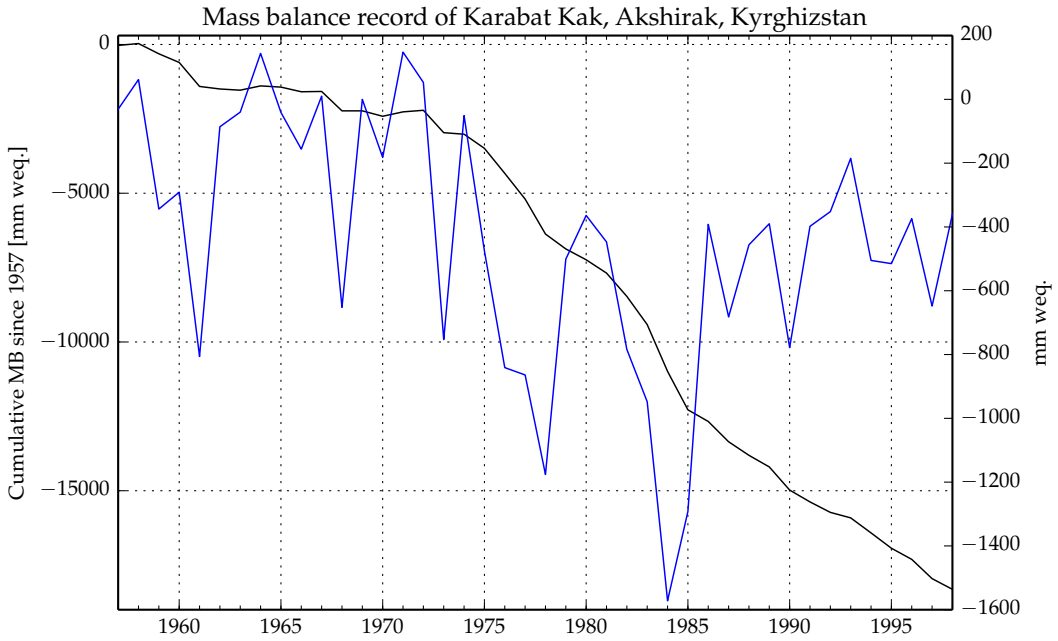

Figure 3.14: Annual mass balance (right axis in mm water equivalent per year) and cumulative mass balance of the reference glacier Karabat Kak, Kyrgyzstan, since the start of the in situ measurements. Data provided by WGMS and UNEP (2008).

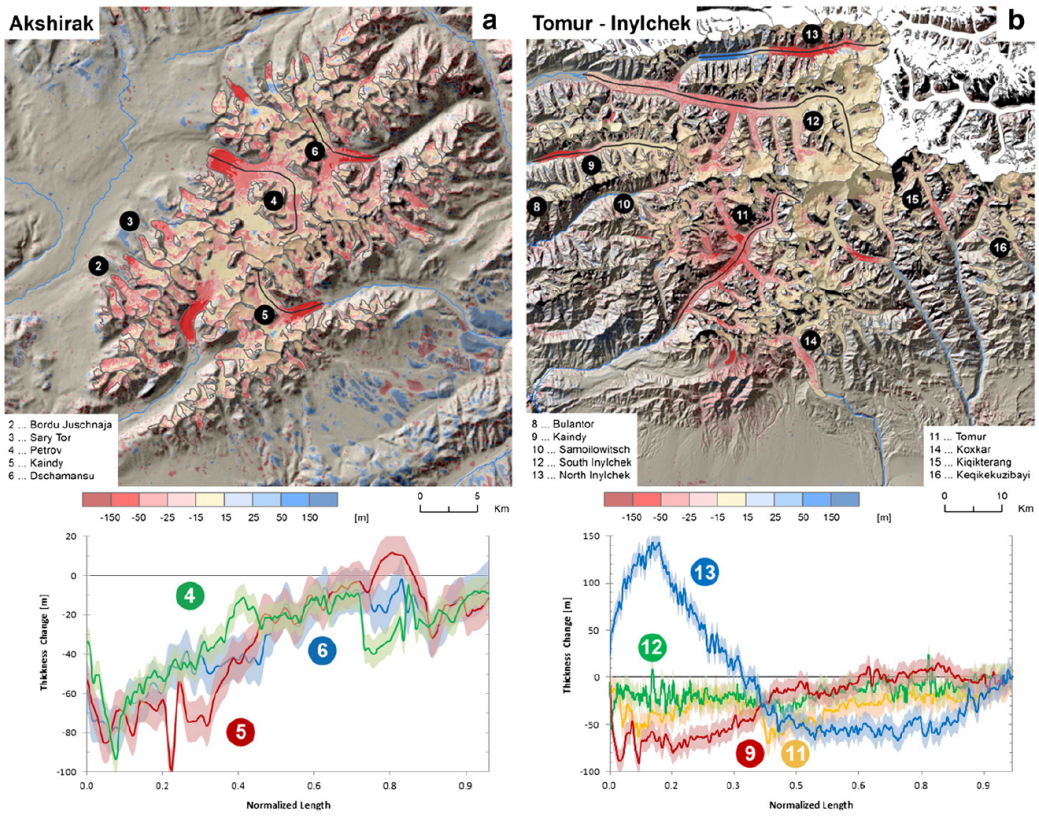

Figure 3.15: Geodetic glacier mass balance of the Khan-Tengri and Akshirak massifs in the Aksu headwater for the period 1975–2000, reproduced from Pieczonka and Bolch (2015).

available analyse changes only within the last 10–15 years (Table 3.6). The positive mass balance stand in contrast to the global trend of mass loss, a phenomenon term 'Karakoram anomaly' (Hewitt, 2005). The mass gain within the first decade of the 21st century ranges from $0.04\,\mathrm{m\,weq.\,a^{-1}}$ to $0.25\,\mathrm{m\,weq.\,a^{-1}}$ across various glacier groups within the Tarim catchment. Yet uncertainty ranges are large in comparison to the magnitudes of change ($\pm 0.14 - -0.22\,\mathrm{m\,weq.\,a^{-1}}$) and there are contrasting estimates for the greater Karakoram range (Gardner et al., 2013; Kääb et al., 2015).

So far, the explanations for this positive mass balance include the strengthening of the Westerlies and the extremely steep and high topography of the region. Despite temperature increases, the glaciers remain stable or even grow through increased accumulation at high elevations, while an extensive debris cover dampens ablation rates (Hewitt, 2005; Scherler et al., 2011). However, these short investigations are only of indicative value for hydrological assessments with longer reference periods.

3.5 Hydrology

The hydrology of the Tarim headwaters is dominated by the semi-arid climate as well as the mountainous and glacierised terrain. Runoff regimes exhibit a strong summer melt peak (see day-of-year mean discharge in Figure 3.16) with discharge 10–15 times higher in summer than in winter (Table 3.1). Catchment-wide runoff varies between 109–356 mm a^{-1}. Besides annual precipitation, it mainly depends on glacier cover and the melt as well as the area of steep terrain. The two Aksu catchments of the Xiehela and Shaliguilanke gauging stations with a fairly similar climate, for example, show strongly different runoff totals with 356 mm a^{-1} and 144 mm a^{-1}, respectively, due to their different glacier covers (20% and 4%, respectively) and topography. This runoff provides close to the only source of surface water for the settlements in the river oases in the Taklamakan desert downstream.

The mountain streams descend down the glacial valleys leaving behind glacial till and forming large braided flow patters (Figure 3.17). Downstream of the five headwater stations the rivers reach the desert through large alluvial fans, where their unconsolid-

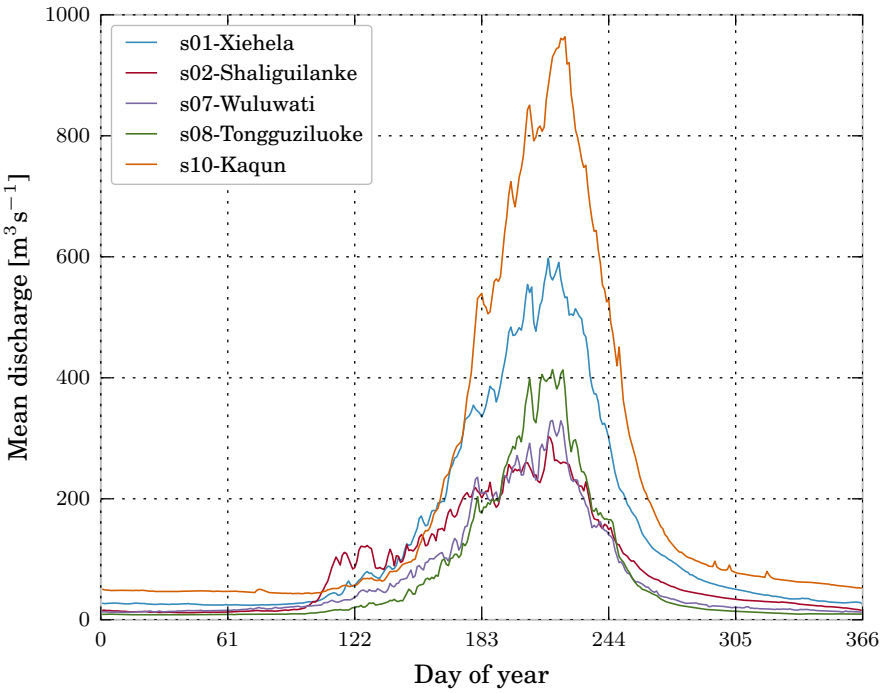

Figure 3.16: Mean day of year discharge at the five headwater stations over the period with available data (1964–1989).

ated flow patterns are restricted by large-scale hydraulic development. River alignments and diversion weirs and barrages have been build over the past 50 years to cater for the expansion of irrigation agriculture as is visible on satellite imagery (Figure 3.18). The oases along the river are made up of an extensive network of irrigation channels, where much of the surface water is used for irrigation or is lost through channel seepage and evaporation (Thevs, 2011). The irrigation agriculture sustains an intensive cotton industry as well as fruit orchards and subsistence farming (Feike et al., 2015).

3.5.1 Trends in discharge

Many studies agree that discharge of several tributaries to the Tarim River has seen an increasing trend over the past five decades, but especially the Aksu headwater (Krysanova et al., 2015a; Tao et al., 2011; Wang et al., 2008; Xu et al., 2010b). The two headwater catchments of the Aksu have experienced a rise of 30 % according to Xu et al. (2010a) between 1957 and 2004 with similar trends in the Yarkant headwaters. Chen et al. (2006) found an increase of 10.9 % from the 1950s to the 1990s, suggesting that increases since the 1990s may have been more pronounced. While rises in the Aksu are in no doubt, statistically significant trends for the Yarkant and Hotan catchments could not be confirmed by Tao et al. (2011). They detected a stagnant or even slight negative trend (only at 10% significance level). In contrast, discharge at the gauging stations downstream of the agricultural oases has been on the decline due to the rapid expansion of the irrigated cotton industry (Thevs, 2011; Wang et al., 2010).

Although these findings are largely in-line with patterns of climatic trends (Tao et al., 2011), attributing the changes to either increases in precipitation or temperature has been difficult. While increases in temperature lead to higher glacier mass loss, simultaneous increases in precipitation can counteract mass losses (through increased glacier accumulation) and/or amplify increases in discharge. Duethmann et al. (2015) examined the influence of both temperature and precipitation on the rising discharge of the Aksu through both a multiple regression and a hydrological model analysis. They found a greater influence of precipitation in the less glacierised Shaliguilanke catchment, but the opposite in the four times more glacierised Xiehela catchment, where the precipitation trend had close to no effect (Figure 3.19). Although trends were not

Figure 3.17: Top: The Sary-Djaz River in Kyrgyzstan about 100km upstream of the Xiehela gauging station, where it is known by its Chinese name as Kumarik He and later becomes the Aksu River. Bottom: The Kaindy River (Aksu headwater), a typical braided glacial river with a shallow slope and large amounts of bed material. Pictures from late August, 2012 (ca. midday) by the author.

Figure 3.18: River alignments and diversion barrages at the confluence of the Toshkan and Kumarik rivers to form the Aksu River (left) and the Yarkant River at the entry into the Yarkant river oasis. Imagery curtsey of Google/CNES/Astrium.

observed in the Hotan and Yarkant catchments, the glaciological studies described in Section 3.4 indicate stable to increasing glacier conditions, which may indicate increases in precipitation at high altitudes leading only to increased glacier accumulation.

3.5.2 Glacier Lake Outburst Floods (GLOFs)

Besides the annual summer flooding regime of the Tarim River headwaters, region has also seen several catastrophic flood events from glacial lakes, so called Glacier Lake Outburst Floods (GLOFs) (Hewitt and Liu, 2010; Krysanova et al., 2015a). The Aksu and the Yarkant rivers have experienced frequent flooding with discharge peaks 5–10 times the average summer discharge as evident in gauge data from the Xiehela and Kaqun station, respectively. GLOFs are caused by the rapid drainage of meltwater lakes either as a result of mechanical dam breaching or the accelerated opening of drainage conduits within the ice. Lakes are created by proglacial moraines or ice dams. Zhang (1992) show the origin of the Yarkant River floods from the Kyagar glacier (Karakoram) that is blocking the Shaksgam valley (presumably as a result of a glacier surge).

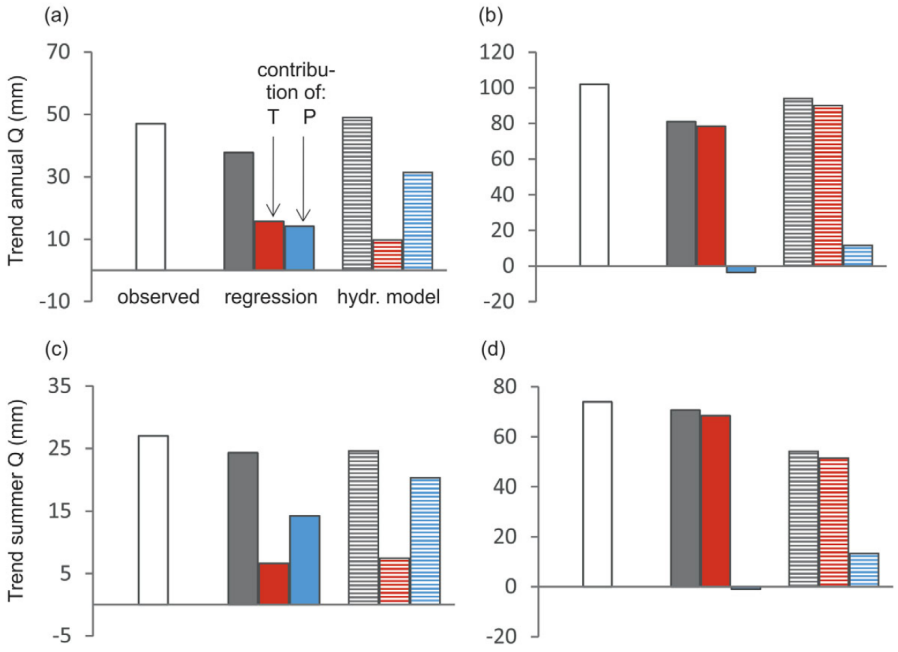

Figure 3.19: Trend attribution in the two Aksu catchments, a) Shaliguilanke b) Xiehela, of annual (top) and summer runoff (bottom) by Duethmann et al. (2015). The observed trend (white bars) is the trend in the discharge observations, the regression trend (filled bars) is from the multiple regression model run with observed discharge and the striped bars show the trend calculated using a hydrological model.

The GLOFs in the Aksu River are special because they are quasi-annually reoccurring. They are produced by the Merzbacher Lake located in the Inylchek valley in Kyrgyzstan at an altitude of 3250 m asl, ca. 200 km upstream of Xiehela gauging station (marked in Figure 3.1) (Glazirin, 2010). The outbursts usually occur at the end of summer or beginning of autumn, with peak floods at the Xiehela station exceeding 1000 $m^3 s^{-1}$, i.e. 6.5 times the mean annual discharge (151 $m^3 s^{-1}$ based on data from 1964–1987) or 2.5 times the mean summer discharge (JJA, 406 $m^3 s^{-1}$ in the same period). These floods have proven destructive to downstream communities, infrastructure as well as agricultural and industrial land in the Aksu-Tarim region. Research has become vital in providing information about the floods and their future development under a warming climate (Liu, 1992; Shen et al., 2009).

The hydrological and climatic controls of the Merzbacher Lake outburst floods are still unclear. Ng et al. (2007) inferred melt water supply during the flood events to the lake via inversion of the Nye subglacial drainage equations taking into account peak discharge and graphically inferred flood volumes. Correlations of the melt water supply

with daily surface temperature averaged over the first third of the flood period at lake level ($r^2 = 0.77$) and graphically separated baseflow at Xiehela station ($r^2 = 0.86$) were found, suggesting high dependence of peak discharge on prevailing weather conditions. They could not define conditions triggering the outburst. This thesis is contributing to the discussion of this special GLOF setting in Section 4.6 by modelling the normal catchment discharge at Xiehela to achieve a more reliable baseflow separation as well as a better analysis of interdependencies between climate and the hydrological phenomena.

3.5.3 Data acquisition

A considerable effort and time was directed towards data acquisition for the upper Tarim River basin. Not only are meteorological and hydrological data scarce in the region (as was shown in Section 3.3.1), but they are also subject to a restrictive data sharing policy in China for international partners. Raw data may not be officially transferred to institutions outside of China. This led to a prolonged negotiation with the Chinese partners at the National Climate Centre (NCC) at the Chinese Meteorological Administration (CMA, Beijing) and at the Xinjiang Institute of Ecology and Geography (Urumqi) to establish the exact data availability, approaches of data processing to overcome the data sharing policy and shared interests for closer cooperation. Distinguishing between restricted data and data not actually recorded proved to be a particular problem, for example in the case of irrigation abstraction data.

Access to preprocessed hydrological and meteorological data was eventually granted under a cooperation agreement, including providing opportunities for knowledge transfer at Potsdam Institute for Climate Impact Research (PIK) (summer schools, exchanges) and shared authorships on future publications. Meteorological data (min., mean, max. temperature, precipitation) was interpolated to a 0.25° grid for the period 1961–2010. River gauge data is available for nine stations on the three main tributaries (three for the Aksu River, three for the Hotan River, two for the Yarkant River) and the first station on the Tarim River after the confluence of all three tributaries, referred to as Alar station (S11). This daily data, however, was only shared for the period 1964 – 1988, with three stations also for 3 to 4 years in the 2010s.

An additional source of data was provided by a published book on the Aksu River (Wang, 2006, in Chinese), that included tables of monthly mean discharge for the three stations on the Aksu River and Alar station on the Tarim River. It also included valuable information on irrigation abstractions and diversions in the river oases, including a monthly abstraction regime of the years 1998–1999 and annual abstractions for the years 1998–2003.

Under a more open data sharing policy, hydrological data was also acquired for the small yet important part of the Upper Aksu River basin that lays in Kyrgyzstan, where the river is called Sary-Djaz. The Aksu River originates in the Kyrgyz part of the Tian Shan mountains, where Soviet gauging stations were operated until 1994. Undigitised daily data from hydrological yearbooks for three stations were sourced from the Central-Asian Institute for Applied Geoscience (CAIAG, Bishkek), mainly covering the period 1974–1992 with gaps.

3.6 Land cover and soils

Land-use in the headwaters is confined to the valley floors that are only sparsely roamed by semi-nomadic cattle (sheep) herders. Vegetation is sparse and dominated by shrubs, grassland and the some coniferous trees below elevations of ca. 3500 m asl, with the rest made up of gravel and scree slopes as well as rock faces (visible in Figure 3.17). Most valleys have a U-shape with shallow slopes, scoured by glaciers that have retreated to higher elevations. Meltwater streams fill these valleys with glacial till forming large braided flow patters.

A land cover map of the Chinese part of the catchment was provided by the Chinese Meteorological Administration (CMA) for ≈ 2000 (Figure 3.20). The parts outside of China (mainly in Kyrgyzstan, the Aksu catchment, marked in Figure 3.20) were filled with the Moderate Resolution Imaging Spectroradiometer (MODIS) land cover product (MCD12Q1, Friedl et al., 2002) from the year 2001. Both maps were reclassed to Soil and Water Integrated Model (SWIM) land cover classes, as shown in Table 3.7. Since glaciers are a variable of the model with the validation data introduced in Section 3.4, the land cover classes from the two maps were assigned the ‘rocks, bare soil’ class.

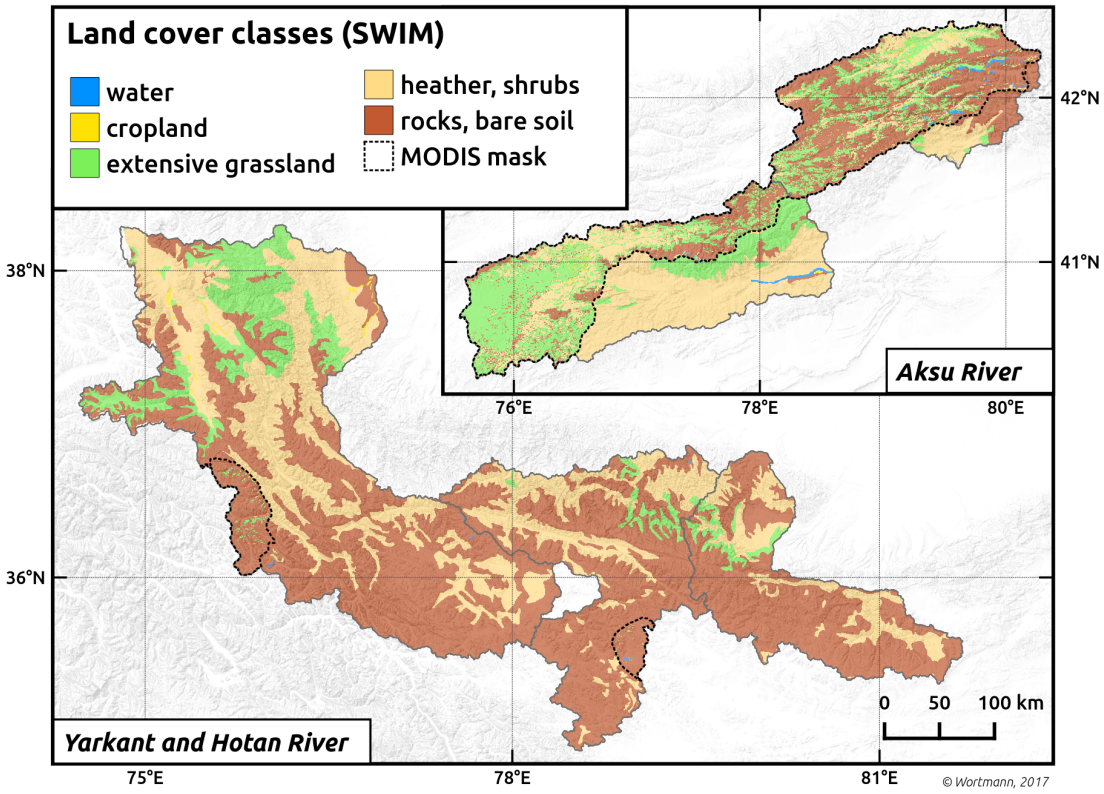

Figure 3.20: Land cover in SWIM classes from the CMA and MODIS (areas marked) land cover maps. See Table 3.7 for details.

Table 3.7: Land cover from the CMA and MODIS land cover classes in SWIM land-use classes with proportional coverage in the Tarim headwater. See map in Figure 3.20.

SWIM	%	CMA	MODIS
rocks, bare soil	52.26	glacier and snow	snow and ice
		desert	barren/sparsely vegetated
		bare soil	
		bare rock	
heather, shrubs	31.78	grassland (20-50%)	closed shrublands
		grassland (5-20%)	open shrublands
			savannas
			woody savannas
extensive grassland	15.46	grassland (>50%)	grasslands
cropland	0.26	non-irrigated agriculture	croplands
water	0.24	river	water

The dominant soils in the catchments are shallow Leptosols and Calcisols in the lower-laying arid parts of the catchments, as shown in Figure 3.21. These sandy soils are common for semi-arid regions and are as shallow as 10–30 cm on the slopes and 100–200 cm in the valley floors or plateaus. Permafrost is widespread above elevations of ca. 3200 m asl, while rock glaciers and large debris moraines dominate the periglacial zones (Zhu, 1996).

The soil information was sourced from the Harmonized World Soil Database (HWSD), a database that attempts to homogenise all national soil inventories providing a consistent dataset for use in earth-sytem models (FAO et al., 2011). A set of pedotransfer functions was used to relate the information given in the HWSD (mainly particle size distributions) to the information needed by SWIM according to

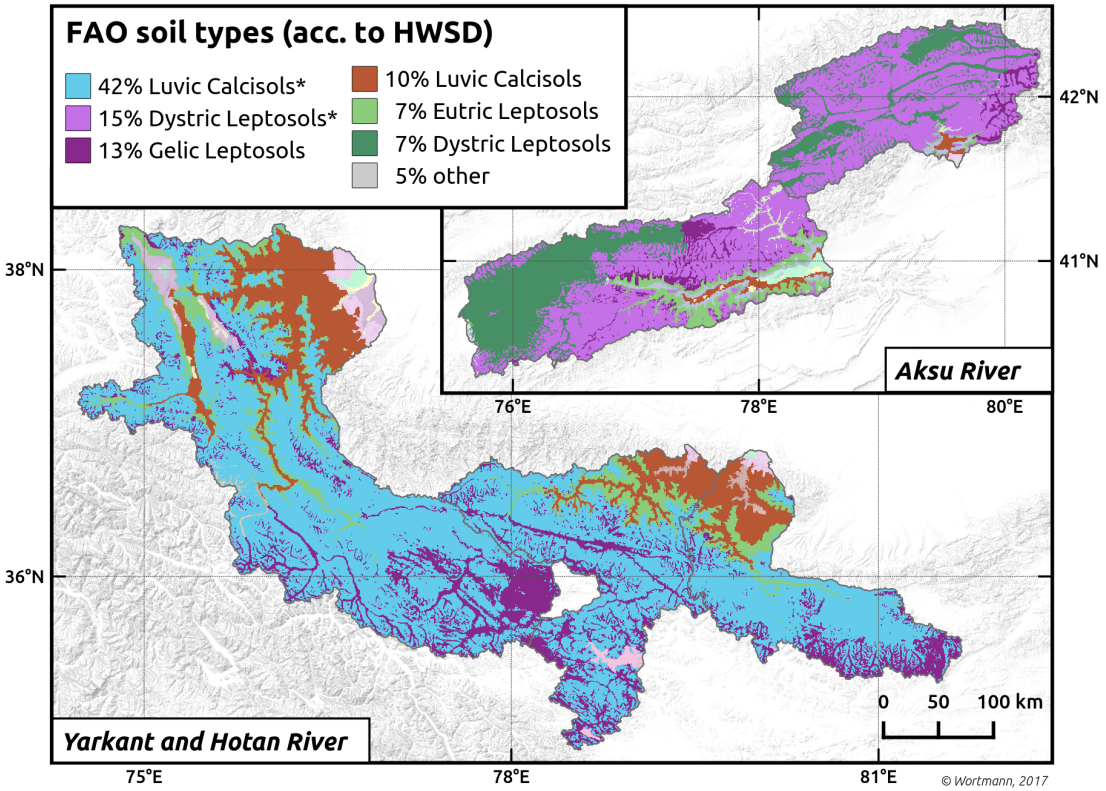

Figure 3.21: Soil types according to the mapping units of the Harmonized World Soil Database (HWSD) in the Tarim headwaters. The soil depths of soil types marked with * have been reduced to 10 cm to reflect the thin soils on the slopes. The proportional coverage over the catchment area is given in the legend, with others (<1%) displayed in shaded colours.

Woesten et al. (2001). That is: bulk density, porosity, available water capacity, field capacity and saturated conductivity.

While in inhabited parts of China this information has a relatively high spatial resolution, it is spatially rather inexplicit with large units in Kyrgyzstan and the higher elevation zones. Those units were split into two soils for valleys and slopes by applying a slope threshold of 15°, as visible in Figure 3.21. The soil depth of the slope soil was reduced to 10 cm (Barontini et al., 2005).

3.7 Summary

This chapter has provided a description of the main region of investigation, the five headwater catchments of the Tarim River, with a particular focus on data availability for hydrological modelling. The main available datasets utilised in the remainder of the thesis are discussed, including the critical gaps in available data and recent studies aiming to close them. The basic catchment statistics are introduced first, followed by a description of their climate, glaciology and hydrology. The available precipitation dataset have received particular focus, as the quality is important to both glaciological and hydrological modelling. The great variability and uncertainties are assessed, providing the ground for the model-based precipitation correction implemented in Chapter 6. Heterogeneous changes in the glaciers of the regions are described, showing general trend of glacier recession in the Aksu catchments, but inconclusive evidence from the Hotan and Yarkant catchments. The chapter is closing by describing how key discharge data were acquired and global datasets were used to close necessary data gaps.

Chapter 4

The Upper Aksu SWIM model and the impact of the Merzbacher Lake outburst floods

4.1 Introduction

The purpose of this chapter is to demonstrate the initial SWIM model setup without any model improvements and to apply it to the case study catchment of the Upper Aksu River. The applied model is shown to be useful to investigate the reoccurring Glacier Lake Outburst Floods (GLOFs) of the catchment in the historical discharge data. The chapter addresses the following research questions as set out in Chapter 1:

1. How well does the standard Soil and Water Integrated Model (SWIM) model code as described by Huang et al. (2010, 2013b) perform in a highly glacierised catchment compared to discharge observations without accounting for glaciological observations?

2. How can a hydrological catchment model aid the analysis and detection of glacial lake outburst floods in discharge timeseries of mountainous catchments?

The Upper Aksu catchment (Section 4.2) and the input data (Section 4.3) are first introduced, complementing the general site description given in Chapter 3. Then, the model construction, calibration and validation are described in Sections 4.4 and 4.5. The model is then used to detect periods from the discharge observations affected by GLOFs. The flood volumes are evaluated and the effect on model performance is assessed (Section 4.6). Finally, the deficiencies of the standard SWIM model for long-term simulations, such as climate change scenario assessments, are shown in Section 4.7.

4.2 The Upper Aksu catchment and the Merzbacher Lake

The Aksu River, originating in the Tian Shan mountains in Kyrgyzstan, is the largest and principal tributary to the endorheic Tarim River in NW China (Figure 4.1). It provides 70–80 % to the total water flow of the Tarim and has two main tributaries, the Toshkan and the Kumarik rivers (Wang et al., 2008). The Kumarik River is the larger of the two tributaries and is the focus of this chapter.

The catchment terminated by the Xiehela gauging station (S1 in Figure 4.1) defines the model domain with a drainage area of 12 991 km^2. This station provides the only long-term hydrological record of the GLOFs in this region. Most of the catchment area is located in Kyrgyzstan, where the river is called Sary-Djaz. Downstream of its confluence with the Inylchek and Ak-Shirak rivers, it flows into China, where the river is known by the name Kumarik, and after joining the Toshkan River, it is called the Aksu River (see Figure 4.1).

Table 4.1 provides details of the entire catchment, one internal subcatchment, for which data was also available, and the ungauged Merzbacher Lake subcatchment. With mean winter and summer discharge of 28 $m^3 s^{-1}$ (DJF) and 406 $m^3 s^{-1}$ (JJA) for the study period 1964-1987, the Kumarik catchment has a pronounced nival regime. Warm and moist frontal systems from the west trigger both snow and glacier melt and orographic rain during summer (Aizen et al., 1995). The catchment's topography, climate, land cover and soils were already described in Chapter 3.

In a rare physiographical setting, the Merzbacher Lake is located between the Northern Inylchek and the much larger Southern Inylchek glacier at an elevation of 3250 m asl

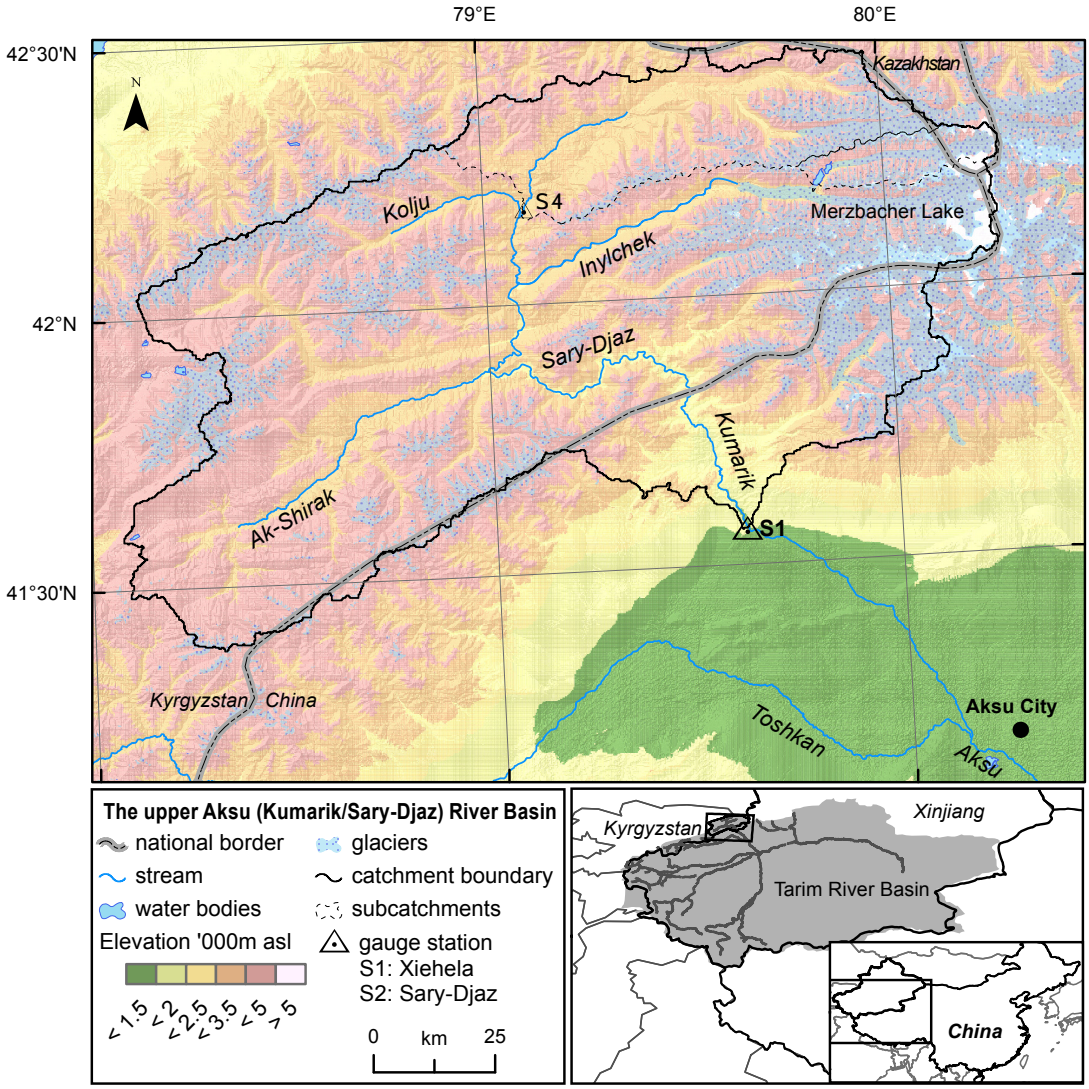

Figure 4.1: The upper Aksu River Basin, the headwater reaches are called Sary-Djaz River in Kyrgizstan and Kumarik River in China. The outlet station Xiehela records approx. 64% of the Aksu River discharge and by that roughly 45% of the Tarim River.

Table 4.1: Catchment details according to the four hydrological stations and the Merzbacher Lake; drainage area, mean discharge Q as annual mean and summer mean for the month June to August (over 1964–1987) and glacier cover. See Table 4.2 for sources.

Station	River	Area $[km^2]$	Mean Q $[m^3 s^{-1}]$	Mean JJA Q $[m^3 s^{-1}]$	Glacier [%]
S1	Kumarik R.	12991	151.8	406.6	22
S4	Sary-Djaz R.	1927	37.4	91.3	18
Merzbacher L.	Enylchek R.	325			55

($79°52'E$, $42°13'N$, Figures 4.1 and 4.2). The northern glacier provides most of the discharge to the lake, while the southern glacier acts as a perpendicular dam to the lake with a valley-blocking tongue reaching into the lake. In the event of an outburst, this tongue floats up triggering the subglacial channels to widen in turn emptying the lake. First discovered by Gottfried Merzbacher in 1903 (Merzbacher, 1905), Merzbacher Lake has since been known to outburst almost every year and in some years even twice, mostly in the period from July to October (Glazirin, 2010). The lake has split into an upper and a lower part with a difference in elevation of ca. 100 m divided by a 2–3 km field of debris.

Investigating possible trigger mechanisms, predicting peak discharges and flood volumes and, by that, predicting the occurrence of the floods, have become the focus of discussion about the Merzbacher Lake GLOFs (Glazirin, 2010). Ajrapetyants and Bakov (1971) proposed the so far unverified hypothesis that the lake empties once the water volume is able to float the damming part of the Southern Inylchek glacier. Cracks

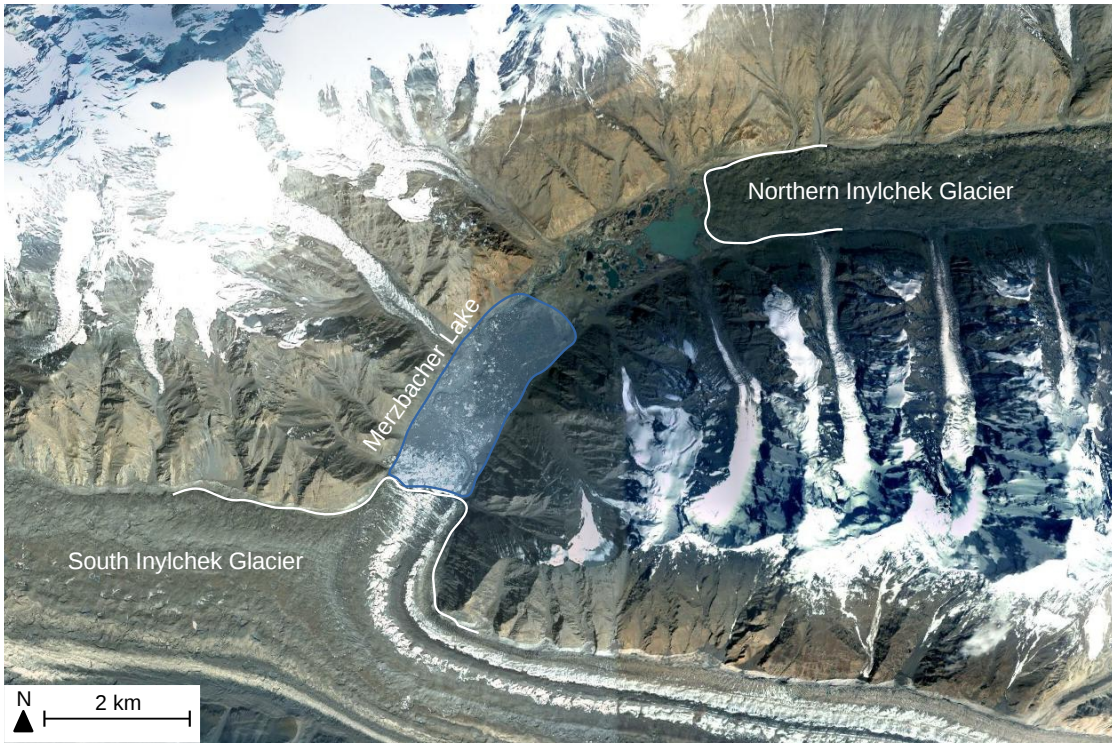

Figure 4.2: Annotated composite satellite imagery of the Merzbacher Lake (lower part marked) in between the North and South Inylchek glaciers (2002–2005). The frontal lobe damming the lake produces small icebergs that cover the lake. Copyright Google/CNES/Airbus/DigitalGlobe, 2017.

and crevasses then open up to form englacial channels which are enlarged by the slightly warmer lake water, a self-accelerating process fueled by the increasing kinematic energy. Once the lake water is drained through the Southern Inylchek glacier tongue, the dam and channels close again and the lake refills. Validation of this hypothesis has so far been limited by accessibility for measurements. Detailed understanding of the interplay between glacier dynamics and lake volumes is therefore lacking.

Uncertainty over Merzbacher Lake GLOF occurrence, peak discharge and volume increases in view of the general increase in temperature and precipitation in the Tian Shan. It is suggested that this trend may lead to more frequent and higher magnitude GLOFs in the entire Tarim catchment (Shen et al., 2009). Merzbacher Lake GLOFs have been found to occur earlier in the year compared to the 1930s. It has also been suggested that peak discharges have increased (Glazirin, 2010; Liu and Fukushima, 1999; Ng et al., 2007).

4.3 Input data

An overview of the data used for the model and their sources is given in Table 4.2. Most of the datasets were already introduced in Chapter 3. In the following, the preparation of the driving data is described.

The model is driven by six climate variables: mean, maximum and minimum temperature, precipitation, relative humidity and solar radiation. All variables except for precipitation were sourced from Water and Global Change project (WATCH) dataset, a reanalysis dataset created for hydrological investigations, while the APHRODITE (Asian Precipitation Highly Resolved Observational Data Integration Towards the Evaluation of Water Resources) dataset was used for the precipitation. The model was previously tested with a gridded precipitation and temperature dataset supplied by the Chinese Meteorological Administration (CMA), with the other variables and temperature and precipitation for the Kyrgyz merged from WATCH. This was, however, replaced by the APHRODITE that covers both countries and showed matching results. The sparse meteorological station data from Kyrgyzstan, such as the Tian Shan meteor-

Table 4.2: Input data used to drive, calibrate and validate the model. A detailed description of the datasets is given in Chapter 3. Topography and glaciers are shown in Figure 4.1.

Data	Source
Climate	WATCH (Weedon et al., 2011), 0.5° grid, temperature, radiation and relative humidity.
	APHRODITE (Yatagai et al., 2012), 0.25° grid, for precipitation.
Topography	SRTM hole-filled digital elevation model at 90m resolution (Jarvis et al., 2007)
Land cover	Chinese Meteorological Administration for Chinese part, MODIS 500 m land cover (2001) (Friedl et al., 2002) for Kirghiz part, reclassified to SWIM land cover classes
Glaciers	Improved GLIMS glacier distribution with individual glacier delineation by Bolch et al. (2012b)
Soil	Harmonised World Soil Database (FAO, 2011), includes the 1:1 Mil. soil map for China
Discharge	Daily river discharge at gauge Xiehela (S1) from Chinese hydrological year books and Sary-Djaz River (S4) from Kyrgiz hydrological yearbooks (both for the period 1964-87)

ological station data as well as some precipitation stations with many gaps (as described in Section 3.3), were omitted in favour of homogeneity between the gridded datasets.

The climate data was merged and interpolated, as illustrated in Table 4.2. The gridded daily data was interpolated to the subbasin centroids using an inverse distance weighted interpolation (IDW). The subbasin precipitation and temperature are corrected at run time using the difference between the WATCH reference elevation and the mean hydrotope elevation. A constant temperature lapse rate of $6.7\,^{\circ}\mathrm{C}\,\mathrm{km}^{-1}$ was used according to Aizen et al. (1995). The precipitation remained uncorrected for this investigation, but is used and described in detail in Chapters 5 and 6.

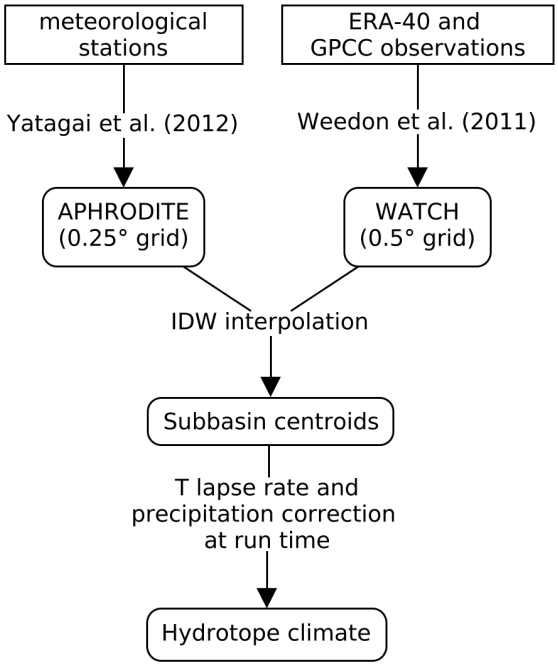

Figure 4.3: Sources and interpolation steps for the climate data used in the SWIM model for the Kumarik catchment. The ERA-40 data was interpolated to the WATCH grid by Weedon et al. (2011).

4.4 Model construction

The SWIM model was set up following the same procedures as Huang et al. (2010, 2013b) have done in the Alpine parts of the Rhine and Danube River including glaciers. The model including its recently improved snow module are described in Section 2.8. The Kumarik catchment with the final gauge at Xiehela was delineated into 346 subbasins, using the 90 m SRTM Digital Elevation Model (DEM) as shown in Figure 4.4, with an average (minimum, maximum) area of 37.5 km^2 (2.2 km^2, 184.7 km^2). The hydrotopes were created from unique combinations of subbasins, land cover and soils as well as 100-meter elevation zones, producing 26371 computational units.

Improved Global Ice Measurment from Space Project (GLIMS) glacier outlines from ≈1975 to designate glacier hydrotopes (Kargel et al., 2014, updates by Bolch, pers. com. and used in Duethmann et al., 2015). The initial ice thickness was determined through an empirical area-volume relationship (Equation (4.1)), also following Huang et al. (2010,

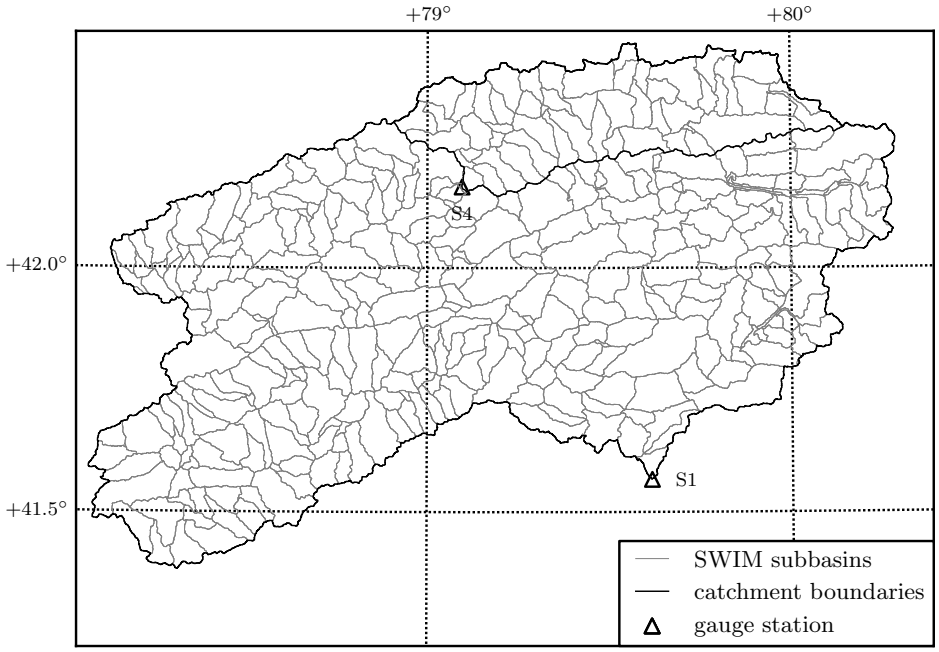

Figure 4.4: Delineation of the 346 subbasins used by the SWIM model (with an average area of 37.5 km^2).

2013b), who use parameter values for this relationship by Klein and Isacks (1998).

$$V = 48.4 \cdot A^{1.36} \cdot \rho_i \tag{4.1}$$

with glacier volume V [m^3 water equiv.] and area A [km^2] and the ice density ρ_i (910 kg m^{-3}).

4.5 Calibration and validation strategy

The model was first manually calibrated to observed discharge at the Xiehela station (S1) and the internal Kyrgyz station on the Sary-Djaz River (S4). In a second step, the simulations were automatically fine-tuned using the local optimisation algorithm PEST (Blasone et al., 2007; Doherty, 2003; Kunstmann et al., 2006). The calibration and validation periods for outlet station are 1964–1975 (calibration) and 1976–1987 (validation), where the observations are only briefly interrupted in the winters of 1973 and

1974. Discharge observations of the internal Kyrgyz station are of much poorer quality with interruptions between 1972–1979 and in 1981. Bank freezing and intermittent observations in winter are suspected to cause some spurious data. The calibration and validation periods are 1964–1971 and 1980–1987, respectively.

Seven calibration parameters were used as listed in Table 4.3. The four snow and ice related parameters were already described in the snow and glacier module description in Section 2.8 (the glacier Degree-Day factor in also in Section 2.5). The routing coefficients are the empirical parameters of the Muskingum routing method, with R_2 for the surface flow component and R_4 for the subsurface flow component. Smaller values mean faster routing. The saturated conductivity of the soil information is corrected with S_c. The large possible range of conductivity is reflected in the range of the correction factor. The evapotranspiration correction factor E_c is used to correct the potential Priestly-Taylor potential evapotranspiration. Since no precipitation correction was used, the use was not warranted here and it was left at 1. It would otherwise compensate for the a low precipitation bias. Four other parameters of SWIM, mainly correction factors (e.g. of curve numbers, sky emissivity), were left at their standard value (i.e. 1). To reduce the effect of initial storage assumptions (e.g. groundwater, snow cover), the model was run with one initialisation year, which was not used in the analysis.

Table 4.3: Calibration parameters with valid ranges, units and calibrated values for the two stations as well as the calibration without GLOF events at Xiehela (S1*).

Parameter / description		Range	S1	S1*	S4	Unit
δ_s	Snow Degree-Day factor	1 – 5	1.1	1.1	1.7	$\mathrm{mm\,K^{-1}\,d^{-1}}$
T_s	Snow fall threshold temperature	0 ± 5	2.9	3.0	-0.1	°C
T_m	Snow melt threshold temperature	0 ± 5	1.7	2.3	-1.6	°C
δ_g	Glacier Degree-Day factor	3 – 10	5.4	6.1	7.1	$\mathrm{mm\,K^{-1}\,d^{-1}}$
R_2	Routing coefficients	1 – 20	1.1	1.0	2.6	
R_4			4.7	5.1	14.9	
S_c	Saturated conductivity correction	0.1 – 10	9.8	2.4	8.5	

The most sensitive model parameters were the ice and snow melt factors as well as the snow melt temperature, indicating that model uncertainties are largest in the snow and glacier melt periods.

Two widely used measures of model performance were employed (Huang et al., 2010; Thompson et al., 2013), the Nash and Sutcliffe efficiency (NSE, Nash and Sutcliffe, 1970) and the relative deviation in water balance (or percent bias). Model performance for the two stations is summarised in Table 4.4. Figure 4.5 and Figure 4.6 show observed and simulated discharge for both the calibration and validation periods at the Xiehela and Sary-Djaz stations, respectively. Numerous measures of model performance or 'objective functions' exist and are used to adapt hydrological models to the region and the study's focus (Gupta et al., 2006; Krause et al., 2005). For highly seasonal catchments, Nash-Sutcliffe Efficiency (NSE) values are misleadingly high in comparison to temperate catchments as the strong seasonal fluctuations lead to large residuals to the mean discharge already that are relatively easy to reproduce (Schaefli and Gupta, 2007). As such, the NSE is a relative performance measure but not absolute across all modelling domains. However, NSE and the bias in the water balance are used here as the aim of this chapter is to apply the SWIM model as it was done in previous studies (Hattermann et al., 2005; Krysanova et al., 2015b), in particular the study by Huang et al. (2013b) that implemented several improvements to the snow module.

For the calibration and validation periods, NSE values of 0.82 and 0.81 respectively at the Xiehela station indicate a good agreement between simulated and observed discharge. A relatively high negative bias in the water balance, however, shows an average underestimation of between 10% and 16%. Closer investigation of the daily discharge

Table 4.4: Performance statistics for the calibration and validation periods. For station S1, performance is listed for the two cases: with and without GLOFs included in the observations.

		Calibration		Validation	
Station	River	NSE	bias [%]	NSE	bias [%]
S1 w GLOFs	Kumarik R.	0.82	-10	0.81	-16
S1 w/o GLOFs		0.90	-2	0.92	-5
S4	Sary-Djaz R.	0.87	-2	0.81	-9

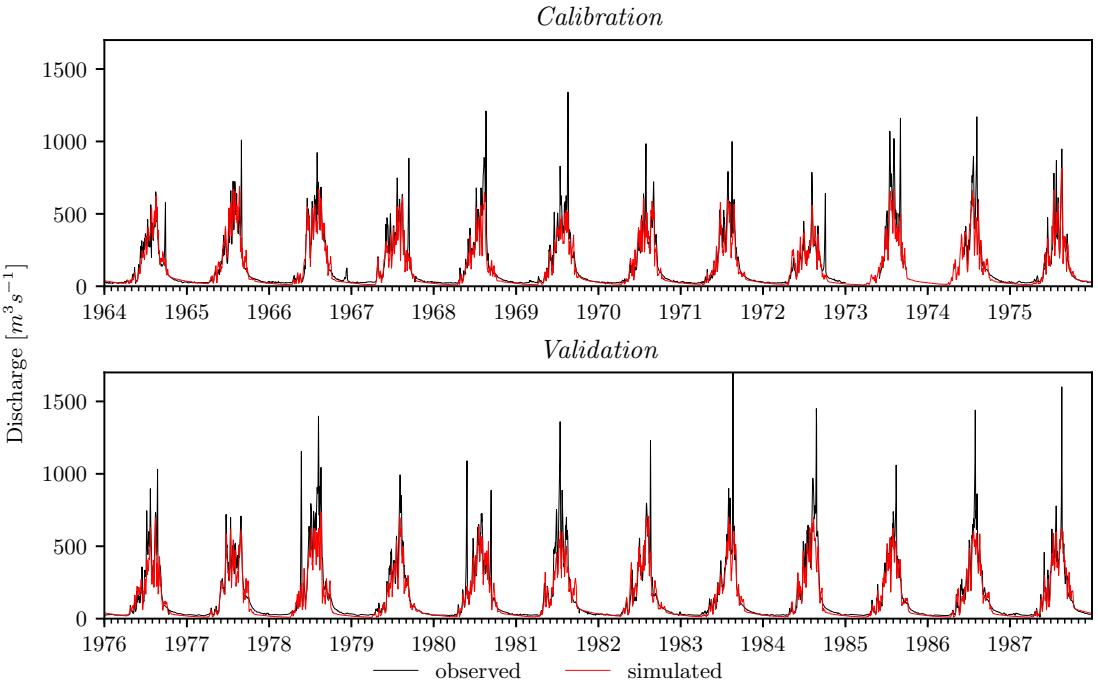

Figure 4.5: Daily observed and simulated discharge for the calibration (top) and validation (bottom) periods at the outlet Xiehela station (S1) with GLOF periods included in the observations.

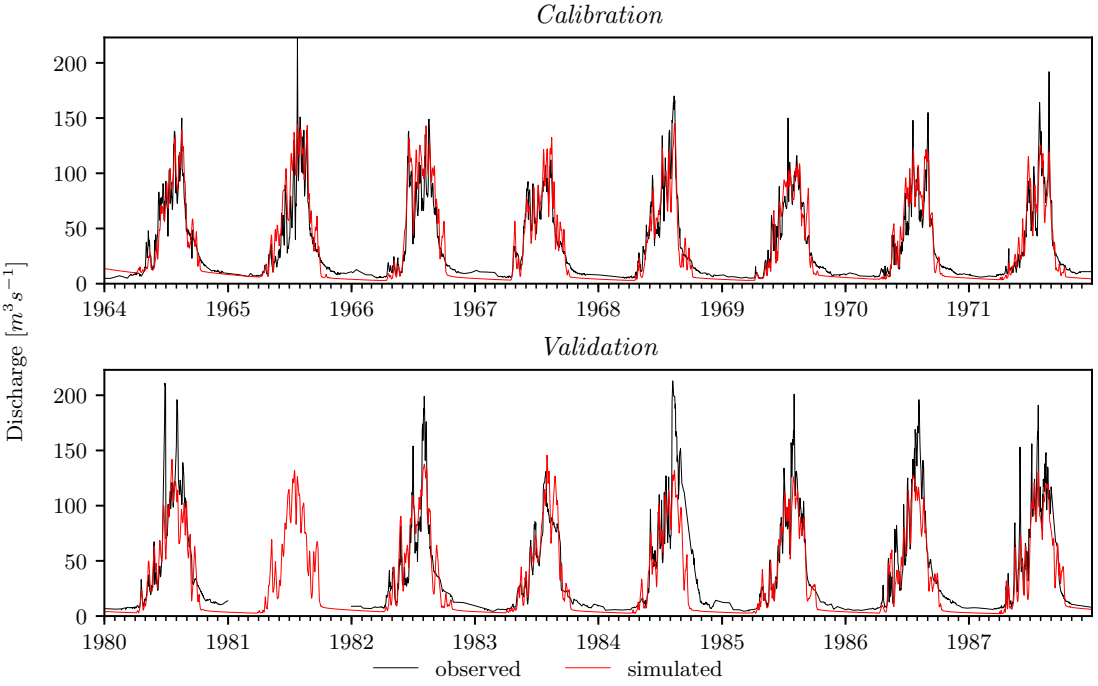

Figure 4.6: Daily observed and simulated discharge for the calibration (top) and validation (bottom) periods at the internal Sary-Djaz station (S4).

dynamics for the Xiehela station shows that large late summer peaks are underestimated in the simulation results while other peaks are slightly overestimated. This simulation mismatch is also reflected by the negative bias in the water balance, suggesting an overall underestimation. The hypothesis is that these peaks are caused by the outbursts of the Merzbacher Lake, as is shown in the next section.

In contrast, results for the internal station on the Sary-Djaz River yielded an NSE of 0.87 and 0.81 for the calibration and validation period, respectively (Figure 4.6). A bias of -2% was achieved in the calibration period, although this was larger in the validation (-9%). Some summer peaks are also underestimated and the performance as well as the visual fit is worse in the validation period. However, considering the much smaller drainage area and the poorer data quality of this station, the results can be evaluated as satisfactory and generally better than the Xiehela station. Since this station is not located downstream of the Merzbacher Lake catchment, its discharge record does not contain the GLOF signal.

4.6 Investigation of Glacial Lake Outburst Floods

The underestimated peak flow periods at the Xiehela station typically last for 5 to 10 days. During these periods, the model underestimated discharge by between 200–1000 $\mathrm{m^3\,s^{-1}}$. These deviations stand out markedly from the typical model errors and mostly occur in late summer or early autumn.

The search for possible causes, *i.e.* processes that are not represented in the model, led to the review by Glazirin (2010) of research on the glacier-dammed Merzbacher Lake. Glazirin (2010) lists approximate dates and durations of some GLOF events during the period 1931–2005. These are based on a range of different sources including scientific publications and data from glaciologists as well as reports from frontier guards who witnessed these events first hand. It is acknowledged by Glazirin (2010) that sometimes the various sources differ in the reported dates for GLOF events. The GLOF dates given were compared to the underestimated peaks at the Xiehela station. In the period 1964–1987 (the simulation period with available river discharge data) there are 14 years with witnessed outbursts, which are also recorded at the Xiehela station.

Figure 4.7 shows selected late summer or autumn peaks for six years not simulated by SWIM, with dates reported by Glazirin (2010) marked. Generally, a good agreement between the reported outbursts and unrepresented peaks is found with a time lag of 5–10 days from the recorded date to the observed peak date at the Xiehela station. Some dates, however, are probably misreported such as in July 4, 1966.

As reported for the catchment earlier (Krysanova et al., 2015a), a high positive and statistically significant correlation was found between the daily temperature (averaged over the catchment) and lagged (by 1–3 days) river discharge at the Xiehela station which breaks over short periods in the end of summer and beginning of autumn. This study concluded that the high (over 95^{th} percentile) flow peaks at the end of summer or beginning of autumn at Xiehela are, to a large extent, caused by the outburst floods from the Merzbacher Lake. For the sub-periods with GLOFs, river flow is not correlated with instantaneous temperature. These high peaks coincide with the unrepresented peaks in the SWIM simulation confirming that they are a result of the regular outbursts from the Merzbacher Lake.

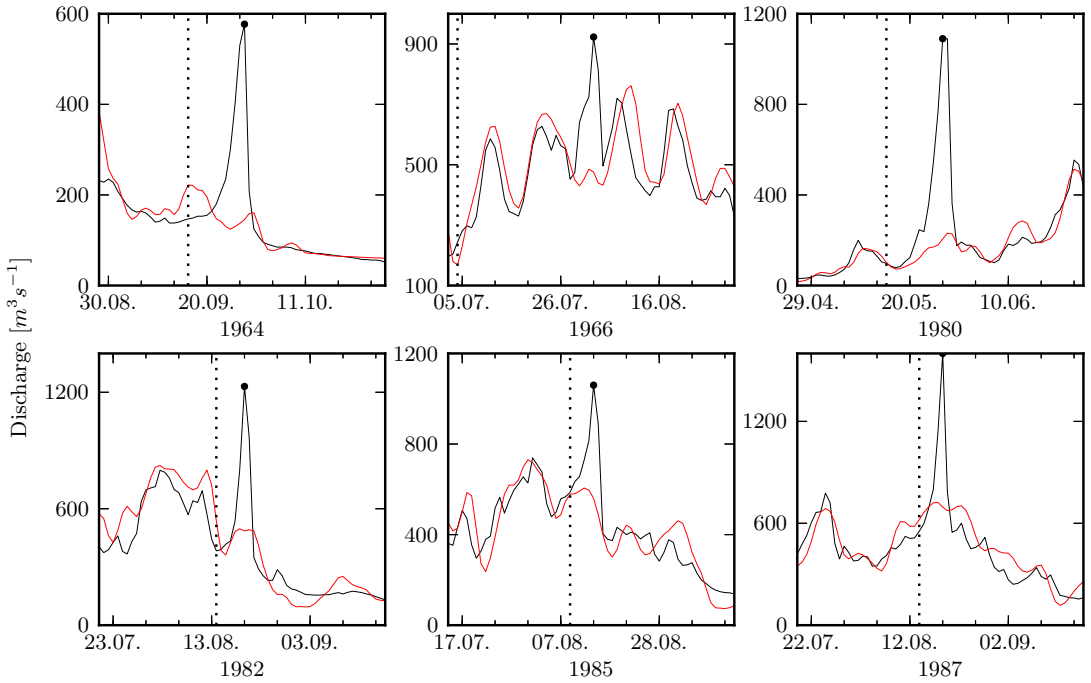

Figure 4.7: Selected periods with unrepresented peaks in the period 1964-1987: simulated (red) and observed (black) discharge. GLOF dates indicated by Glazirin (2010) are marked with a dashed vertical line.

An improvement of the model calibration and validation for the Xiehela station requires either the GLOF processes be incorporated into the model or that the GLOF periods are excluded from the observation data. The former option is not currently feasible since the processes leading to the outbursts from the lake are not fully understood and it would require more accurate data on the dynamics of the damming glacier than are available at present. In the following the model is recalibrated without the GLOF peaks in the observations and a method is proposed to detect GLOFs in discharge timeseries. Then the simulated discharge is used to assess the flood volumes.

4.6.1 Calibration excluding GLOFs in observations

The high late summer peaks including their rising and receding limbs which were attributed to GLOF events were excluded from the observation data and the calibration and validation were repeated. This was done for two purposes. First, as the GLOFs have a strong influence on the total river discharge, the hypothesis that excluding GLOFs from the observation data will improve the model performance was tested. Second, the resulting simulated discharge should represent the normal catchment discharge.

A new manual calibration and again followed by an automatic optimisation rendered a modified parameter set (Table 4.3) which improved the model performance considerably (Table 4.4). Figure 4.8 shows the calibration and validation results for the Xiehela station after the exclusion of GLOF periods. The model performance was improved, i.e. NSE increased to between 0.90 and 0.92 whilst the bias in the water balance declined to between -2% and -5%, in the calibration and validation periods, respectively.

Some deficiencies in the discharge simulation are still apparent in the melt period where some peaks are still slightly underestimated. The same is true for the months of October and November, when discharge tends to be underestimated. However, in general the results are considered to be good, especially taking into account the quality of the input data.

The simulated normal discharge can be used for the following: a) to provide a physical basis for the visual interpretation of the GLOF peaks or even to detect GLOFs in the observations for which no reported sightings are available and b) to act as a

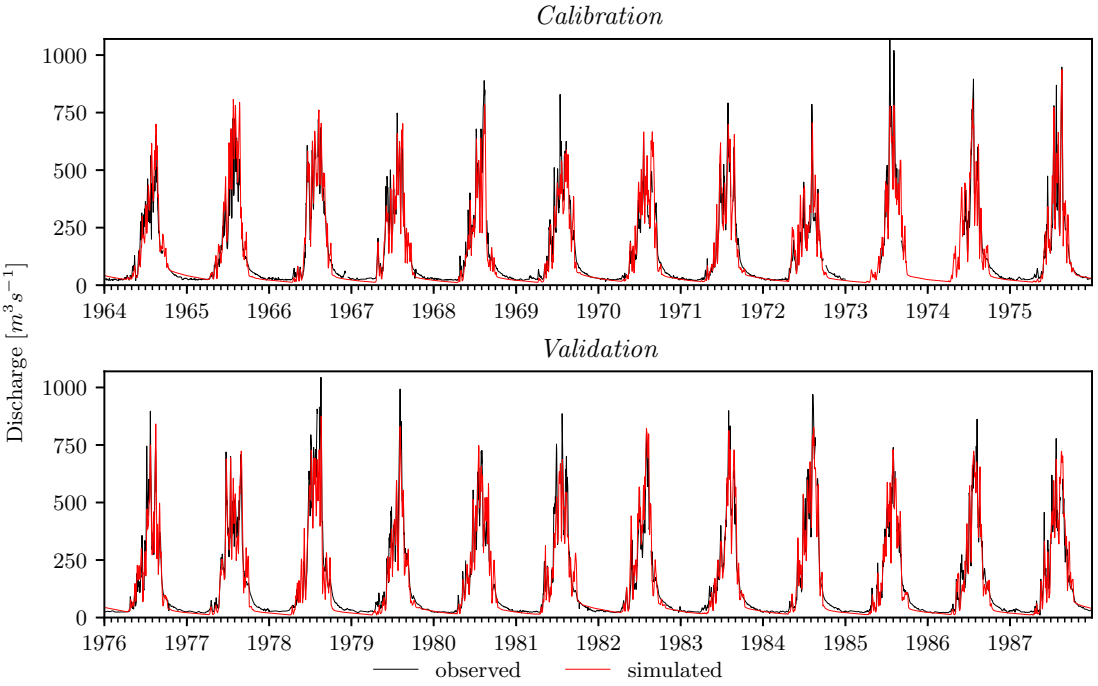

Figure 4.8: Daily observed and simulated discharge in the calibration (top) and validation (bottom) periods without GLOFs included in the observations at Xiehela station (S1).

baseflow for the separation of the GLOF peaks to estimate the flood volume, a proxy for the volume discharged from the Merzbacher Lake during these events. These two examples are presented in the next two sections.

4.6.2 GLOF identification in observation record

The occurrence of GLOFs, which are not included in the model, can influence modelling performance (as described in section 4.1 for the Kumarik catchment). In the following an approach is suggested to identify and filter them out. The identification of GLOF events at the Xiehela station could employ the simulated normal discharge and a criterion based on the deviation of this simulated discharge from that in the observational record. This could provide a method to detect GLOFs in the observations that were not reported and to provide a physically-based proof for the visually identified GLOFs.

The most basic criterion for the GLOF detection would be to apply a threshold to the observation-simulation residuals (hereafter referred to as residuals), using the non-corrected observations and the normal simulated discharge. That is, asking by what

value does the simulation have to deviate from the observed discharge to be identified with a high probability as a GLOF event. As can be seen from the comparison for the total simulation period (Figure 4.5), most GLOF peak discharges deviate from the simulated normal discharge by more than $500\,m^3\,s^{-1}$ and up to $1100\,m^3\,s^{-1}$.

Simulation residuals are, however, dependent upon the magnitude of observed discharge; this is true for both the GLOF peak discharges and model errors. While typical August GLOFs have peak discharges of above $1000\,m^3\,s^{-1}$ with typical normal flows of 500–$600\,m^3\,s^{-1}$, the December GLOF in 1966 peaked at $126\,m^3\,s^{-1}$ with a residual of $25\,m^3\,s^{-1}$. Therefore, the threshold applied to the residuals needs to vary according to the observed discharge. This approach was therefore employed to find this linearly varying threshold empirically using the simulated normal discharge and confirmed GLOFs reported by Glazirin (2010).

First, all local (GLOF and non-GLOF) peaks were extracted from the observation data to only consider the maximum discharge without their rising and receding limb. A 10-day moving average filter was used to calculate the discharge anomalies. The maximum discharge of periods during which the anomaly was above the 75^{th} percentile yielded the largest 5–10 peaks in every year, most of them occuring in summer.

The witnessed GLOFs described by Glazirin (2010) were used to find a suitable threshold to discriminate between GLOFs and model uncertainties. A constant threshold of $400\,m^3\,s^{-1}$ is able to capture most of the reported GLOFs. However, in order to capture the above mentioned non-summer GLOFs, a linear threshold depending on the observed discharge is required.

This was found empirically. The average plus one standard deviation of the ratio between residuals and observations was found as the slope of the linearly varying threshold. To exclude most non-GLOF peaks, a constant component equal to the 75^{th} percentile of the residuals ($23\,m^3\,s^{-1}$) was used. The following equation describes the varying threshold t_q:

$$t_q = (\overline{rq} + \sigma_{rq}) \times Q_{obs} + r_{p75} \tag{4.2}$$

or

$$t_q = 0.434 \times Q_{obs} + 23 \tag{4.3}$$

where rq is the ratio of residual and observation, $\overline{rq}$ its mean and σ_{rq} its standard deviation, and r_{p75} is the 75^{th} percentile of the residuals.

Figure 4.9 (top) shows the simulation residuals r ($Q_{obs} - Q_{sim}$) against the extracted peak discharges for the modelled period 1964–1987. All GLOFs except one reported by Glazirin (2010) are delineated by this varying threshold. This one peak below the threshold line corresponds to a GLOF on September 1, 1970 with a peak discharge of $721\,\mathrm{m^3\,s^{-1}}$. This is, however, preceded by a GLOF on July 31, 1970 peaking at $984\,\mathrm{m^3\,s^{-1}}$ (both listed by Glazirin, 2010 and by Liu, 1992). Considering the short time since the last event and the low simulation residual, it is plausible to conclude that this event was misreported.

The GLOF peaks visually identified by Liu (1992) for the same period were included in Figure 4.9 (bottom). It provides verification that the linearly varying threshold correctly delineates all 25 GLOFs in the observational record and suggests that the threshold line can be used for the identification of GLOFs in other periods. This method could also be employed for other catchments with glacial lakes in which the same processes lead to intermittent peak discharges associated with GLOFs.

4.6.3 Merzbacher Lake flood volume estimations

Once GLOF events have been identified, it is possible using the simulated normal discharge and observed discharges to evaluate the flood volume, a proxy for the volume discharged from the Merzbacher Lake.

The form of the GLOF peak hydrograph at the Xiehela station is different from the one directly at the glacier outlet due to river hydraulics. However, water conservation means that the hydrograph area approximately equals the volume of the water exiting the lake during the outburst. The flood hydrograph is separated using the normal catchment discharge simulated by SWIM as baseflow. Earlier studies used graphical hydrograph separation instead (Liu, 1992; Ng et al., 2007).

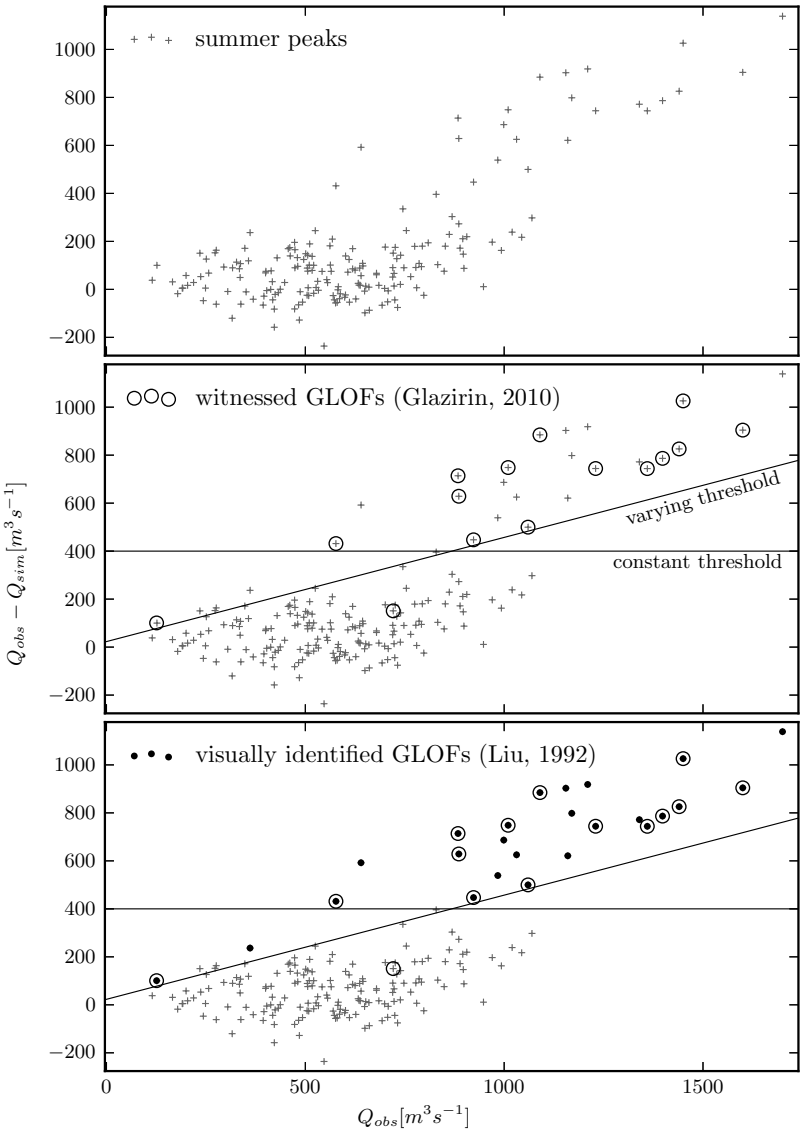

Figure 4.9: Observed discharge against the observation-simulation residuals for only the extracted summer peaks (top), including GLOFs following reported dates by Glazirin (2010) with the constant ($Q = 400\,\mathrm{m^3\,s^{-1}}$) and the varying threshold (middle) and including the visually identified GLOF peak discharges by Liu (1992).

The method of hydrograph separation using the simulated normal discharge is presented in Figure 4.10. The deviation of observed and simulated discharge at the start and end of the flood period requires the simulated discharge to be firstly locally corrected, to account for the model uncertainties. The onset ($d_{\nearrow}$) and end ($d_{\searrow}$) dates are variable, but are typically 5 days before and 3 days after the peak date, respectively (Liu, 1992). The simulated discharge is corrected to these dates, as indicated in Figure 4.10. The deviation in observed and simulated discharge on those days determines the start and

end correction factor which is then linearly interpolated for the days in between. This linearly varying correction factor f shown in Figure 4.10 (bottom) is applied to each day of the GLOF period. After the correction of the simulated discharge, the flood volume is estimated by the difference between the integrated observed and simulated discharge.

GLOF flood volume estimations for the whole simulation period are shown in Figure 4.11 (black columns). Volumes range from 56 to 291 million m^3 with an average of 167 million m^3. High variability between the volumes is evident, supported by a standard deviation of 55 million m^3. The highest volumes are estimated for the two GLOFs which occurred in May 1978 and 1980 both after years without a GLOF. The lowest volumes are found outside the melting season, *e.g.* in December, 1966.

Volume estimations without the local correction of simulated discharge are also shown in Figure 4.11. The large volume differences arise from the model uncertainties before and after the GLOF periods. Relatively small discrepancies between observed and simulated discharge can still lead to large volume changes. For example, a mean underestimation of $70\,m^3\,s^{-1}$ over a typical 8-day GLOF period would lead to an addi-

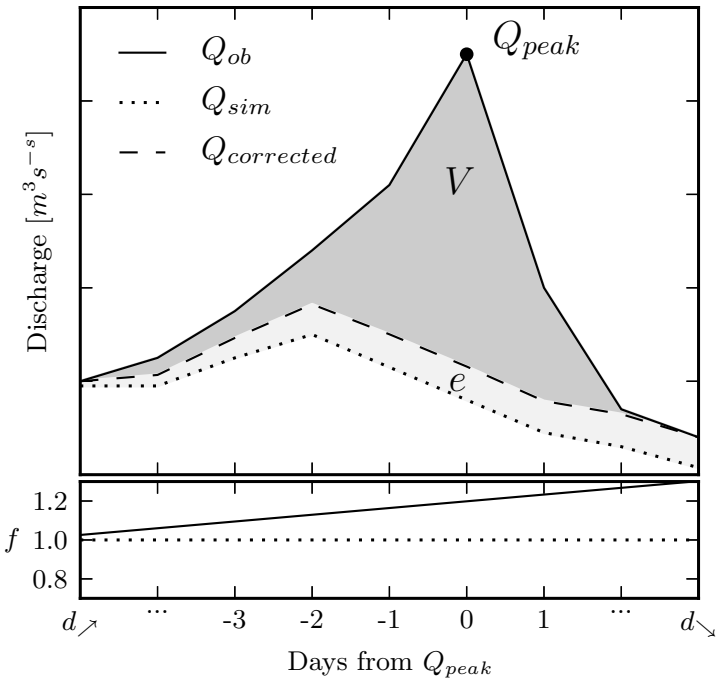

Figure 4.10: The GLOF hydrograph separation via the corrected simulated discharge $Q_{corrected}$. A linearly varying correction factor f is used to locally correct the simulated Q_{sim}, the area between $Q_{corrected}$ and Q_{sim} is the error e. See explanation in the text.

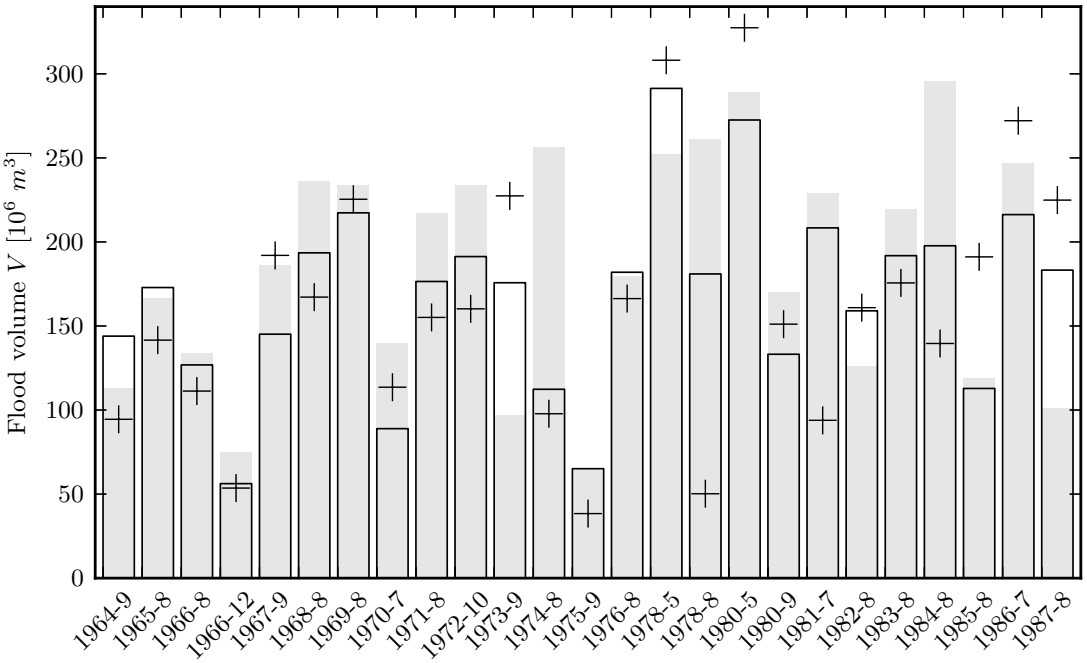

Figure 4.11: Estimated flood volumes for all GLOF events in the period 1964–1987 derived from corrected (black columns) and uncorrected discharge (light shaded bars) in comparison to volumes estimated by graphical hydrograph separation by Liu (1992) (crosses). Year and month of the peak discharge are given.

tional 50 million m^3 in volume. These errors are, however, removed through the linear correction while retaining the daily discharge dynamics.

Volumes reported by Liu (1992), also shown in Figure 4.11 (crosses), vary on average by ±25% from the estimated volumes presented here. Large differences (more than 50%) in estimated volumes exist for three GLOFs: the August, 1985 GLOF volume is 69% higher, while the August, 1978 and July, 1981 events have volumes that are 55% and 72% respectively lower than the estimates presented here.

4.6.4 Significance of the GLOF analysis and comparison to other studies

There are many glacial lakes in mountainous catchments around the world and their number is increasing, under a general trend of glacier retreat induced by a warming climate (Dussaillant et al., 2010; Huggel et al., 2003; ICIMOD and UNEP, 2001). Research has been dedicated to identifying those lakes (Bolch et al., 2008; Jain et al., 2012) and understanding the impacts their potential outbursts might have for riparian com-

munities, infrastructure and ecosystems downstream (Dussaillant et al., 2010; Osti and Egashira, 2009; Osti et al., 2013). The implemented SWIM model was used to investigate these impacts at the catchment scale and provides an approach to both understanding the GLOF impacts as well as analysing them, using the simulated catchment discharge without the GLOFs.

Identifying the Merzbacher Lake GLOFs in the Kumarik catchment using the simulated discharge proved to be useful for several reasons. Although many flood events markedly stand out in the discharge records and could be visually identified, many others occur during the melting season and could well be spring surge events, *i.e.* temperature induced peaks in glacier melt discharge. This problem was already highlighted in a previous study (Krysanova et al., 2015a), where discharge correlations with temperature were found to be interrupted. Considering the remoteness and erratic outburst of most glacial lakes, this problem is likely to be common to other discharge records of glaciated catchments.

For example, Osti et al. (2013) describe the highly GLOF-prone catchment of the Pho Chu, Bhutan with a total of 549 lakes, eight of which are deemed vulnerable to breaching. Finding other flood occurrences by the proposed method would reveal frequencies and magnitudes of smaller outburst floods, though it would not locate their origin. This would also provide proof for large but less documented GLOFs, especially those from ice-dammed lakes that outburst with a degree of regularity but with different magnitudes (*e.g.* Anderson et al., 2003; Dussaillant et al., 2010).

Although estimating outburst flood volumes is a routine procedure in most GLOF analyses, it is subject to several sources of uncertainty, especially where GLOFs are recorded some distance downstream of the lake. Using a hydrological model to simulate the catchment discharge as 'naturalised flow' during the flood event, adds a physical basis to the hydrograph separation. Yet the model uncertainties are propagated, an effect reduced by the correction of the simulated to the observed discharge at the onset and end of the GLOF. Resulting volumes for the Kumarik catchment are comparable to volumes found by Liu (1992) but are generally higher. Huss et al. (2007) performed a similar hydrograph separation at hourly time steps using a coupled glacier melt and

linear reservoir model at the Gornersee, Switzerland. They benefited from lake volume measurements and were able to quantify the error to $\pm 5-30\%$. Weighing up between the higher resolved observations in their study and the greater complexity of a process-based model, these error values may apply in the case presented here.

The presented modelling results bring to light how GLOFs are superimposed on normal catchment discharge, which may be relatively low during the event as in 1964 or high during the melting season as in 1987. Hydrological models might therefore be useful in attempts to reconstruct and predict GLOF hydrographs as has been common in GLOF research (Björnsson, 2011). The hydrological model can then serve as a framework for integrated investigations of GLOFs and their impacts downstream under various discharge scenarios, i.e. a first step to modelling a GLOF. It also allows simulating the melt water supply to the lake, which has been shown to play an important role in the triggering of a GLOF (Ng et al., 2007).

4.7 Deficiencies of SWIM in glacierised catchments

The results presented in Section 4.6 show that the model is suited to the analysis of historical discharge, with a calibration that only considers the correlation between simulated and observed discharge. Glaciological observations such as mass balance and area changes were not considered due to the purpose of the study. Simulating these variables accurately is crucial, however, when considering the long term water availability of a glacierised catchment. To test the model's performance of glacier mass and area change against catchment-wide study of Pieczonka and Bolch (2015), the model was run for the study period of 1975–2000.

Although the simulated mass balance of $-0.46\,\mathrm{m\,weq.\,a^{-1}}$ compared well with the estimates by Pieczonka and Bolch (2015) of $-0.35 \pm 0.34\,\mathrm{m\,weq.\,a^{-1}}$, the glacier area increased drastically in the first years of simulation and fluctuating strongly thereafter. Since the remaining snowpack at the end of the melting season (here September 30th) is converted to glacier ice, the glacier area varies strongly with interannual snow cover. If considering only glacier-covered hydrotopes with an ice thickness larger than 1 m, the glacier area is slightly growing with an average rate of 0.001 %/a, lower than estimates of

Pieczonka and Bolch (2015) (−0.11 %/a, 1975–2010) or Osmonov et al. (2013) (−0.2 %/a, 1990–2000). Despite a mass loss the glacier area remains nearly constant or expands revealing the problem of the direct conversion of the snowpack into ice regardless of the underlying glacier processes.

To evaluate the long-term evolution of glacier area and volume, the model was run for 100 years driven by a repeated 12-year climate slice of 1963–1974. This period was chosen as the climate of the 1960s and early 1970s has been shown to result in near stable glacier conditions in the Tian Shan (Farinotti et al., 2015) and in many other glacierised regions of the world (Dyurgerov, 2010). Glacier volume is decreasing strongly over the first 40 years, similarly to the 1975–2000 simulation described above, but increases again their after, as illustrated in Figure 4.12. After about 50 years of simulation, the mass balance turns positive essentially accumulating an ever growing ice cover. Glacier area on the other had is redistributed from lower elevations to higher ones as shown in Figure 4.13 and Figure 4.14. Since there is no downslope redistribution of snow and ice, the glacier cover increases indefinitely at higher elevation (Figure 4.14) outweighing the mass losses of lower laying valley glaciers after about 40 year (Figure 4.12).

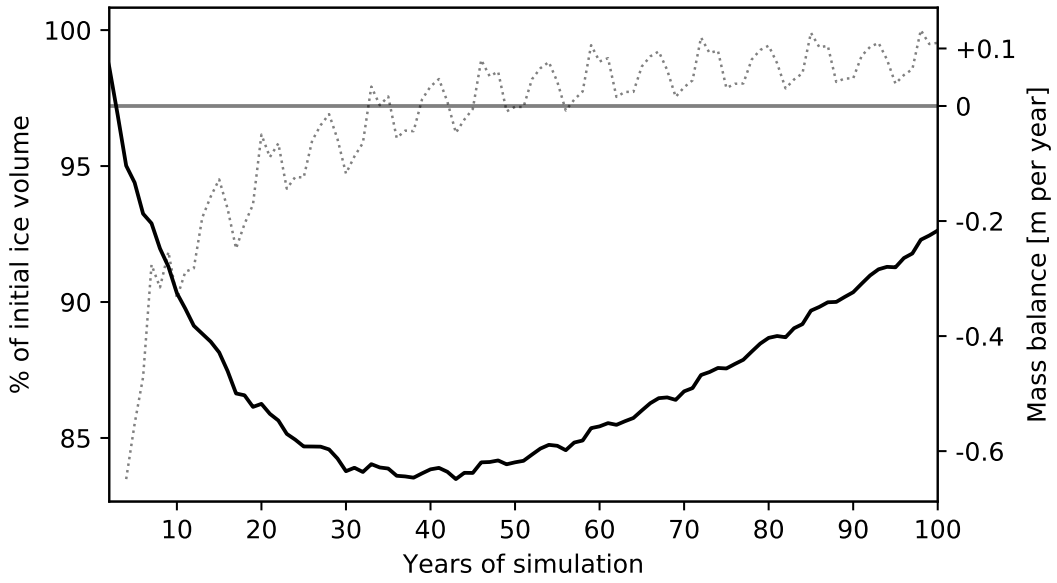

Figure 4.12: Percent of initial glacier volume (solid line) and annual mass balance (dashed grey line) over the 100-year simulation with a constant climate.

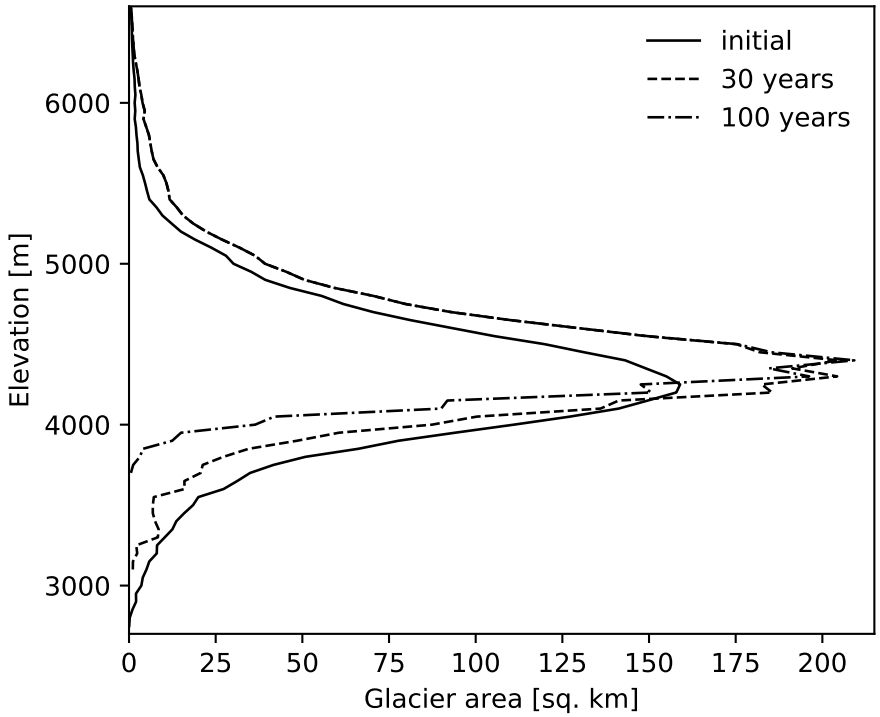

Figure 4.13: Elevation distribution of glacier area in the Xiehela catchment at the start of the simulation and after 30 and 100 years. Only hydrotopes with ice thicker than 1 mw eq were considered.

In conclusion, mass changes over shorter simulation periods (<40 years), may seem reasonable, but they are the result of a compensating effect of indefinitely increasing accumulation zone glacier thickness and rapidly receding valley glaciers. Glacier area is fluctuating strongly with interannual snow cover variability and is retreating to higher elevations with little change in the total glacierised area. Using the standard SWIM code for purely hydrological purposes with the current linear reservoir produces reasonable results in the first 20–40 years of simulation, but weaknesses of this simple implementation become apparent thereafter.

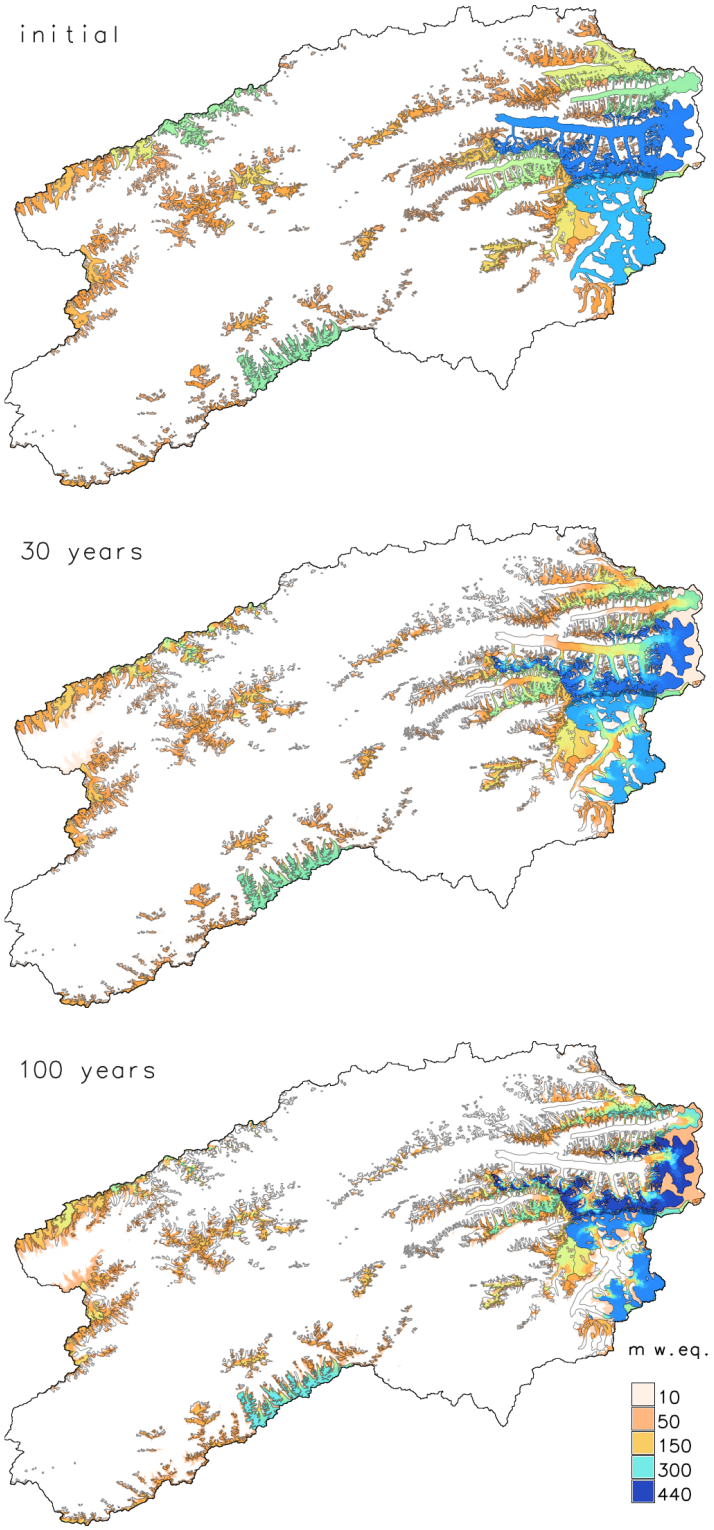

Figure 4.14: Glacier distribution in the Xiehela catchment at the start (top), after 30 (middle) and 100 (bottom) years of continuous simulation with a constant climate. Only glacier thickness larger than 1 m are shown. The initial glacier outlines are drawn in grey.

4.8 Summary

The standard SWIM model code without any improvements was implemented in the highly glacierised case study catchment of the upper Aksu River and used for an investigation of GLOFs. The model was calibrated and validated to observed discharge without taking glacier observations into account. The model shows a good performance with the exception of some late-summer peaks. These peaks were shown to originate from Merzbacher Lake outburst floods and they were filtered out using residual threshold approach, which improved the overall model performance. The simulated discharge was used to estimate flood volumes. Finally the deficiencies of the standard SWIM code to perform long-term assessments of glacierised catchments are described that serve as a motivation for the next chapter.

Chapter 5

Development of a glacier dynamics module for SWIM

5.1 Introduction

In this chapter, the development of a glacier dynamics module for the hydrological model SWIM is described, addressing one of the central objectives of this thesis. The single research questions addressed is: 'How can the SWIM model be improved to account for all major glacier processes, especially ice dynamics?' The module development draws on existing glacier dynamics and mass balance approaches that are described in Chapter 2, integrating them into the existing semi-distributed model structure. The validated model is later implemented in all five Tarim headwaters in Chapter 6 for the climate impact assessment in Chapter 7. The developed Fortran module code can be found in Appendix A. The new SWIM version is subsequently called SWIM-Glacier dynamics (SWIM-G).

First, the spatial representation of glaciers and the implemented processes are described in Sections 5.2 to 5.10 and the initialisation and calibration strategy in Section 5.11. The improved model is then validated in two catchments, the relatively data-abundant Upper Rhone catchment, Switzerland (introduced in Section 5.12) and the data-scarce Upper Aksu catchment (already introduced in Section 4.2 and Chapter 3).

The results are provided in Section 5.13. The chapter ends by showing the similarities of previous studies and the limitations of the model (Section 5.16).

5.2 Spatial disaggregation of glaciers

SWIM is a semi-distributed, hydrological model with three levels of disaggregation: the basin, subbasins and the hydrological response units (or hydrotopes). The latter subdivide the subbasins typically by unique combinations of land cover, soil class (as described in Section 2.8), but this can be refined by other variables, such as elevation zones or geological formations. They provide an adaptive spatial unit depending on the process scale and available data. Taking on this proven hydrological concept, they were here used to represent glaciers. The hydrotopes were used to model the complex mountainous terrain that determines glacier geometry and distribution by considering slope and aspect classes as well as elevation zones. This type of terrain abstraction is common in geomorphology with established threshold values and classification methods (Bishop et al., 2003; Cronin, 2000; Rasemann et al., 2004). It was here used with the focus on glacier properties.

The hydrotopes are unique combinations of three terrain classifications that are derived from the Digital Elevation Model (DEM), as illustrated in Figure 5.1 and described as followed:

a) a valley and hillslope class (using a slope threshold),

b) elevation zones with small intervals in valleys and larger intervals on hillslopes,

c) four, regularly spaced aspect classes on hillslopes only.

The unique combinations produce a noisy map that needs to be aggregated to a minimum area threshold (Figure 5.1). These 'glaciological response units' are only produced in the potential glacier region of the catchment, i.e. all areas above a suitable lower elevation depending on the current glacier cover and allowing some space for possible glacier advances. The hydrological response units in the remaining part of the catchment are created using the standard combinations of land cover, soil and elevation zone maps.

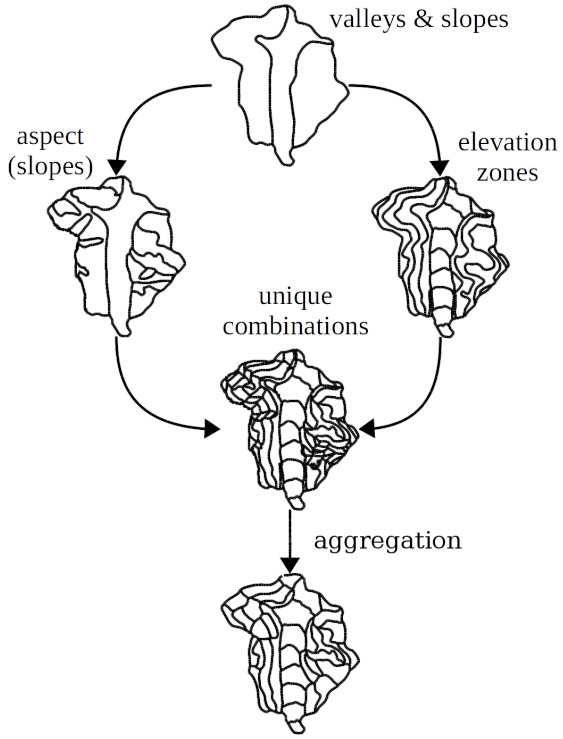

Figure 5.1: Spatial disaggregation within a subbasin as the representative glacier units.

Typical elevation zones in hydrological models vary between 20–200 m (Hagg et al., 2007; Lindström et al., 1997; Mayr et al., 2013). The variable elevation zone intervals in valleys and hillslopes stems from the desire to have equally sized spatial units. Typical slope angles for the two classes should thus govern the choice of ratio between intervals. If typical or average slope angle for valleys and hillslopes are α_s and α_v, then the ratio R_i is described by:

$$R_i = \frac{\tan \alpha_s}{\tan \alpha_v} \tag{5.1}$$

For example, equal unit distances are produced with typical slope angles of 3.9° and 34° if hillslope interval i_s is 10 times as large as the valley interval i_v, as illustrated in Figure 5.2.

Distinguishing between slope aspect is important to subdivide elevation zones. The aspect classes break these into distinct hillslope units that are more representative of glacial hillslopes than an entire elevation zone and distinguish glaciers with different exposure. The minimum area threshold limits the model to glaciers larger than this threshold, although fractional coverages are possible as a glacier retreats or with avalanche prone

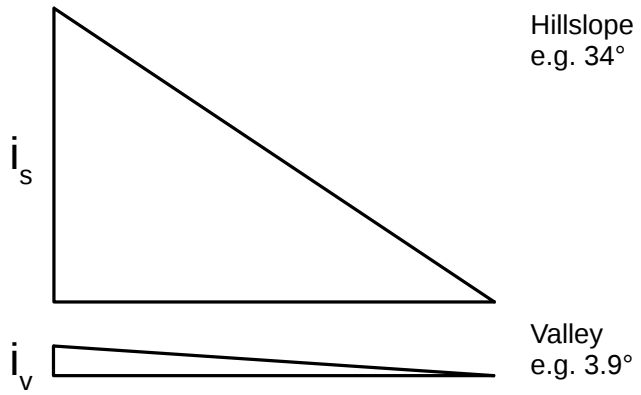

Figure 5.2: Example of similarly sized units when choosing hillslope and valley elevation intervals with average slope angles of the catchment.

areas. These representative units resolve the glacial systems of the catchment as well as the hillslopes contributing to glacier accumulation.

The slope threshold, the elevation intervals, the number of aspect classes and the minimum area of aggregation are threshold values that were adapted to the desired level of terrain discretisation. For the two catchments used here to validate the model, the threshold values and resulting unit statistics are summarised in Table 5.1.

The aggregation was achieved through a successive remove and neighbourhood filling routine. That is, first all areas below a defined minimum threshold are removed and the voids are then filled by growing the neighbouring units. This is done for each subbasin individually, so that subbasin boundaries remain intact. The aggregation and

Table 5.1: Threshold and interval values for the creation of the glaciological response units with the resulting unit statistics.

	Upper Aksu	Upper Rhone
Valley threshold angle	15°	
Valley elevation interval	40 m	30 m
Hillslope elevation interval	400 m	200 m
Aspect classes	4	
Minimum unit threshold	0.5 km^2	0.1 km^2
Unit count	12980	12179
Average unit area	0.95 km^2	0.33 km^2
Maximum unit area	3.48 km^2	2.30 km^2

suitable thresholds are important for the creation of similarly sized units, preventing numerical issues when routing ice between irregular units (Marshall and Clarke, 1999; Sanzana et al., 2013).

Other spatial attributes relevant to the hydrological model were mapped onto the spatial structure of the glacier units, i.e. for each hydrotope the dominant land cover and soil class were used. As soil inventories in mountainous areas mainly apply to valleys (alluvial fans, plateaus) and the hillslopes are mainly composed of bare rock and extremely shallow soils, the soil depth on the hillslope units was reduced to 300 mm in line with typical soil depths in steep terrain (Dietrich et al., 1995; Heimsath et al., 1999). All hillslopes are given the land cover category bare soil, i.e. the soil cover is treated as loosely consolidated, unvegetated soil that describes the loose gravel and small fluvial vans of high mountain terrain.

In comparison to other discretisation schemes of glacio-hydrological models, the 'glaciological response units' use fewer computational units than grid-based models (Immerzeel et al., 2011; Lutz et al., 2014; Naz et al., 2014), but retain more of the terrain geometry than hypsometry-based models (Duethmann et al., 2015; Hagg et al., 2007; Huss et al., 2008), as illustrated by Figure 5.3. This enables the model to be applied

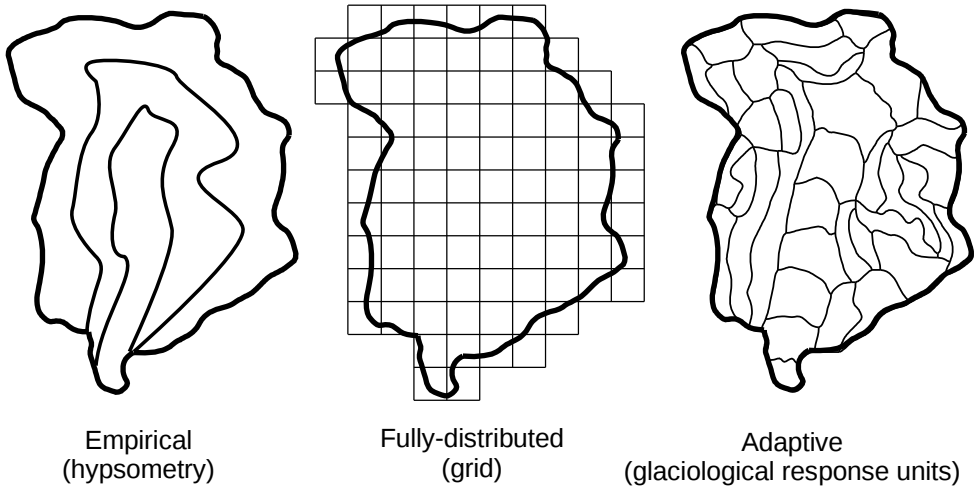

Figure 5.3: The 'glaciological response units in comparison of the other two discretisation schemes in a single subbasin.

over large catchments and also simulate every glacier individually. The size of the units may be adapted to the desired level of detail and model domain.

5.3 Glacier formation and accumulation

All snow processes are governed by the existing snow module, including a description of the ice and water content of the snowpack calculating melt accordingly (based on the snow module, see Section 2.8). If at the end of the ablation season (defined as 90 days after the summer solstice, i.e. end of September in the northern hemisphere) snow or firn is left in the hydrotope and the snowpack exceeds a critical height H_c, it turns into glacial ice and is subject to ice flow. H_c is dependent on both slope α and shear stress τ_s, the force the ice needs to overcome to deform under its own weight. Although this varies between glaciers and regions, a global average of 100 kPa is widely accepted (Cuffey and Paterson, 2010; Dudeja, 2011; Linsbauer et al., 2012). H_c [m] is determined by the equation:

$$H_c = \frac{\tau_s}{\rho \cdot g \cdot \tan(\alpha)} \tag{5.2}$$

with glacier ice density ρ ($900\,\mathrm{kg\,m^{-3}}$), gravity g ($9.8066\,\mathrm{m\,s^{-2}}$) and slope angle α [°]. The glacier module is only active if down-slope mass redistribution is viable (i.e. the snowpack exceeds H_c) through ice creep and slip or avalanching, while the snow module is simulating all snow processes including firn and also where snow is covering glacial ice.

It is fully acknowledge that shear stress deviates locally and between glaciers from the global mean. Cuffey and Paterson (2010) give a typical range of 50–200 kPa. Since actual observed estimates depend on ice thickness measurements, the average value remains the best estimate for the majority of glaciers. Haeberli and Hoelzle (1995) and Huss et al. (2010a) proposed an empirical approach to spatially distribute this estimate for individual glaciers at central flow lines, using the elevation range of a glacier as a proxy. This approach is now used to assess glacier volumes over larger domains (Huss et al., 2010c; Linsbauer et al., 2012). This approach, however, relies on empirical relationships with several parameters that need to be estimated for individual glaciers or glacier groups, disagreeing with the parameter parsimony of the proposed model.

5.4 Ice flow

The routing between the glacier units is processed similarly to the subbasin routing, i.e. according to the flow direction given in the DEM. Ice flow occurs if the critical height H_c is exceeded; if the thickness decreases below H_c, the ice area of the unit is proportionally decreased to simulate a slow terminus recession. Figure 5.4 shows the routing between the glacier units in a single subbasin and a valley cross-section of three units. The flow volume Q_i [m^3 weq. a^{-1}] is based on Glen's Flow Law and the semi-empirical adaptation suggested by Marshall et al. (2011):

$$Q_i = \chi \cdot A_u \cdot H^5 \cdot \tan(\alpha)^3 \tag{5.3}$$

with area of the glacier unit A_u [m^2], glacier thickness H [m weq.], slope α [°] and the rheology term χ [$m^{-4}a^{-1}$] that is subject to calibration. The flux Q_i is routed to the next glacier unit, but is constrained to the volume above the critical height.

Independent thickness measurements or simulations (using physically-based ice models) may be used to calibrate the rheology term χ. GlabTop2 simulations were used

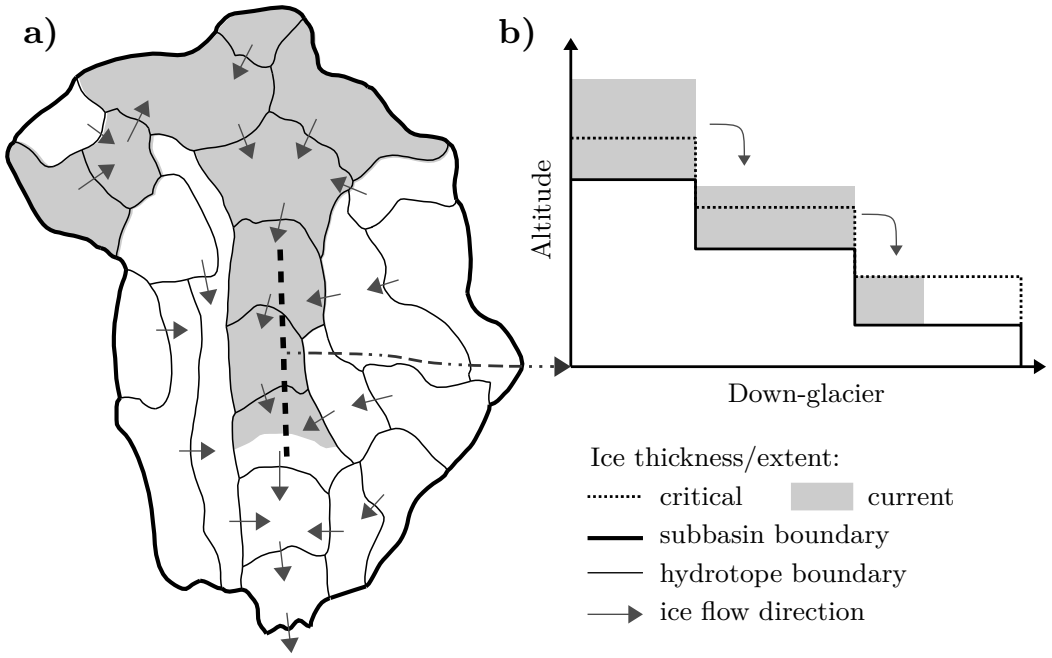

Figure 5.4: Schematic representation of ice routing in a single subbasin (a) and through a valley cross-section of three glacier units (b).

here for both catchments. The GlabTop approach uses an empirical relation between average shear stress and elevation range of individual glaciers and is calibrated with geometric information from paleoglaciers and radio echo soundings on contemporary glaciers (Linsbauer et al., 2012). The average vertical error was shown to be 7–25 % (Frey et al., 2014), which is comparatively small given the uncertainties of the catchment-wide uniform shear stress assumption in the model.

To account for more accurate glacier area changes that in turn have a strong impact on catchment wide glacier melt, the glacier critical height is maintained if melting occurs and the fraction of glacier area is reduced instead (as illustrated in Figure 5.4b). This simulates the gradual recession of a glacier front up-slope, exposing a decreasing area to melting after the glacier falls below the critical height. An approximation of the frontal melt area is necessary, however, to adequately account for melt of the receding glacier unit. Since the glacier units have irregular shapes, width and length may be approximated by $\sqrt{A_u}$, assuming the average shape to be close to a square block. A wedge-shaped glacier front is assumed with a constant height equal to H_c and a length l proportional to the changing volume below the critical hight, as described by:

$$l = \sqrt{A_u} \cdot \frac{H}{H_c} \tag{5.4}$$

The melt area A_m [km^2] is thus:

$$A_m = \sqrt{A_u} \cdot \sqrt{l^2 + H_c^2} \tag{5.5}$$

This subgrid treatment of glacier area allows for a more accurate sensitivity to temperature.

Observed elevations (i.e. the SRTM-3 DEM at 90m spatial resolution) were used to vertically distribute melt temperatures, rather than relying on modelled bed elevations and using the evolving glacier surface elevation. This eliminates the dependency on more complex thickness simulations (e.g. GlabTop2) that are only used where available to calibrate the rheology parameter χ. This simplification is warranted because the simulated ice thickness does not decrease below the critical hight, keeping the thickness variations relatively small.

5.5 Avalanching

Avalanching represents a more rapid form of snow and ice redistribution as the majority of the snow or firn column is removed and transported downslope (Cuffey and Paterson, 2010). The avalanche-prone areas are identified by a simple slope threshold that is physically based and well constrained to a range of 35–45° (Schweizer et al., 2003) and should be adapted to the observed glacier hypsometry and distribution. If the snow and glacier height exceed the critical height, the snow is accumulated on the remaining fraction of the glacier unit or if the avalanche proportion is greater than 90%, all snow is transported down-slope to the next glacier unit (illustrated in Figure 5.5. This upper threshold is needed for numerical stability to avoid large snow masses 'piling up' on small fractions of the glacier unit. Although the impact of avalanching on catchment-wide discharge simulations was found to be insignificant, the process is needed to account for glacier area variations above the Equilibrium Line Altitude (ELA) that are present in observed glacier outlines. Excluding it would lead to even very steep slopes – common for elevations above the ELA – to be ice covered and in turn would erroneously increase the total glacier area.

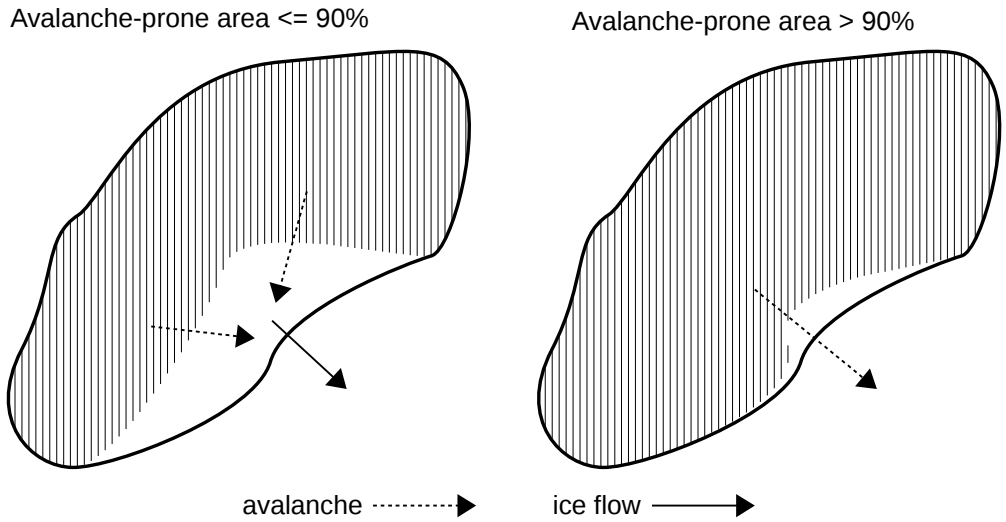

Figure 5.5: Avalanching in a glacier unit with less than 90% avalanche-prone areas (left) and a unit with more than 90% (right).

5.6 Glacier melt

The well-tested Degree-Day approach was implemented to simulate glacier melt, as temperature is the 'least uncertain' available climate variable (Hock, 2003). Glacier meltwater is collected in a linear reservoir together with liquid precipitation over the glacier and released as glacier discharge Q_g with a delay described by the residence time. This reservoir simulates the water storage capacity of glaciers and the observed delay of glacier discharge after intensive melting periods (Cuffey and Paterson, 2010). The following equations describe the glacier melt M_g and water outflow Q_w from the linear reservoir V_w:

$$M_g = \begin{cases} \delta_g \cdot T & \text{if } T > T_m \text{ and } H_s = 0 \\ 0 & \text{otherwise} \end{cases} \tag{5.6}$$

with the Degree-Day factor δ_g [mm K^{-1} d^{-1}], daily mean temperature T [°C] and melt threshold temperature T_m [°C], glacier height H_g and snow height H_s.

$$\frac{\Delta V_w}{d} = M_g + P_l - Q_w \tag{5.7}$$

$$Q_w = \frac{V_w}{t_r} \tag{5.8}$$

with liquid precipitation P_l and residence time t_r [d] ranging between 1–10 days, which may be calibrated, for example, using individual melt events without rain (Cuffey and Paterson, 2010). Since glaciers are situated above SWIM's soil column, glacier water outflow (Q_q) is subject to the same infiltration and surface runoff processes as liquid precipitation as is illustrated in Figure 5.6. The soft glacier bed till is described by a shallow, highly permeable soil, which saturates quickly resulting in high rates of surface runoff throughout the melt season.

The effects of an evolving subglacial channel network were neglected because it has little impact on catchments larger than a single glacier group and with significant contributions of precipitation to discharge, especially at daily time steps (Cuffey and Paterson, 2010; Hock and Hooke, 1993). Including the process would have led to additional parameter redundancy. Similarly, evaporation over glaciers is not accounted for since it is a negligible component of the glacial water balance at the catchment scale

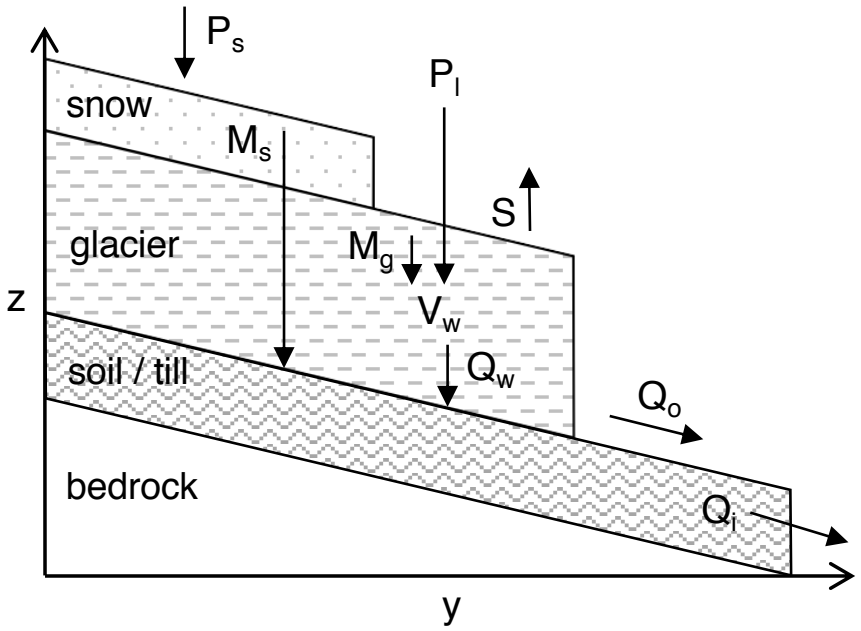

Figure 5.6: Schematic representation of a longitudinal glacier cross-section with water fluxes leading to runoff generation from the soil or glacial bed till. Symbols are as defined in Equations (5.7) and (5.8) and M_s for snow melt, Q_o for surface runoff, Q_i for subsurface runoff, P_s for solid precipitation and S for sublimation.

(Cuffey and Paterson, 2010). Most approaches are based on the surface energy balance and requires information on free supraglacial water surfaces, both of which are beyond the complexity of the developed model.

Two processes were considered that alter the melt rate over space and time: a) slope aspect and terrain shading (Section 5.8) and b) supraglacial debris cover (Section 5.9). Both processes have been shown to have a significant influence on glacier melt and in turn the spatial distribution of glaciers over longer time scales, as described below. Although their governing processes are highly complex, two simple approaches are used to approximate their effects and to spatially distribute Degree-Day melting rates.

5.7 Sublimation

In most glacieriesed regions sublimation from the glacier is considered a negligible factor, with rates often far below the error of accumulation rates (Gascoin et al., 2011; Hock, 2005). This is mainly due to the fact that sublimation consumes 8.5 times as

much energy (latent heat of sublimation: $2.838 \times 10^6\,\mathrm{J\,kg^{-1}}$ versus latent heat of fusion: $0.334 \times 10^6\,\mathrm{J\,kg^{-1}}$). In dry and high elevation zones, however, the proportion of energy consumed by sublimation rises to significant levels, suppressing melt rates and meltwater runoff as a result (Mölg et al., 2009; Zhang et al., 2006). High wind speeds and large vapour pressure deficits (or low relative humidity) favour sublimation and are common in high elevations. Modelling day-to-day variations in sublimation rates is only possible with a full energy balance model. However, approximate average ratios of energy used for sublimation in the annual mass balance allow the coupling of sublimation with melting and consider the process at least on annual timescales. Assuming ablation is made up of sublimation S and melting M_g, the energy balance with a sublimation ratio Γ (share of energy used for sublimation) can be described as follows:

$$M_g = E \cdot \frac{1-\Gamma}{L_f} \tag{5.9}$$

$$S = E \cdot \frac{\Gamma}{L_s} \tag{5.10}$$

with the total available energy E $[\mathrm{J\,kg^{-1}}]$ and the latent heat of fusion L_f $[\mathrm{J\,kg^{-1}}]$ and of sublimation L_s $[\mathrm{J\,kg^{-1}}]$. Using the Degree-Day approach from Equation (5.6) with positive degrees of temperature as T_+, M_g can be replaced to solve for E as follows:

$$E = \delta_g \cdot T_+ \cdot \frac{L_f}{1-\Gamma} \tag{5.11}$$

Using Equation (5.10), sublimation can be described by:

$$S = \delta_g \cdot T_+ \cdot \frac{\Gamma \cdot L_f}{(1-\Gamma) \cdot L_s} \tag{5.12}$$

This allows the inclusion of sublimation from glaciers using the proven Degree-Day factor approach while only adding a single parameter that can be estimated from general climatic conditions and sparse energy balance studies. This first order approximation ensures the inclusion of sublimation in the annual mass balance. While it is acknowledged that the fraction of energy used may vary significantly at the daily timescale, it is implemented at that timescale due to its simultaneous calculation with melt.

Low observed or calibrated Degree-Day factors are an indication of high proportions of energy used for sublimation (Winkler et al., 2009; Zhang et al., 2006). Observed degree-Day factors (mostly measured by ablation stakes) include sublimation and should therefore be compared to simulated ablation and not used for the ice melt term without calibration.

5.8 Slope aspect and terrain shading

Slope aspect and terrain shading alter the amount of short-wave solar radiation a glacier area receives, which is the dominant driver of glacier melt (Paul, 2010). A first order approximation of this variability is given by the potential sunshine duration per day a slope receives ignoring clouds, a variable readily inferable from a DEM (Figure 5.7).

Although clear-sky solar radiation would provide a more accurate variable (as used in other models, e.g. Huss et al., 2008), it requires additional calibration parameters, which was sought to be keep to a minimum. Hours of sunlight were computed for both

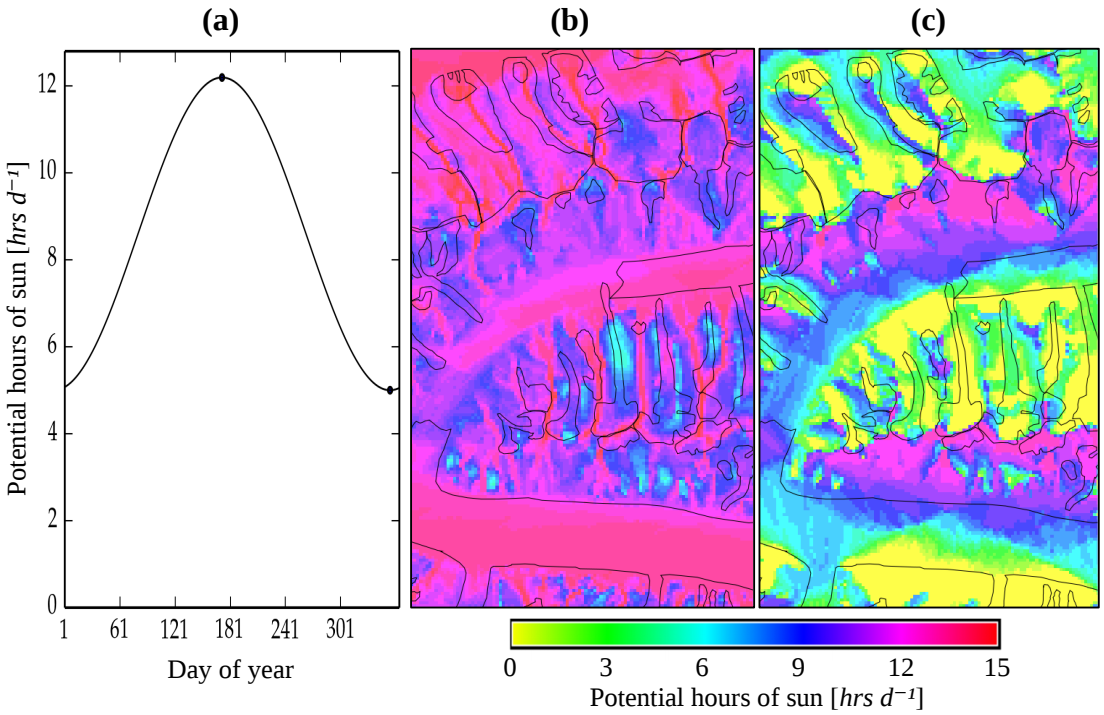

Figure 5.7: An example of DEM-derived potential sun hours on the summer solstice (June 21) (b) and winter solstice (December 21) (c) including glacier outlines. The days are marked in the day of year sine interpolation (a) for an example glacier unit.

the summer h_s and winter h_w solstice and interpolated for all days in between with a sine curve (the HBV-ETH model uses a similar sinusoidal differentiation of the Degree-Day factor, but with empirical boundaries, Hock, 2005). The basin-wide Degree-Day factor δ_g is localised by linear scaling as δ_i:

$$h_i = h_w + \frac{h_s - h_w}{2} \cdot \left(1 + \cos \frac{2\pi \cdot i}{365}\right) \tag{5.13}$$

$$\delta_i = \delta_g \cdot \frac{h_i}{12} \tag{5.14}$$

where i are the days since the winter solstice, sun hours on day i, on the summer and winter solstice are h_i, h_s, h_w (12 signifying the potential hours at the equinox on an unshaded horizontal surface). Although potential sun hours neglect cloud shadowing and the fact that melting is also driven by turbulent heat flux and diffuse radiation, it provides an efficient method to vary the melt rate over complex terrain without introducing additional parameters (as using potential short-wave radiation would do). The Degree-Day approach allows to calibrate the other melt terms implicitly.

5.9 Debris cover

A supraglacial debris cover has long been shown to first increase glacier ablation up to a thickness of a few centimetres and then significantly decrease ablation (Bozhinskiy et al., 1986; Nicholson and Benn, 2006; Östrem, 1959). The initial increase in melting is caused by the decreased albedo of thin debris or aerosol deposition and enhanced thermal conductivity to the glacier ice. This effect, however, is rapidly decreased by the thermal shielding effect of debris layers thicker than a few centimetres. Observing the initial increase has been difficult and including the effect in modelling would require estimating debris thickness with errors smaller then the threshold thickness. Since this is beyond the precision of the model, only the decreasing effect of such a debris layer is considered here.

Several in situ studies have linked debris cover to subdebris ablation rates using a negative exponential relationship based on the pioneering work by Östrem (1959) (Mattson, 1993; Nicholson and Benn, 2006, e.g. in the Himalaya and several other

regions). Considering the measured daily mean temperature, the ablation can be expressed in terms of Degree-Day factors. The simplified Östrem curve without the initial increase is described by the following empirical equation:

$$\delta_d = \delta_i \cdot e^{-\gamma \cdot H_d} \tag{5.15}$$

with the clean ice melt factor δ_i [mm K^{-1} d^{-1}], the debris thickness H_d [cm] and the slope factor γ. Although the latter parameter varies between studies and glaciers, it tends to be similar, while the clean ice melt factor varies much more between regions (Nicholson and Benn, 2006).

Observations of subdebris ablation are sparse, so that mean values for the slope factor must be used in most cases. Here the findings from the largest glacier of the Tien Shan, the heavily debris-covered South Inylchek glacier, Kyrgyzstan (located in the Upper Aksu catchment) by Hagg et al. (2008) were used. They found a value of $\gamma = 0.0572$ that is able to describe their ablation observations with a correlation of 0.94.

As delineating the spatial distribution and estimating the thickness of debris cover over an entire river catchment is near to impossible, let alone knowing its development in the future, a dynamical approximation of the glacier cover was implemented. Supraglacial debris has several origins: deposition of colluvial material from rock avalanches and landslides as well as emergence of subglacial moraines and melt out of englacial debris are the main processes involved (Bolch, 2011). While the first two processes are highly local and glacier specific, englacial debris melt out is the only one mainly driven by meteorology and universally applicable to a wider region (with varying intensity between regions). To simulate the evolution of debris produced by this process, an englacial debris concentration approach was implemented (previously proven by Bozhinskiy et al. (1986) in a more complex form). While snow accumulation decreases the concentration, melting increases it and ice flow 'dilutes' the downstream concentration with the one upstream.

An assumed initial debris concentration C_0 (dimensionless) is altered by melting and accumulation in a glacier unit with the specific debris concentration C_g over the daily

time step d according to the following equation:

$$\frac{\Delta C_g}{d} = C_g \cdot \frac{A - H_s}{H_g} + (C_u - C_g) \cdot \frac{H_q}{H_g}, \quad C_0 \leq C_g < 1 \tag{5.16}$$

with glacier thickness H_g, glacier ablation A (melt and sublimation), firn accumulation H_s, ice flux height H_q and debris concentration of the upstream unit C_u. The first term changes the concentration according to the ratio of the specific mass balance $(A - H_s)$. The second term describes the 'dilution' of the ice flux from the upstream unit. This debris concentration approach is schematically illustrated in Figure 5.8.

The debris concentration above the initial concentration was assumed to cover the glacier surface. The actual debris height H_d is a fraction of the critical glacier height H_c (see Section 5.3) for simplicity taking account of the slope dependence and the minimum glacier thickness. This is expressed by the following equation:

$$H_d = H_c \cdot (C_g - C_{init}) \tag{5.17}$$

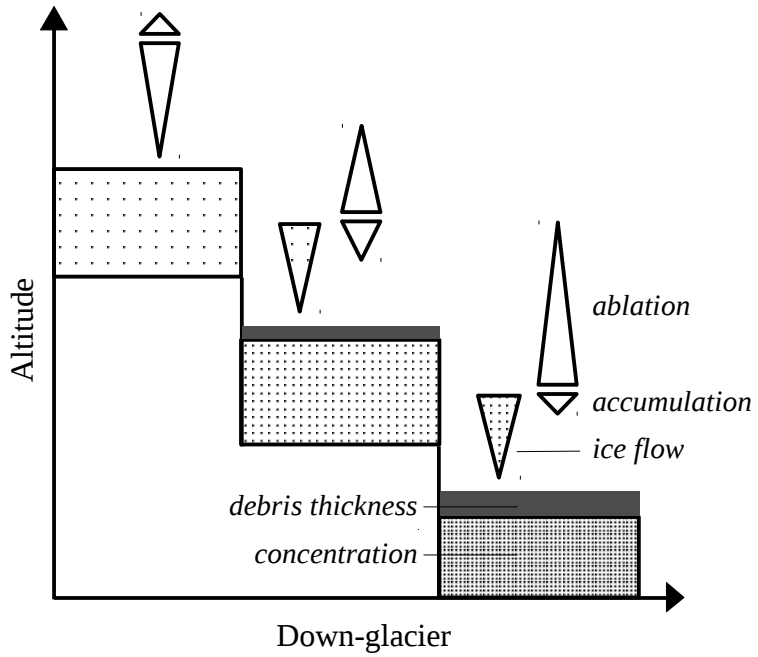

Figure 5.8: Schematic representation of the debris cover concentration approach for three glacier units with increasing concentrations. Mass fluxes with their respective debris concentration (fill) are shown as arrows.

While this method is relatively simple approximation of the actual local debris conditions, it reproduces the basin-wide response of an increasing debris cover with increasing melt, typical for low-lying glacier snouts. The calibration parameter C_{init} is used to adjust debris thickness to comparable observed values.

5.10 Precipitation correction

In Section 3.3.2 it was shown that precipitation dataset vary widely in the Aksu and the other Tarim River headwater catchments. Insufficient meteorological station density leads to a low-elevation bias in observation-based datasets, generally underestimating precipitation at higher elevations. Therefore, a precipitation correction was used for the Upper Aksu catchment. Since it is the focus of Chapter 6 and described in detail in Section 6.4, it is only briefly described here.

Precipitation was corrected by a function of altitude and three physically-based parameters. taking account of varying gradients and an eventual decrease at very high elevations. The correction factor remains 1 over lower laying elevations for which observations are available, but increases exponentially up to a maximum gradient a. It then reduces the gradient until a maximum correction factor c at altitude m is reached and decreases again at higher elevations thereafter.

Since the Upper Rhone catchment has a much higher density of meteorological stations, the above form of altitude-dependent correction was not necessary. Instead, all available precipitation data were interpolated via the Inverse-Distance-Weighting method and corrected by factors published in the Swiss Hydrological Atlas (Kirchhofer, 2000; Sevruk, 1985).

5.11 Calibration strategy

5.11.1 Glacier initialisation

Glacier dynamics need decades to centuries to reach an equilibrium under a given stable climate (Cuffey and Paterson, 2010). To take account of these long-term dynamics at the start of the modelling period, the ice cover has to be initialised by the model

using a representative quasi-stable climate of this length. This ensures consistency between glacier cover and the driving data, as the interpolated climate data is inherently imprecise compared to the observed glacier cover. Also, the model processes and spatial routing structure are an imperfect representation of actual conditions, so that observed glacier areas and volumes can not be directly used as initial conditions.

For the proposed model, the glacier area and volume were initialised using a climate period in which the glacier mass balance is known to be close to 0, i.e. in a quasi-equilibrium state (Clarke et al., 2015; Marshall et al., 2011). Since this period is in most cases shorter than the time it takes for a glacier to reach an equilibrium, shorter periods are used successively for 200–1000 years.

Mass balance records around the world have exhibited balanced or even positive budgets in the 1960s until the mid-1970s (Dyurgerov, 2010; Dyurgerov and Meier, 1997; Sorg et al., 2012; WGMS and UNEP, 2008). This is also true for reference glaciers in and close to the case study catchments of this study: The long-term mass balance records of the Griess glacier in the Rhone catchment show a mean of $-79\,\mathrm{mm\,a^{-1}}$ between 1962–1980. For the Tien Shan, Dyurgerov (2010) puts forward a regional average mass balance that shows a mean balance of $-82\,\mathrm{mm\,a^{-1}}$ between 1960–1975 (also confirmed by Farinotti et al., 2015). These periods were chosen for the initialisation of the glacier cover in the respective catchments.

Glaciers are never in a perfect equilibrium state, as the two examples above show. But typically, near-stable periods can be identified and the 1960s and 1970s are the latest periods known that also overlap with meteorological observations. Since the model initialisation assumes a perfect equilibrium, the residual mass balance must be represented by a calibration parameter that either adds or subtracts mass from the annual balance during the initialisation period. Clarke et al. (2015) use a similar bias approach in their mass balance model to initialise glaciers of western Canada. The residual mass balance parameter b_r ensures that the equilibrium assumption of the initialisation does not lead to wrong parametrisations of accumulation (precipitation correction) or ablation (glacier melt). The calibration strategy of this and other parameters is discussed in the following section.

5.11.2 Multi-objective calibration

Constraining the parameters of a glacio-hydrological model is necessarily a multi-objective problem, when both glacier and river discharge observations are used. It is the concurrent simulation of both physical systems that makes it a mutually beneficial exercise at the catchment scale: Accurate glacier behaviour validates the precipitation correction and glacier melt, that is important for the accurate simulation of discharge.

An overview of the parameters used for calibration and were they have been described is given in Table 5.2. The glacier-relevant parameters are mainly calibrated during the glacier initialisation. They are the precipitation correction, the snow and ice melt rates, the ice rheology and the residual mass balance. The most important hydrological parameters are the saturated conductivity correction, evapotranspiration correction and the routing parameters with some less important ones left at typical values. Their ranges are catchment and input data dependent and were tightly constrained by values reported in the literature.

The model was calibrated to daily discharge observations, observed glacier area and catchment-wide, annual mass balances with approximately the same time coverage for each basin. For the Upper Rhone catchment, the mass balance calibration period was 1981–2010 to match the catchment-wide assessment of Fischer et al. (2015), while the hydrological calibration was only for the first half of that period (1981–1995) with the other half used for validation (split-sample approach). For the Upper Aksu catchment the mass balance assessment of Pieczonka and Bolch (2015) was for the period 1975–1999, which was used as the glacier calibration period. Daily discharge data was only available for the period 1971–1987 at the Xiehela station. Observations for the Sary-Djaz station are often interrupted, with only 12 years available between 1971–1994. The available data was split in half with the first 8/12 years used for calibration and the rest for validation.

Four objective functions were chosen to rate the quality of the simulation: The quality of the discharge simulations is evaluated by the commonly used Nash-Sutcliffe Efficiency (NSE) (Nash and Sutcliffe, 1970) and the bias in water balance, as was done in Chapter 4. The model's accuracy in simulating the glacier area is quantified by the

Table 5.2: Calibration parameters ordered by model component with typical ranges. Depending on the catchment, the parameter ranges are further constrained based on available information. Parameter ranges used for the calibration presented here are given in the results section.

Symbol	Description	Introduced in	Range	Unit
Snow and glaciers				
δ_s	Snow Degree-Day factor	Section 2.8.1	1 – 5	$\mathrm{mm\,K^{-1}\,d^{-1}}$
T_s T_m	Snow fall and melt threshold temperatures	Section 2.8.1	0 ± 4	°C
t_e	Temperature lapse rate	Section 2.8.1	-0.45 – -0.80	$\mathrm{°C100m^{-1}}$
δ_g	Ice Degree-Day factor	Section 5.6	5 – 15	$\mathrm{mm\,K^{-1}\,d^{-1}}$
b_r	Residual mass balance during initialisation	Section 5.11.1	0 ± 300	$\mathrm{mm\,a^{-1}}$
*Precipitation**				
c	Max. correction factor	Section 5.10	1–6	
a	Max. precipitation gradient	Section 5.10	0.05 – 0.9	$\mathrm{\%\,m^{-1}}$
m	Max. precipitation altitude	Section 5.10	3000–7000	m asl.
Hydrology				
E_c	Potential evaporation correction factor	Section 4.5	0.7 – 1.5	
R_2 R_4	Routing coefficients	Section 4.5	1 – 5	
S_c	Saturated conductivity correction factor	Section 4.5	0.5 – 2	

*only used for the data-scarce Aksu catchment

Root Mean Square Error (RMSE) between simulated and observed hypsometry. The RMSE is also used to quantify the error in annual, catchment-wide mass balances.

While manually calibrating the model to four objectives is possible, it is a painstaking and time-consuming exercise. After initial manual tests, the widely used automatic calibration algorithm, the Non-dominated Sorting Genetic Algorithm 2 (NSGA-2) (Bekele and Nicklow, 2007; Deb et al., 2002; Duethmann et al., 2014; Efstratiadis and Koutsoyiannis, 2010), was chosen to provide multiple parameter sets. NSGA-2 employs

evolutionary computation paired with the multi-objective Pareto optimality to rank and select well-performing 'individuals' (i.e. parameter sets). The result is a collection of archived parameter sets that all produce 'good' results by at least one objective function. 'Good' here means that no other objective function can be improved without degrading any other, making them all 'Pareto-optimal' (together forming a Pareto front, Efstratiadis and Koutsoyiannis, 2010). It is up to the user to choose acceptable trade-offs between them.

A population size of 50 individuals was chosen that are concurrently evaluated over 100 generations, i.e. 5000 evaluations. Considering the 10–13 dimensional parameter space, these do not ensure finding all optimal solutions for the model. However, the method does provide an efficient way to find some of them within a manageable computing time. The parallel evaluation reduces the calibration time to approximately the number of generations times model runtime, keeping the calibration time to 1–2 days rather than several weeks. To select acceptable trade-offs from the final archive of parameter sets, the best 25 parameter sets were chosen by excluding results that do not meet the following minimal criteria: Nash-Sutcliffe Efficiency > 0.5, percentage bias in the water balance $< 20\%$, absolute error of the glacier hypsometry as percent of total glacier area $< 40\%$ and RMSE of mass balance as percent of observed $< 40\%$. These values were successively improved (i.e. NSE increased and errors lowered) at 1% increments until the best 25 sets remain, for which median, minimum and maximum performance values are reported.

5.12 Catchments and input data

Two catchments similar in size and glacier coverage were chosen to test and validate the model (Table 5.3 and Figure 5.9). The relatively data-scarce catchment of the Upper Aksu River has already been described as part of the Tarim River headwaters in Chapter 3 and in more detail in Section 4.2. A second catchment, that of the Upper Rhone River, Switzerland was chosen to test the model under 'data-abundant' conditions. It is described in more detail below and an overview of the data sources used in both models is provided in Table 5.4.

Table 5.3: Catchment details according to the gauging stations used for calibration; drainage area, mean discharge Q as annual mean and summer mean for the month June to August (over all available data) and glacier cover. See Table 5.4 for sources.

Gauge station	River	Area $[km^2]$	mean Q $[m^3s^{-1}]$	mean JJA Q $[m^3s^{-1}]$	Glacier [%]
Upper Aksu					
Xiehela	Kumarik R.	12991	151.8	406.6	22
Sary-Djaz	Sary-Djaz R.	1927	37.4	91.3	18
Upper Rhone					
Port du Scex	Rhone R.	5220	180.3	349.5	11.9
Blatten	Massa R.	192	2.8	7.6	57

Table 5.4: Input data used to drive SWIM and to calibrate/validate the model. Topography and glaciers are shown in Figure 5.9. Climate variables are: temperature T (mean, min., max.), precipitation P, radiation and relative humidity.

Variable	Upper Aksu	Upper Rhone
Climate	WATCH (Weedon et al., 2011) for T, radiation and relative humidity; P from APHRODITE (Yatagai et al., 2012)	climate reference data from Oesterle et al. (2003) with additional precipitation observations from MeteoSwiss
Topography	SRTM digital elevation model at 90m (hole-filled) (Jarvis et al., 2007)	ASTER digital elevation model at 30m (GDEMv2, hole-filled)
Land cover	Chinese Meteorological Administration for Chinese part, MODIS 500 m land cover (2001) (Friedl et al., 2002) for Kyrghyz part	CORINE Land Cover (European Environment Agency, 2006)
Glaciers	Outlines for 1975 by Osmonov et al. (2013) and Pieczonka and Bolch (2015) and GlabTop simulated volume (Duethmann et al., 2015)	Outlines for 1973 by Paul (2003) and GlabTop simulated volumes by Linsbauer et al. (2012).
Soil	Harmonised World Soil Database (FAO, 2011)	
Discharge	Xiehela station from Chinese hydrological yearbooks (daily 1971–1987; annual 1971–2000) and Sary-Djaz station from Kirghiz hydrological yearbooks (daily 1971–1996).	Port du Scex and Blatten from GRDC (2016) (daily 1980–2010).

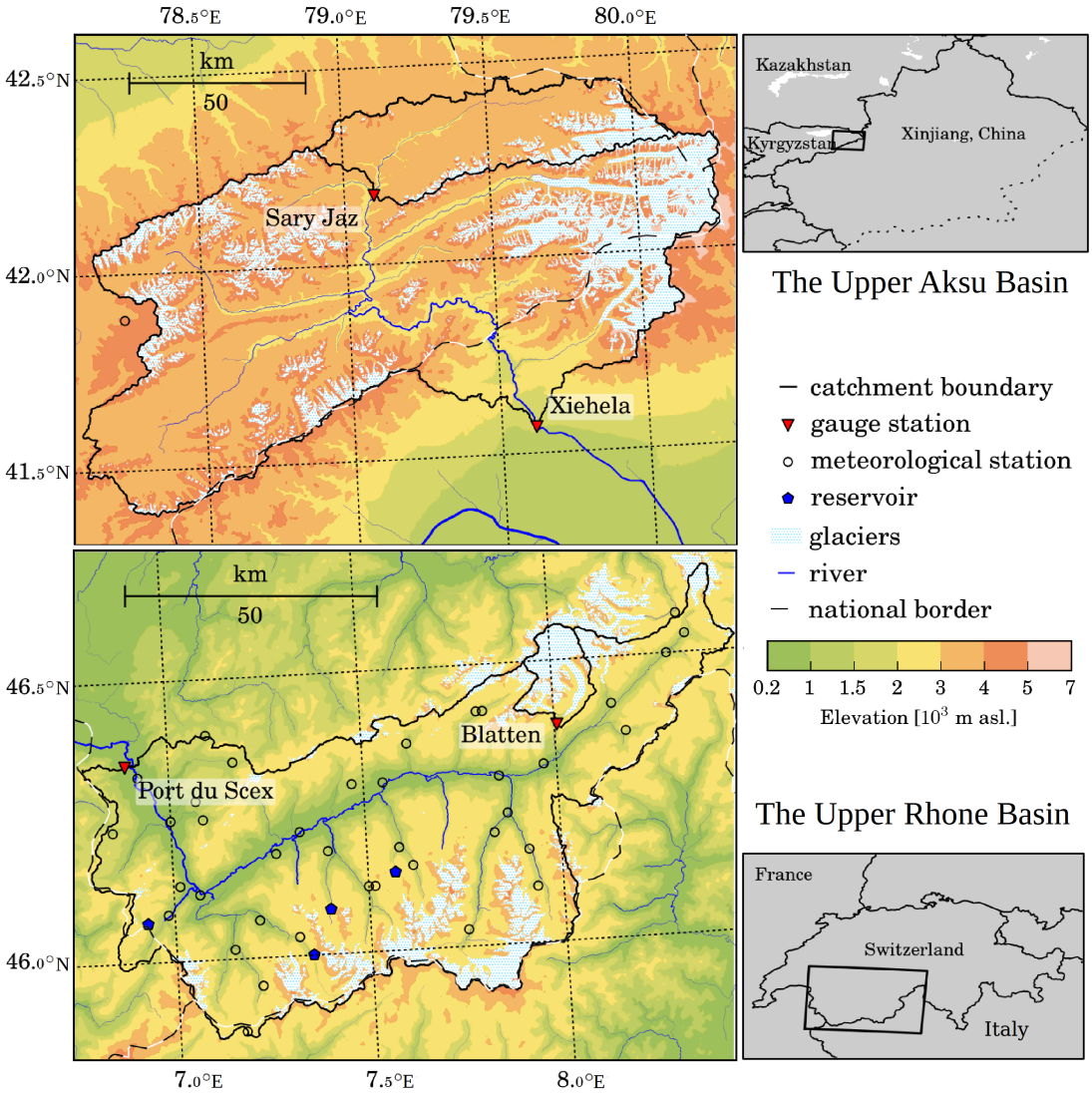

Figure 5.9: Overview maps of the two case study basins. Glacier cover is only shown inside the catchments.

5.12.1 The Upper Rhone catchment

The Rhone River originates from the Rhone glacier in southern Switzerland and its catchment has the largest glacier cover (11.9%) in Europe (Figure 5.9). The focus here is on the Alpine part of the catchment terminating just before Lake Geneva at the gauging station Port du Scex. The catchment incorporates the Alps' largest glacier, Great Aletsch Glacier, in the north-east and many other well studied glaciers in the south. It is dominated by a temperate climate with a strong elevation dependency:

While the valley floors receive 500–800 mm a^{-1} of precipitation, elevations above 2000 m receive 2000–3000 mm a^{-1} (Kirchhofer, 2000).

As with the rest of the Alps, the glaciers in the Upper Rhone catchment have seen rapid glacier retreat over the past three decades, but also follow the global trend of near-stable or even advancing conditions in the 1960s and 1970s (Huss et al., 2010b). Between 1973 and 2010, glacier area has shrunk from 722 km^2 to 569 km^2, a relative change of $-0.57\,\% a^{-1}$ (Fischer et al., 2014; Paul, 2003). Mass loss in the Rhone catchment between 1980–2010 was shown to be heterogenous in magnitude ranging from 200–1200 mm weq. a^{-1} with an average of 590 mm weq. a^{-1} (Fischer et al., 2015). Griesgletscher, one of two WGMS reference glaciers in the Alps located in the southeast of the catchment (Zemp et al., 2009) has an average mass balance of -1002 mm weq. a^{-1} over the same period. This long-term mass balance record is scaled by the geodetic catchment-wide mass balance for the calibration of the model.

The Upper Rhone catchment is regulated by 11 high head hydropower dams that were constructed between 1951–1975. A cumulated reservoir capacity of 1186×10^6 m^3 is installed to date up to Lake Geneva (Meile et al., 2010). Although reservoirs are not a focus of this study, it was found essential to represent the largest reservoirs in the model to adequately simulate downstream discharge that is important for the calibration of the glacier model. The four largest dams (Lake Dix, Lake Emosson, Lake Mauvoisin and Lake Moiry; see Figure 5.9) were implemented using SWIM's reservoir model (Koch et al., 2013). In the absence of reservoir discharge data due to the power companies' data restriction, average monthly filling quotas of Switzerland from Schaefli et al. (2005) were used because they were shown to highly correlate with most of the reservoirs in the catchment (a notable exception is the Lake Dix that has a more complex pumping network). While monthly average filling quotas do not reproduce the daily variability of the reservoir discharge, it is sufficient to reproduce the storage effect from summer to winter discharge. The effect of Sunday closures of the reservoirs on calibration results was reduced by excluding them from the observation data. The implementation of the reservoir module also demonstrates the benefits of the glacier assessment within an integrated hydrological model.

The reason for choosing this catchment for the validation of the model is the relative data abundance in comparison to other glacierised catchments: There are eight long-term meteorological stations available with temperature, radiation and humidity observations as well as a further 70 precipitation stations. In addition, the region has received extensive research yielding verified results on glaciological development (e.g. Braithwaite and Zhang, 2000; Farinotti et al., 2009; Fischer et al., 2015), climatic variability with elevation (e.g. Kirchhofer, 2000; Sevruk and Mieglitz, 2002) and successful hydrological modelling including glacier melt and large reservoirs (e.g. Fatichi et al., 2015; Rahman et al., 2012; Uhlmann et al., 2013). The research confirms many of the concepts and methods used in the presented model. Rahman et al. (2012) implemented the semi-distributed model SWAT to the same model domain. They demonstrate the complexities in modelling this highly glacierised and regulated mountainous catchment focusing on the extensive hydropower network of the Grande Dixence reservoir. Uhlmann et al. (2013) implemented a conceptual, semi-distributed glacio-hydrological model that has an empirical parameterisation of glacier flow in between elevation zones.

5.13 Calibration and validation results

From the Pareto-optimal solutions, the 25 best runs were selected following the approach described in Section 5.11. The calibrated parameter values (min., median, max.) are largely similar between the two catchments as expected for mid-latitude glaciers (Table 5.5). The drier climate of the Upper Aksu catchment becomes apparent in lower temperature lapse rates and slightly lower snow and ice melt factors. The precipitation correction, only applied to the Upper Aksu catchment as described in Section 5.10, leads to a catchment-wide correction of 45–53 % (464–490 mm a^{-1}), in line with previous studies (Aizen et al., 1996; Duethmann et al., 2015).

Table 5.6 provides an overview of the performance for both the hydrological and glaciological objective functions: Median values are given with parameter uncertainty ranges indicated by minimum and maximum values in brackets, i.e. the performance ranges over all 25 runs. The glacier area objective is given in two measures: the sum of absolute errors between the observed and simulated hypsometry and the deviation in the total area from the observed. Both values are given as fractions of the total

Table 5.5: Calibrated parameters (min., median, max.) for both investigated catchments over the best 25 parameter sets. Refer to Table 5.2 for a description and upper and lower bounds of the parameters.

Parameter		*Upper Aksu*			*Upper Rhone*		
		min	median	max	min	median	max
δ_s	Snow Degree-Day factor	3.2	3.8	4.1	2.7	4.0	5.0
T_s	Snow fall threshold	2.2	3.3	3.8	-2.3	1.3	1.9
T_m	Snow melt threshold	-2.0	-1.2	-0.7	-1.2	-0.5	1.6
t_e	Temperature lapse rate	-0.78	-0.72	-0.68	-0.60	-0.56	-0.49
δ_g	Ice Degree-Day factor	5.8	8.6	11.6	6.1	8.8	10.3
b_r	Residual mass balance	-281	-250	-182	-129	-79	149
c	Max. P correction factor*	3.1	3.6	3.9			
a	Max. P gradient*	0.31	0.34	0.37			
E_c	Potential evap. correction	0.61	0.79	1.15	0.74	1.08	1.41
R_2	Routing coefficients	0.5	1.1	3.1	1.3	3.8	5.0
R_4		0.9	2.7	4.1	1.6	4.6	5.0
S_c	Sat. conductivity correction	0.6	1.2	1.9	1.0	1.3	1.7

*only used for the data-scarce Aksu catchment

observed area for better comparison between the catchments. Simulated mass balances are contrasted with the geodetic mass balances given by the respective studies for both regions.

After the presentation of the discharge and glacier simulation results, a sensitivity analysis of the calibration parameters with regard to the four objectives is given to evaluate the effects and relative importance of the various parameters on the model outcomes. This is followed by an assessment of the annual water balance of the two catchments.

5.13.1 Daily discharge

The daily simulated and observed discharge for the calibration period is shown in Figure 5.10 and for the validation period in Figure 5.11. The day-of-year mean over the entire calibration/validation periods are also given. The hydrological model efficiency NSE in the calibration period ranges from 0.60 to 0.90 with a range in bias of the water

Table 5.6: Model performance for all four objectives: median (min., max.). The Nash-Sutcliffe Efficiency **NSE** and the bias in the water balance **PB** are given for the calibration and validation period (split-sample approach). The absolute and relative error of the glacier area hypsometry **A** is given as a fraction of total glacier area. The simulated annual mass balances **MB** are compared to observed values by Pieczonka and Bolch (2015) (Upper Aksu) and Fischer et al. (2015) (Upper Rhone).

Station	**NSE**	**PB** [%]	**A** [%]	**MB** [m weq. a^{-1}]
	calibration	*calibration*	*abs. residuals*	*simulated*
	validation	*validation*	*rel. total*	*observed*
Upper Aksu				
Xiehela	0.82 (0.81, 0.83)	0.8 (-4.4, 2.3)	16.3 (14.2, 19.5)	-0.36 (-0.37, -0.34)
	0.84 (0.82, 0.85)	-2.4 (-7.7, -1.1)	-1.1 (-11.5,2.4)	-0.35 ± 0.34
Sary-D.	0.63 (0.60, 0.70)	0.8 (-2.6, 5.3)	25.9 (18.7, 31.2)	-0.33 (-0.37, -0.33)
	0.66 (0.61, 0.72)	-7.9 (-11, -3.7)	11.3 (-5.3,18.5)	-0.35 ± 0.34
Upper Rhone				
Port d. S.	0.67 (0.66, 0.68)	-1.8 (-2.8, -1.4)	12.6 (10.8, 15.8)	-0.67 (-0.72, -0.58)
	0.62 (0.60, 0.64)	0.8 (-0.3, 1.4)	-8.8 (-13.8,6.8)	-0.59 ± 0.07
Blatten	0.89 (0.86, 0.90)	-0.1 (-1.0, 1.0)	8.4 (7.2, 10.0)	-0.87 (-0.96, -0.80)
	0.89 (0.85, 0.90)	-2.7 (-4.7, 0.6)	-1.0 (-6.7,2.1)	-0.80 ± 0.07

balance within ±5.3% indicating a good model performance. However, differences in performance reflect the data quality and the impact of water regulation.

In the data-scarce Upper Aksu catchment, the model performance is significantly higher at the outlet station Xiehela with a NSE of 0.81–0.85, while in the much smaller subcatchment Sary-Djaz, it is only 0.60–0.72. This is an indication that poor precipitation data influences the performance more the smaller the catchment size. In the data-abundant Rhone catchment, the best performing catchment is that of the smaller Blatten station with values of NSE of 0.85–0.90. The outlet station Port du Scex, however, shows a significant decline in performance with NSE values of 0.60–0.68. This is most probably due to the many reservoirs that were only implemented on an average monthly basis, although day-to-day fluctuations (e.g. reduced flows on Sundays) are clearly visible (Figures 5.10 and 5.11). This performance pattern is repeated in the divergence from calibration to validation period; the performance of the Sary-Djaz

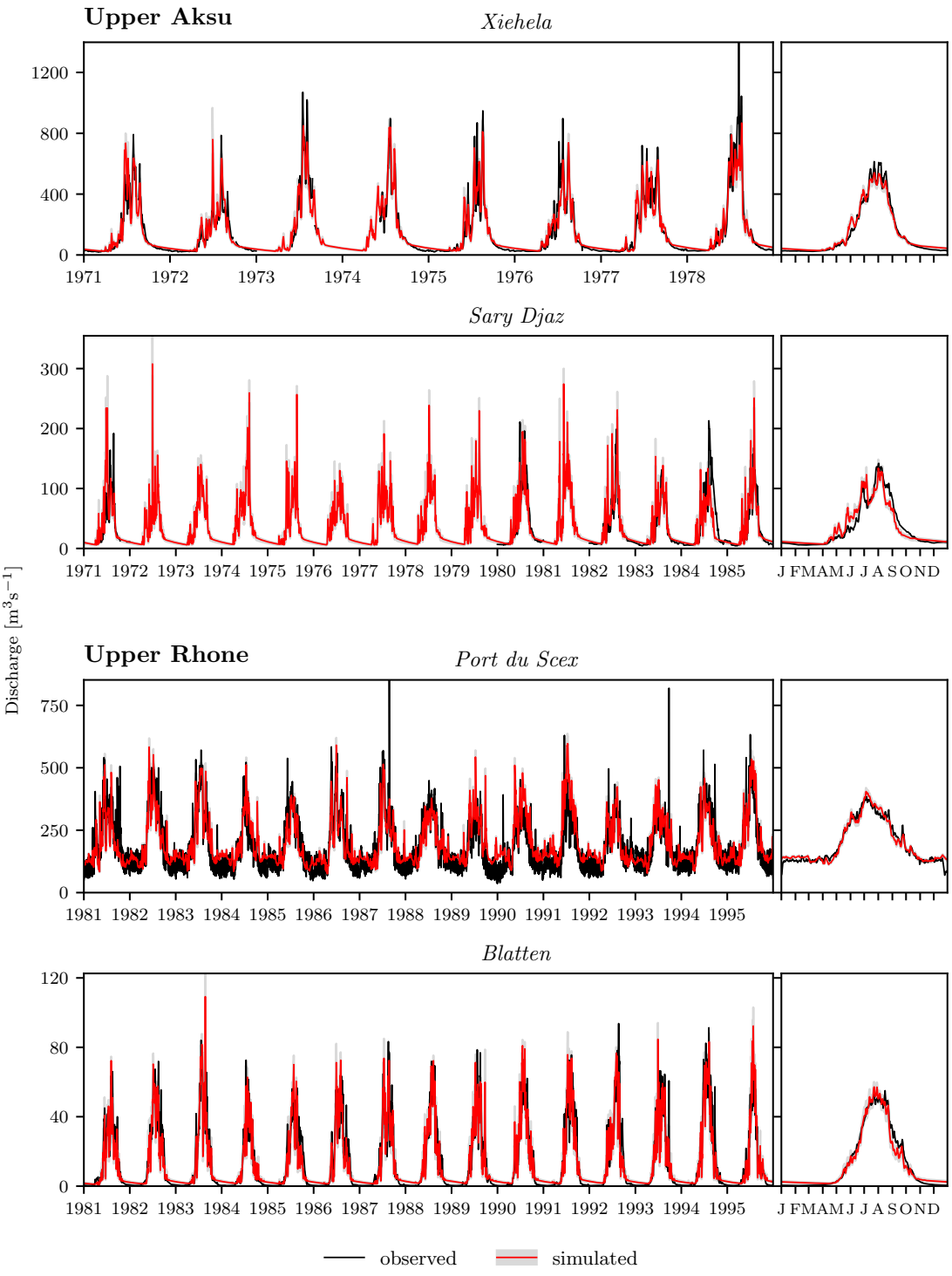

Figure 5.10: Simulated versus observed discharge in the calibration period for the outlet stations (Xiehela and Port du Scex) and intermediate stations (Sarj Djaz and Blatten) of both catchments. Daily discharge (left) is shown for a selected period while day of year mean discharge (right) is taken over the entire calibration and validation period. The oscillations in the Port du Scex discharge are the effects of weekend dam closures.

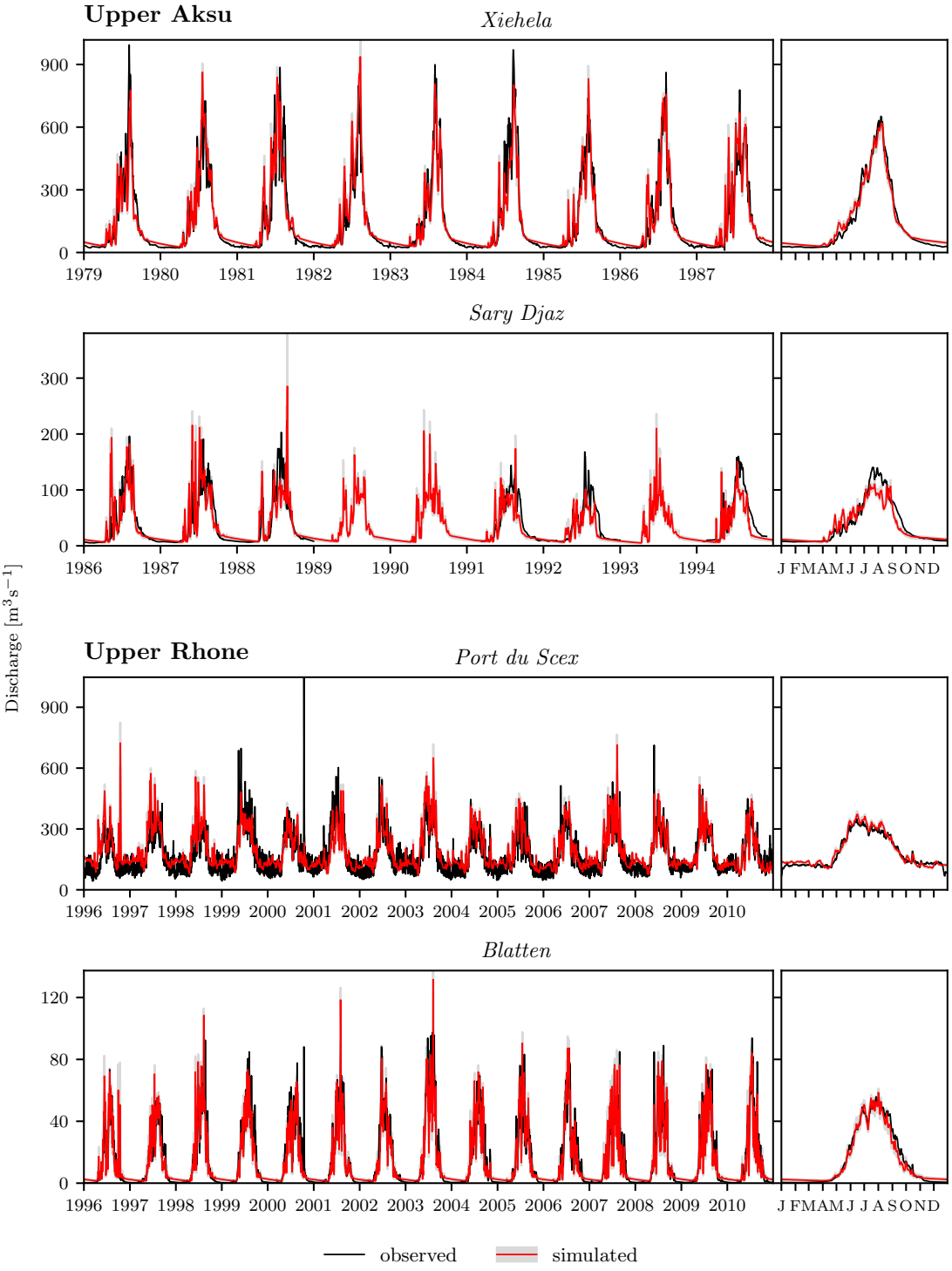

Figure 5.11: Same as Figure 5.10 but for the validation period.

catchment and the Port du Scex catchment is degrading more than at the other stations, but remains within acceptable limits (NSE 0.58–0.72, bias -11–+5%).

5.13.2 Glacier initialisation

The objective of the initialisation was to optimise the catchment parameters (mainly, the precipitation correction, ice rheology and the residual mass balance) to match the total catchment glacier area and volume as well as the elevation distribution (hypsometry) of glaciers in the individual subcatchments. An initialisation period of 300 years was judged to be sufficient to reach stability and is within the range of time length used in previous studies (Marshall et al., 2011; Naz et al., 2014).

The catchment-wide observed areas and estimated volumes are matched well by the modelled equilibrium of both area and volume over the initialisation period (Figure 5.12) and helped to rigorously correct the precipitation in conjunction with the observed and simulated catchment discharge (discussed above). While uncertainties in the estimated 'observed' volumes (modelled by Duethmann et al. (2015) for the Upper Aksu catchment and Linsbauer et al. (2012) for the Rhone catchment) undoubtedly exist, the initialised volume is mainly controlled by the rheology parameter of the ice flow equation and the assumed shear stress of 10^5Pa.

The area hypsometry is reproduced well by the model in both catchments (Figure 5.13). The sum of absolute residuals ranges from 7.2 to 31.2% of the total glacier area, while total area error is within −13.8–18.5 %. The largest mismatches exist in the data-scarce Sary-Djaz catchment, where insufficient driving data is likely affecting the accurate simulation of glacier area distributions. Discrepancies also exist in the elevation range with the largest glacier cover where the model overestimates cover in individual elevation zones by up to 25 % in the Upper Aksu catchment and by up to 18 % in the Rhone catchment.

5.13.3 Mass balances and area changes

The simulated mass balance was calibrated against reference glacier mass balance records, that were scaled by the catchment-wide geodetic mass balances provided by

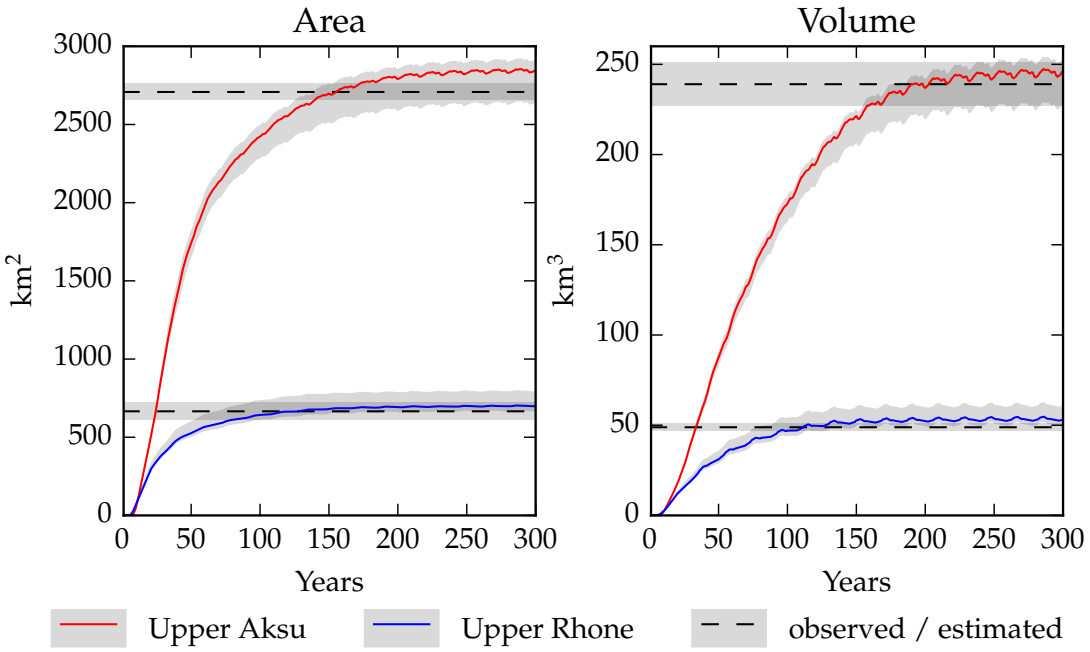

Figure 5.12: Development of area and volume over the 300-year initialisation period in the Upper Rhone and the much larger Upper Aksu catchment. Observed area ranges are taken from Paul (2003) and Osmonov et al. (2013) and Pieczonka and Bolch (2015). Volume estimations are based on modelled glacier thicknesses in the Upper Aksu catchment and in the Upper Rhone catchment by Linsbauer et al. (2012).

Pieczonka and Bolch (2015) for the Upper Aksu and by Fischer et al. (2015) for the Upper Rhone catchment. The comparison of both simulated and 'observed' mass balances is shown in Figure 5.14 including the parameter uncertainty ranges. Simulated and observed annual mass balances are generally in good agreement (Table 5.6). Parameter uncertainty ranges in the Upper Aksu catchment are at 0.03–0.04 m weq. a^{-1} significantly smaller than the error of observations. This is not the case in the Upper Rhone catchment, where the parameter uncertainty range is 0.14–0.16 m weq. a^{-1} and comparable to the uncertainties of observations. This is due to the fact that Fischer et al. (2015) used higher resolution elevation data (25m, DHM25 and SwissAlti3d), while Pieczonka and Bolch (2015) relied on the SRTM3 DEM (90m resolution) and Hexagon KH-9 stereo data.

Glacier area changes over the simulation period 1970–2000 in the Upper Aksu and 1980–2010 in the Upper Rhone catchment are shown in Figure 5.15. They are not part of the calibration, but are compared to geodetic area change values from the literature. There is a good agreement in the Upper Aksu catchment where the parameter uncer-

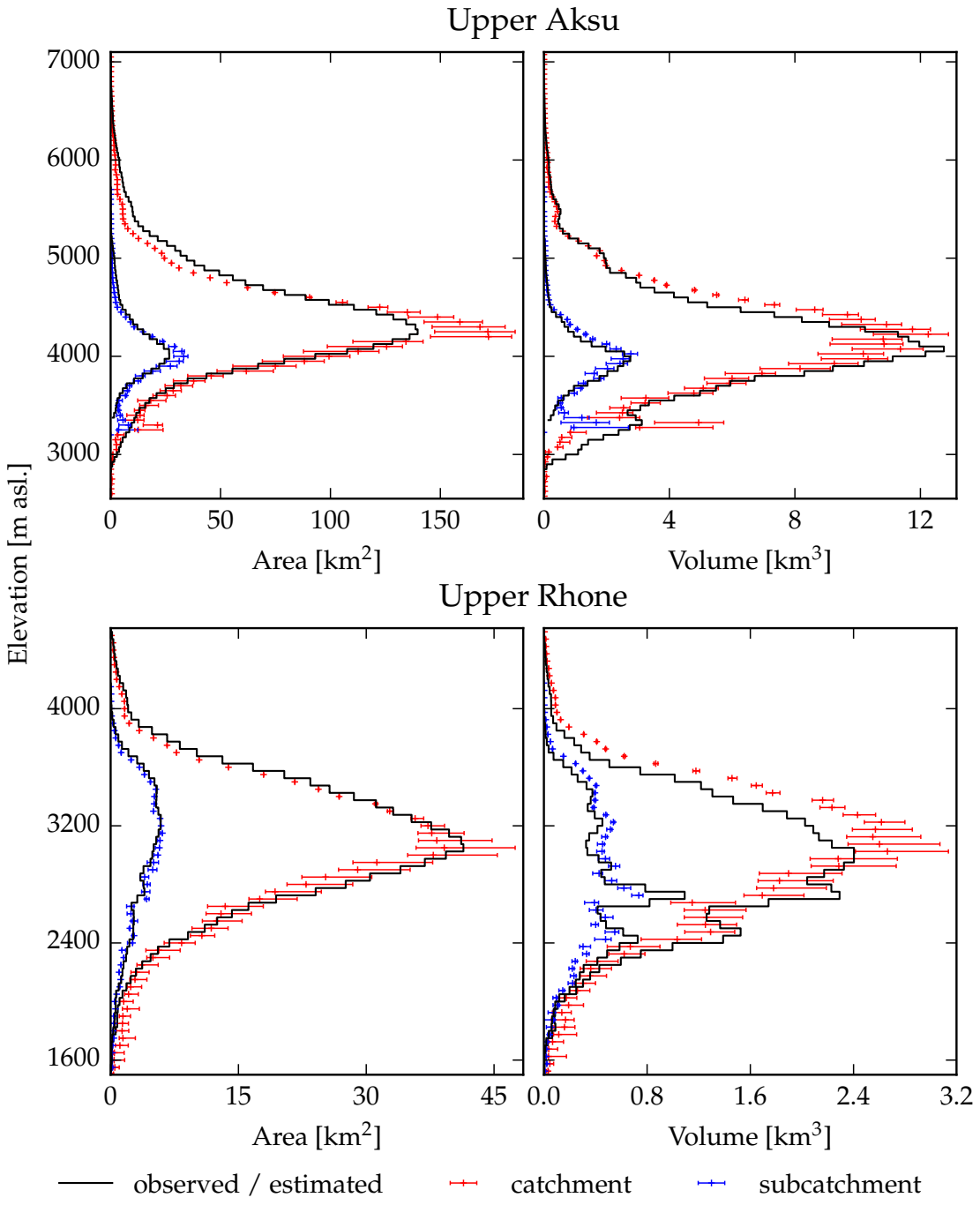

Figure 5.13: Initialised glacier area and volume hypsometry (i.e. distribution over 50m elevation zones). The catchment-wide hypsometry is shown with the subcatchments of the Sary-Djaz gauging station in the Upper Aksu catchment and the Blatten station in the Rhone catchment, which encompasses the Great Aletsch Glacier. Observed areas are taken from Pieczonka and Bolch (2015) in the Upper Aksu catchment and from Paul (2003). Volume estimations are based on modelled glacier thicknesses in the Upper Aksu catchment by Pieczonka and Bolch (2015) and in the Upper Rhone catchment by Linsbauer et al. (2012).

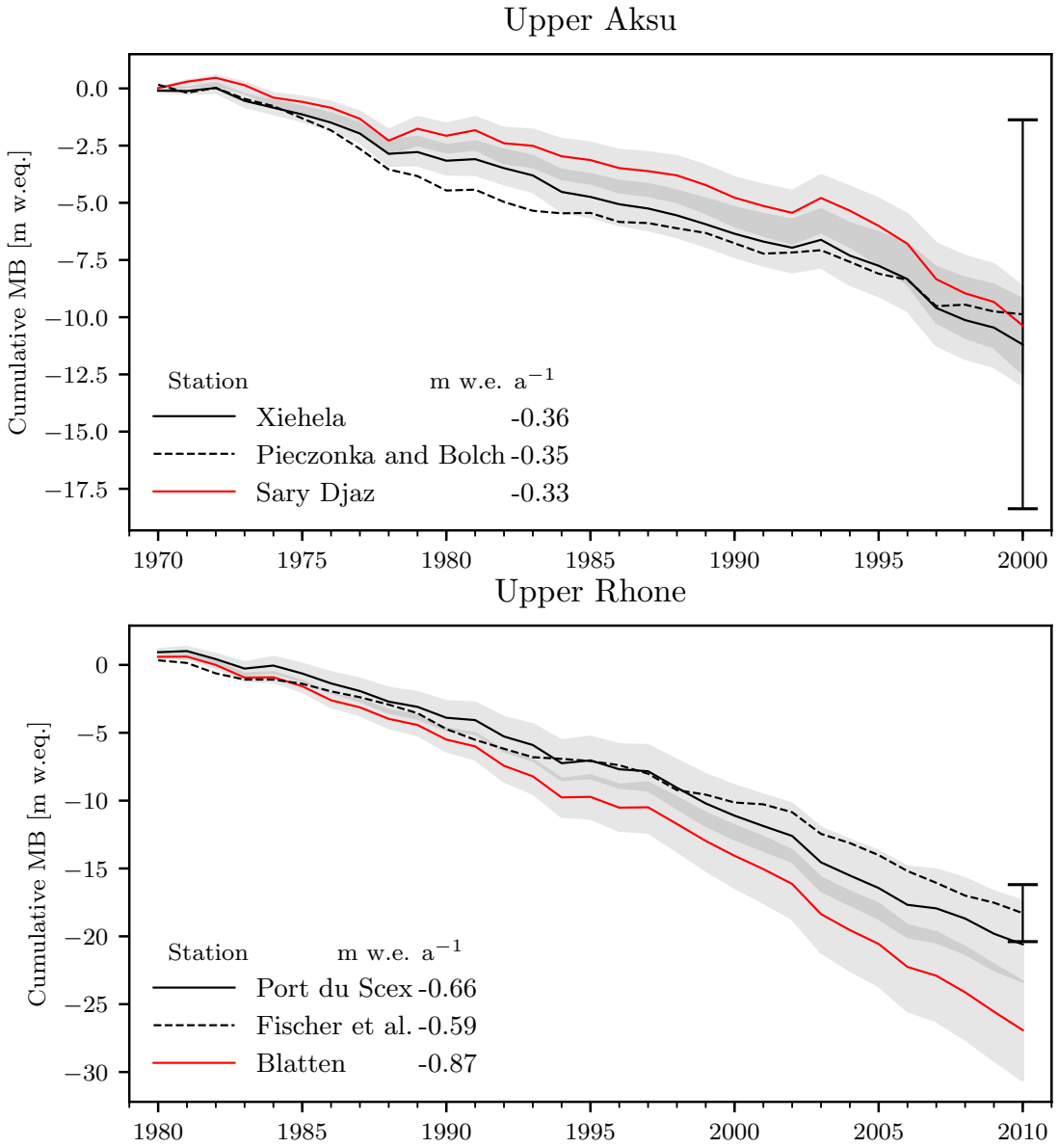

Figure 5.14: Median of simulated mass changes including ranges induced by the parameter uncertainty. The dashed black line shows the reference glacier mass balance scaled by the catchment-wide geodetic mass balance from the indicated studies including uncertainty bars from those studies. Note that the scaled/observed mass balance and the uncertainty bar (black) only refers to the entire catchment, i.e. the outlet station. Annual mean values over the simulation period are indicated in the legend.

tainty range fully overlaps the error range of the observations. In the Upper Rhone, the observed shrinkage is slightly higher, but the uncertainty ranges still overlap. The area changes in the much smaller Blatten catchment (Great Aletsch glacier) are significantly smaller than the catchment-wide values. This is in line with the catchment's mean ice

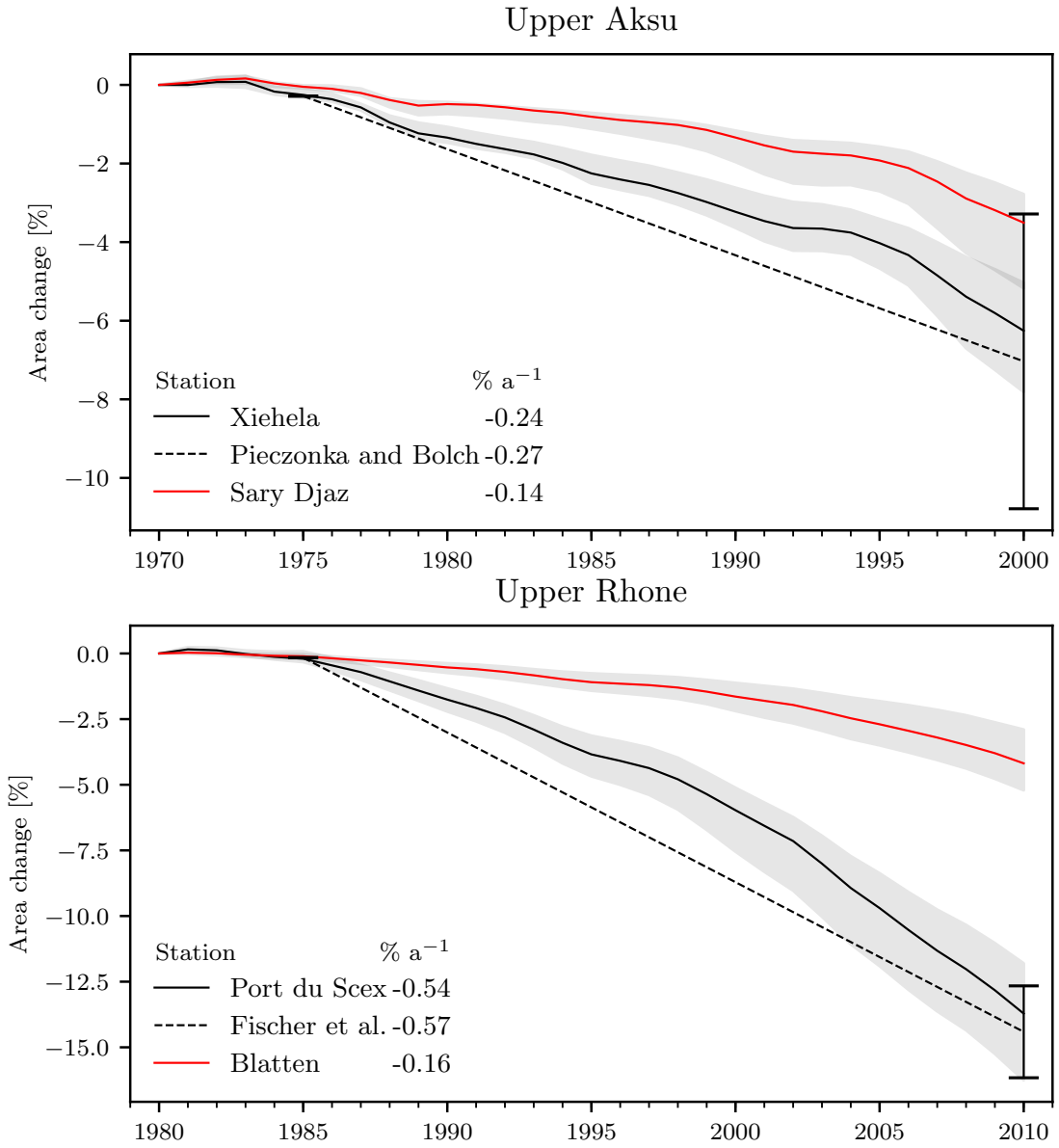

Figure 5.15: Median of simulated relative glacier area changes including ranges induced by the parameter uncertainty. The observed geodetic area changes from the indicated studies are shown by the dashed line with uncertainty ranges. Mean values over the simulation period are indicated in the legend.

thickness of 115 m Linsbauer et al. (2012) and large glacier tongue that make it less sensitive to area changes despite strong mass losses.

5.13.4 Annual water balance and long-term annual discharge

The hydrological effects of glacier changes are most evident in long-term river discharge. Trends in annual discharge may reflect changes in the glaciers' mass balance but also

reflect changes in precipitation. For example, Pieczonka and Bolch (2015) estimate that 20% of discharge increases in the Upper Aksu catchment are due to the glacier imbalance. Glacio-hydrological models are able to decompose those trends to understand changes in river discharge and project possible 'peak discharge' due to glacier decline.

Figure 5.16 shows annual runoff (annual discharge divided by catchment area) together with precipitation and glacier melt over the 30-year simulation period of the most glacierised catchments of both rivers terminated by Xiehela and Blatten station. Both show a good fit between observed and simulated discharge, including reproduced trends. However, comparing both catchments also exposes the data quality; the inter-annual variations are reproduced much better in the Upper Rhone and show some larger deviations in the 1990s in the Upper Aksu. This coincides with the decline in precipitation observations that contributed to the APHRODITE reanalysis set with the collapse of the Soviet Union.

Figure 5.16 also shows the annual precipitation and glacier melt distributed over the catchment area (not to be confused with mass balance, i.e. accumulation–melt over the glacier area). Both variables are the principal drivers of inter-annual variability of discharge, as their magnitudes are indicative of the year's weather. The increasing discharge in the Upper Aksu in the last 4 years is caused by both increasing glacier melt and precipitation, for example. Similarly, the increasing trend in discharge at the Blatten (Upper Rhone) station is driven by increasing glacier melt in the 2000s, while precipitation is generally lower than in the previous two decades (hence the strongly negative mass balances). Comparing glacier melt to discharge also highlights the importance of the glaciers in the catchment: The mean glacier melt to discharge ratio is 44% and 43% in the Xiehela and Blatten catchment respectively, although their glacierisation vary significantly with mean glacier coverage of 22% and 57%, respectively.

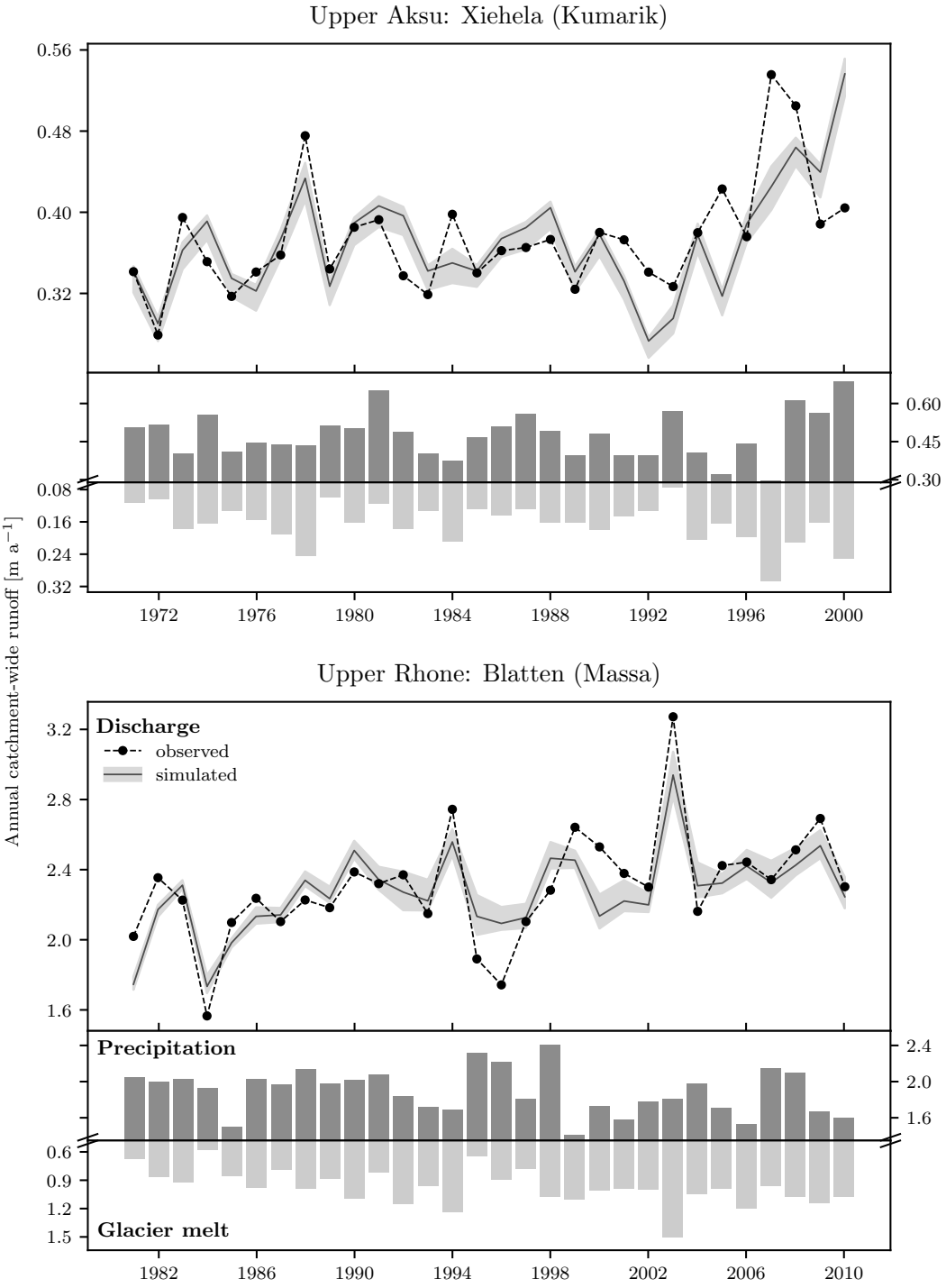

Figure 5.16: Simulated (median, min., max.) and observed mean annual runoff (station discharge divided by catchment area) of the Xiehela (Kumarik) and Blatter (Massa) catchments with annual precipitation and glacier melt distributed over the catchment area.

5.14 Calibration parameter sensitivity

In order to investigate the relative importance of the calibration parameters implemented in the model, the parameter sensitivity is indicated by the partial correlation of the parameter values with the objective functions using the results of the calibration runs. Although this assumes a linear relation between parameters objective functions, which is most likely not the case, it gives an indication of the strength of the relationship but without its characteristics. Stronger correlations indicate greater effects on the particular model result. Alternative approaches to sensitivity analyses include measures of result changes with only a single parameter changing or statistical tests on the distribution of the results (Hamby, 1994). The partial correlation coefficients between the calibration parameters and the four objective functions were calculated using the results of the 5000 calibration runs and averaged over both catchments.

Results show a generally lower correlation with the hydrological objectives (NSE and PB) than the glaciological objectives (Figure 5.17). This is due to the differences in implemented process complexity of simulated discharge compared to simulated glacier area and mass balance. A notable exception are the precipitation correction parameters, that were only used in the Upper Aksu catchment. They have a much stronger effect on discharge than, for example, the potential evaporation correction or the snow and glacier melt factors.

The glacier area objective function is most strongly affected by the snow Degree-Day factor, the melt temperature and the temperature lapse rate. In addition, the mass balance objective is strongly correlated to the residual mass balance during initialisation and the glacier Degree-Day factor. The residual mass balance is implemented to create the mass balance equilibrium during initialisation and has thus by definition a strong control over subsequent mass balances.

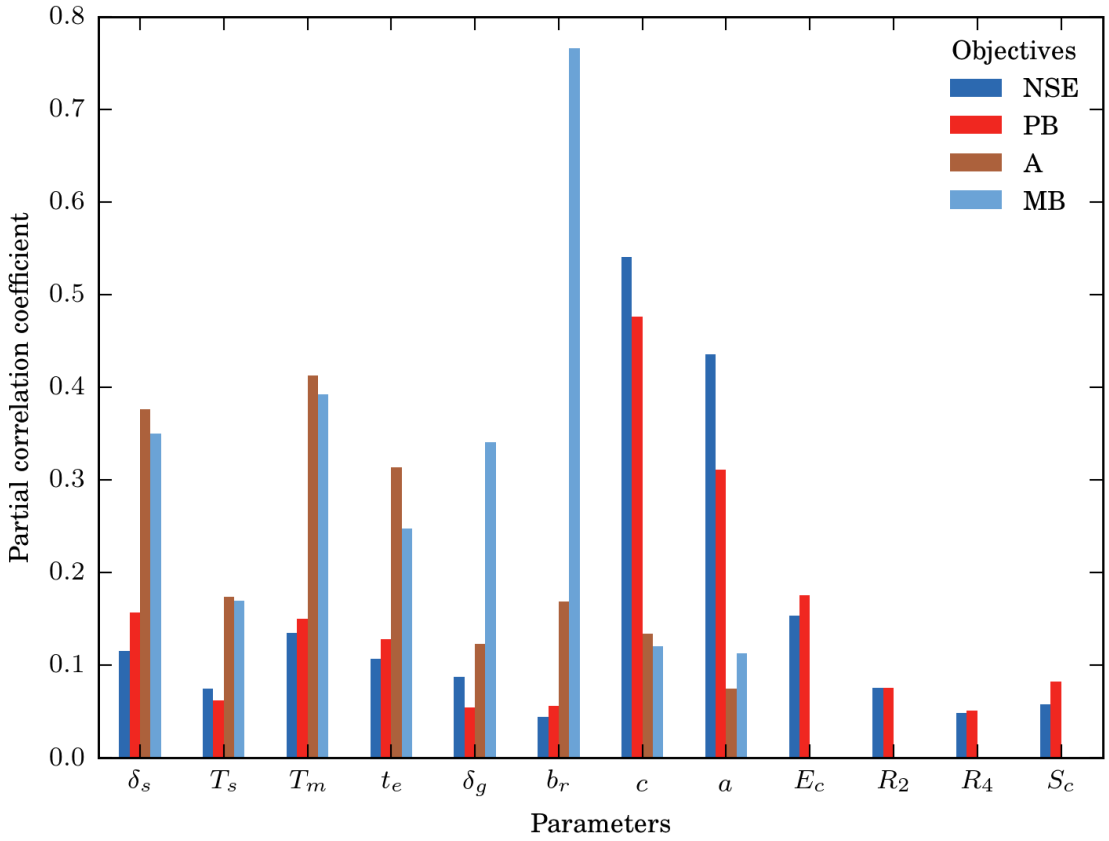

Figure 5.17: Calibration parameter sensitivity with regard to the four objective functions: Nash-Sutcliffe Efficiency (NSE), percentage bias in the water balance (PB), RMSE of the initialised glacier area hypsometry (A) and the RMSE of annual mass balance (MB). The parameters are (further details given in Table 5.2 and Table 5.5): δ_s (Snow Degree-Day factor), T_s, T_m (Snow fall and melt threshold temperatures), t_e (Temperature lapse rate), δ_g (Ice Degree-Day factor), b_r (Residual mass balance during initialisation), c and a (Maximum precipitation correction factor and maximum precipitation gradient, both only applied to the Aksu catchment), E_c (evaporation correction factor), R_2, R_4 (routing coefficients) and S_c (saturated conductivity correction). The partial correlation coefficient of the parameters over the 5000 calibration runs were averaged over all catchments. As the parameters E_c, R_2, R_4 and S_c have no impact on A and MB, the coefficients were excluded here.

5.15 Numerical stability with varying unit sizes

The stability of the model results was tested by setting up the model for the Upper Rhone catchment with three different sets of values for the minimum area, the contour interval of valleys and hillslopes. The initial values were decreased and increased by factors of 0.5 and 1.5 to produce two additional model setups (Table 5.7). The resultant unit counts are roughly half and double the initial counts and the mean unit area is halved

and nearly doubled. A single parameter set was chosen out of the calibration ensemble that is close to the median values of all objective functions, and used throughout the analysis.

The main model results remain largely stable across the three model setups and variability is within the calibration uncertainty range (Table 5.7 and figs. 5.18 and 5.19). Overall, the larger units lead to a slightly larger initialised area than the smaller units (4%), while the volume is marginally lower (2%). Similarly, glacier area recession over the 30 year simulation period is also higher with the larger units, but mass changes are only slightly different (Figure 5.19). The increase in area shrinkage with increased unit sizes may be due to the greater reliance on the fractional area representation when units become partly glacierised. They are then assumed to be glacier termini and are subject to frontal melting.

Table 5.7: Statistics of the three Upper Rhone model setups to investigate the numerical stability with changing unit sizes.

		smaller	same	larger
Glacier unit parameters				
valley contours	m	15	30	45
slopes contours	m	100	200	300
min. area	km^2	0.05	0.10	0.15
Glacier unit statistics				
count		25053	12179	7745
mean area	km^2	0.16	0.33	0.52
std. area	km^2	0.11	0.24	0.41
Summary results				
initial. area	km^2	692	712	721
mean Q	$m^3 s^{-s}$	193.11	194.33	194.57
area change	% a^{-1}	-0.34	-0.37	-0.43
mass balance	m w.e. a^{-1}	-0.74	-0.72	-0.70

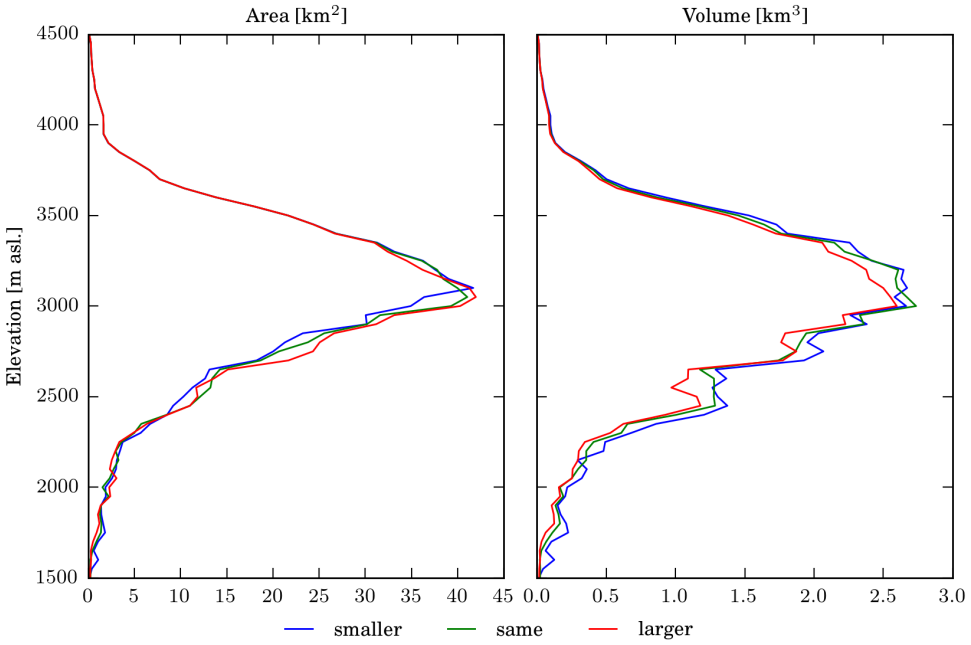

Figure 5.18: Initialised glacier area and volume hypsometry for the Upper Rhone catchment for three different glacier unit configurations. See Table 5.7 for details.

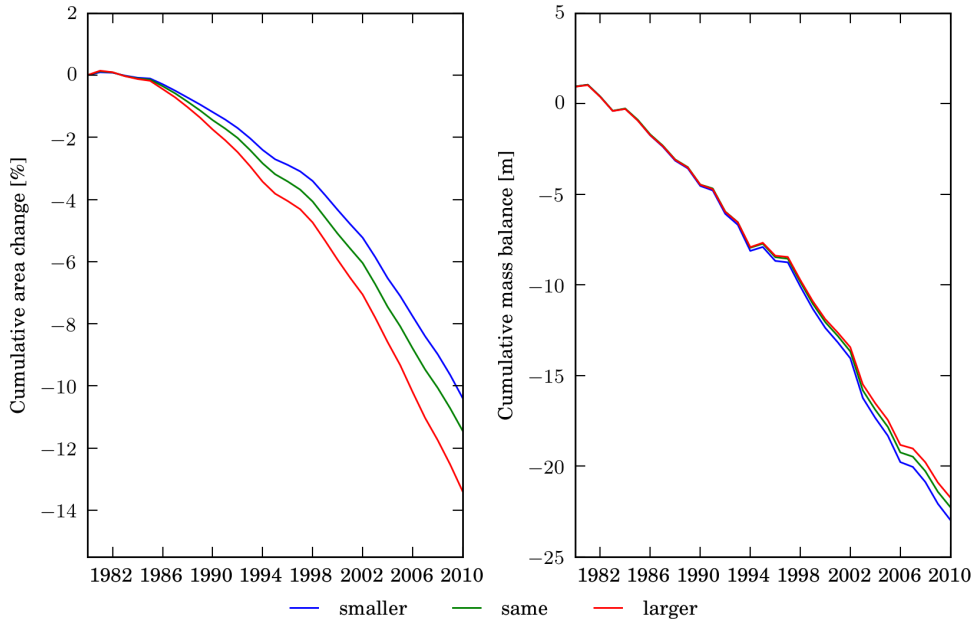

Figure 5.19: Glacier area and cumulative mass balance over the period 1980–2010 for the Upper Rhone catchment for three different glacier unit configurations. See Table 5.7 for details.

5.16 Comparison to other studies and limitations

SWIM-G, the model presented here bridges the gap between semi-distributed, empirical glacio-hydrological catchment models and fully distributed and more physically based models for small scales. It includes a representation of individual glaciers on the catchment scale without being computationally too demanding and excessively precise. The model integrates ice flow over the spatially adaptive glaciological response units, avoiding computationally expensive finite difference schemes such as those used by Clarke et al. (2015). It represents glacier dynamics of individual glaciers as distributed glacio-hydrological models have done, such as Naz et al. (2014) and Immerzeel et al. (2011), but can do so for much larger catchments at an intermediate resolution appropriate for the catchment hydrology. Previous semi-distributed or empirical approaches to bridge this scale gap such as Uhlmann et al. (2013) and Huss et al. (2010b) have made important advances in this regard, yet do not include a process-based description of glacier dynamics on an individual glacier basis. Some other important glaciological or hydrological processes (e.g. debris cover, sublimation, reservoirs) are so far also missing in these or similar models. While more physically-based (Clarke et al., 2015; Naz et al., 2014) approaches exist, the scope of the model presented here lies in larger catchments, where those approaches fail due to their data and computational requirements.

Hydrological modelling of larger glacierised catchments is plagued with data scarcity, often yielding results with high uncertainty. However, recent advances in glaciological remote sensing (Fischer et al., 2015; Gardelle et al., 2012; Pieczonka and Bolch, 2015), in the modelling of climatic parameters (e.g. Immerzeel et al., 2015; Maussion et al., 2014) and the increasing availability of glaciological baseline data have helped to overcome some of these data gaps. More glacier outlines, mass balance and glacier thickness data from the global terrestrial network for glaciers (www.gtn-g.org) and other databases have become available to modellers. The model presented here attempts to incorporate these advances, while keeping the driving data to a minimum. It is calibrated not only to measured discharge, but also to glacier distribution and observed mass balance. A larger number and more diverse observations constrain the parameter ranges greatly, which is especially important for those parameters with the largest effects on discharge, i.e. precipitation correction and glacier melt. The multi-objective calibration

reduces the overall uncertainty of discharge simulations in mountainous catchments with insufficient observations. This contributes to other recent studies concerned with data scarcity, such as using remotely sensed snow cover data in conjunction with discharge (Duethmann et al., 2014), the output of regional climate models as weights for a discharge-based precipitation correction (Duethmann et al., 2014) or a precipitation correction solely based on a glacier equilibrium assumption (Immerzeel et al., 2012). Thus, the glacier dynamics module integrated into the hydrological model SWIM and the multi-objective calibration procedure are well adapted to data-scarce catchments with various kinds – yet limited – observations.

Another approach to overcome the data scarcity and to also formulate a comprehensive representation of glacier processes is the use of expert parameters, i.e. those that are only constrained by expert knowledge, empirical values or point-based measurements (also known as soft information) (Winsemius et al., 2009). For example, the ratio of energy consumed by sublimation or the debris concentration in glaciers are constrained by values reported in the literature that are transferred to the catchments' climates. Similarly, the thresholds used for the spatial disaggregation (elevation zone interval, hillslope threshold, cleaning threshold) are empirical values and depend on the desired level of detail. These parameters are difficult to calibrate because they have little or indirect influences on the calibration objectives and may be easily compensated for by other more dominant parameters (Refsgaard, 1997). They are mostly unique to a particular catchment but constrained by ranges reported in the literature or by model results that are not part of the calibration. While using these parameters leads to a high risk of parameter equifinality and may seem like excessive complexity with high uncertainty (Beven, 2006a), they are intended to make the model more robust on longer time scales (i.e. 30 to 100 years) and physically more complete than other empirical and conceptual models of mountain hydrology (Merz et al., 2011). The use of expert parameters allows the scarce information about not systematically observed processes to be included in the modelling, a type of parameter upscaling (Blöschl and Sivapalan, 1995) that is warranted where little to no data exists (Dornes et al., 2008; Krogh et al., 2014). In cases where more observations of driving variables exist, the model could be extended to more physically based approaches of glacier processes, such as calculating the full energy

balance for ablation or the inclusion of an explicit glacier sliding term (e.g. Wertman's sliding law in Immerzeel et al., 2011). However, this would only yield better results if reliable driving data for these approaches (radiation, humidity etc.) are available and can be spatially distributed over the entire catchment.

An important process considered in the model is the evolution of debris cover in response to glacier mass changes. This introduces a much discussed negative feedback into modelling of glaciers under climate change, i.e. the increased shielding of ice as glaciers retreat (Kirkbride and Deline, 2013; Scherler et al., 2011). The implementation here is a starting point for a more general treatment of debris on glaciers because so far the model only considers the relative effect of a negative mass balance on melt rates while absolute debris thicknesses are unknown at the catchment scale. The approach could be further developed by initialising debris cover along with the ice cover, effectively modelling debris thickness that could be verified against point observations. However, this would require finding a debris equilibrium between debris production and fallout rates. Although several processes governing debris production and deposition are understood (e.g. Hambrey et al., 2008), they have not been systematically described and the implementation has just started (e.g. Rowan et al., 2015) and requires further research. The influence of ice cliffs or supraglacial lakes on glacier melt was also not considered although they occur frequently on debris-covered glaciers (Cuffey and Paterson, 2010; Juen et al., 2014). These hot spots of glacier melt may be significant on some glaciers but are of lesser importance than the shielding effect of debris cover (Juen et al., 2014; Sakai et al., 1998; Sakai et al., 2000). It is nearly impossible to predict their occurrence, persistence and size at a catchment level as they are mostly erratic features. Similarly local processes that are also not considered are wind drifted snow, aerosol deposition and glacier surges. The limited influence of these processes on the catchment hydrology and glacier evolution clearly does not justify the difficulties of implementation and the added uncertainties. However, testing and including more debris processes may be part of future additions to the model.

The successful validation in the two case study catchments has shown that SWIM-G is transferable to a range of glacierised catchments. This is especially due to the following four aspects: a) the adaptive and cross-scale spatial disaggregation, b) the process-based

and comprehensive process implementation, c) the flexibility in required driving data with emphasis on data scarcity as well as d) the wide applicability of the hydrological model SWIM. Its primary purpose will be to serve as a tool for integrated climate change impact assessments of glaciological and hydrological changes, making use of climate change scenarios, such as the scenario ensembles of CMIP5 (Taylor et al., 2011) of global climate models or regional scenarios from the CORDEX initiative (Giorgi and Gutowski, 2015).

5.17 Summary

A new catchment-wide glacier model was developed and integrated into the hydrological model SWIM (SWIM-G). It covers most glacier processes relevant to simulating catchment discharge including glacier dynamics, debris melt-out and sublimation. This ensures robustness over long timescales and a range of climatic and glaciological settings, although it was primarily developed for data-scarce catchments of High Asia. The new approach to representing individual glaciers and their ice dynamics in a hydrological model bridges the gap between distributed, physically based glacier dynamics models – that are typically only applicable to single glaciers or small glacier groups – and large-scale empirical glacio-hydrological models. This allows for accurate and integrated glaciological and hydrological assessments of entire, highly glacierised catchments. The intermediate complexity enables ensemble modelling approaches for calibration and scenario analysis by radically reducing computing time compared to fully distributed glacier models.

SWIM-G was implemented and validated in a data-scarce catchment in Kyrgyzstan/NW China and a data-abundant catchment in Switzerland. The calibration yielded good results compared to both discharge and glaciological observations, but performance depends on data quality – precipitation observations in particular. The model was automatically calibrated using a multi-objective evolutionary optimisation that is widely used in hydrological modelling. The parameter uncertainty is comparable to uncertainties of glaciological observations (e.g. glaciological or geodetic area and mass balance observations) but may become large over longer simulation periods due to the variable initialisations. In data-scarce catchments, the model highlights the need for precipita-

tion correction and is able to inform the method of correction by initialising ice cover and calibrating the model using discharge, glacier distribution and glacier mass balance in the multi-objective calibration procedure. The model helps to prevent overestimations of glacier melt in-lieu of negative biases in precipitation observations that are ubiquitous in mountainous catchments. The application to the arid Upper Aksu catchment shows that adequately simulating glacier dynamics (including accurate rates of accumulation and ablation) is vital to properly model this and similar river basins due to their high contribution of glacier melt to discharge. The intermediate complexity of the developed glacio-hydrological model means that it is well adapted to large, partially glacierised and data-scarce catchments, as they are often found in High Asia and other mountain ranges of the world. Its main purpose is to serve as a model for long-term glacio-hydrological climate change impact assessments of IPCC scenarios for the 21st century, as will be shown in Chapter 7.

Chapter 6

Implementation of SWIM-G to the Tarim headwaters with a glacier consistent precipitation correction

6.1 Introduction

After the glacier dynamics module for the Soil and Water Integrated Model (SWIM) was developed and validated in Chapter 5, it is here implemented to all five headwater catchments of the Tarim River and calibrated to both discharge and glacier cover. The catchments and their limited databases were introduced in Chapter 3 with a particular focus on the quality of precipitation datasets. The calibrated model is used in this chapter to provide a better estimate of annual precipitation that is both consistent with hydrological and glaciological observations. The following research questions are addressed:

1. How well does the SWIM-G model reproduce hydrological and glaciological observations over the reference period in the data-scarce Tarim headwaters?

2. How can the glacio-hydrological model inform the correction of precipitation data by using inverse modelling, as previously tested in other high mountain catchments?

3. What is the simulated mean catchment precipitation and how does it compare to other precipitation datasets?

The chapter begins with a description of the model implementation and a summary of the input data that were discussed in Chapter 3. It continues with the calibration strategy and the precipitation correction method in Section 6.3 and Section 6.4, respectively. The calibration results of discharge and glacier cover are then presented (Section 6.5) and the results of the precipitation correction in the following section (Section 6.6).

6.2 Model implementation

The SWIM-Glacier dynamics (SWIM-G) model was set up for five headwater catchment of the Tarim River in the same way as the Upper Aksu River model described in Chapter 5. The catchments were described in detail in Chapter 3 along with the available data, so the input data is only summarised here with an overview provided in Table 6.1. The hole-filled, 90 m SRTMv3 (Jarvis et al., 2007) Digital Elevation Model (DEM) is used to delineate the catchments, subbasins and the glacier units as well as to derive relevant topographic information for these units. 1287 subbasins were delineated with a mean subbasin size of 88.3 km^2. The subbasin map is shown in Figure 6.1 and the size distribution is shown in Figure 6.2. To delineate the glacier units, a glacier area was chosen by applying the lower elevation boundaries of the observed glacier cover minus an extra 300m to the DEM (2500 m asl). This glacier area covers 78% of the catchment area with 92893 glacier units (107691 hydrotopes over the entire catchment area). The glacier unit size distribution is shown in Figure 6.3 with a mean area of 0.96 km^2.

The hydrotopes were constructed using the subbasin, soil and land cover map, with the most common class of the latter two maps assigned to the glacier units. The soil map and information were taken from the Harmonised World Soil Database (HWSD, FAO et al., 2011), which includes the relatively high resolution Chinese Soil Map (1:10^6)

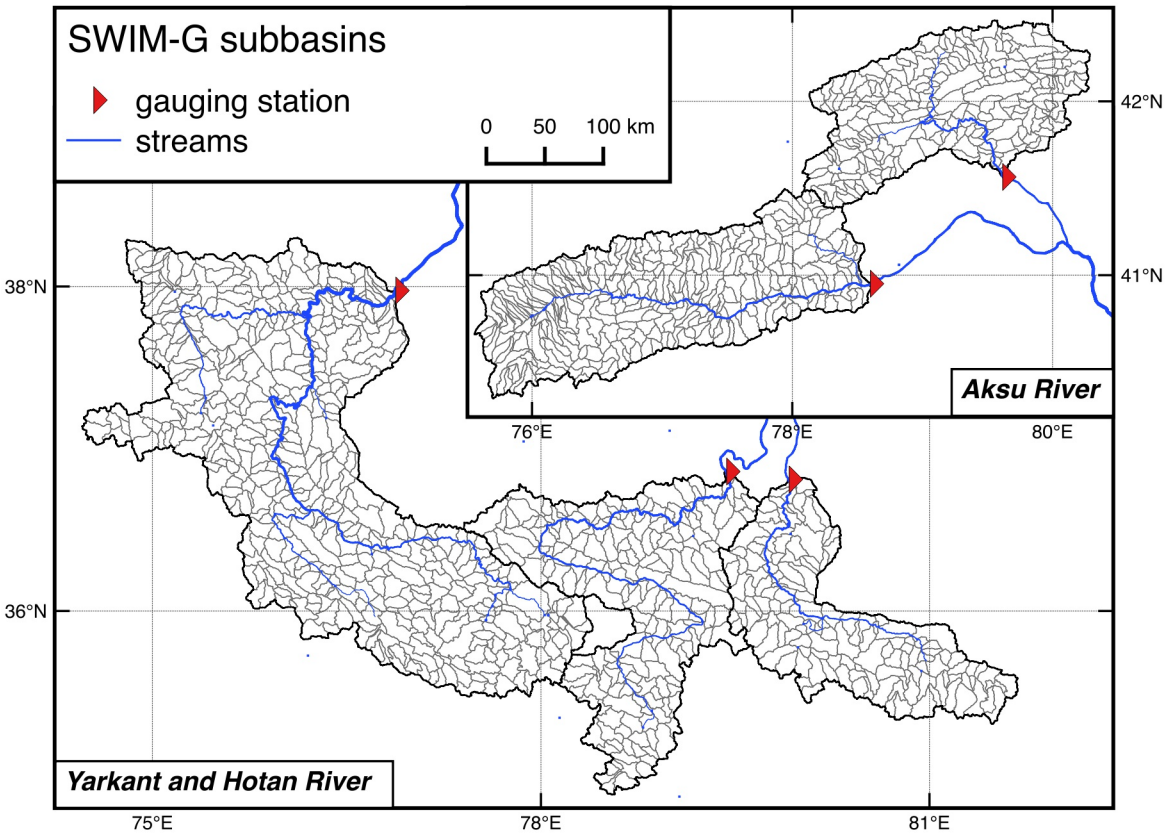

Figure 6.1: Map of the delineated subbasins for all five headwaters including outlet stations and streams.

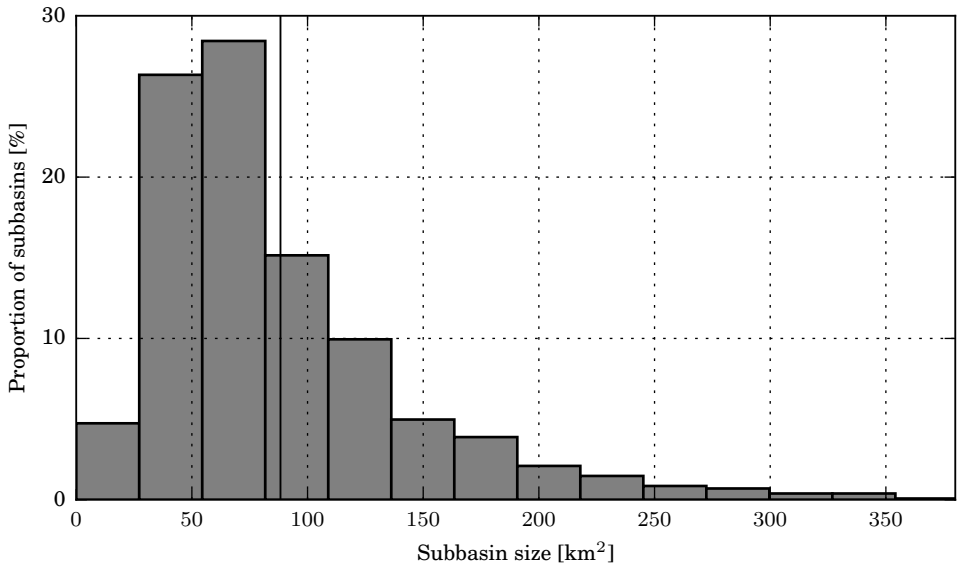

Figure 6.2: Subbasin size distribution (n=1287) of the SWIM-G model for all five headwaters. The mean value is indicated by a vertical line.

Table 6.1: Input data used to drive SWIM-G and to calibrate/validate the model. Climate variables are: temperature T (mean, min., max.), precipitation P, radiation and relative humidity.

Data	Source
Climate	WATCH (Weedon et al., 2011) for temperature (mean, min., max.), radiation and relative humidity
	AHPRODITE (Yatagai et al., 2012) for precipitation
Topography	SRTM hole-filled digital elevation model at 90m resolution (Jarvis et al., 2007)
Land cover	Chinese Meteorological Administration for Chinese part, MODIS 500 m land cover (2001) (Friedl et al., 2002) for Kirghiz part, reclassified to SWIM land cover classes
Glaciers	Glacier inventory based on Landsat TM and ETM+ data generated within the SuMaRiO project (www.sumario.de) (Osmonov et al., 2013; Pieczonka and Bolch, 2015 and unpublished data)
Soil	Harmonised World Soil Database (FAO et al., 2011), includes the $1{:}10^6$ soil map for China
Discharge	Daily river discharge at 5 gauges from Chinese hydrological year books (Wang, 2006) for the period 1964-87 (with some gaps)

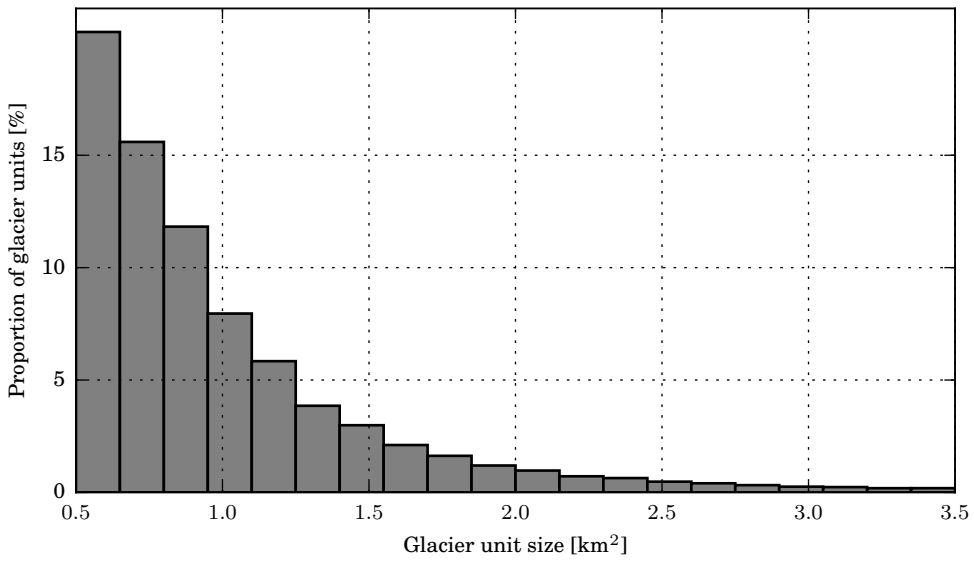

Figure 6.3: Glacier unit size distribution (n=92893) of the SWIM-G model for all five headwaters, with a mean and maximum size of 0.96 km^2 and 3.48 km^2, respectively. The minimum area size is constraint by the aggregation threshold to 0.50 km^2.

with full particle size distributions (Shi et al., 2004), resulting in 24 soil classes. The land cover map of China was provided by the Chinese Meteorological Administration (CMA) for the year 2000 and supplemented by the MODIS 500m Land Cover (MCD12Q1, Friedl et al., 2002) for the year 2002 for parts of the catchment outside of China.

The model was driven by the APHRODITE precipitation dataset (described in Section 3.3.1) and the WATCH forcing data (Weedon et al., 2011) for temperature (daily mean, minimum, maximum), radiation and relative humidity. The gridded driving data were interpolated to the subbasin centroids using inverse distance weighted interpolation (IDW) at the preprocessing stage. At model runtime, temperature is lapsed to the hydrotope elevation using a calibration parameter (see Section 6.3) and precipitation is corrected to the same elevation according to the approach described in Section 6.4.

6.3 Model initialisation and calibration

The model was calibrated using a multi-objective automatic optimisation, considering observed discharge at the five outlet gauging stations, observed glacier area and mass balances, where they were available. A calibration run consisted of the glacier initialisation and a full hydrological run over the reference period 1971–2000. The reference period was chosen because daily discharge data were only available for the 1970s and 1980s for most stations (with 1–4 years missing) and the geodetic mass balance analysis for the Aksu catchment by Pieczonka and Bolch (2015) is for the period 1975–2000. The calibration of the Aksu catchments was supported by these recent findings of catchment-wide glacier mass balances.

However, since catchment-wide mass balances or representative local mass balance records for the Hotan and Yarkant catchments were not available, three initial mass balance scenarios were used and compared to regional research findings (see Section 6.5.1). The mass balance scenario range also contributed to the model uncertainty.

The model's calibration parameters were described in Section 5.11. In comparison to the calibration in Chapter 5, two parameters were left out due to parameter redundancy: The snow fall threshold temperature T_s was found to correlate strongly with the temperature lapse rate and was thus kept constant at 0 °C. The routing coefficients

R_2 and R_4 were combined to $R_{2,4}$ and set to equal values. The complete list of used calibration parameters is given in Table 6.2 with ranges specific to the five headwater catchments.

Glacier dynamics models need to be initialised over typical equilibrium time frames (200–1000 years) in order to ensure consistency between driving data, model structure and ice cover (Clarke et al., 2015; Marshall et al., 2011). The model here was initialised over 300 years and the resultant glacier cover is compared to the observed glacier inventory. The fit of the ice hypsometry in each catchment was used to match the ini-

Table 6.2: Calibration parameters and ranges used for the multi-objective calibration. Where different ranges were used, they are differentiated for either the Aksu or the Hotan and Yarkant catchments.

Parameter / description		Range	Unit
Precipitation			
c	Maximum correction factor	a) 1 – 6	
		b) 1 – 15	
a	Maximum precipitation gradient	0.1 – 0.9	%/100m
m	Maximum precipitation altitude	4000 – 7000	m asl.
Snow and glaciers			
δ_s	Snow Degree-Day factor	a) 2 – 7	$\mathrm{mm\,K^{-1}\,d^{-1}}$
		b) 1 – 5	
T_m	Snow melt threshold temperature	0 ± 3	°C
t_e	Temperature lapse rate	-0.80 – -0.55	°C/100m
δ_g	Ice Degree-Day factor	a) 6 – 14	$\mathrm{mm\,K^{-1}\,d^{-1}}$
		b) 2.5 – 7	
Γ	Proportion of energy	a) 0.2 – 0.6	
	consumed by sublimation	b) 0.4 – 0.9	
b_r	Residual mass balance	a) 0 ± 0.34	$\mathrm{m\,weq.\,a^{-1}}$
	during initialisation	b) -0.1 / 0 / +0.1	
Hydrology			
E_c	Potential evaporation correction	0.7 – 1.3	
$R_{2,4}$	Routing coefficients	1 – 20	
S_c	Saturated conductivity correction	0.1 – 2	

a) Aksu catchments, b) Hotan and Yarkant catchments

tialised glacier area to the observed, through the calibration of all parameters affecting the glaciers. It was quantified by the χ^2 objective function for histogram comparison between the two hypsometries as follows:

$$\chi^2 = \sum \frac{(A_{s,i} - A_{o,i})^2}{A_{s,i} + A_{o,i}} \cdot 100 \tag{6.1}$$

with observed A_o and simulated A_s glacier area for the 50-meter elevation band i, expressed as percent. It ensures good fit also at the tail ends of the hypsometries due to the sum of observed and simulated areas in the denominator. The χ^2 was calculated for each glacier group of the catchment and weighted by the observed glacier area in each group.

As described in Section 5.11.1, the initialisation requires a climate period with known, quasi-stable mass balance conditions that is representative for the observed glacier cover. Although glaciers are never in a perfect equilibrium state, glaciers are globally identified as having stable conditions between the 1960s and the mid-1970s (Dyurgerov, 2010). This is also true for the Tien Shan (Farinotti et al., 2015; Sorg et al., 2012). However, historic observations are limited for Kunlun Shan and Karakoram. Recent findings based on declassified satellite imagery indicated that glaciers in the Karakoram have been stable or showed only slight mass loss since the 1970s until today (Bolch et al., 2017; Zhou et al., 2017). Dyurgerov (2010) provided 'best-guess' regional glacier mass balances since the 1960s for all major glacier regions. For the initialisation period between 1960–1975, mean mass balances of $-82\,\mathrm{mm\,weq.\,a^{-1}}$ were given for the Tian Shan, $-37\,\mathrm{mm\,weq.\,a^{-1}}$ for the Tibetan Plateau, $176\,\mathrm{mm\,weq.\,a^{-1}}$ for the Karakoram and $-52\,\mathrm{mm\,weq.\,a^{-1}}$ for the Pamir. While these values should be used as guidelines only, as they mostly originate from single glaciers, they show mass balances less negative than the global mean of $-330\,\mathrm{mm\,weq.\,a^{-1}}$ in the period 1976–2005 (Zemp et al., 2009). This imbalance was corrected for by the residual mass balance term that was calibrated in the Aksu catchment, where mass balances estimates existed, and prescribed in a scenario approach in the Hotan and Yarkant catchment where they were absent.

Pieczonka and Bolch (2015) provide a catchment-wide mean mass balance including uncertainty range for the Xiehela (Aksu) catchment for the period 1975–2000. Due to their proximity and topographical similarities, these average values were also used in the neighbouring Shaliguilanke catchment. The objective function for the automatic calibration assigns a score between 1 (worst) and 0 (exact match) based on the normal distribution probability function using the mass balance as mean value and the uncertainty range as standard deviation. It is defined as follows:

$$\mathrm{MB}_i = 1 - \exp\left(-\frac{(\overline{b_s} - \overline{b_o})^2}{\varepsilon^2}\right) \tag{6.2}$$

where $\overline{b_o}$ is the mean annual mass balance over the study period by Pieczonka and Bolch (2015) ($-0.35\,\mathrm{m\,weq.\,a^{-1}}$) with an uncertainty range of ε ($\pm 0.34\,\mathrm{m\,weq.\,a^{-1}}$) and the simulated mass balance $\overline{b_s}$ over the same period. The Hotan and Yarkant catchments were calibrated for three initial mass balance scenarios of $+0.1, 0, -0.1\mathrm{m\,weq.\,a^{-1}}$, with the simulated mass balances results discussed in Section 6.5.1 and more recent mass balance studies in Section 6.5.1. These values are guided by the 'best-guess' values mentioned above. The $0.1\,\mathrm{m\,weq.\,a^{-1}}$ max./min. values represent about 30% of the expected catchment precipitation and nearly twice as much as is recorded in the APHRODITE data. A mass balance outside of that range would mean a strong glacier imbalance that has not been observed elsewhere in High Asia during the 1960s and 1970s and was thus considered unlikely.

In addition to the simulated glacier dynamics, the catchment hydrology was calibrated to the available discharge records from the five outlet gauging stations (described in Section 3.2). The hydrological performance was measured by one objective function for the daily discharge and a second objective function for annual discharge. The first objective function applied to daily discharge is a combination of the standard and logarithmic Nash-Sutcliffe Efficiency (NSE, Nash and Sutcliffe, 1970) to optimise both the summer peak discharge but also the winter low flows. The logarithmic NSE was included to prevent the strong summer peaks from receiving the greatest weight in the common NSE measure, as was recommended by Duethmann et al. (2014, 2015). The objective function is given by the following equation:

$$\mathrm{NSE}_c = \frac{1}{2}\left(2 - \frac{\sum (Q_s - Q_o)^2}{\sum (Q_o - \overline{Q_o})^2} - \frac{\sum (\log Q_s - \log Q_o)^2}{\sum (\log Q_o - \log \overline{Q_o})^2}\right) \tag{6.3}$$

with observed Q_o and simulated Q_s daily mean discharge and the observed long-term average $\overline{Q_o}$. As Schaefli and Gupta (2007) note, it is relatively easy to calibrate a model to high NSE values in strongly seasonal catchments. That is, the NSE is a relative performance measure that allows comparison in the same catchments or between catchments of the same climatic region but not to those with a less pronounced seasonality. Reported NSE values should thus not be interpreted in absolute terms. The even years of the available data were used for calibration and the odd years were used to evaluate NSE_c for validation (split-sample approach). This reduces the impact of changes in the quality of the precipitation data that were evident in the 1980s.

A second objective function using the annual discharge was used to also optimise the model to the annual water balance and the inter-annual variability. This was done through a simple root mean square function as described by:

$$\mathrm{RMSE}_{QA} = \frac{\sqrt{(QA_s - QA_o)^2}}{\overline{QA_o}} \cdot 100 \tag{6.4}$$

with squared residuals between observed QA_o and simulated QA_s annual mean discharge weighted by the observed long-term average discharge $\overline{QA_o}$ expressed in percent.

The S-Metric-Selection Evolutionary Multi-Objective Optimisation Algorithm (SMS-EMOA) (Beume et al., 2007; Emmerich et al., 2005) was employed here to optimise the four objective functions using the twelve calibration parameters listed in Table 6.2. The algorithm successively finds Pareto optimal solutions out of a parameter set population of 100 'individuals' by optimising the hypervolume enclosing the space of dominated (not Pareto-optimal) solutions. Its advantage over other commonly used multi-objective optimisation algorithms (e.g. NSGA-2) is the preference for solutions well spaced out on the Pareto front, rather than clustering many solutions over smaller parts of the front. It has been used successfully in hydrological modelling studies with similar multi-criteria problems before (Ficklin et al., 2014; Stagge and Moglen, 2014).

The model was optimised for each of the five catchments individually and run for a population of 100 in parallel on a large computer cluster over 100 generations. Satisfactory convergence results were attained after 50–70 generations, i.e. 5000–7000 model runs. The remaining 'Pareto-optimal' solutions were inspected and the following minimum criteria were defined: a) a NSE_c of at least 0.6, b) a $RMSE_Q A$ less than 25%, c) a χ^2 less than 20% and d) a MB likelihood lower than 0.1 (only in the Aksu catchments). These criteria were used to filter out solutions at the edges of the Pareto-front. The remaining count out of 100 will be reported in the results along with median values from all remaining ones.

6.4 Precipitation correction

Where meteorological information has to be extrapolated over great distances both horizontally and/or vertically, a method to correct for orographic precipitation is paramount to the accurate modelling of both the glaciers and the catchment hydrology (Immerzeel et al., 2014; Stisen et al., 2012). Glacio-hydrological models have proven useful tools in finding accurate correction factors and gradients with elevation when a near-glacier equilibrium is assumed or mass balances are known (Immerzeel et al., 2015; Immerzeel et al., 2012).

Most studies used linear gradients to vary precipitation with elevation over a complex terrain with typical ranges of 0.05–0.5 $\% \, m^{-1}$ (Hock, 2005; Immerzeel et al., 2014; Sevruk and Mieglitz, 2002). However, representing variance of precipitation as a linear function of elevation is inherently local, highly variable over varying altitude ranges and generally unsuitable for elevations below the reference altitude, as precipitation would diminish to 0.

In this thesis, precipitation was corrected by a non-linear function of altitude taking account of varying gradients and an eventual decrease at very high elevations. The correction factor f_c described by Equation (6.5) and plotted in Figure 6.4 remains close to 1 over lower laying elevations for which observations are available, but increases exponentially up to a maximum gradient a [$\% \, m^{-1}$]. It then reduces the gradient until a maximum correction c [dimensionless] at altitude m [m asl] is reached and decreases

again at higher elevations thereafter.

$$f_c(z) = (c-1) \cdot \exp\left[-\left(\frac{a}{(c-1)\cdot 100}\right)^2 \cdot (z-m)^2\right] + 1 \tag{6.5}$$

This is a more continuous approach than the combination of two linear functions proposed by Immerzeel et al. (2012). c is effectively the greatest correction factor applied, while the altitude m is the physical limit of the atmosphere to lose more moisture. For the Tien Shan, Aizen et al. (1995) described this exponential change in precipitation and provided valuable observations to constrain the parameters of the correction function for the multi-objective calibration. The investigations by Immerzeel et al. (2015) and Immerzeel et al. (2012) helped to constrain the parameter ranges for the Karakoram region.

To account for local differences in precipitation underestimation across a catchment, the correction term c is distributed over selected glacier groups similar to Immerzeel et al. (2015). There are 5–11 groups in each catchment as shown in Figure 6.5. They were manually identified according to major glacier clusters at mountain massifs and expos-

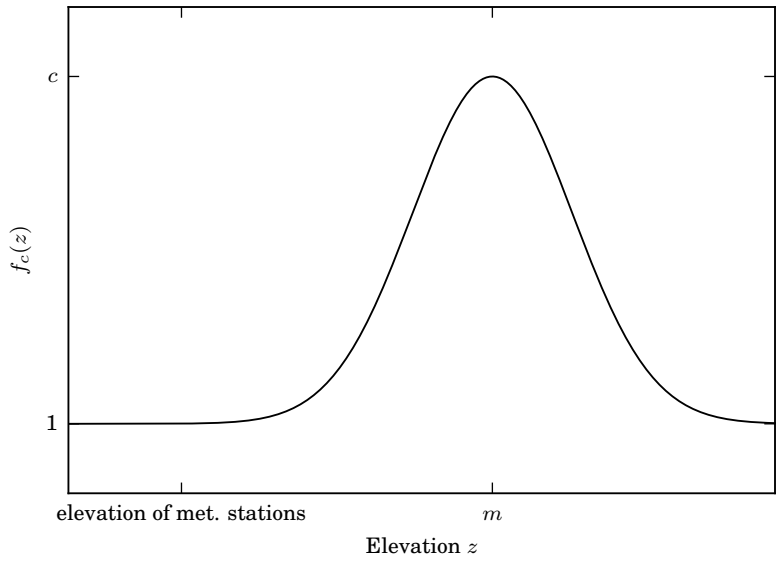

Figure 6.4: An exemplary plot of the precipitation correction function described by Equation (6.5).

ition. For subbasins without any glaciers, the values were interpolated between the groups using an IDW interpolation.

Since the precipitation correction is part of the model calibration it is evaluated as part of the model validation. Direct observations of precipitation over the elevation profile do not exist to permit explicit validation approaches. Instead cited literature and the analysis of various satellite and model-based datasets (Section 3.3,Figure 3.9) show that precipitation totals generally behave as described by Equation (6.5) in relation to elevation in this region.

6.5 Calibration and validation results

The automatic calibration of the SWIM-G yielded good results, but performances vary with meteorological station density. The Pareto fronts for the final calibration ensemble of 100 parameter sets are shown in Figures 6.6 to 6.10. While the multi-dimensional

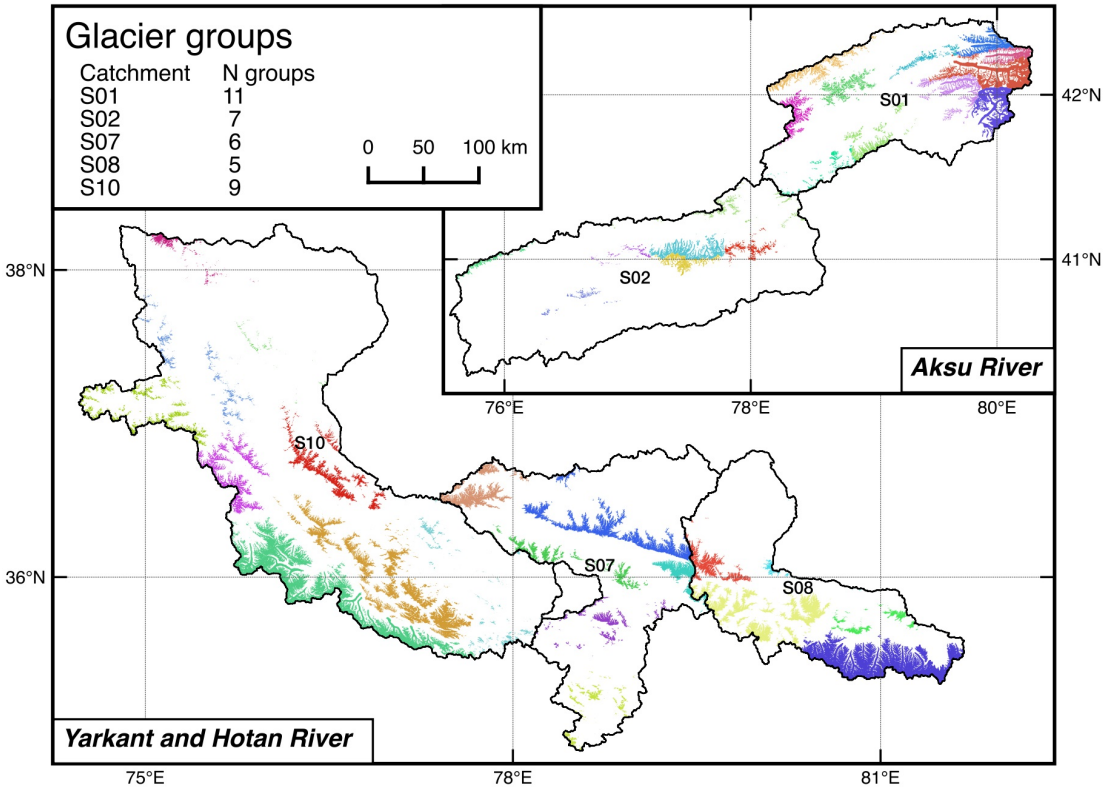

Figure 6.5: Manually identified glacier groups for the which different values of the correction term c were found in each catchment. The number of groups in each catchment are given in the legend.

(3 or 4 dimensions) fronts are difficult to visualise, outliers are clearly visible with the majority of parameter sets falling within acceptable ranges of the objective functions. The population size of 100 parameter sets was subset using acceptable threshold values (see Section 6.3 and top of Table 6.3) for the four objective functions (NSE_c, RMSE of annual discharge, χ^2 of glacier hypsometry and MB). The subsets include all of the runs in the Xiehela (Aksu) catchment, 49 runs for the Shaliguilanke (Aksu catchment), 48–83 in the Hotan catchments and 85–97 in the Yarkant catchment. The results for the Hotan and Yarkant catchments are given with uncertainty ranges over the three mass balance assumptions in the initialisation period. The mean performance values are provided in Table 6.3 and the calibrated values for the precipitation, snow and glacier and hydrological parameters are listed in Table 6.4, Table 6.5 and Table 6.6, respectively.

Table 6.3: Model performance according to the mean values of the four objective functions over the calibration ensemble plus the validation evaluation of daily discharge (NSE_c*). By applying the thresholds shown in the table header, the 100 Pareto-optimal calibrations are reduced to number N. In the Hotan and Yarkant catchments, mean values are provided for three mass balance assumptions (+0.1, 0, -0.1m weq. a^{-1}), instead of the MB performance.

		N	NSE_c	NSE_c*	$RMSE_{QA}$ [%]	χ^2 [%]	MB
(threshold)			0.60		25.0	20.0	10.0
Aksu							
Xiehela		100	0.923	0.909	13.2	10.2	0.1
Shaliguilanke		49	0.832	0.820	16.0	14.4	2.3
Hotan							
Wuluwati	+0.1	48	0.732	0.718	21.6	10.6	
	0	73	0.750	0.731	20.5	10.4	
	-0.1	67	0.751	0.739	19.5	12.5	
Tongguziluoke	+0.1	73	0.726	0.708	23.1	4.4	
	0	83	0.757	0.741	22.4	4.2	
	-0.1	83	0.776	0.761	21.9	3.7	
Yarkant							
Kaqun	+0.1	93	0.849	0.829	16.0	9.8	
	0	85	0.848	0.822	15.4	11.0	
	-0.1	97	0.872	0.858	15.8	10.8	

Table 6.4: Calibrated precipitation correction parameter median values (standard deviations) of the calibration ensemble for all catchment and initial mass balance scenarios. See Table 6.2 for parameter descriptions and ranges.

		c	a	m
Aksu				
Xiehela		3.38 (0.279)	0.542 (0.0387)	4644 (31.6)
Shaliguilanke		3.53 (0.385)	0.431 (0.0702)	4672 (57.9)
Hotan				
Wuluwati	+0.1	2.87 (0.698)	0.402 (0.0454)	6028 (54.8)
	0	3.45 (1.076)	0.424 (0.0630)	6110 (63.7)
	-0.1	3.93 (1.167)	0.521 (0.1097)	5884 (45.1)
Tongguziluoke	+0.1	7.71 (1.015)	0.355 (0.0385)	6103 (117)
	0	5.98 (1.197)	0.245 (0.0242)	6450 (261)
	-0.1	5.76 (0.660)	0.266 (0.0204)	6290 (81.4)
Yarkant				
Kaqun	+0.1	7.93 (0.917)	0.596 (0.0356)	6665 (38.0)
	0	6.28 (1.355)	0.554 (0.0557)	6228 (212)
	-0.1	5.55 (0.758)	0.431 (0.0447)	6358 (211)

The glaciological calibration is mainly characterised by the match between the observed and simulated (initialised) ice hypsometries (Figure 6.11), evaluated by the objective function χ^2. The overall hypsometry is generally in good agreement with the observed one, with median χ^2 deviations of 3.7–14.4 %. Departures from the observations mainly occur at overestimated hypsomety peaks, as a result of the χ^2 objective function that weighs errors relative to the observed magnitude, compromising overestimations in the peaks against better fits at the lower ends. Differences between the initial mass balance assumptions for the Hotan and Yarkant catchments are small (0.7–1.9% in the median χ^2), giving evidence that the precipitation correction has compensated for the loss/gain in ice for positive/negative mass balances in the initialisation period.

The hydrological calibration, gauged by the combined NSE and the RMSE of annual mean discharge, yielded good results, but differences with meteorological station densities are apparent (Figure 6.12). The NSE_c for the validation (odd years) are only slightly lower than those for the calibration (even years), as would be expected. Whereas the

Table 6.5: Same as Table 6.4 but for calibrated snow and glacier parameters. The residual mass balance for the Aksu catchments is discussed in Section 6.3.

		δ_s	T_m	t_e	δ_i	Γ
Aksu						
Xiehela		2.2 (0.21)	-1.1 (0.28)	-0.70 (0.006)	6.7 (0.34)	0.24 (0.05)
Shaliguilanke		2.2 (0.11)	-0.5 (0.28)	-0.68 (0.011)	6.6 (0.24)	0.26 (0.04)
Hotan						
Wuluwati	+0.1	2.6 (0.52)	1.4 (0.52)	-0.78 (0.011)	5.9 (0.70)	0.54 (0.03)
	0	1.7 (0.18)	-0.1 (0.16)	-0.79 (0.005)	5.2 (0.47)	0.51 (0.03)
	-0.1	3.0 (0.49)	1.0 (0.36)	-0.79 (0.014)	6.1 (0.48)	0.59 (0.04)
Tongguziluoke	+0.1	1.5 (1.22)	-1.9 (1.36)	-0.80 (0.003)	4.0 (0.42)	0.52 (0.02)
	0	2.3 (0.62)	-0.6 (0.75)	-0.79 (0.005)	4.2 (0.39)	0.52 (0.02)
	-0.1	1.9 (1.07)	-1.7 (0.84)	-0.79 (0.003)	4.0 (1.01)	0.56 (0.03)
Yarkant						
Kaqun	+0.1	2.0 (0.48)	0.4 (1.01)	-0.76 (0.015)	4.8 (0.40)	0.55 (0.04)
	0	1.6 (0.71)	-0.8 (1.28)	-0.78 (0.019)	4.9 (0.52)	0.59 (0.07)
	-0.1	2.0 (0.49)	0.8 (0.84)	-0.77 (0.020)	4.4 (0.30)	0.52 (0.03)

Table 6.6: Same as Table 6.4 but for calibrated hydrological parameters.

		E_c	$R_{2,4}$	S_c
Aksu				
Xiehela		0.89 (0.092)	7.5 (1.11)	0.82 (0.027)
Shaliguilanke		0.83 (0.076)	3.5 (0.80)	0.80 (0.049)
Hotan				
Wuluwati	+0.1	0.72 (0.017)	2.9 (1.48)	0.34 (0.185)
	0	0.83 (0.056)	1.6 (0.65)	0.39 (0.281)
	-0.1	0.88 (0.051)	1.8 (0.57)	0.42 (0.317)
Tongguziluoke	+0.1	0.76 (0.173)	5.1 (2.41)	0.33 (0.240)
	0	0.72 (0.046)	5.6 (1.75)	0.27 (0.277)
	-0.1	0.74 (0.051)	2.1 (1.53)	0.31 (0.391)
Yarkant				
Kaqun	+0.1	0.80 (0.086)	2.4 (1.64)	0.42 (0.274)
	0	1.00 (0.064)	2.2 (1.18)	0.38 (0.136)
	-0.1	0.75 (0.100)	0.7 (0.95)	0.44 (0.057)

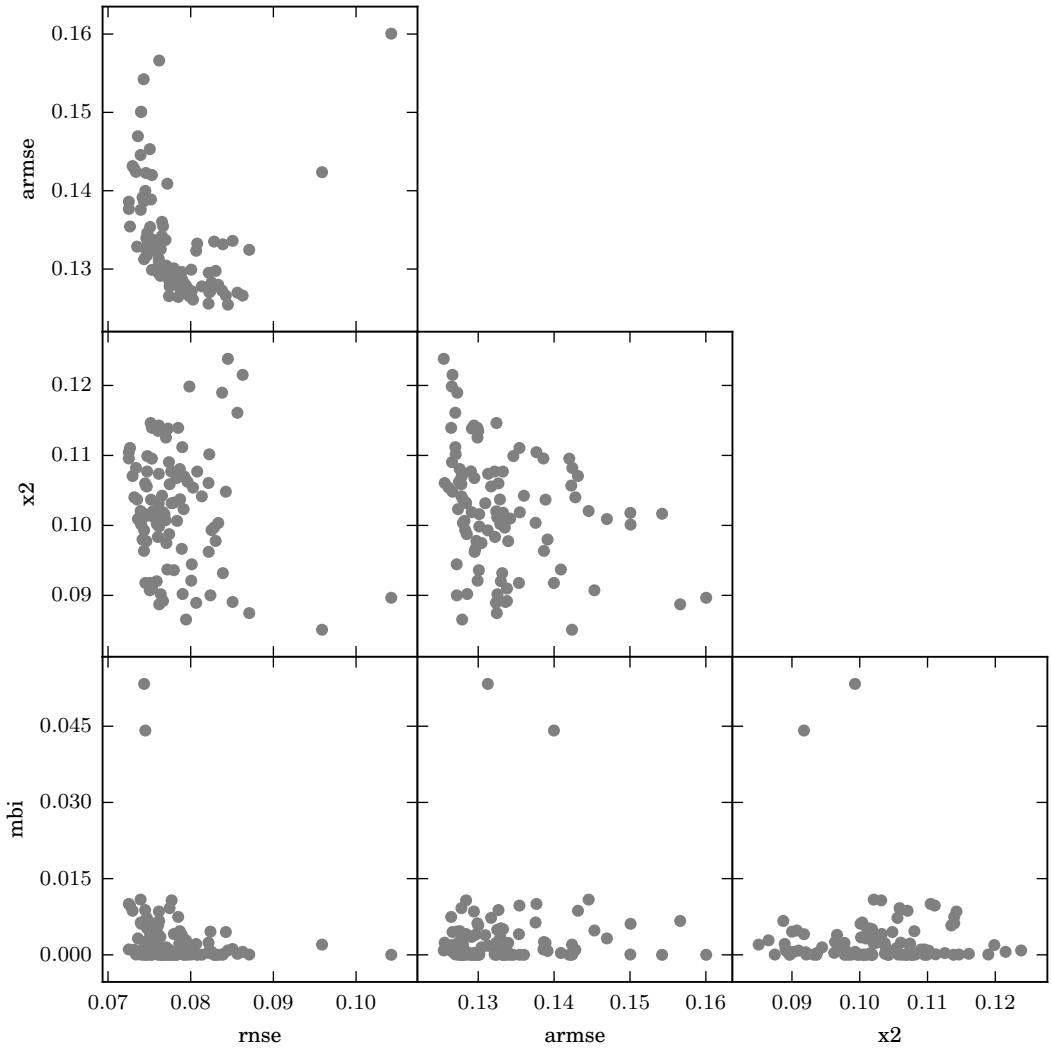

Figure 6.6: Performances of all 100 calibrated parameter sets for the Xiehela (Aksu, S01) catchment. All four objective functions are plotted against each other showing the multi-dimensional Pareto front. rnse: the combined NSE_c (reversed, i.e. 1-NSE_c), armse: annual discharge $RMSE_{QA}$, x2: glacier hypsometry χ^2, mbi: mass balance probability MB_i.

two Aksu catchments and the Yarkant catchment have NSE_c values of above 0.83 and an annual discharge error of less than 16%, the performance declines to around 0.74 and 21% in the Hotan catchments. The day-to-day variability as well as the day of year mean seasonality are reproduced well, but the erratic discharge peaks in summer are often missed by the simulations, especially in the Hotan catchments. The range in discharge over the calibration ensemble is relatively small but is usually greatest in autumn, with some exceptions in the Yarkant catchment. While catchment discharge

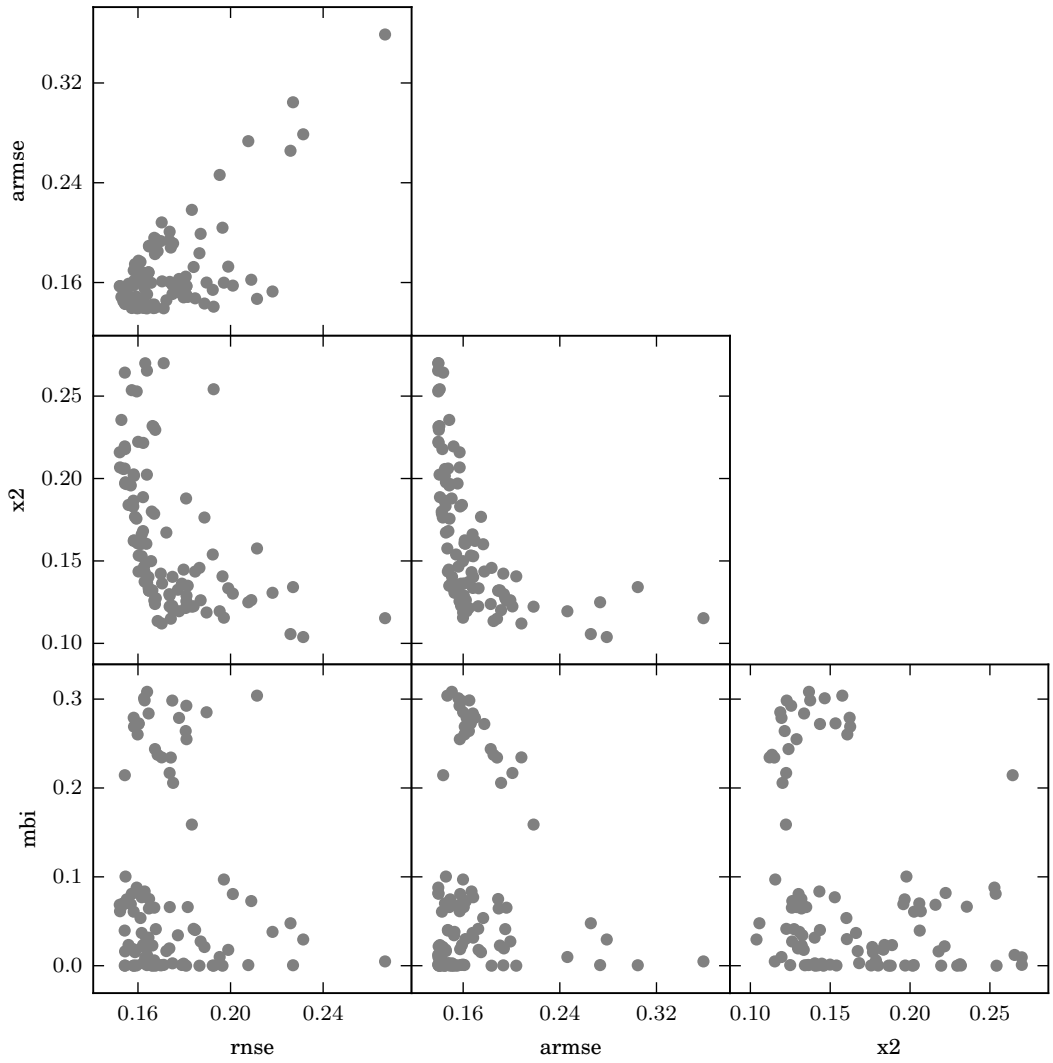

Figure 6.7: Same as Figure 6.6 but for the Shaliguilanke (Aksu, S02) catchment. rnse: the combined NSE_c (reversed, i.e. 1-NSE_c), armse: annual discharge $RMSE_{QA}$, x2: glacier hypsometry χ^2, mbi: mass balance probability MB_i.

was used for the automatic calibration, it is only one component of the catchment hydrology. Results of the other components (snow melt, evapotranspiration etc.) will be presented in the next section and should also be considered in the model calibration and its hydrological plausibility.

The simulated glacier mass balance in the two Aksu catchments was accurately calibrated to the catchment-wide values found by Pieczonka and Bolch (2015) for the period 1975–2000 (Figure 6.13, top). While the simulated annual variability is close to the in situ mass balance record at Karabatkak Glacier (scaled in Figure 6.13, top), it is more

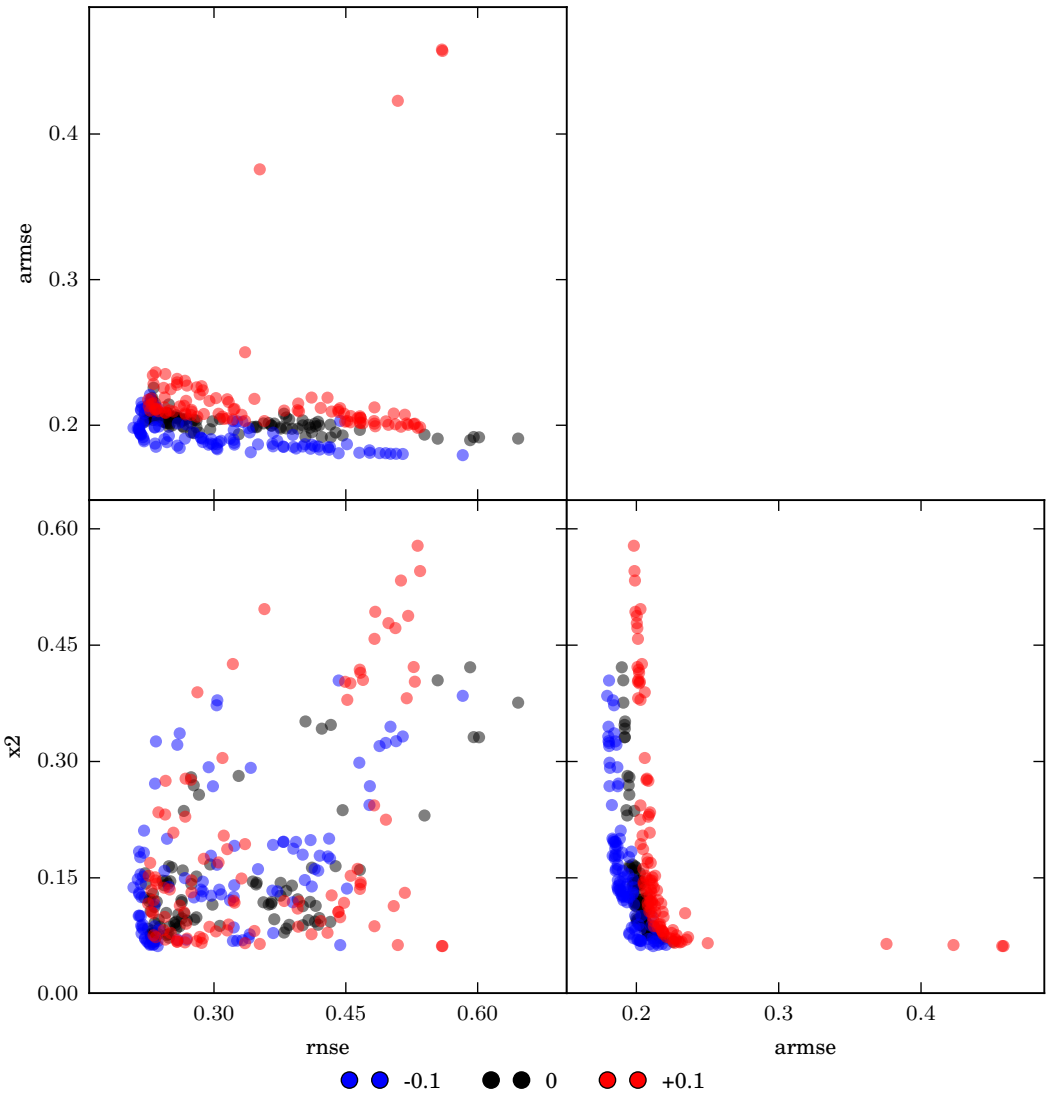

Figure 6.8: Performances of all 300 calibrated parameter sets for the Wuluwati (Hotan, S07) catchment. 100 parameter sets were produced for three initial mass balance assumptions. All three objective functions are plotted against each other showing the multi-dimensional Pareto front. rnse: the combined NSE_c (reversed, i.e. 1-NSE_c), armse: annual discharge $RMSE_{QA}$, x2: glacier hypsometry χ^2.

positive in the early 1980s and slightly more negative in the late 1990s. The calibration ensemble range is with -0.36 ± 0.18m weq. a^{-1} lower than the accumulated uncertainty provided by Pieczonka and Bolch (2015) (-0.35 ± 0.34m weq. a^{-1}). Mass balance is mainly calibrated via snow and ice degree-day melt rates as well as the residual mass balance during initialisation. The calibrated residual mass balance median (standard deviation) is -0.19 ± 0.02 m weq. a^{-1} for the Xiehela catchment and -0.16 ± 0.04 m weq. a^{-1}

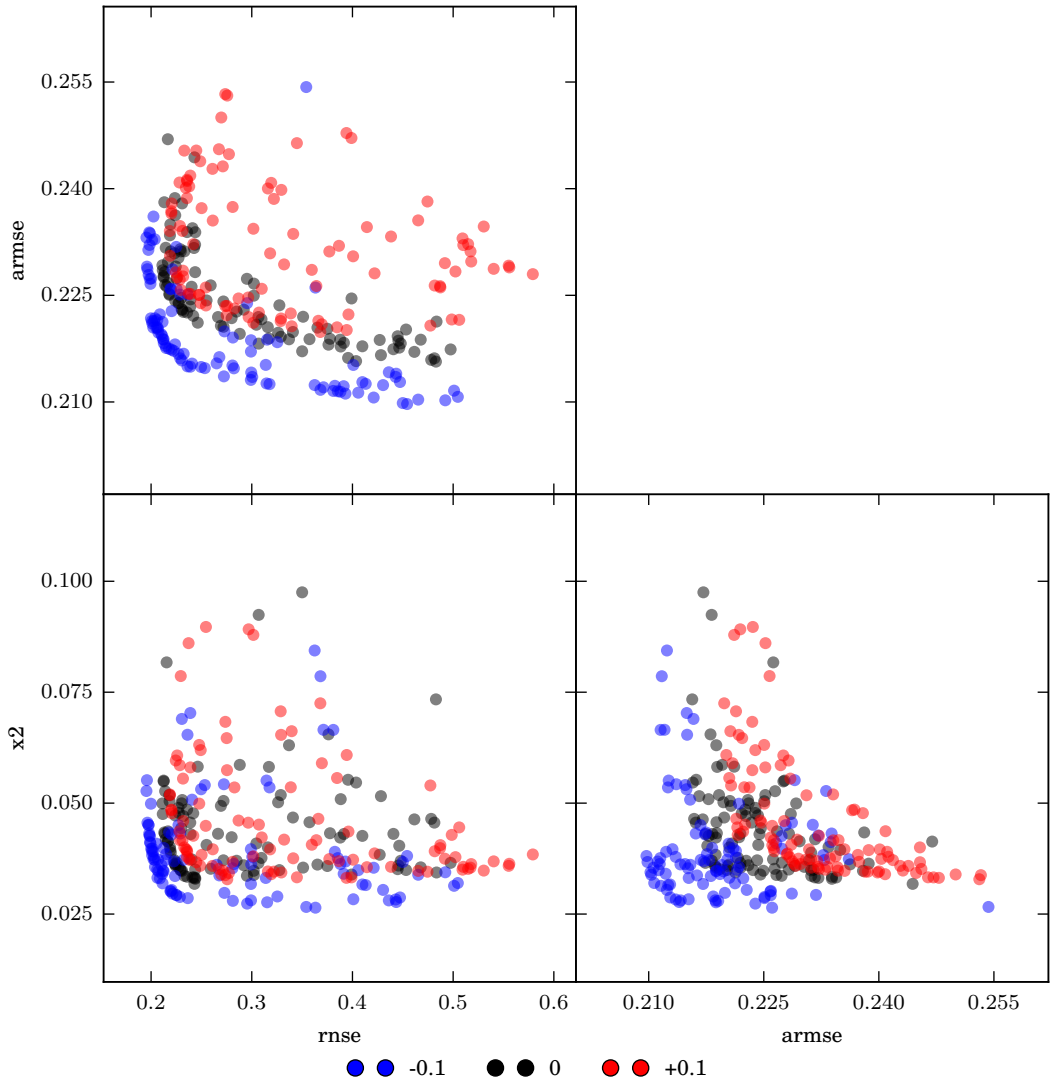

Figure 6.9: Same as Figure 6.8 but for the Tongguziluoke (Hotan, S08) catchment. rnse: the combined NSE_c (reversed, i.e. 1-NSE_c), armse: annual discharge $RMSE_{QA}$, x2: glacier hypsometry χ^2.

for the Shaliguilanke catchment, which is within the range of values found in a modelling study for the Tien Shan for the same period (Farinotti et al., 2015).

The simulated mass balances in the Hotan and Yarkant catchments are stable or increasing under all three initial mass balance assumptions (Figure 6.13, bottom two). Increasing with the residual mass balance assumption, median values range between 0.03–0.20 m weq. a^{-1} in the Hotan and 0.05–0.27 m weq. a^{-1} in the Yarkant catchment, with uncertainty ranges (half-range over all runs) of 0.03–0.07 m weq. a^{-1}. The annual

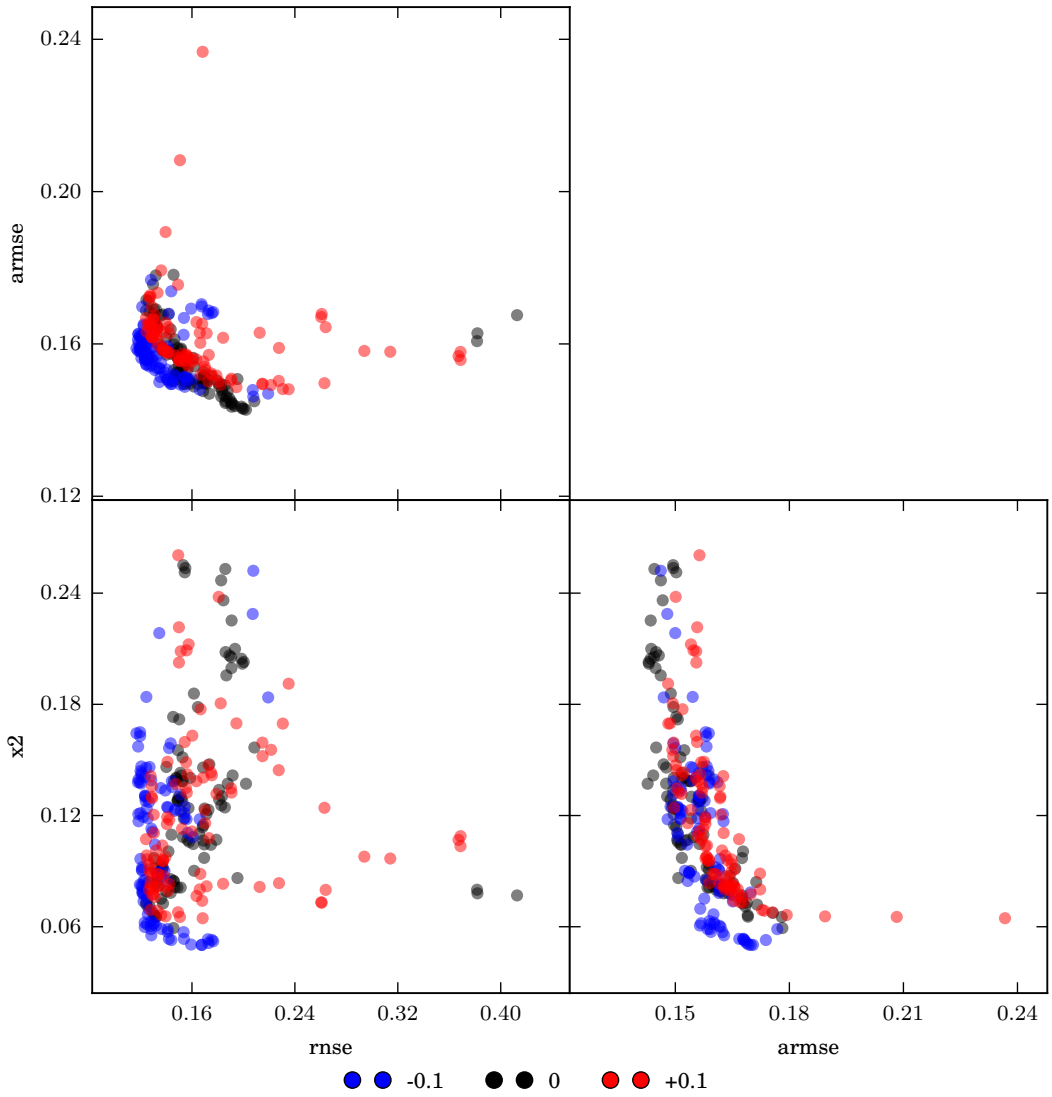

Figure 6.10: Same as Figure 6.8 but for the Kaqun (Yarkand, S10) catchment. rnse: the combined NSE_c (reversed, i.e. 1-NSE_c), armse: annual discharge $RMSE_{QA}$, x2: glacier hypsometry χ^2.

variability is similar in these two catchments; it is stable to slightly negative between 1975–1985 and increasing thereafter. These simulations are in line with several, mostly local, glaciological studies from the Kunlun Shan and the Karakoram, as is discussed in more detail in Section 6.5.1. The increasing trend, even with a negative initialisation mass balance, is driven by increases in precipitation in comparison to the initialisation period (1961-1975), while temperature changes are moderate.

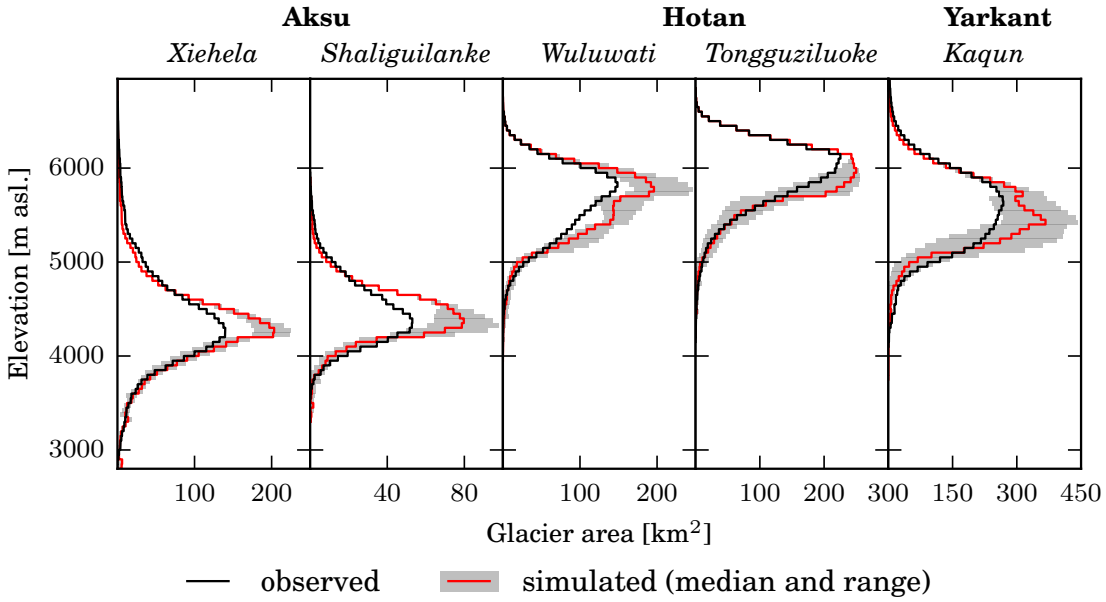

Figure 6.11: Initialised and observed glacier hypsometry of the five headwater catchments. Hypsometry intervals are 50m. Note the variable horizontal scales.

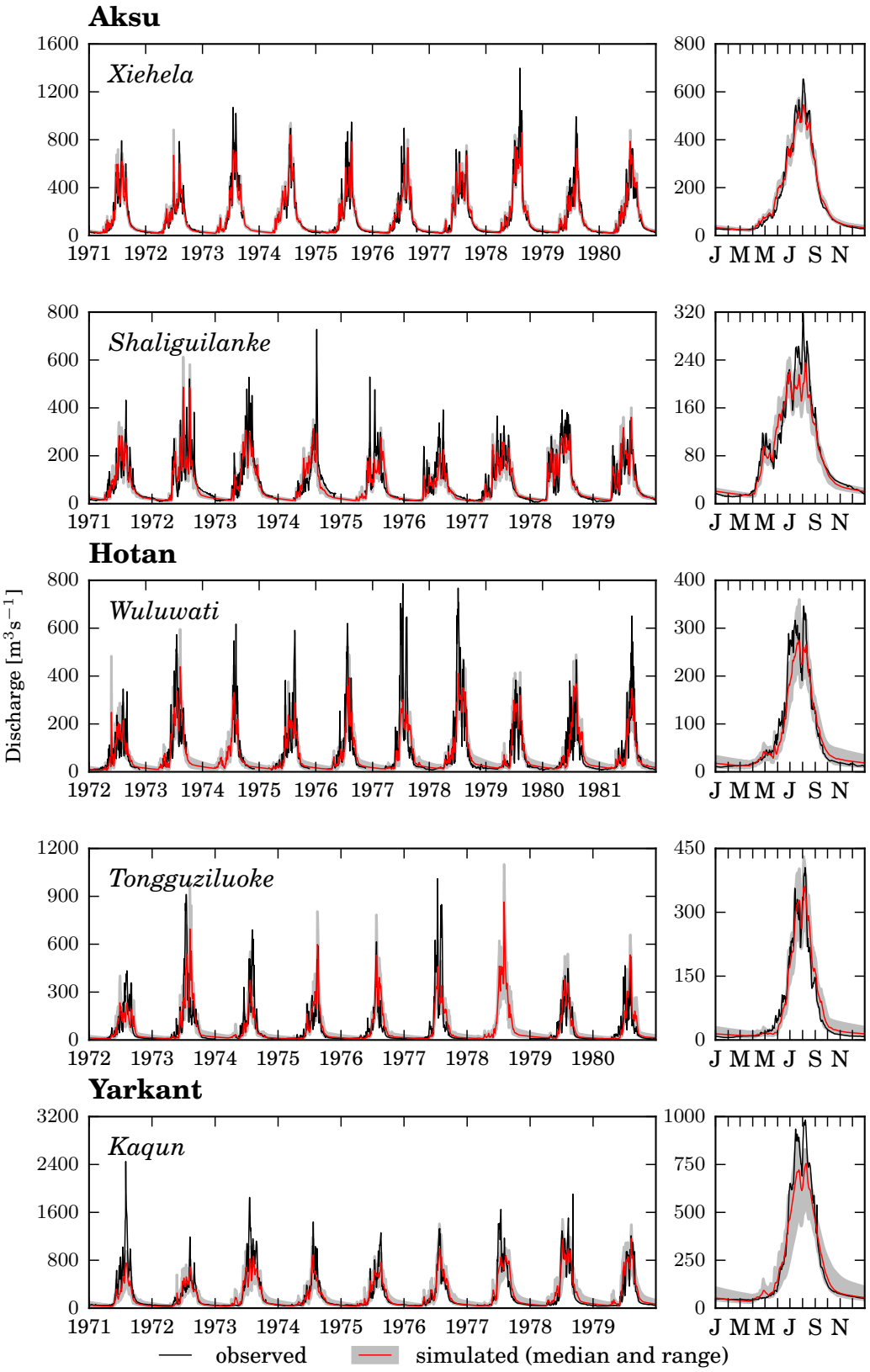

Figure 6.12: Simulated and observed daily and day-of-year mean discharge for all five gauging stations over the period with available data. Even years were used for calibration and odd years for validation.

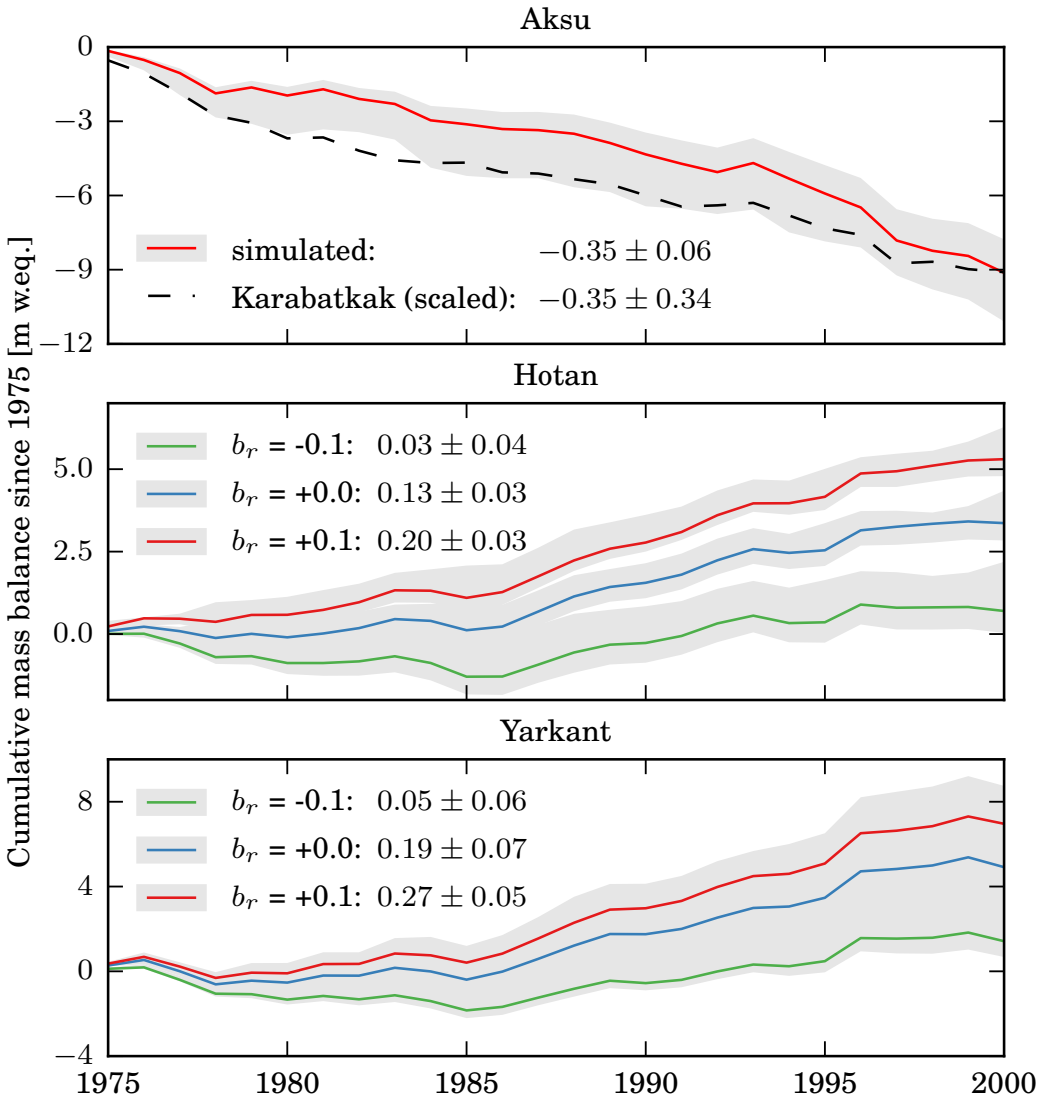

Figure 6.13: Simulated mass balance in the period investigated by Pieczonka and Bolch (2015) with median and min./max. ranges drawn and annual mean values [m weq. a^{-1}] with uncertainties (half-range over all runs) given in the legend. The Karabatkak mass balance is scaled to the catchment-wide mean value found by Pieczonka and Bolch (2015) for the Aksu catchments. As observations for the Hotan and Yarkant catchments do not exist, the outcomes of the three initialisations with different mass balance assumptions are shown.

6.5.1 Mass balances scenarios in the Hotan and Yarkant catchments

Despite the uncertainty about mass balances in the Hotan and Yarkant catchments, the parameter uncertainty of the precipitation correction with three reasonable mass balance assumptions is lower than the overall parameter uncertainty. Differences over the simulation period between the three scenarios are most significant in simulated mass balance, precipitation and snow fall. Under all scenarios glacier mass balances are positive over the simulation period, although not in every year.

Despite a general trend of glacier recession in High Asia, glaciers in the Karakoram (Yarkant) and Kunlun Shan (Hotan) have shown strong signs of opposing this trend (sometimes referred to as the Karakoram anomaly). Hewitt (2005) show many advancing and thickening glacier tongues in the Karakoram in the late 1990s and Liu et al. (2006a) find evidence of advancing glaciers in the Kunlun Shan between 1968–1999. Recent investigations in the Karakoram based on declassified satellite imagery (Hexagon KH-9) from the 1970s indicate stable or only slight mass loss: Bolch et al. (2017) find mass balance of $-0.01 \pm 0.09\,\mathrm{m\,weq.\,a^{-1}}$ over the 1973–1999 and $-0.08 \pm 0.21\,\mathrm{m\,weq.\,a^{-1}}$ over 1999–ca.2009 for the Hunza catchment. For the central Karakoram, Zhou et al. (2017) give a mass balance of $-0.04 \pm 0.05\,\mathrm{m\,weq.\,a^{-1}}$ (1973–2000). Similar findings were made for the Mutztagh Ata massif (Eastern Pamir) in the north of the Yarkant catchment (Holzer et al., 2015). Studies of changes in the 2000s using ICSat satellite measurements show a positive trend in the Kunlun Shan and Tarim part of the Karakoram with mass balances of $0.03 \pm 0.25\,\mathrm{m\,weq.\,a^{-1}}$ (2003–2009) (Neckel et al., 2014), $0.05 \pm 0.07\,\mathrm{m\,weq.\,a^{-1}}$ (2003–2008) (Kääb et al., 2015) and $0.17 \pm 0.15\,\mathrm{m\,weq.\,a^{-1}}$ (2000–2010) (Gardelle et al., 2013). The strengthening of the Westerlies is assumed to be the cause of these stable conditions (Yao et al., 2012). In combination with the extremely high elevations, increases in precipitation lead to greater glacier accumulation even with slightly increasing temperatures (Hewitt, 2005).

In light of these studies, the stable or increasing mass trend simulated here (Figure 6.13) are reasonable. Although spatial and temporal domains vary, the lower initial mass balance assumption of $-0.1\,\mathrm{m\,weq.\,a^{-1}}$ is the most likely scenario with

0.03 ± 0.04 m weq. a^{-1} and 0.05 ± 0.06 m weq. a^{-1} for the Hotan and Yarkant catchments, respectively, over the period 1975–2000.

6.6 Corrected precipitation

The simulated and corrected precipitation is far higher than the DPD; at the catchment average by a factor of about 1.5 in the Aksu catchments, 2.2 in the Wuluwati (Hotan) and the Kaqun (Yarkant) catchments and by a factor of about 4.3 in the Tongguziluoke (Hotan) catchment (Figures 6.14 to 6.16). In the calibration ensemble median, the highly glacierised Xiehela (Aksu) catchment receives 487 mm a^{-1} (corrected from 314 mm a^{-1}) on average over the reference period 1971–2000 and the less glacierised, lower lying Shaliguilanke (Aksu) catchment to the south-west 327 mm a^{-1} (corrected from 230 mm a^{-1}). Correction factors over the large massifs, the Kokshal-Too in the west and the Inylcheck-Tomur regions, are between 2–5 with precipitation totals of up to 1400 mm a^{-1}. The two Hotan catchments south of the Taklamakan Desert were strongly corrected due to the absence of any meteorological station to 285 mm a^{-1} (from 62 mm a^{-1}) in the highly glacierised Tongguiziluoke catchment and 230 mm a^{-1} (corrected from 98 mm a^{-1}) in the drier Wuluwati catchment with large parts on the Tibetan Plateau. The West Kunlun Shan massif in the south-west of Tongguiziluoke catchment requires factors of 5–10 to sustain its vast glacier cover. The precipitation patterns are more heterogeneous in the much larger Yarkant catchment; the catchment-wide average was corrected to 267 mm a^{-1} (from 113 mm a^{-1}). The Karakoram in the south of the catchment, however, receives 500–1200 mm a^{-1} much more than the rest of the catchment, with high correction factors of 5–9.

The coefficient of variation (standard deviation as % of mean) over the calibration ensemble is used here to describe the spatial pattern of the uncertainty, referred to as just uncertainty hereafter (Figure 6.17). Since the mass balance of the Aksu catchments is calibrated, the uncertainty is at around 10–20% smaller than in the Hotan and Yarkant catchments, where most parts have uncertainties of about 20% and in some locations of up to 45%. The mean catchment uncertainty, however, is much smaller at 5–7% in the Aksu catchments and 12–15% in the Hotan and Yarkant catchments. Uncertainties are generally greater at higher altitudes, but are mainly distributed according to the

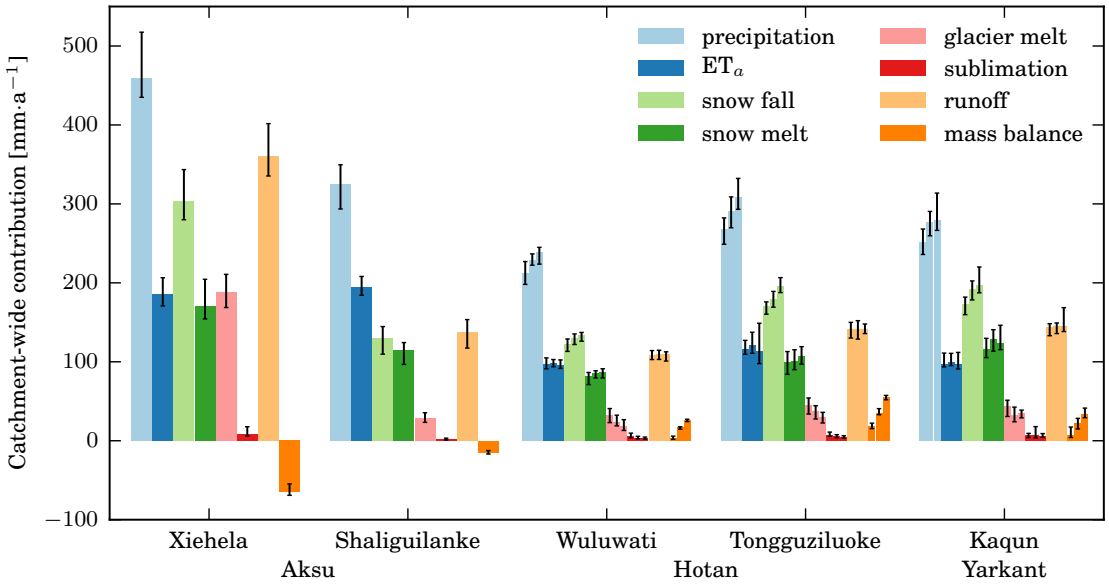

Figure 6.14: Simulated water balance components averaged over all five catchments, median (solid bars) and ensemble min. and max. (error lines). The three initial glacier mass balance assumptions for the Hotan and Yarkant catchments are indicated by divided bars and three error lines for those catchments (l-r: MB = -0.1, 0.0, +0.1 m a^{-1}).

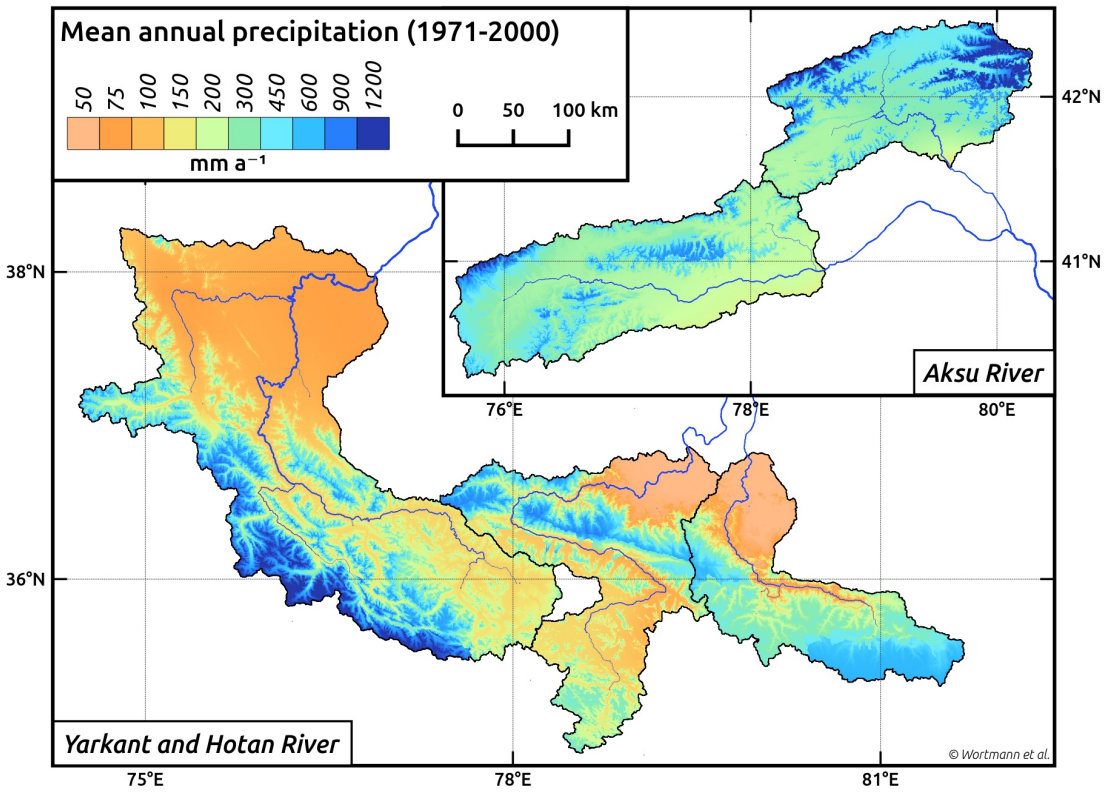

Figure 6.15: Corrected mean annual precipitation (1971–2000) over the five catchments, based on the APHRODITE reanalysis dataset.

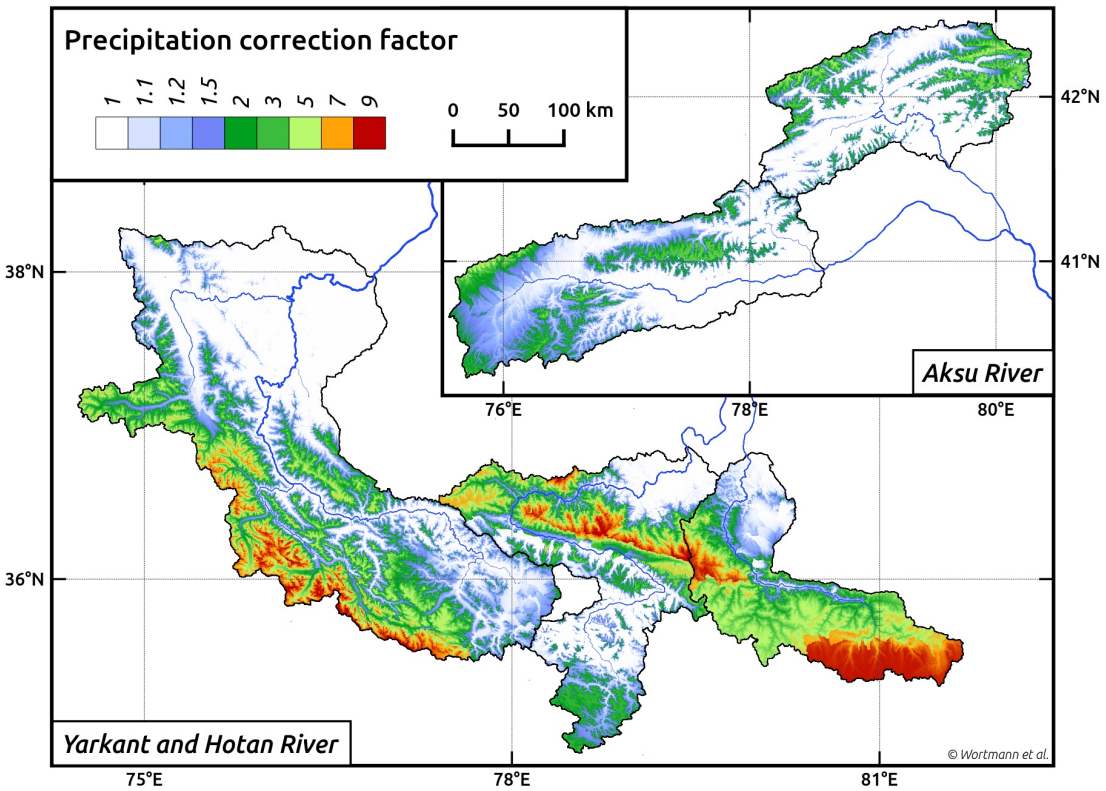

Figure 6.16: Ensemble median precipitation correction factors for the APHRODITE reanalysis dataset (1971–2000).

glacier area of the glacier groups that the simulated ice hypsometry is compared to. For example, the precipitation estimations in the central east of the Wuluwati (Hotan) and the south-east of the Yarkant catchment with uncertainty values of around 40% are based on a relatively small glacier group with predominantly smaller glaciers.

6.6.1 Comparison to precipitation datasets

In comparison to the six analysed precipitation datasets described in Sections 3.3.1 and 3.3.2, the corrected values fall between the SPD and the MPD. In the Aksu catchments, they are closest to the TMPA and CCLM catchment averages and in the Hotan and Yarkant catchment they are between the TMPA and HAR values. The spatial distribution is much closer to higher resolution datasets than the original APHRODITE data (compare Figure 3.8 and Figure 6.15), the HAR dataset in particular. For the catchment average, the two SPD and MPD covering the simulation period, CCLM and ERA-Interim (only from 1979), show larger values with catchment means greater by a

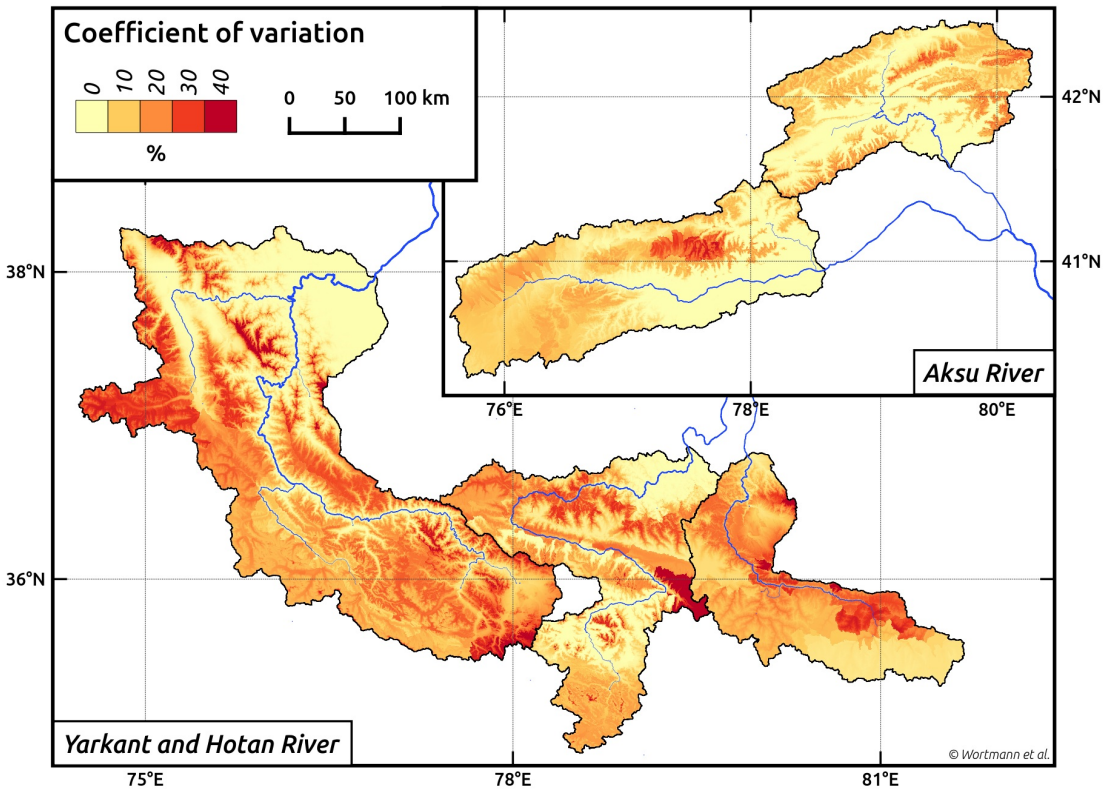

Figure 6.17: Coefficient of variation over the calibration ensemble over all five catchments.

factor of 1.2–2.1 and 1.5–2.3, respectively. Although it covers a different period, the high resolution HAR dataset is closer in the Hotan and Yarkant catchment with deviations of 1.2–1.5 times greater. The precipitation patterns around the large massifs are similar to the high resolution HAR and the GPM datasets. Although they are only available for more recent periods, they provide evidence for high orographic precipitation of up to 1000–1500 mm a^{-1}, for example on the northern ridge of the Karakoram or at the crests of the Kunlun Shan, corroborating the large correction factors found within the calibrated model results. The corrected values, however, deviate from most other SPD and MPD in the north of the Yarkant catchment: Corrected values range between 80–200 mm a^{-1}, but most SPD and MPD indicate higher values of around 200–500 mm a^{-1}. This is also reflected in relatively high uncertainties (Figure 6.17) that are probably a result of the contrast between sparse and relatively small glaciers in the north and an extensive glacier cover in the south in this large catchment.

6.6.2 Comparison to other studies

The results compare well with similar studies. For example, Immerzeel et al. (2015) found similar discrepancies with existing datasets, such as APHRODITE or TRMM-based products in the neighbouring Upper Indus Basin, south-west of the Yarkant and Hotan catchments. Similar to the results of this chapter, they obtained corrected precipitation of around 800–1200 mm a^{-1} along the Karakoram range, with similar correction factors of up to 10 for the APHRODITE dataset. They also found much drier conditions at the south-eastern edge of the Yarkant catchment and south of the Wuluwati (Hotan) catchment with similar precipitation totals of 200–500 mm a^{-1}. Parameter uncertainties also compare well around the Karakoram between 10–50 % (35% mean).

Similarly high correction factors were found by Sakai et al. (2015), who used a glacier mass balance model of High Asian glaciers and correct the APHRODITE precipitation data by tuning the model to independently estimated equilibrium line altitudes. But their relatively coarse model resolution (0.5°) fails to represent the heterogeneity of the terrain and is based on the assumption that glacier median elevation represents the equilibrium line altitude.

Although the approach used here and the two above differ in time covered, model and calibration strategy, the results provide new insights into poorly gauged and investigated catchments and reduce the uncertainty for future modelling studies. They highlight the importance of in situ and geodetic glaciological measurements of both glacier outlines and mass balance. While not immediately obvious, they are vital to constrain models that provide a greater understanding and management tools for downstream communities. The approach presented here has particular merit in other catchments with only discharge observations and preferably geodetic mass balance estimates available.

Uncertainties remain in the calibration strategy and model structure, but they are quantified through a calibration ensemble (Figure 6.17). Parameter conflicts due to better correlation of discharge with snow/ice melt than precipitation are addressed by using the agreement in annual discharge as one objective function. Incorporating snow cover maps in the automatic calibration, as was done by Duethmann et al. (2014), could further reduce the parameter uncertainty, but this is outside the scope of this thesis.

Temporal changes in correction factors as well as valley and slope specific precipitation patterns were also not considered This would require a greater coupling of a high resolution climate model (such as the HAR dataset) with the glaciological model.

6.7 Summary

The model implementation, calibration and validation to the five headwaters of the Tarim River were described in this chapter with an additional analysis of the corrected precipitation. SWIM-G was set up using the available datasets described in Chapter 3 and calibrated to discharge and glacier cover using a multi-objective, evolutionary optimisation algorithm with satisfactory to good performance results. The corrected precipitation of the calibration ensemble was then further examined and compared to the precipitation datasets presented in Chapter 3. The implemented model suggests that actual precipitation must be higher by factors of 1.5–4.3 at the catchment average to support the observed glacier area and to attain reasonable mass balances for the reference period 1971–2000. Although high uncertainty ranges in local precipitation fields are still present (especially in areas with sparse glacier cover) and model results that are inherently imperfect cannot replace in situ observations, the calibration ensemble represents a hydrologically and glaciologically consistent correction of high mountain precipitation. The results are indicative of data discrepancies across High Asia and other sparsely gauged mountainous regions. The calibrated model is used in the next chapter for the climate change impact assessment.

Chapter 7

Climate change impact assessment for the Tarim headwaters

7.1 Introduction

After the model construction in Chapter 5 and model implementation in Chapter 6, this chapter describes the climate change impact assessment for the headwaters of the Tarim River. With assessments of water resources at the global and regional scale widely available (IPCC, 2014b; Radić et al., 2013), catchment-scale assessments are important to reduce uncertainty for local water managers. Such an assessment has so far been missing for the Tarim headwaters. As outlined in Chapter 1, the following research questions are addressed:

1. What are the projected impacts on river discharge of the Tarim headwaters considering three IPCC climate change scenarios simulated by an ensemble of climate models in three periods of the 21st century with regards to the reference period 1971–2000?

2. How will the glacier cover (area and volume) change under these climate projections?

3. What are the uncertainties of the discharge and glacier cover projections induced by the climate model ensemble and the calibration parameters and how do both sources compare to the scenario uncertainty?

The chapter begins with introducing the established methods for climate change impact assessments in the hydrological sciences and the climate scenarios used in this study (Section 7.2). It then continues with the evaluation of the climatic changes projected under the used scenarios in Section 7.3, the simulated glaciological and hydrological changes under the scenarios in Sections 7.4 and 7.5, respectively. The chapter closes with an analysis of uncertainty contributions of climate change models, hydrological model parameters and climate change scenarios (Section 7.6).

7.2 Modelling the impacts of climate change

As already discussed in Section 2.10 including its assumptions and limitations, the accepted approach to conduct climate change impact assessments in the hydrological sciences is broken down into three steps: a) Model definition, construction, calibration and validation, b) climate change scenario definition and construction, and c) driving the model with the perturbed climate data and comparing the results to the reference period (Arnell, 1999). While the first step has already been the subject of Chapters 5 and 6, the details of the second and third step are described in this section and the results of the third step are provided in the Sections 7.3 to 7.5.

Climate change scenarios are available from the latest IPCC Assessment Report (IPCC, 2014b) that established the Represenative Concentration Pathwayss (RCPs) as a simple representation of possible future atmospheric greenhouse gas concentration trajectories over the 21st century (Moss et al., 2010). As such, they eschew the complex socio-economic storylines of the previous generation of IPCC climate change scenarios that focused on emissions rather than concentrations (IPCC, 2007). The following three scenarios were chosen (their radiative forcing is shown in Figure 2.9): a) RCP-

2.6 (peaking at 490 ppm $CO_2 - eq$ and eventual decline), b) RCP-4.5 (stabilisation at 650 ppm $CO_2 - eq$) and c) RCP-8.5 (continuous rise above 1370 ppm $CO_2 - eq$).

The climate realisations of these scenarios are created by climate models. Here the output of eight general circulation models (GCMs) from the Climate Model Intercomparison Project (CMIP) and one regional climate model (RCM) from the Sustainable Management of River Oases in the Tarim Basin (SuMaRiO) project were used. The models were selected to cover the full range of precipitation and temperature change signals from the CMIP ensemble over the Tarim catchments, i.e. the moderate and strong cases of wetter-warmer, wetter-colder, dryer-warmer, dryer-colder signals (see Table 7.1). The GCMs have spatial resolutions ranging from 1.5–3° and all data was provided at a daily temporal resolution. To provide an alternative realisation of the future climate at a finer spatial resolutions, the CCLM regional climate model was considered with a resolution of 0.44° (Wang et al., 2013).

Both regional and global climate model results were bias-corrected to the original driving data that the SWIM-G model was calibrated to (APHRODITE for precipitation and Water and Global Change project (WATCH) all other variables) by the data

Table 7.1: List of selected GCMs as well as the one RCM for the climate impact assessment.

Model name	Institute
CNRM-CM5	Centre National de Recherches Meteorologiques, France
GFDL-ESM2M	Geophysical Fluid Dynamics Laboratory, US
HadGEM2-ES	Met Office Hadley Centre, UK
IPSL-CM5A-LR	Institut Pierre-Simon Laplace, France
MIROC5, MIROC-ESM-CHEM, MIROC-ESM	Japan Agency for Marine-Earth Science and Technology, Atmosphere and Ocean Research Institute, Japan
MRI-CGCM3	Meteorological Research Institute, Japan
Regional climate model	
CCLM*	Potsdam Institute for Climate Impact Research (PIK), Germany

*driven by the GCM MPI-ESM-LR

providers (Wang et al., 2013, Duethmann et al., 2016, Menz, pers. com.). The method chosen was a non-parametric quantile mapping approach with a trend preservation as was previously used by Hempel et al. (2013). Despite concerns of the validity of using a bias-correction for climate change impact assessments (Ehret et al., 2012), it was considered necessary in the Tarim headwaters because of considerable deviations in precipitation between calibration and scenario driving data as well as the great sensitivity of the glacier cover to even slight differences in climate.

Due to the nature of the SWIM-Glacier dynamics (SWIM-G) model, the calibration strategy and the data-scarcity of the Tarim headwaters, the third step of the standard assessment approach had to be altered and extended for two reasons: First, since glaciers evolve over time scales of decades and centuries, the model had to be initialised using the climate model data and then run continuously over the baseline and scenario periods for each scenario. This ensures that the glacier cover is consistent with the driving data at the start of the simulation and evolves seamlessly from the baseline period and over the entire scenario period.

Second, each scenario and climate model combination was run using several parameter configurations to allow for an uncertainty range and analysis. The model calibration (as described in the previous chapter) yielded several 'non-dominated' parameter sets, all of which are considered equally valid. Since assessing each scenario-model combination with each of the 50–100 parameter sets would lead to an excessive number of model evaluations, only those parameter sets were selected performing best by each objective function as well as the best trade-off between all objective functions. Figure 7.1 illustrates this selection for a Pareto front with two objective functions. Choosing the best performing parameter sets ensures that the full range of model performances is covered because the best set according to one objective function is simultaneously the worst of another. The best trade-off is the parameter set with the shortest distance to the origin when all objective axes are scaled to the largest (worst) value. For the two Aksu catchments, this selection yields five parameter sets (4 objective functions plus best trade-off) and for the Hotan and Yarkant catchments twelve because they were calibrated for three initial mass balance assumptions with three objective functions. These configurations are multiplied by the number of climate models for the total number of

model evaluations for each scenario (45 for the Aksu catchments, 108 for the Hotan and Yarkant catchments).

7.3 Changes in temperature and precipitation

The temperature and precipitation of the Tarim headwaters under all of the scenarios selected as projected by the RCM and GCMs is presented in Figure 7.2. All scenarios project increases in both temperature and precipitation relative to the reference period (1971–2000) with significant changes across all headwater catchments. All ensemble median values in the three projection periods – the near (2011-40), medium (2041-70) and far (2071-2100) future – indicate increases across all regions. Only ensemble minimum signals indicate negative changes in precipitation, especially in the Aksu. Strong increases in temperature and precipitation from the reference period to the near future (often stronger than changes in subsequent periods) are primarily caused by the 10-year gap (2001-2010) between those periods.

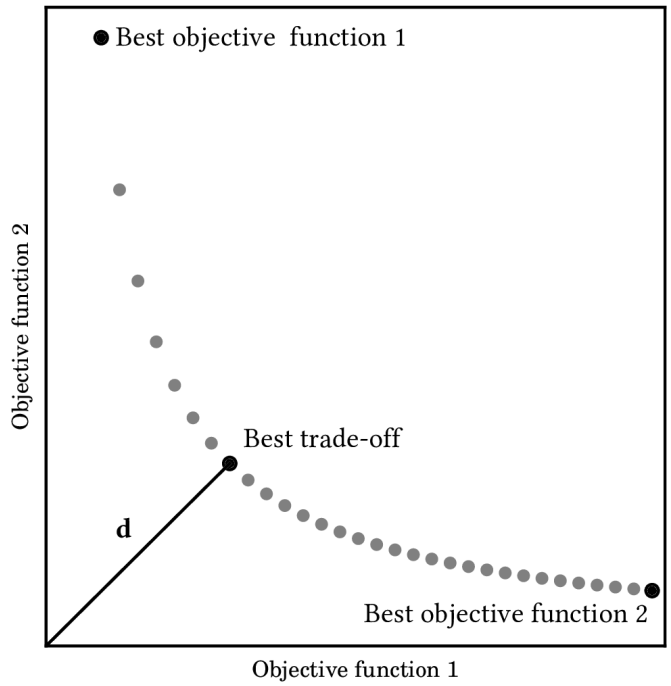

Figure 7.1: Exemplary plot of model solutions positioned on a idealised Pareto front to illustrate the selection of parameter sets used for the climate impact assessment. The best trade-off parameter set has the minimum distance to the origin (d) after the axes have been scaled to the highest value of its objective function.

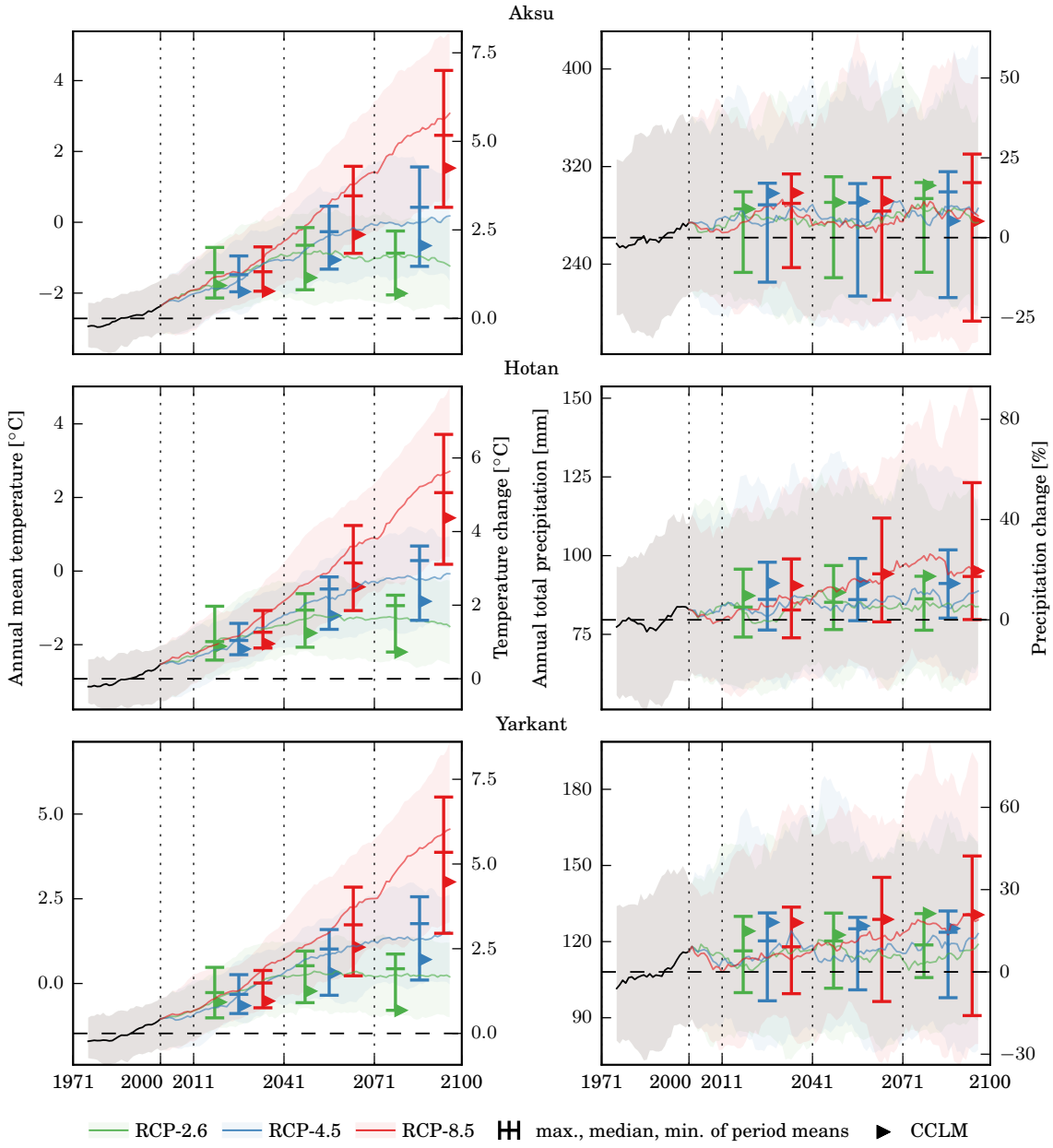

Figure 7.2: 21st century climate change scenarios for the Tarim headwaters including the reference period 1971–2000. Ensemble maximum, median and minimum values are shown as 10-year running means and signals averaged over the near (2011-40), medium (2041-70) and far (2071-2100) future. Period mean values are also given for the RCM CCLM as triangles. Absolute values are given on the left vertical axis and changes relative to the reference period along the right axis.

Temperature increases are similar across all regions. In the near future, they range between 0.5 °C and 2.4 °C with only small differences between the scenarios. Those differences become more striking in the later two periods, when ensemble median changes increase with RCP scenario. In the medium future, they peak for the RCP-2.6 scenario at about 2.5 °C and decrease thereafter, while for the higher RCP scenarios they continue to increase up to 7 °C in the far future for RCP-8.5. The ensemble variability generally increases with time leading to ranges of about 2–4 °C in the far future. The regional model CCLM consistently projects lower changes; signals fall between the median and minimum values in all regions.

Changes in precipitation are less uniform across regions and projection periods, but nevertheless drastic and they exhibit an even greater ensemble variability, a pattern common in other regions (Thompson et al., 2013; Vetter et al., 2013). Relative changes in the near future are modest and similar across the regions and scenarios with median values between 6–8 %. Scenario differences become more pronounced in the later two periods, as ensemble median changes vary with RCP scenario (with the exception of the medium term in the Aksu catchments). Changes in the Aksu catchments range from decreases of up to 25 % to increases of the same magnitude, but median changes still indicate increasing precipitation of 11–18 %. These increases are similar in the Hotan and Yarkant catchments, but the spread is larger and mostly positive (−15–54 %).

7.4 Changes in glacier area and volume

Impacts on the catchments' glaciology are characterised by changes in glacier area and volume; changes in the latter are mostly described by the mass balance. Figure 7.3 gives the simulated area changes compared to the reference period for the 21st century for all catchments and scenarios. Solid lines describe the median of the best trade-off (optimal) parameter configurations including the initial mass balance assumption of $-0.1\,\mathrm{m\,weq.\,a^{-1}}$ for the Hotan and Yarkant catchments (as described in Section 6.5.1). Median values of the regional climate model, CCLM, driven simulations are shown by dashed lines. Uncertainty ranges (5th–95th percentile ranges) refer to the entire parameter set and model distribution. Mean values over three future climate periods – the near (2011–2040), medium (2041–2070) and long-term (2071–2100) – are provided

in Table 7.2. The uncertainty is discussed in more detail in Section 7.6. An example of spatial changes in modelled glacier area over the reference and scenario period is given in Figure 7.4 for the RCP-8.5 for the Xiehela (Aksu) catchment using the optimal parameter set and the CCLM climate input.

A receding trend over the 21st century is evident in all catchments for the ensemble median and strengthening with RCP concentration, although the upper boundaries of the uncertainty ranges in the Hotan and Yarkant catchment maintain stable glacier areas at least in the RCP-2.6 and 4.5 scenarios. For the ensemble median, areas shrink by 2–21 % in the near future, 8–45 % in the medium future and 11–71 % in the far future compared to the reference period across the three scenarios. In the Xiehela and Shaliguilanke (Aksu) catchments, area shrinkage for the high-end RCP-8.5 scenario steadily rises to 58% and 81% by the end of the century, respectively. Both lower scenarios nearly stabilise at 30–40% and 50–60%. The CCLM driven simulations are around 5–20% weaker (smaller decreases in area). Changes in the highly glacierised Tongguziluoke (Hotan) catchment are similar to the Xiehela (Aksu) catchment (both with a glacier cover ≈ 20%). Those of the less glacierised Wuluwati (Hotan) and Kaqun (Yarkant) catchments are similar to the Shaliguilanke (Aksu) catchment (7, 12 and 5% glacier shrinkage, respectively). Differences between the lower two scenarios, however, are larger in the Hotan and Yarkant catchments than in the Aksu and they show a slower recession in the first half of the century.

Similar to the area changes in Figure 7.3, volume changes are provided in Figure 7.5 and their mean values over the three future climate periods are given in Table 7.3. In line

Table 7.2: Ensemble median values of the glacier area change projections shown in Figure 7.3 averaged over three future climate periods.

Catchment	2011-2040			2041-2070			2071-2100		
RCP	2.6	4.5	8.5	2.6	4.5	8.5	2.6	4.5	8.5
Xiehela	-11.5	-10.6	-10.9	-24.1	-23.4	-27.1	-31.5	-36.0	-47.7
Shaliguilanke	-21.2	-20.2	-20.7	-40.8	-39.8	-44.5	-49.7	-55.6	-70.8
Wuluwati	-4.8	-4.3	-6.1	-15.3	-19.6	-26.0	-30.4	-46.3	-57.0
Tongguziluoke	-2.2	-2.3	-2.2	-8.2	-10.6	-12.1	-10.9	-19.9	-32.3
Kaqun	-6.8	-7.4	-8.0	-16.8	-20.7	-25.4	-29.0	-43.9	-54.8

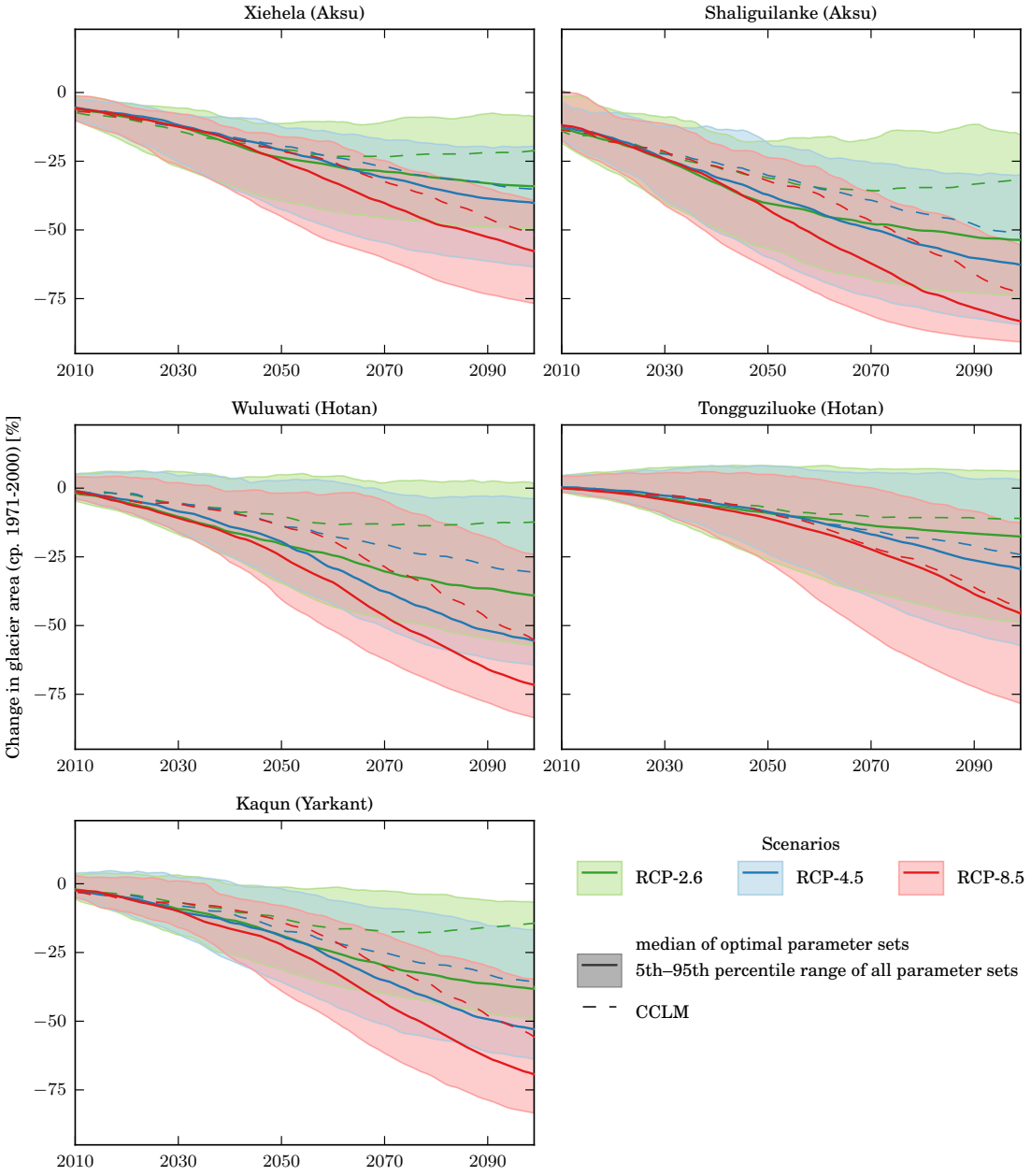

Figure 7.3: Projected glacier area changes over the scenario period for the three RCP scenarios and the five catchments (indicated by their outlet station and main Tarim headwater). Median values are computed from the best trade-off (optimal) parameter set simulations and all climate models, while the 5th–95th percentile uncertainty ranges are calculated from all parameter sets and all climate models. Medians of the RCM-driven simulations are shown as dashed lines.

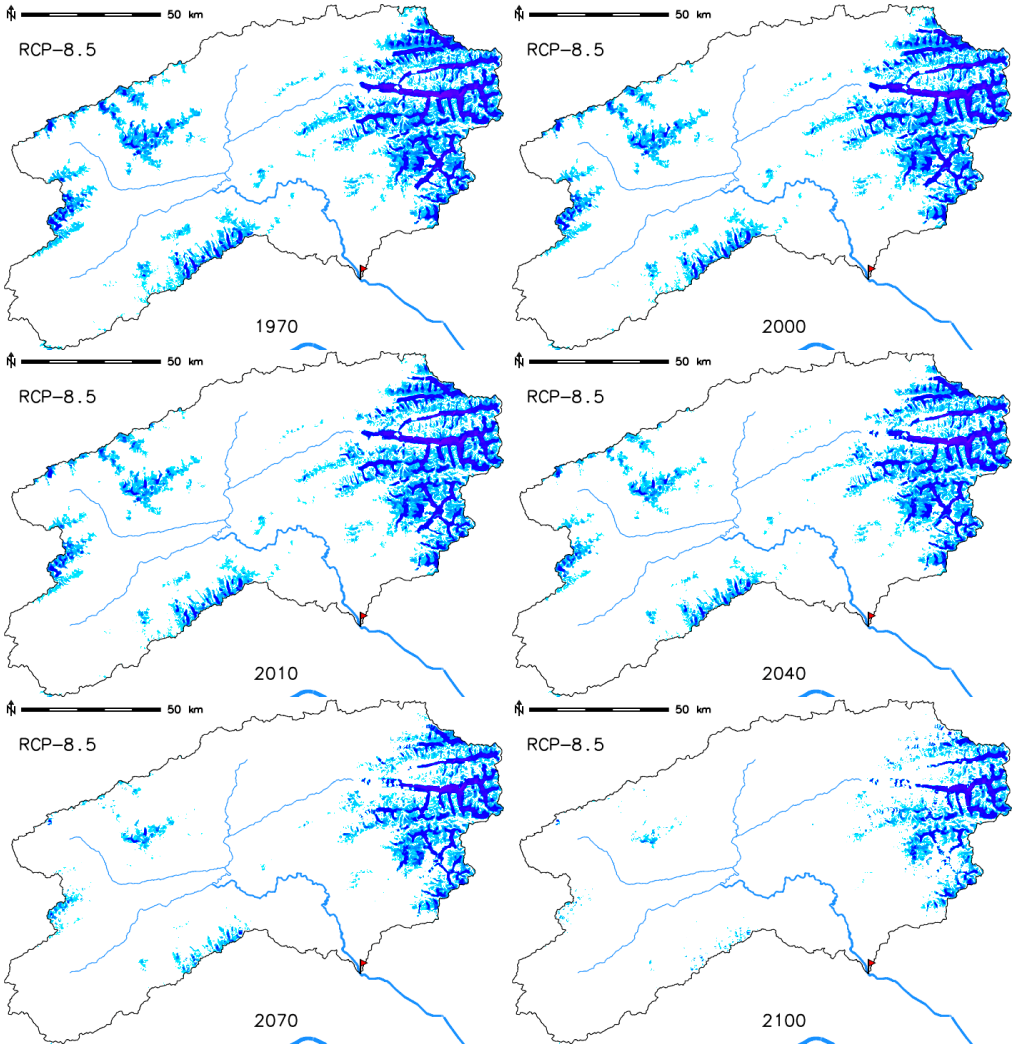

Figure 7.4: Example of glacier area changes over the Xiehela (Aksu) catchment for the reference period (top two maps) and the scenario period (bottom four maps) for the RCP-8.5 scenario driven by CCLM results and using the optimal parameter set. Colours indicate ice thickness from 10 m weq (cyan) to 300 m weq (dark blue).

with area changes, ice volume is also projected to decrease under all scenarios (with the exception of upper uncertainty bounds in the Hotan and Yarkant catchments). Projected mass loss is 4–24 % in the near, 12–54 % in the medium and 14–78 % in the far future across all catchments and scenarios for the ensemble median. Losses are consistently the greatest in the Shaliguilanke (Aksu) catchment with similar magnitudes in the Xiehela (Aksu) catchment and they are the lowest in the Tongguziluoke (Hotan) catchment with similar magnitudes in the Wuluwati (Hotan) and Kaqun (Yarkant) catchments. CCLM-driven projections are close to the ensemble median values in the Xiehela (Aksu) and

Tongguziluoke (Hotan) catchments and project lower losses in the other three catchments (5–25% less).

Glacier mass balances, that is rates of change in ice volume, give an indication of the glacier imbalance, the hydrological impact thereof and they may be better compared to studies of the past glacier evolution. Decadal mean annual mass balances are provided in Figure 7.6. The glacier recession described above is associated with negative mass

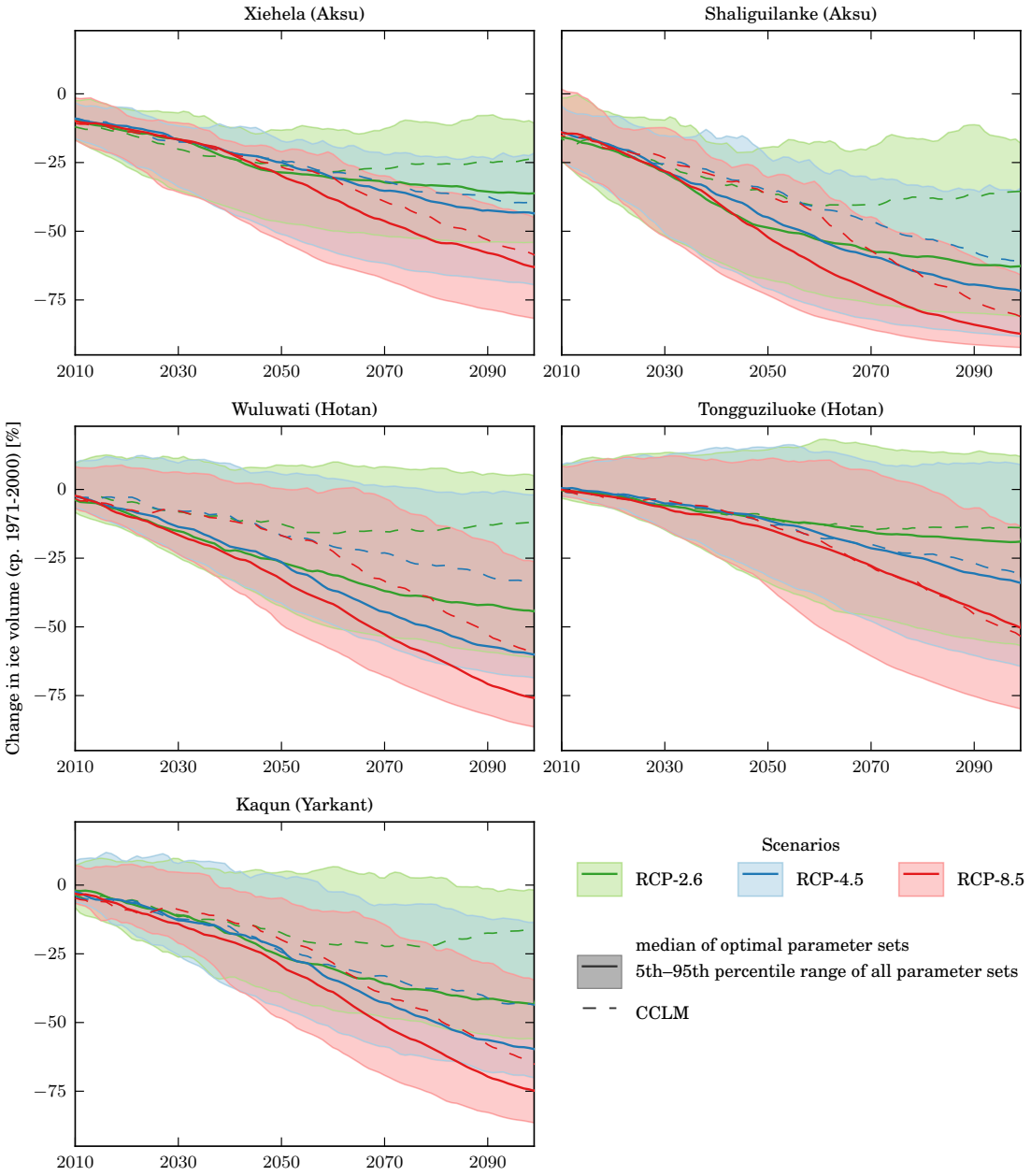

Figure 7.5: Same as in Figure 7.3 but for ice volume changes.

Table 7.3: Ensemble median values of the glacier volume change projections shown in Figure 7.5 averaged over three future climate periods.

Catchment	2011-2040			2041-2070			2071-2100		
RCP	2.6	4.5	8.5	2.6	4.5	8.5	2.6	4.5	8.5
Xiehela	-16.3	-14.9	-15.2	-28.9	-27.8	-32.3	-34.0	-39.3	-53.9
Shaliguilanke	-24.9	-23.3	-24.3	-48.8	-47.9	-53.5	-59.0	-65.1	-78.4
Wuluwati	-7.9	-6.2	-9.5	-20.7	-25.3	-32.5	-35.8	-51.7	-61.7
Tongguziluoke	-4.3	-3.9	-4.0	-11.5	-14.6	-16.5	-13.9	-25.4	-40.7
Kaqun	-8.4	-9.5	-11.0	-20.7	-27.4	-30.6	-32.7	-51.2	-60.8

balances that experience a strengthening in the first half of the 21st century with a recovery for the RCP-2.6 and 4.5 scenarios and an acceleration for the RCP-8.5 scenario by the end of the century. The near future (2011–2040) shows similar mass balances to those observed in the past across the region – -0.4–$0\,\mathrm{m\,weq.\,a^{-1}}$ – with little differences between scenarios. The largest negative mass balances for the lower two scenarios are projected for the middle of the century, while they continue to grow more negative in the high-end scenario until they reach -0.8–$-1.2\,\mathrm{m\,weq.\,a^{-1}}$ by the end of the century. A recovery to stable or even positive mass balances is only projected under the RCP-2.6 scenario in the far future.

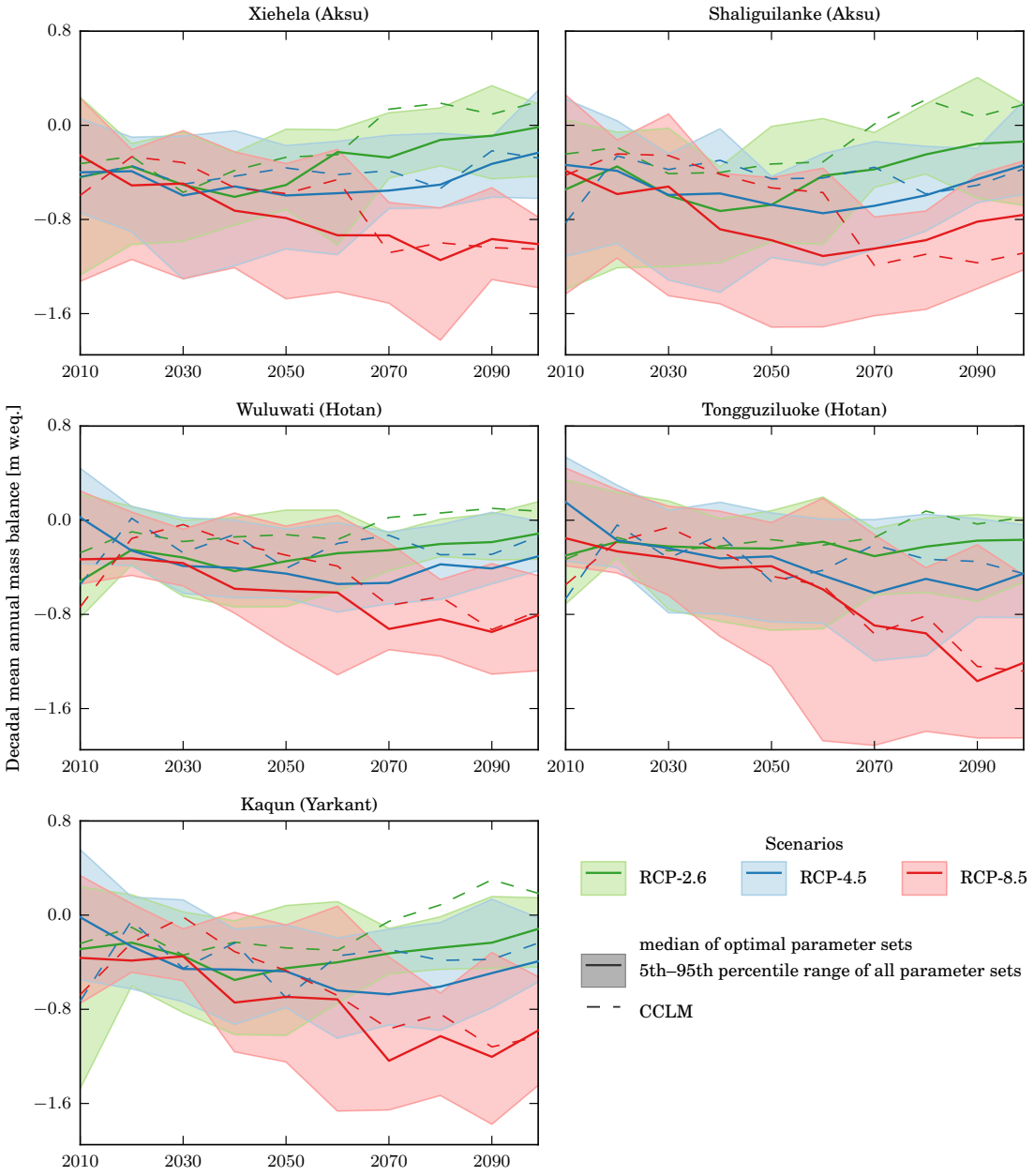

Figure 7.6: Same as in Figure 7.3 but for decadal mean mass balances.

7.5 Changes in river discharge

The discharge results of the multi-parameter set and multi-climate-model simulations are summarised in Figure 7.7 for each catchment and each scenario in asymmetric violin plots. The distributions of changes in annual mean discharge over three future climate periods and relative to the baseline period 1971–2000 are shown. The two sides of the violin plots give the distributions in changes considering all parameter configurations

and climate models on the right and on the left only the best trade-off parameter sets (and most plausible mass balance assumptions for the Hotan and Yarkant catchments) for all climate models. The simulated change in discharge driven by the regional climate model CCLM is explicitly highlighted by the diamond markers. The comparison of the two sides and the overall spread is an indication of different degrees of uncertainties, which will be discussed further in Section 7.6.

There is a general trend of increasing mean annual discharge apparent at all stations but not for all future periods. In the Aksu catchments, this increase is most pronounced in the near-future (2011–2040) but recedes in subsequent periods except for the RCP-8.5 scenario in the Xiehela catchment. This initial increase is 10% for the ensemble median relative to the 1971–2000 reference period with a slight increase relative to the RCP forcing. In the medium and long-term the increase reduces progressively and turns to a decreasing trend under the RCP-2.6 scenario in the Xiehela catchment and for the RCP-8.5 in the Shaliguilanke catchment for the ensemble median. In the Xiehela catchment, the CCLM-driven simulations generally show smaller increases and greater decreases in comparison to the entire ensemble.

Changes in mean annual discharge in the Hotan and Yarkant catchments show an uniformly increasing trend at greater magnitudes as in the Aksu catchments. The initial increase in the near future is around 30 to 40% (ensemble median, best parameter sets). Subsequent periods show stronger increases yet for at least the RCP-8.5 scenario with the RCP-4.5 simulations peaking in the medium term at 35–48% compared to the baseline period. The RCP-2.6 scenario shows lower discharges in the later periods than in the first, reducing to 5% higher in the Yarkant catchment in the far future. Simulations driven by the regional climate model CCLM are generally far below (in the RCP-2.6 scenario and the near future) or close to the ensemble median.

To show what these changes mean for the monthly discharge regime for the three rivers, the CCLM best trade-off simulations are plotted in Figures 7.8 to 7.10 at the monthly time scale for all three scenarios. Rather than relative change for each month in comparison to the reference period, the monthly contributions to the annual discharge changes are shown to account for the highly seasonal flows. For example, since winter

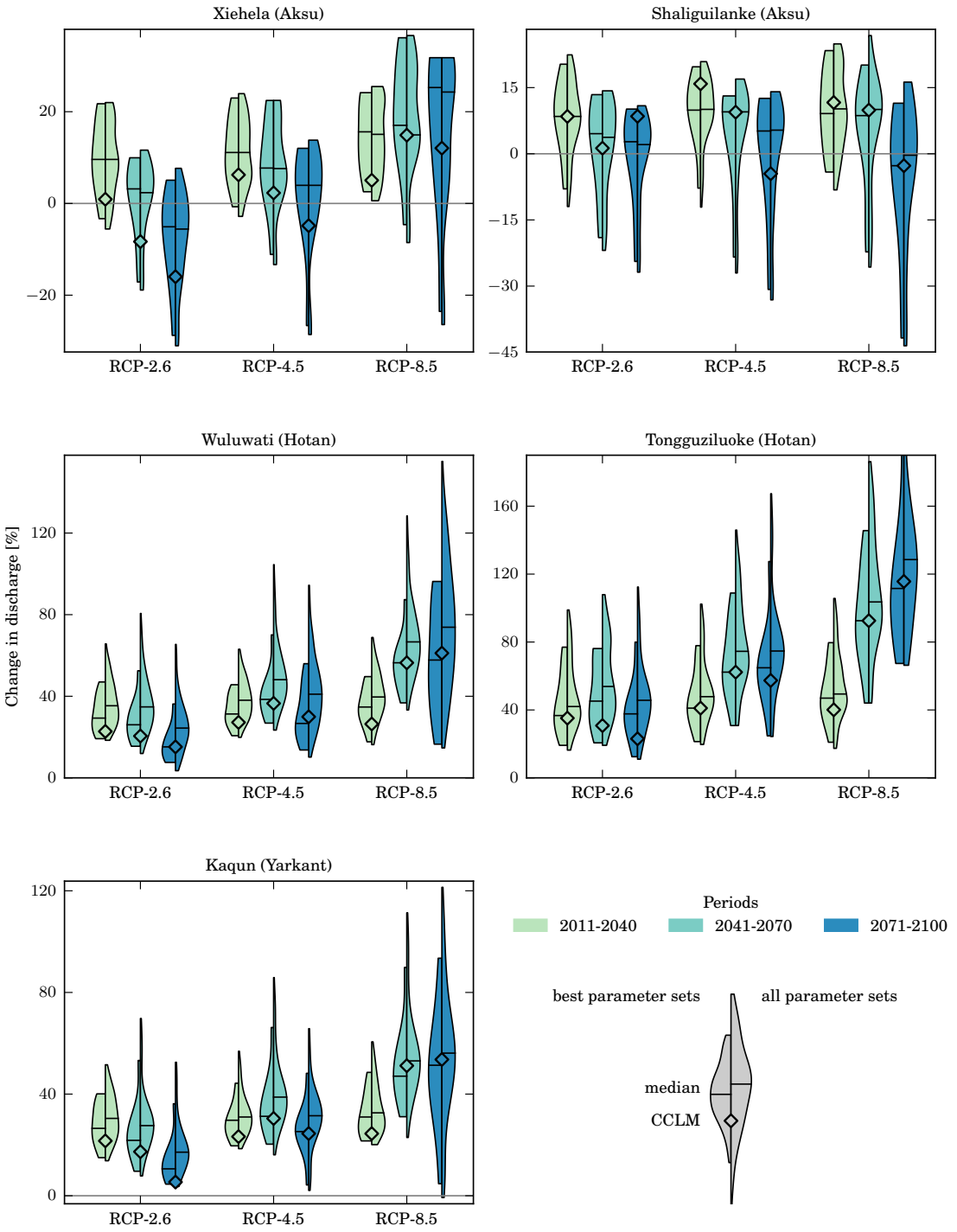

Figure 7.7: Changes in annual mean discharge simulated by SWIM-G driven by various climate models and various parameter configurations (see text). Changes are relative to the baseline period 1971–2000. The asymmetric violin plots indicate the distributions considering all parameter sets (right) and only the best trade-off parameter configurations as well as most plausible mass balance assumptions (Hotan and Yarkant) on the left. The median simulations driven by the regional climate model CCLM are indicated by a diamond.

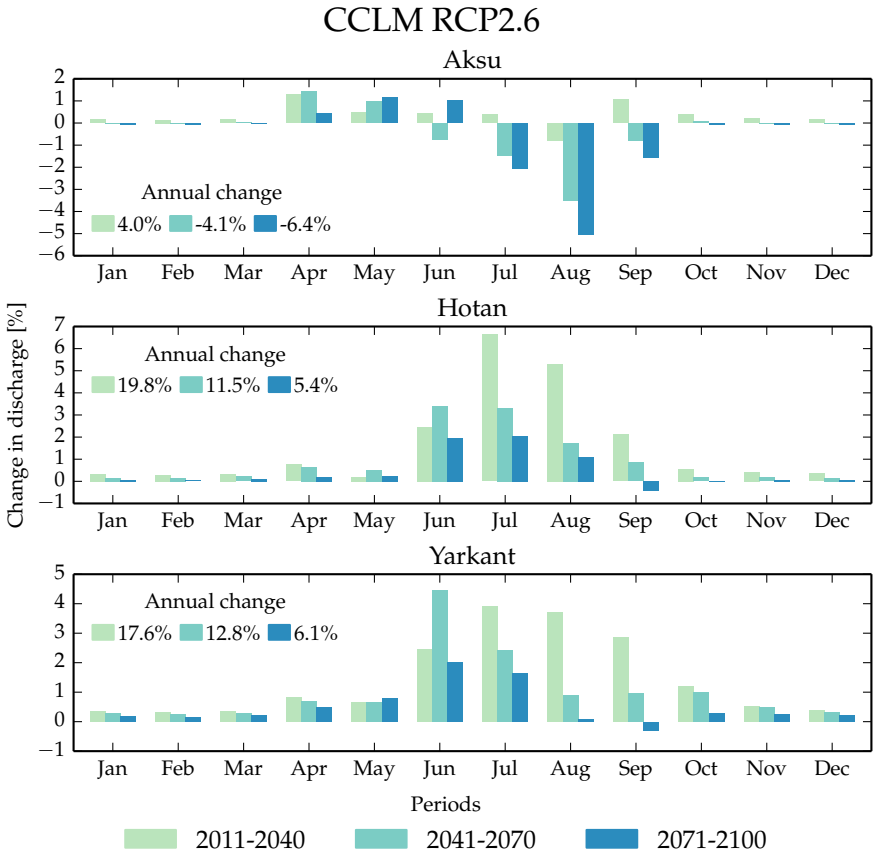

Figure 7.8: Changes of mean annual discharge decomposed over the monthly regime aggregated to the three main headwaters of the Tarim River for the scenario RCP-2.6. Values are median values of the CCLM driven simulations using the best model parameter sets.

discharge is very low (5–10% of mean annual flow) a small absolute increase would lead to drastic relative changes, but only has a small impact on overall changes. April to June discharge predominantly increases in the Aksu catchments for all scenarios, while middle and late summer discharge (July–September) tends to decrease. This signal is stronger in the RCP-2.6 and weaker in the RCP-8.5 scenario especially in the far future. The Hotan and Yarkant catchments show increases especially in the summer months (June to September) that progress with period and RCP concentration. Only under the RCP-2.6 scenario does discharge decrease in September in the far future. Winter discharge changes in all catchments are mostly positive but represent only small fractions of the increase in the annual discharge.

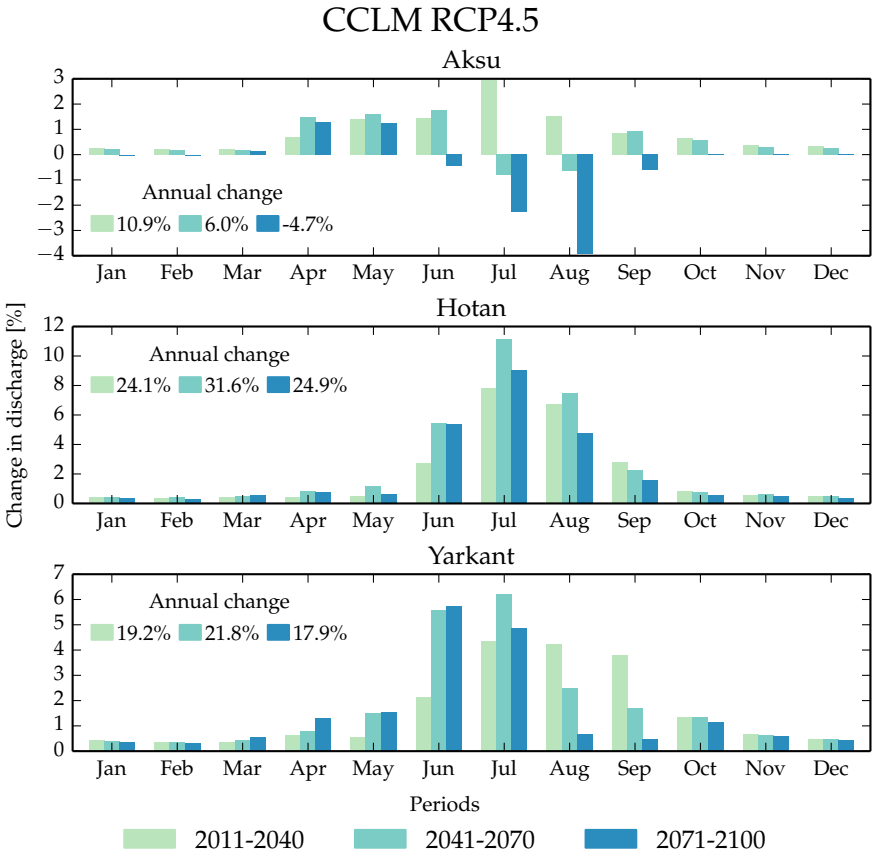

Figure 7.9: Same as Figure 7.8 but for the RCP-4.5 scenario.

The origin of these changes can be traced by investigating the changes in the runoff generating water inputs, i.e. rain, glacier and snow melt (Figure 7.11). As would be expected under a warmer and wetter climate, the share of rain is increasing in all catchments under most scenarios and the contribution of glacier melt is decreasing. An exception is the highly glacierised Tongguziluoke (Hotan) catchment, where the share of rain and glacier melt is increasing, indicating an increased redistribution of ice into the ablation zone. The contribution of snowmelt is nearly constant, although slightly increasing under the RCP-2.6 and 4.5 scenarios in the Xiehela (Aksu) catchment and slightly decreasing under the RCP-8.5 scenario. Absolute input values reveal the peak in glacier melt predominently in the first half of the 21st century for the Hotan and Yarkant catchments (Figure 7.12). Under the RCP-8.5 scenario the peak is shifted further into the second half of the century, especially evident in the Tongguziluoke (Hotan) catchment. There is no peak in the Aksu catchments under the RCP-2.6 and 4.5 scenarios, leading to the decline in discharge as described above.

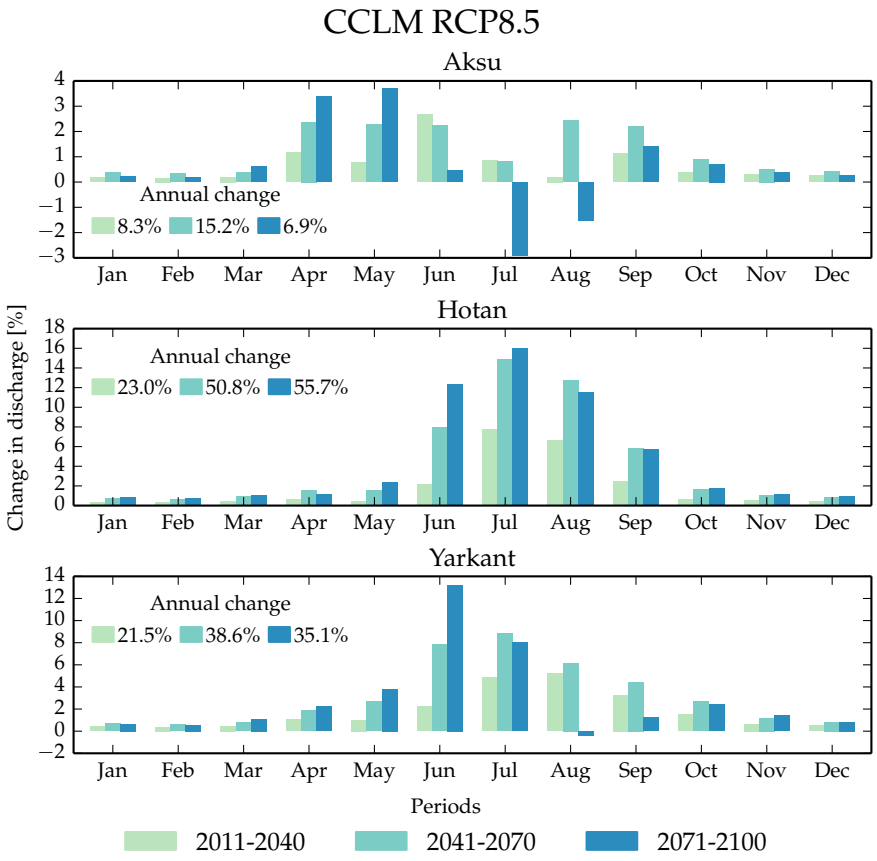

Figure 7.10: Same as Figure 7.8 but for the RCP-8.5 scenario.

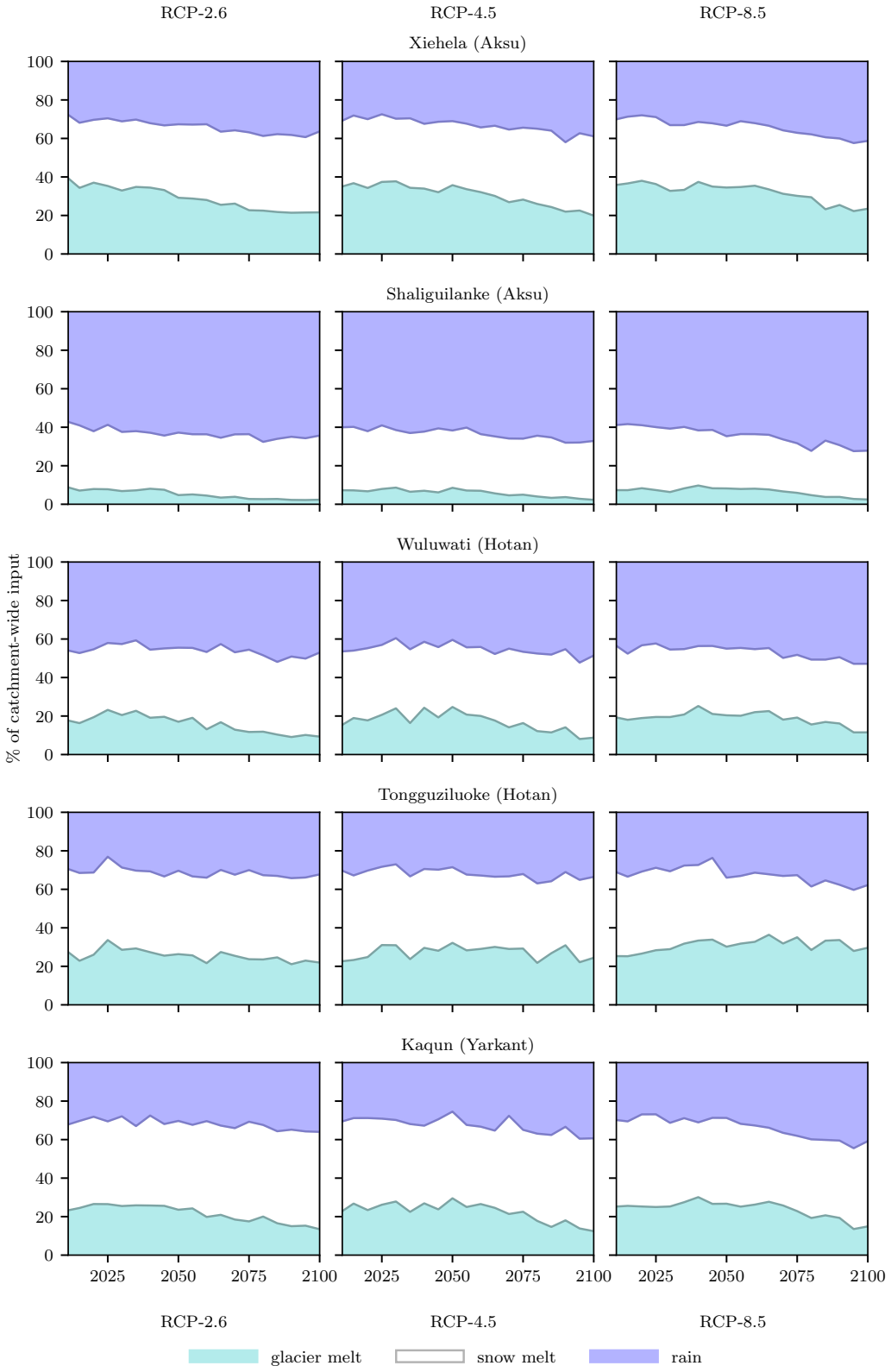

Figure 7.11: Projected contribution of glacier melt, snow melt and rain to runoff generation. Five-year average values are shown of the climate model median and using the optimal parameter sets.

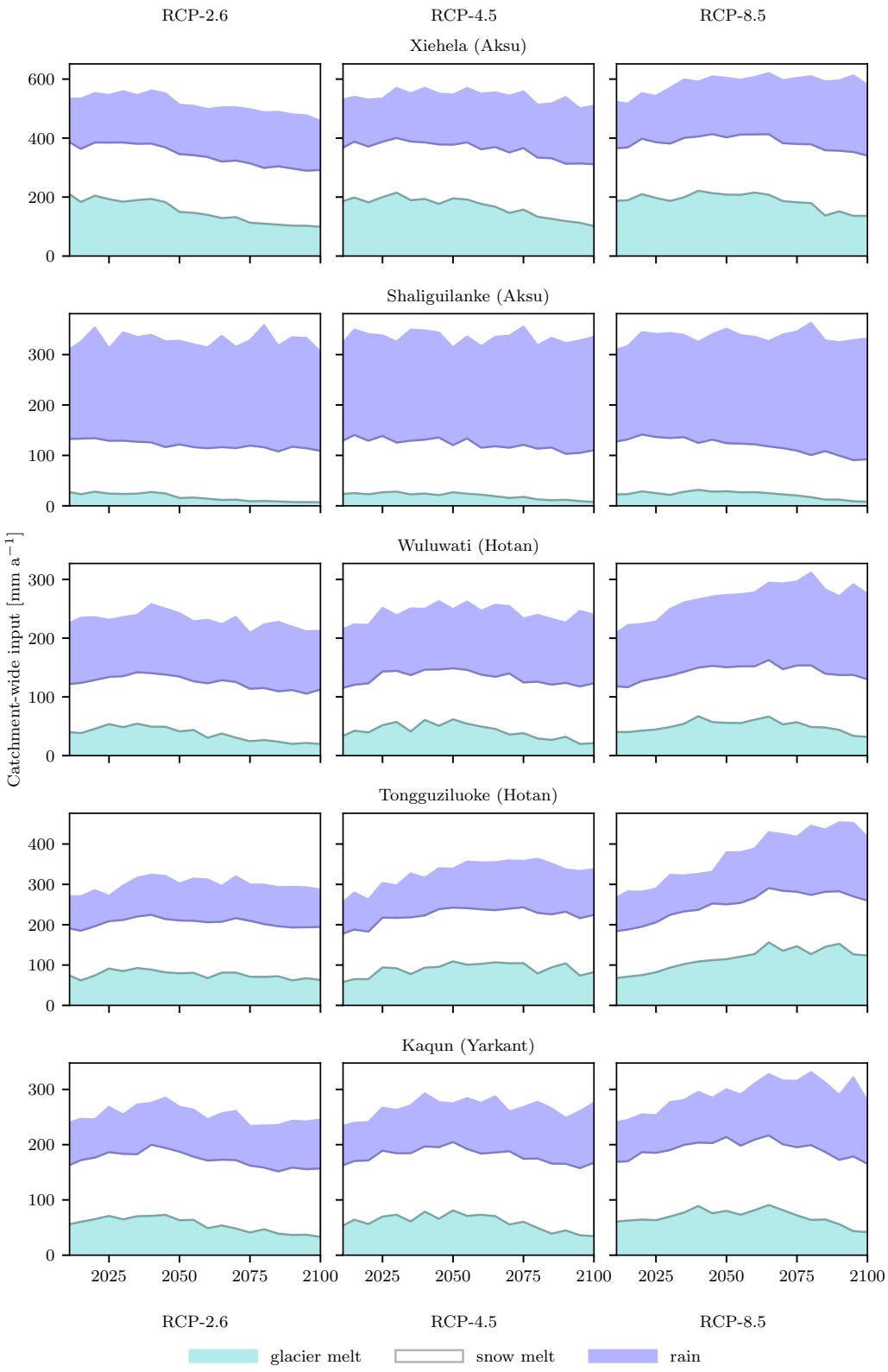

Figure 7.12: Same as Figure 7.11 but with absolute input values in mm a^{-1}.

7.6 Uncertainty analysis

The uncertainties in the climate (Figure 7.2), glacier (Figures 7.3, 7.5 and 7.6) and discharge (Figure 7.7) projections are evidently large. Uncertainty ranges span large fractions of the change signal and increase in time. Due to the greater knowledge of historic mass balances in the Aksu catchments, uncertainty ranges are narrower than in the Hotan and Yarkant catchments (e.g.25–40 % versus 50–75 % by the end of the century for glacier area simulations), where initial mass balance assumptions had to be made. Ranges markedly increase in the second half of the 21st century in the Hotan and Yarkant catchments, while a moderate increase or even a decrease in the range is evident in the Aksu catchments.

RCP scenario ranges are widely overlapping for all simulation results and catchments, suggesting that the model uncertainty exceeds the scenario uncertainty even by the end of the century where the scenarios diverge most.

While the results presented above only show the overall uncertainties, the individual contributions may be analysed through the variance of the uncertainty terms, the model's driving data (CMIP climate model results) and the parameter configurations. The total variance maybe decomposed into the variance of only those terms and reported as fractions of the total variance, an analysis known as analysis of variance (ANOVA) (Bosshard et al., 2013; Vetter et al., 2015). The unbiased variance (normalised to sample size) is calculated for the simulations of the different components and divided by the total sum of variances. Differences between scenarios are also considered to compare them to the sources of uncertainties.

Figure 7.13 shows the results of the ANOVA analysis for glacier area and annual mean discharge simulations over both the reference and scenario period. Over the reference period scenarios do not differ and thus do not contribute to the variance. Differences in glacier area simulations are initially mainly determined by differences in the model's parameter sets, but the contribution of variance between climate models increases steadily after the reference period. Parameter set variance decreases to below 0.2 in the second half of the 21st century, but is larger for the Hotan and Yarkant

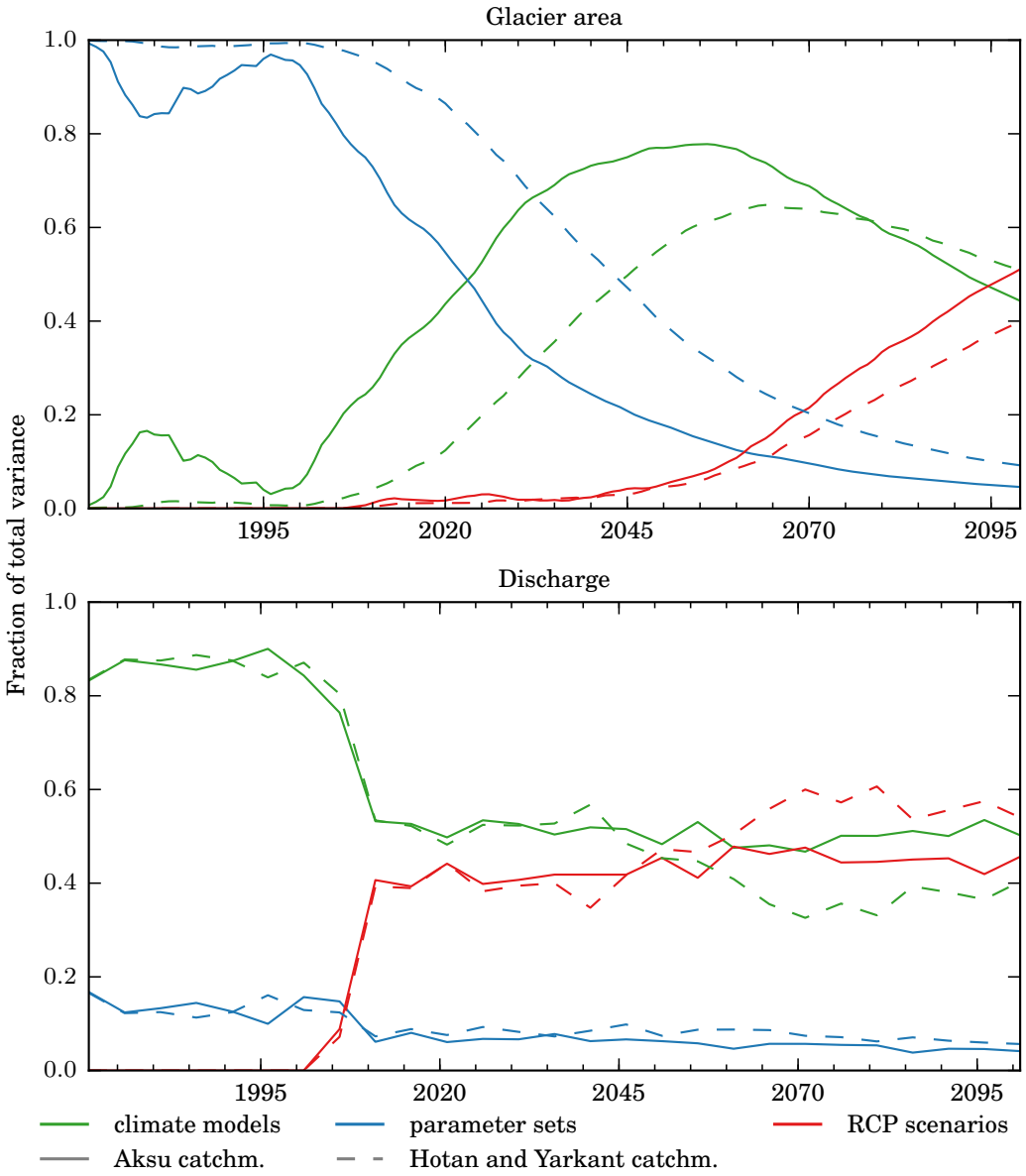

Figure 7.13: The fraction of the total variance for glacier area (top) and discharge (bottom, 5-year mean) simulations for the three components (climate models, parameter sets and RCP scenarios). For the Aksu catchments (solid lines), mass balances were known over the reference period, while the Hotan and Yarkant catchments (dashed lines) were calibrated for three initial mass balance assumptions.

catchments due to the mass balance uncertainties. The variance induced by the climate models peaks around the middle of the century, from which point the contribution of scenarios increases steadily to about 0.5.

The strong influence of the driving climate data is apparent in the variance components of annual mean discharge. Over the reference period, the differences between the

model's parameter sets contribute less than 20% of the variance. The contribution of the scenarios rises to 0.4 at the start of the scenario period and only marginally increases over the 21st century overtaking the climate model contributions only in the Hotan and Yarkant catchments. The parameter set contribution is below 0.1 over the scenario period with the Hotan and Yarkant catchment simulations only marginally above those of the Aksu catchments.

7.7 Comparison to other studies

Climate change projections of future glacier cover are scarce in High Asia and those assessing river discharge simultaneously are even more rare (Bolch et al., 2012b; Chaturvedi et al., 2014; Kulkarni, 2014). This is especially true for the Tarim River, where only two studies are known to assess state of the art climate scenarios. Projected glacier area changes of these two studies, in the Yarkant and Aksu catchments, are listed in Table 7.4 along with other studies from the wider region. The glacier area projections of these studies compare well with results presented here (Table 7.2).

Zhang et al. (2012) assessed three IPCC SRES scenarios in the Yarkant catchment only until 2050. Glacier area changes (−17−−13 %) are close to the findings presented in this chapter (−25−−17 %). Since they only employed a glacier mass balance model, there is no accounting for catchment discharge or glacier dynamics.

Table 7.4: Climate change impact studies of glacier area and/or discharge change in catchments of High Mountain Asia using both IPCC SRES and RCP scenarios. Changes approximately refer to the reference year 2000.

Reference	Study area	Glacier area change [%]	
		2050	2100
Duethmann et al., 2016	Aksu headwaters	-69 to -12	-90 to -32
Zhang et al., 2012	Yarkand basin	-17 to -13	
Sorg et al., 2014	Chon Kemin basin	-88 to -14	-100 to -50
Gan et al., 2015	Naryn basin		-65 to -36
Lutz et al., 2013	upper Amu & Syr Darya	-65 to -55	
Hagg et al., 2013	Tanimas basin	-45 to -35	
Immerzeel et al., 2011	Langtang basin, upper Ganges	-50 to -30	-90 to -60

In a study similar to the research of this chapter, Duethmann et al. (2016) projected glacier cover and discharge changes for the Aksu headwaters. The results agree well with the ones presented here, but the glacier recession is a lot steeper in the first half of the 21st century than those presented in Figure 7.3. This is likely to be caused by the use of an empirical, hypsometry-based glacier geometry change approach, rather than accounting for the ice flow of individual glaciers (as shown in Chapter 5).

7.8 Summary

This chapter used the model constructed in Chapter 5 and implemented in Chapter 6 to conduct a climate change impact assessment of both glacier and discharge changes over the 21st century. The scenario modelling approach incorporates climate driving data from eight GCMs and one RCM over three state of the art climate change scenarios (RCP-2.6, 4.5, 8.5) and considers the uncertainties introduced by the different model parameter configurations.

Both temperature and precipitation are projected to rise significantly over all five catchments (up to 6 °C warmer and up to 60 % wetter), but climate models show a large spread in both variables with also decreasing precipitation. This climatic trend produces a strong glacier recession with about 50% of glacier area lost by the end of the century, but the large climate model uncertainty is propagated. Discharge projections show strong increases in the near future, then decreases in the Aksu catchments and further increases in the Hotan and Yarkant catchments in the middle and at the end of the century. Discharge increases are greatest in the summer months (JJA) and decreases in the Aksu catchment mainly occur in late summer due to a shrinking glacier coverage. An ANOVA uncertainty analysis revealed the climate model uncertainties to be larger than the differences between scenarios over almost all of the 21st century. Although glacio-hydrological model parameters lead to differences in initial glacier area, they are responsible for a much smaller fraction of the uncertainties by the middle and at the end of the century and all discharge simulations.

Chapter 8

Summary, conclusions and recommendations

8.1 Summary of research conducted

The research conducted in this thesis addressed the difficulties of modelling mountainous, glacierised catchments and the benefits of integrating glacier dynamics into a semi-distributed hydrological model. These included problems of data scarcity, the spatial representation of individual glaciers at the catchment scale and the calibration of the model to multiple and diverse observations. The main objective of the thesis was to develop a glacier dynamics module for the Soil and Water Integrated Model (SWIM), based on validated approaches from glaciological as well as hydrological models. The research questions as outlined in Chapter 1 address both the need and the value of integrating glaciers into hydrological modelling of mountainous catchments.

The structure of the thesis reflects the typical steps of implementing and improving an existing model: Chapters 1 and 2 introduced the background of the research, Chapters 3 and 4 described the scientific problems in the Tarim headwaters, Chapter 5 covered the module development and validation and Chapters 6 and 7 provide a wider implementation and use of the improved model.

8.2 Key findings and answers to research questions

As described in Chapter 1, the research questions this thesis has addressed fall into three themes (data scarcity, model implementation and improvement, climate change impact assessment) and focus on the headwater catchments of the Tarim River. In the following sections, conclusions for all research questions are provided with reference to all relevant parts of the thesis. Where the conclusions are also relevant outside the focus region of the Tarim River, the generality of the findings are highlighted and discussed.

1. Data scarcity

(a) *What is the quality and uncertainty of the available regional precipitation datasets?*
The six selected gridded precipitation datasets exhibited strong differences between each other considering catchment mean annual values, monthly regimes as well as the spatial distribution of precipitation (in Chapter 3). In general, satellite and climate model based datasets indicate much higher precipitation than the observation-based datasets (1.2–8 times larger), while the latter show a much more homogeneous spatial distribution than would be expected. It is found that the sparse network of the observation-based datasets, with some catchments completely devoid of meteorological stations, leads to severe underestimations of the high-mountain discharge, where most of the discharge of the Tarim River originates. Since the satellite and model-based datasets are largely unsuitable for daily hydrological modelling due to coarser temporal resolutions, short periods of operations and insufficient correlation with discharge, a correction of the best observation-based dataset (APHRODITE) is found to be indispensable.

(b) *How can the glacio-hydrological model inform the correction of precipitation data by using inverse modelling, as previously tested in other high mountain catchments?*
The implemented model was calibrated to river discharge and glacier area (as well as glacier mass balance where data were available). As the observed catchment precipitation was found to be far below values needed to sustain the glacier cover due to data quality (see previous question), a three-parameter precipitation correction was used as part of the calibration (Chapter 6). The application of a

glacio-hydrological model allowed for a precipitation correction that is in line with both the discharge and the glacier cover, assuming these two observations are more robust than the precipitation observations. A similar inverse modelling approach has been tested in the neighbouring Upper Indus basin (Immerzeel et al., 2015; Immerzeel et al., 2012), but only through a simple water balance calculation. The glacier dynamics module in SWIM-G is able to incorporate glacier cover and test mass balance scenarios where mass balance information is unavailable, as has been shown in the Hotan and Yarkant catchments.

(c) *What is the simulated mean catchment precipitation and how does it compare to other precipitation datasets?*

The calibrated or corrected precipitation according to SWIM-G (as shown in Chapter 6) is on average 1.4–4.3 times higher than the observation-based APHRODITE dataset, that is 327–487 $\mathrm{mm\,a^{-1}}$ (1.4–1.5 times higher) in the Aksu catchments, 229–285 $\mathrm{mm\,a^{-1}}$ (2.4–4.3 times higher) in the Hotan catchments and 267 $\mathrm{mm\,a^{-1}}$ (2.1 times higher) in the Yarkant catchment. Although the magnitudes of correction factors are large, the values fall between the observation-based datasets and the climate model-based ones that were assessed in Chapter 3. The corrected precipitation also produces much more plausible runoff coefficients ranging from 0.4–0.8 depending on the catchments' proportional glacier cover.

2. Model implementation and improvement

(a) *How well does the standard SWIM model code as described by Huang et al. (2010, 2013b) perform in a highly glacierised catchment compared to discharge observations without accounting for glaciological observations?*

Implemented in the Xiehela (Aksu) catchment with a glacier cover of 20% (in Chapter 4), the standard SWIM model code reproduced the observed discharge with very good results, indicated by a high performance in Nash-Sutcliffe Efficiency (NSE) (0.81–0.92) and bias in water balance (−16–−2 %) over both the calibration and validation period. Negative biases in the water balance were found to be caused by near-annually reoccurring Glacier Lake Outburst Floods (GLOFs). However, the disregard for glaciological changes during the calibration leads to a

strong compensation of underestimated precipitation by freely increasing glacier melt. This leads to highly unlikely negative mass balances, i.e. $-0.7\,\mathrm{m\,weq.\,a^{-1}}$ compared to the $-0.25\,\mathrm{m\,weq.\,a^{-1}}$ global average. Further, the standard SWIM code does not account for ice dynamics. As a result the snowpack at higher elevations builds up indefinitely, while the lower-lying valley glaciers recede quickly without resupply from the accumulation zones. This presents the basis for the model improvement in Chapter 5.

(b) *How can a hydrological catchment model aid the analysis and detection of glacial lake outburst floods in discharge timeseries of mountainous catchments?*

The discharge simulations of the Xiehela (Aksu) catchment (modelled in Chapter 4) deviate considerably from observations for short periods (mostly in late summer for 5–10 days), when recorded values show large flood events that are not represented by the model. Closer inspection revealed that these flood events originate from the glacial lake outburst floods of the glacier-dammed Merzbacher Lake. The fact that this process is not represented by the hydrological model can be exploited to identify such outburst floods in discharge timeseries and estimate the flood volume. By applying a threshold that is linearly varying with observed discharge to the observation-simulation residuals, the developed method is able to identify all witnessed flood events reported in the literature (Glazirin, 2010), while also casting doubt on one reported flood event that may have been falsely identified as a GLOF. After identification and exclusion of the flood events from the observation data, a new model calibration yielded performance improvements: NSE increased from 0.82 to 0.90 and the bias in the water balance was reduced from -16% to -2%. Flood volumes are estimated to range from $56\,\mathrm{m^3}$ to $291\,\mathrm{m^3}$ and are similar to estimates obtained through visual hydrograph separation. The model-based estimates offer the advantage of accounting for weather-induced signals in the flood baseflow.

(c) *How can the SWIM model be improved to account for all major glacier processes, especially ice dynamics?*

The shortcomings of the SWIM model in highly glacierised catchments (as found in Chapter 4) were addressed by developing and validating a glacier dynamics module

in Chapter 5. A spatial disaggregation scheme for the potentially glacierised part of the catchment was developed that is based on combinations of topographical characteristics (elevation zone, exposure and subbasin) in a similar fashion to the traditional hydrotopes. This allows the meaningful downslope redistribution of ice and snow (in avalanches) as well as a tight coupling of the glacier processes with the hydrological model. Mass balance processes were improved mostly adopting tested approaches from the literature, such as melting based on Degree-Day factors, slope aspect and terrain shading and reduced melt rates under supra-glacial debris, with a strong focus on parameter and data parsimony. A simple approach to estimating sublimation based on Degree-Day factors was developed to represent this often neglected process in high elevation catchments, where it can have a considerable influence on the annual glacier mass balance. The model validation in two highly glacierised catchments (the data-scarce Upper Aksu and the data-abundant Upper Rhone catchments) showed good results in terms of the initialised glacier area hypsometry, river discharge as well as glacier area and mass changes over the reference period.

(d) *How well does the improved model reproduce hydrological and glaciological observations over the reference period 1971–2000 in the data-scarce Tarim headwaters?*

The improved SWIM model, SWIM-G, was applied to all five headwater catchments of the Tarim River in Chapter 6 with largely satisfactory results, despite missing mass balance information in the Hotan and Yarkant catchments. Daily discharge observations were reproduced with a mean NSE of 0.73–0.92 and annual discharge was simulated with average root mean square errors of 13.2–23.1 % of mean discharge. The glacier hypsometry was initialised with a χ^2 accuracy of 3.7–14.4 % of total glacier area, while the glacier area and mass changes compare well to studies in the Aksu catchment. Out of the three initial mass balance assumptions assessed in the Hotan and Yarkant catchments, the $-0.1\,\mathrm{m\,weq.\,a^{-1}}$ scenario confirms current research findings from the Karakoram and Kunlun Shan mountain ranges that report stable to slightly positive glacier mass balances (Bolch et al., 2017; Kääb et al., 2015). The differences in calibration results are largely aligned with

data quality, with the Hotan and Yarkant catchments showing lower performance ratings than the Aksu catchments.

3. Climate change impact assessment

(a) *What are the projected impacts on river discharge of the Tarim headwaters considering three IPCC climate change scenarios simulated by an ensemble of climate models in three periods of the 21st century with regards to the reference period 1971–2000?*

All three climate scenarios project warmer conditions over the climate model ensemble (0.5–7.0 °C), while most models also project strong increases in precipitation across the 21st, especially in the Hotan and Yarkant catchments (up to 54 %). As a consequence, the SWIM-G model projects largely strong increases in discharge, in particular in the near future and increasing with RCP scenario intensity. Increases in the Aksu catchments are less intense (10–25 %) than in the Hotan and Yarkant catchments (30–105 %) and discharge is at greater risk of decreasing in the medium to far future, especially in the RCP2.6 scenario. In the Hotan and Yarkant catchments, discharge is projected to be consistently above that of the reference period, despite large uncertainty ranges.

(b) *How will the glacier cover (area and volume) change under these climate projections?*

A general trend of glacier recession is projected in all catchments under most scenarios with the low-end RCP2.6 scenario leading to a stabilisation or even recovery by the end of the 21st century. Ensemble median area losses in the far future are 11–50 % for the low-end RCP2.6 scenario, 20–56 % for the medium RCP4.5 scenario and 32–71 % for the high-end RCP8.5 scenario, with the Shaliguilanke (Aksu) catchment worst affected and the Tongguziluoke (Hotan) catchment least. Volume losses follow the same pattern but slightly greater magnitudes. A complete recovery to reference conditions are only simulated in the Hotan catchments at the upper uncertainty bound.

(c) *What are the uncertainties of the discharge and glacier cover projections induced by the climate model ensemble and the calibration parameters and how do both sources compare to the scenario uncertainty?*

Uncertainty ranges of discharge and glacier change projections spann 20–100 percentage points. At least for the discharge simulations in the Aksu catchments, the uncertainty ranges cover both directions of change. Uncertainty ranges of different climate scenarios are mostly widely overlapping and they are larger in the Hotan and Yarkant catchments than in the Aksu catchments, due to the lack of historic mass balance information. Most uncertainty is induced by the climate model ensemble over the scenario period (ca. 50%) compared to the parameter uncertainty (ca. 10%), although the latter plays a larger role in the glacier area projections at the beginning of the century. In comparison, the scenario uncertainty in the first half of the century is slightly lower (40%) than the climate model uncertainty for the discharge projections and negligible for glacier area. In the second half of the century, the share rises rises to become roughly equal to the climate model uncertainty.

8.3 Recommendations for further research

A significant amount of time during this PhD project was spent on acquiring and homogenising model driving and validation data, such as discharge, meteorological and glaciological observations. First and foremost, the quality and sheer inexistence of precipitation observations over large parts of the catchment area (as described in Chapter 3) lead to numerous failed attempts to adequately model the water balance of the remote Tarim River headwaters. Any improvements, newly available sources, rediscovery or declassification of old data would make a comparison with and an update of the presented results worthwhile. The establishment of a network of automatic weather stations at higher elevations is necessary to drive better models in the future (Bolch et al., 2012a) and to verify precipitation correction methods or validate newly available remote sensing data (such as the GPM data presented in Section 3.3).

Chapter 6 presents a method to correct the inadequate precipitation data using an elevation-dependent equation and three calibration parameters. An exploration of

more sophisticated precipitation correction approaches would also be interesting, but was not feasible as part of this PhD work. For example, exploiting the climatological information of regional climate model (RCM) datasets would be a valuable source of correction factors over space (catchment area) and time (e.g. monthly), an approach that has been shown by Duethmann et al. (2013). The 10-km HAR dataset (presented in Section 3.3) would be an excellent start, although it only covers the Hotan and Yarkant catchments at a fine resolution and covers a relatively short period of time (10 years).

Even better, but as yet prohibitively time consuming, would be the specific deployment of a high-resolution RCM to use the modelled driving variables directly in the glacio-hydrological model, such as liquid and solid precipitation, radiation and latent heat flux. These data could potentially greatly improve the accuracy of the simulations with a full energy balance glacier mass balance accounting model, although in situ validation data would also be needed. This greater integration of the atmospheric components would also allow for an assessment of parameter stability in a future warmer climate ('ungauged climates' Merz et al., 2011). For example, it has been suggested that temperatures rise faster in mountains under climate change, an effect termed 'elevation-dependent temperature rise' (MRIEDWWG, 2015). A high-resolution RCM would provide a unique opportunity to explore such effects.

The scarcity of glaciological studies in the Tarim region also impacted the research presented in this thesis. Fortunately, the glaciological working group of the overarching research project (Sustainable Management of River Oases in the Tarim Basin (SuMaRiO)), produced valuable insights into the historic changes in glacier area and volume of the Aksu catchments, while the lack of this information for the Hotan and Yarkant catchments made a scenario approach necessary. Therefore, further research is needed to assess glacier area changes and mass balance at the catchment scale for these catchments over at least a 20–30-year period. Pieczonka and Bolch (2015) provide valuable approaches for such work. This information would greatly reduce the uncertainty of the results presented here, as the differences in uncertainties between the Aksu and the Hotan/Yarkant catchments have demonstrated.

To further validate the glacier dynamics module presented in Chapter 5, it would be interesting to assess the differences in results of glacio-hydrological models with different spatial representations of glaciers, such as an empirical hypsometry-based model (Duethmann et al., 2016; Hagg et al., 2007)) and a fully distributed, physically-based model (Immerzeel et al., 2011). This would better reveal and quantify performance trade-offs, such as computational time, data requirements and the accuracy of simulation results. However, more detailed validation data would be necessary in the Tarim River headwaters for such an assessment and has for that reason not been conducted as part of this thesis.

Finally, the model could most certainly be refined by collecting more characteristic parameter values in the field and by using more satellite observations to calibrate the model, such as snow cover data (as has been shown by Duethmann et al. (2014)) or evapotranspiration products. The author's reconnaissance field trip to the Aksu catchment yielded valuable insights and a greater understanding of the hydrology of the region, but was too short for systematic data collection. Estimates of soil and root depth as well as soil porosity observations are extremely scarce and would most probably enhance the accuracy of the simulations. The calibration approach used in this thesis (multi-objective automatic calibration) would allow for the incorporation of other research results (such as remote sensing products) or scarce field observations.

First-authored and co-authored publications

Wortmann, M., Bolch, T., Krysanova, V., Buda, S. (in review). "An efficient representation of glacier dynamics in a semi-distributed hydrological model to bridge glacier and river catchment scales".

Wortmann, M., Bolch, T., Menz, C., Jiang, T., Krysanova, V. (2018). "Comparison and correction of high-mountain precipitation data based on glacio-hydrological modelling in the Tarim River headwaters (High Asia)". In: *Journal of Hydrometeorology*. doi: 10.1175/JHM-D-17-0106.1.

Huang, S., D. **M. Wortmann**, Duethmann, C. Menz, F. Shi, C. Zhao, B. Su, V. Krysanova (2018). "Adaptation strategies of agriculture and water management to climate change in the Upper Tarim River basin, NW China". In: *Agricultural Water Management* 203, 207–224. doi: 10.1016/j.agwat.2018.03.004

Rumbaur, C., N. Thevs, M. Disse, M. Ahlheim, A. Brieden, B. Cyffka, D. Duethmann, T. Feike, O. Frör, P. Gärtner, U. Halik, J. Hill, M. Hinnenthal, P. Keilholz, B. Kleinschmit, V. Krysanova, M. Kuba, S. Mader, C. Menz, H. Othmanli, S. Pelz, M. Schroeder, T. F. Siew, V. Stender, K. Stahr, F. M. Thomas, M. Welp, **M. Wortmann**, X. Zhao, X. Chen, T. Jiang, J. Luo, H. Yimit, R. Yu, X. Zhang, and C. Zhao (2015). "Sustainable Management of River Oases along the Tarim River (SuMaRiO) in Northwest China under Conditions of Climate Change". In: *Earth Syst. Dynam.* 6.1, pp. 83–107. doi: 10.5194/esd-6-83-2015.

Krysanova, V., **M. Wortmann**, T. Bolch, B. Merz, D. Duethmann, J. Walter, S. Huang, J. Tong, S. Buda, and Z. W. Kundzewicz (2015). "Analysis of Current Trends in Climate Parameters, River Discharge and Glaciers in the Aksu River Basin (Central Asia)". In: *Hydrological Sciences Journal* 60.4, pp. 566–590. doi: 10.1080/02626667.2014.925559.

Kundzewicz, Z. W., B. Merz, S. Vorogushyn, H. Hartmann, D. Duethmann, **M. Wortmann**, S. Huang, B. Su, T. Jiang, and V. Krysanova (2014). "Analysis of Changes in Climate and River Discharge with Focus on Seasonal Runoff Predictability in

the Aksu River Basin". In: *Environmental Earth Sciences* 73.2, pp. 501–516. doi: 10.1007/s12665-014-3137-5.

Wortmann, M., V. Krysanova, Z. W. Kundzewicz, B. Su, and X. Li (2014). "Assessing the Influence of the Merzbacher Lake Outburst Floods on Discharge Using the Hydrological Model SWIM in the Aksu Headwaters, Kyrgyzstan/NW China". In: *Hydrological Processes* 28.26, pp. 6337–6350. doi: 10.1002/hyp.10118.

Wortmann, M., S. Huang, and V. Krysanova (2012). "Complexities in Modelling Water Availability in the Water-Scarce Aksu Catchment, Northwest China". In: *Proceedings of the Sixth Biannial Meeting of the International Environmental Modelling and Software Society.* International Congress on Environmental Modelling and Software. Leipzig, Germany, pp. 2794–2800.

References

Abbott, M., J. Bathurst, J. Cunge, P. O'Connell, and J. Rasmussen (1986a). "An Introduction to the European Hydrological System – Systeme Hydrologique Europeen, "SHE", 1: History and Philosophy of a Physically-Based, Distributed Modelling System". In: *Journal of Hydrology* 87 (1-2). 01022, pp. 45–59. DOI: 10.1016/0022-1694(86)90114-9.

Abbott, M., J. Bathurst, J. Cunge, P. O'Connell, and J. Rasmussen (1986b). "An Introduction to the European Hydrological System – Systeme Hydrologique Europeen, "SHE", 2: Structure of a Physically-Based, Distributed Modelling System". In: *Journal of Hydrology* 87 (1-2), pp. 61–77. DOI: 10.1016/0022-1694(86)90115-0.

Aich, V., S. Liersch, T. Vetter, S. Huang, J. Tecklenburg, P. Hoffmann, H. Koch, S. Fournet, V. Krysanova, E. N. Müller, and F. F. Hattermann (2014). "Comparing Impacts of Climate Change on Streamflow in Four Large African River Basins". In: *Hydrol. Earth Syst. Sci.* 18.4, pp. 1305–1321. DOI: 10.5194/hess-18-1305-2014.

Aizen, V., E. Aizen, and J. Melack (1995). "Climate, Snow Cover, Glaciers, and Runoff in the Tien Shan, Central Asia". In: *JAWRA Journal of the American Water Resources Association* 31.6, pp. 1113–1129. DOI: 10.1111/j.1752-1688.1995.tb03426.x.

Aizen, V. B., E. M. Aizen, and J. M. Melack (1996). "Precipitation, Melt and Runoff in the Northern Tien Shan". In: *Journal of Hydrology* 186 (1–4), pp. 229–251. DOI: 10.1016/S0022-1694(96)03022-3.

Aizen, V. B., V. A. Kuzmichenok, A. B. Surazakov, and E. M. Aizen (2006). "Glacier Changes in the Central and Northern Tien Shan during the Last 140 Years Based on Surface and Remote-Sensing Data". In: *Annals of Glaciology* 43.1, pp. 202–213. DOI: 10.3189/172756406781812465.

Ajrapetyants, S. and E. Bakov (1971). "Morphology of the Merzbacher glacial lake and mechanisms of its catastrophic outbursts". In: *Some regularities of glacierization of the Tien Shan*. Ed. by S. Ajrapetyants and E. Bakov. Frunze: Ilim, pp. 75–84.

Anderson, S. P., J. S. Walder, R. S. Anderson, E. R. Kraal, M. Cunico, A. G. Fountain, and D. C. Trabant (2003). "Integrated Hydrologic and Hydrochemical Observa-

tions of Hidden Creek Lake Jökulhlaups, Kennicott Glacier, Alaska". In: *Journal of Geophysical Research: Earth Surface* 108 (F1), pp. 4.1–4.19. DOI: 10.1029/2002JF000004.

Arnell, N. W. (1999). "The Effect of Climate Change on Hydrological Regimes in Europe: A Continental Perspective". In: *Global Environmental Change* 9.1, pp. 5–23. DOI: 10.1016/S0959-3780(98)00015-6.

Arnold, J. G., P. M. Allen, and G. Bernhardt (1993). "A Comprehensive Surface-Groundwater Flow Model". In: *Journal of Hydrology* 142 (1-4), pp. 47–69. DOI: 10.1016/0022-1694(93)90004-S.

Arnold, J., J. Williams, A. Nicks, and N. Sammons (1990). *SWRRB: A Basin Scale Simulation Model for Soil and Water Resources Management*. Texas A & M University Press College Station, TX.

Arnold, N., K. Richards, I. Willis, and M. Sharp (1998). "Initial Results from a Distributed, Physically Based Model of Glacier Hydrology". In: *Hydrological Processes* 12.2, pp. 191–219. DOI: 10.1002/(SICI)1099-1085(199802)12:2<191::AID-HYP571>3.0.CO;2-C.

Bamber, J. L. and A. J. Payne, eds. (2004). *Mass Balance of the Cryosphere: Observations and Modelling of Contemporary and Future Changes*. Cambridge University Press. 666 pp.

Barontini, S., A. Clerici, R. Ranzi, and B. Bacchi (2005). "Saturated Hydraulic Conductivity and Water Retention Relationships for Alpine Mountain Soils". In: *Climate and Hydrology in Mountain Areas*. Ed. by C. de Jong, D. Collins, and R. Ranzi. 00008. John Wiley & Sons, Ltd, pp. 101–121.

Barry, R. G. (2005). "Alpine Climate Change and Cryospheric Responses: An Introduction". In: *Climate and Hydrology in Mountain Areas*. Ed. by C. de Jong, D. Collins, and R. Ranzi. 00008. John Wiley & Sons, Ltd, pp. 1–4.

Barry, R. G. (2006). "The Status of Research on Glaciers and Global Glacier Recession: A Review". In: *Progress in Physical Geography* 30.3, pp. 285–306. DOI: 10.1191/0309133306pp478ra.

Barry, R. G. (2008). *Mountain Weather and Climate*. 3rd ed. Cambridge: Cambridge University Press. 532 pp.

Barry, R. G. and T.-Y. Gan (2011). *The Global Cryosphere : Past, Present and Future*. 1 publ. 00016. Cambridge: Cambridge University Press.

Bekele, E. G. and J. W. Nicklow (2007). "Multi-Objective Automatic Calibration of SWAT Using NSGA-II". In: *Journal of Hydrology* 341 (3–4), pp. 165–176. DOI: 10.1016/j.jhydrol.2007.05.014.

Beniston, M. (2006). "Mountain Weather and Climate: A General Overview and a Focus on Climatic Change in the Alps". In: *Hydrobiologia* 562.1, pp. 3–16. DOI: 10.1007/s10750-005-1802-0.

Berghuijs, W. R., R. A. Woods, and M. Hrachowitz (2014). "A Precipitation Shift from Snow towards Rain Leads to a Decrease in Streamflow". In: *Nature Climate Change* 4.7, pp. 583–586. DOI: 10.1038/nclimate2246.

Berry, S. L., G. D. Farquhar, and M. L. Roderick (2006). "Co-Evolution of Climate, Soil and Vegetation". In: *Encyclopedia of Hydrological Sciences*. John Wiley & Sons, Ltd.

Beume, N., B. Naujoks, and M. Emmerich (2007). "SMS-EMOA: Multiobjective Selection Based on Dominated Hypervolume". In: *European Journal of Operational Research* 181.3, pp. 1653–1669. DOI: 10.1016/j.ejor.2006.08.008.

Beven, K. (1989). "Changing Ideas in Hydrology—the Case of Physically-Based Models". In: *Journal of hydrology* 105.1, pp. 157–172.

Beven, K. (2006a). "A Manifesto for the Equifinality Thesis". In: *Journal of Hydrology*. The model parameter estimation experimentMOPEXMOPEX workshop 320 (1–2), pp. 18–36. DOI: 10.1016/j.jhydrol.2005.07.007.

Beven, K. J. (2006b). "Rainfall-Runoff Modeling: Introduction". In: *Encyclopedia of Hydrological Sciences*. John Wiley & Sons, Ltd.

Bishop, M. P., J. F. Shroder Jr., and J. D. Colby (2003). "Remote Sensing and Geomorphometry for Studying Relief Production in High Mountains". In: *Geomorphology*. Mountain Geomorphology - Integrating Earth Systems, Proceedings of the 32nd Annual Binghamton Geomorphology Symposium 55 (1–4), pp. 345–361. DOI: 10.1016/S0169-555X(03)00149-1.

Björnsson, H. (2011). "Understanding Jökulhlaups: From Tale to Theory". In: *Journal of Glaciology* 56.200, pp. 1002–1010.

Blasone, R.-S., H. Madsen, and D. Rosbjerg (2007). "Parameter Estimation in Distributed Hydrological Modelling: Comparison of Global and Local Optimisation Techniques". In: *Hydrology Research* 38 (4-5), pp. 451–476. DOI: 10.2166/nh.2007.024.

Blöschl, G. and M. Sivapalan (1995). "Scale Issues in Hydrological Modelling: A Review". In: *Hydrological Processes* 9 (3-4), pp. 251–290. DOI: 10.1002/hyp.3360090305.

Blöschl, G. (2006). "Rainfall-Runoff Modeling of Ungauged Catchments". In: *Encyclopedia of Hydrological Sciences*. John Wiley & Sons, Ltd.

Bolch, T., M. Buchroithner, J. Peters, M. Baessler, and S. Bajracharya (2008). "Identification of Glacier Motion and Potentially Dangerous Glacial Lakes in the Mt. Everest Region/Nepal Using Spaceborne Imagery". In: *Natur. Hazards Earth Syst. Sci.(NHESS)* 8.6. 00066, pp. 1329–1340.

Bolch, T., A. Kulkarni, A. Kääb, C. Huggel, F. Paul, J. G. Cogley, H. Frey, J. S. Kargel, K. Fujita, M. Scheel, S. Bajracharya, and M. Stoffel (2012a). "The State and Fate of Himalayan Glaciers". In: *Science* 336.6079, pp. 310–314. DOI: 10.1126/science.1215828.

Bolch, T., S. Kutusov, and X. Li (2012b). *Updated GLIMS Glacier Database for the Tian Shan*. Shapefile. Boulder, CO: National Snow and Ice Data Center/World Data Center for Glaciology.

Bolch, T., T. Pieczonka, K. Mukherjee, and J. Shea (2017). "Brief Communication: Glaciers in the Hunza Catchment (Karakoram) Have Been Nearly in Balance since the 1970s". In: *The Cryosphere* 11.1, pp. 531–539. DOI: 10.5194/tc-11-531-2017.

Bolch, T. (2011). "Debris". In: *Encyclopedia of Snow, Ice and Glaciers*. Ed. by V. P. Singh, P. Singh, and U. K. Haritashya. Encyclopedia of Earth Sciences Series. Springer Netherlands, pp. 176–178.

Bolch, T. (2017). "Hydrology: Asian Glaciers Are a Reliable Water Source". In: *Nature* 545.7653, pp. 161–162. DOI: 10.1038/545161a.

Bolch, T., B. Menounos, and R. Wheate (2010). "Landsat-Based Inventory of Glaciers in Western Canada, 1985–2005". In: *Remote Sensing of Environment* 114.1. 00171, pp. 127–137. DOI: 10.1016/j.rse.2009.08.015.

Bosshard, T., M. Carambia, K. Goergen, S. Kotlarski, P. Krahe, M. Zappa, and C. Schär (2013). "Quantifying Uncertainty Sources in an Ensemble of Hydrological Climate-Impact Projections". In: *Water Resources Research* 49.3, pp. 1523–1536. DOI: 10.1029/2011WR011533.

Bozhinskiy, A., M. Krass, and V. Popovnin (1986). "Role of Debris Cover in the Thermal Physics of Glaciers". In: *Journal of Glaciology* 32, pp. 255–266.

Braithwaite, R. J. and Y. Zhang (2000). "Sensitivity of Mass Balance of Five Swiss Glaciers to Temperature Changes Assessed by Tuning a Degree-Day Model". In: *Journal of Glaciology* 46.152, pp. 7–14. DOI: 10.3189/172756500781833511.

Braun, L. N. and C. B. Renner (1992). "Application of a Conceptual Runoff Model in Different Physiographic Regions of Switzerland". In: *Hydrological Sciences Journal* 37.3, pp. 217–231. DOI: 10.1080/02626669209492583.

Bronstert, A (2005). *Coupled Models for the Hydrological Cycle Integrating Atmosphere, Biosphere, and Pedosphere*. Berlin [etc.]: Springer.

Bronstert, A. (2006). "Rainfall-Runoff Modeling for Assessing Impacts of Climate and Land Use Change". In: *Encyclopedia of Hydrological Sciences*. John Wiley & Sons, Ltd.

Bulygina, O. N., V. N. Razuvaev, and N. N. Korshunova (2009). "Changes in Snow Cover over Northern Eurasia in the Last Few Decades". In: *Environmental Research Letters* 4.4. 00059, p. 045026. DOI: 10.1088/1748-9326/4/4/045026.

Bøggild, C. E., C. J. Knudby, M. B. Knudsen, and W. Starzer (1999). "Snowmelt and Runoff Modelling of an Arctic Hydrological Basin in West Greenland". In: *Hydrological Processes* 13 (12-13), pp. 1989–2002. DOI: 10.1002/(SICI)1099-1085(199909)13:12/13<1989::AID-HYP848>3.0.CO;2-Y.

Chaturvedi, R. K., A. Kulkarni, Y. Karyakarte, J. Joshi, and G. Bala (2014). "Glacial Mass Balance Changes in the Karakoram and Himalaya Based on CMIP5 Multi-Model Climate Projections". In: *Climatic Change* 123.2, pp. 315–328. DOI: 10.1007/s10584-013-1052-5.

Chen, Y., K. Takeuchi, C. Xu, Y. Chen, and Z. Xu (2006). "Regional Climate Change and Its Effects on River Runoff in the Tarim Basin, China". In: *Hydrological Processes* 20.10. 00093, pp. 2207–2216. DOI: 10.1002/hyp.6200.

Clarke, G. K. C. (1987). "Fast Glacier Flow: Ice Streams, Surging, and Tidewater Glaciers". In: *Journal of Geophysical Research: Solid Earth* 92 (B9), pp. 8835–8841. DOI: 10.1029/JB092iB09p08835.

Clarke, G. K. C., J. P. Schmok, C. S. L. Ommanney, and S. G. Collins (1986). "Characteristics of Surge-Type Glaciers". In: *Journal of Geophysical Research: Solid Earth* 91 (B7), pp. 7165–7180. DOI: 10.1029/JB091iB07p07165.

Clarke, G. K. C., A. H. Jarosch, F. S. Anslow, V. Radić, and B. Menounos (2015). "Projected Deglaciation of Western Canada in the Twenty-First Century". In: *Nature Geoscience* advance online publication. DOI: 10.1038/ngeo2407.

Collins, M., R. Knutti, J. Arblaster, J.-L. Dufresne, T. Fichefet, P. Friedlingstein, X. Gao, W. J. Gutowski, T. Johns, G. Krinner, M. Shongwe, C. Tebaldi, A. J. Weaver, and M. Wehner (2013). "Chapter 12 - Long-Term Climate Change: Projections, Commitments and Irreversibility". In: *Climate Change 2013: The Physical Science Basis. IPCC Working Group I Contribution to AR5*. Ed. by IPCC. In collab. with M. R. Allen, T. Andrews, U. Beyerle, C. M. Bitz, S. Bony, B. B. B. Booth, H. E. Brooks, V. Brovkin, O. Browne, C. Brutel-Vuilmet, M. Cane, R. Chadwick, E. Cook, K. H. Cook, M. Eby, J. Fasullo, E. M. Fischer, C. E. Forest, P. Forster, P. Good, H. Goosse, J. M. Gregory, G. C. Hegerl, P. J. Hezel, K. I. Hodges, M. M. Holland, M. Huber, P. Huy-

brechts, M. Joshi, V. Kharin, Y. Kushnir, D. M. Lawrence, R. W. Lee, S. Liddicoat, C. Lucas, W. Lucht, J. Marotzke, F. Massonnet, H. D. Matthews, M. Meinshausen, C. Morice, A. Otto, C. M. Patricola, G. Philippon-Berthier, Prabhat, S. Rahmstorf, W. J. Riley, J. Rogelj, O. Saenko, R. Seagar, J. Sedlacek, L. C. Shaffrey, D. Shindell, J. Sillmann, A. Slater, B. Stevens, P. A. Stott, R. Webb, G. Zappa, and K. Zickfeld. Cambridge: Cambridge University Press.

Cronin, T. (2000). "Classifying Hills and Valleys in Digitized Terrain". In: *Photogrammetric engineering and remote sensing* 66.9, pp. 1129–1137.

Cuffey, K. M. and W. S. B. Paterson (2010). *The Physics of Glaciers*. 00292. Amsterdam: Elsevier.

Deb, K., A. Pratap, S. Agarwal, and T. Meyarivan (2002). "A Fast and Elitist Multiobjective Genetic Algorithm: NSGA-II". In: *IEEE Transactions on Evolutionary Computation* 6.2, pp. 182–197. DOI: 10.1109/4235.996017.

Dee, D. P., S. M. Uppala, A. J. Simmons, P. Berrisford, P. Poli, S. Kobayashi, U. Andrae, M. A. Balmaseda, G. Balsamo, P. Bauer, P. Bechtold, A. C. M. Beljaars, L. van de Berg, J. Bidlot, N. Bormann, C. Delsol, R. Dragani, M. Fuentes, A. J. Geer, L. Haimberger, S. B. Healy, H. Hersbach, E. V. Hólm, L. Isaksen, P. Kållberg, M. Köhler, M. Matricardi, A. P. McNally, B. M. Monge-Sanz, J.-J. Morcrette, B.-K. Park, C. Peubey, P. de Rosnay, C. Tavolato, J.-N. Thépaut, and F. Vitart (2011). "The ERA-Interim Reanalysis: Configuration and Performance of the Data Assimilation System". In: *Quarterly Journal of the Royal Meteorological Society* 137.656. 01210, pp. 553–597. DOI: 10.1002/qj.828.

Dickerson-Lange, S. E. and R. Mitchell (2014). "Modeling the Effects of Climate Change Projections on Streamflow in the Nooksack River Basin, Northwest Washington". In: *Hydrological Processes* 28.20, pp. 5236–5250. DOI: 10.1002/hyp.10012.

Dietrich, W. E., R. Reiss, M.-L. Hsu, and D. R. Montgomery (1995). "A Process-Based Model for Colluvial Soil Depth and Shallow Landsliding Using Digital Elevation Data". In: *Hydrological Processes* 9 (3-4), pp. 383–400. DOI: 10.1002/hyp.3360090311.

Ding, Y., S. Liu, J. Li, and D. Shangguan (2006). "The Retreat of Glaciers in Response to Recent Climate Warming in Western China". In: *Annals of Glaciology* 43.1, pp. 97–105. DOI: 10.3189/172756406781812005.

Dobhal, D. P. (2011). "Glacier". In: *Encyclopedia of Snow, Ice and Glaciers*. Ed. by V. P. Singh, P. Singh, and U. K. Haritashya. Encyclopedia of Earth Sciences Series. Springer Netherlands, pp. 376–377.

Doherty, J. (2003). *PEST: Model Independent Parameter Estimation, User Manual*. Brisbane, Australia: Watermark Numerical Computing.

Dornes, P. F., J. W. Pomeroy, A. Pietroniro, S. K. Carey, and W. L. Quinton (2008). "Influence of Landscape Aggregation in Modelling Snow-Cover Ablation and Snowmelt Runoff in a Sub-Arctic Mountainous Environment". In: *Hydrological Sciences Journal* 53.4, pp. 725–740. DOI: 10.1623/hysj.53.4.725.

Dudeja, D. (2011). "Gelisols". In: *Encyclopedia of Snow, Ice and Glaciers*. Ed. by V. P. Singh, P. Singh, and U. K. Haritashya. Encyclopedia of Earth Sciences Series. 00000. Springer Netherlands, pp. 313–313.

Duethmann, D., J. Zimmer, A. Gafurov, A. Güntner, D. Kriegel, B. Merz, and S. Vorogushyn (2013). "Evaluation of Areal Precipitation Estimates Based on Downscaled Reanalysis and Station Data by Hydrological Modelling". In: *Hydrol. Earth Syst. Sci.* 17.7, pp. 2415–2434. DOI: 10.5194/hess-17-2415-2013.

Duethmann, D., J. Peters, T. Blume, S. Vorogushyn, and A. Güntner (2014). "The Value of Satellite-Derived Snow Cover Images for Calibrating a Hydrological Model in Snow-Dominated Catchments in Central Asia". In: *Water Resources Research* 50.3, pp. 2002–2021. DOI: 10.1002/2013WR014382.

Duethmann, D., T. Bolch, D. Farinotti, D. Kriegel, S. Vorogushyn, B. Merz, T. Pieczonka, T. Jiang, B. Su, and A. Güntner (2015). "Attribution of Streamflow Trends in Snow- and Glacier Melt Dominated Catchments of the Tarim River, Central Asia". In: *Water Resources Research*, pp. 4727–4750. DOI: 10.1002/2014WR016716.

Duethmann, D., C. Menz, T. Jiang, and S. Vorogushyn (2016). "Projections for Headwater Catchments of the Tarim River Reveal Glacier Retreat and Decreasing Surface Water Availability but Uncertainties Are Large". In: *Environmental Research Letters* 11.5, p. 054024. DOI: 10.1088/1748-9326/11/5/054024.

Dunn, S. M. and R. J. E. Colohan (1999). "Developing the Snow Component of a Distributed Hydrological Model: A Step-Wise Approach Based on Multi-Objective Analysis". In: *Journal of Hydrology* 223 (1–2), pp. 1–16. DOI: 10.1016/S0022-1694(99)00095-5.

Dussaillant, A., G. Benito, W. Buytaert, P. Carling, C. Meier, and F. Espinoza (2010). "Repeated Glacial-Lake Outburst Floods in Patagonia: An Increasing Hazard?" In: *Natural Hazards* 54.2. 00016, pp. 469–481. DOI: 10.1007/s11069-009-9479-8.

Dye, D. G. (2002). "Variability and Trends in the Annual Snow-Cover Cycle in Northern Hemisphere Land Areas, 1972–2000". In: *Hydrological Processes* 16.15. 00165, pp. 3065–3077. DOI: 10.1002/hyp.1089.

Dyurgerov, M. B. (2010). *Reanalysis of Glacier Changes: From the IGY to the IPY, 1960-2008*. Data of Glaciological Studies 108. Moscow: Glaciological Association, Geographical Institute of the Russian Academy of Sciences.

Dyurgerov, M. B. and M. F. Meier (1997). "Mass Balance of Mountain and Subpolar Glaciers: A New Global Assessment for 1961-1990". In: *Arctic and Alpine Research* 29.4, pp. 379–391. DOI: 10.2307/1551986. JSTOR: 1551986.

Dyurgerov, M. and M. Meier (2004). "Glaciers and the Study of Climate and Sea-Level Change". In: *Mass Balance of the Cryosphere: Observations and Modelling of Contemporary and Future Changes*. Ed. by J. L. Bamber and A. J. Payne. 00000. Cambridge University Press.

Efstratiadis, A. and D. Koutsoyiannis (2010). "One Decade of Multi-Objective Calibration Approaches in Hydrological Modelling: A Review". In: *Hydrological Sciences Journal* 55.1, pp. 58–78. DOI: 10.1080/02626660903526292.

Ehret, U., E. Zehe, V. Wulfmeyer, K. Warrach-Sagi, and J. Liebert (2012). "HESS Opinions "Should We Apply Bias Correction to Global and Regional Climate Model Data?"" In: *Hydrology and Earth System Sciences; Katlenburg-Lindau* 16.9, p. 3391. DOI: http://dx.doi.org.libproxy.ucl.ac.uk/10.5194/hess-16-3391-2012.

Emmerich, M., N. Beume, and B. Naujoks (2005). "An EMO Algorithm Using the Hypervolume Measure as Selection Criterion". In: *Evolutionary Multi-Criterion Optimization*. International Conference on Evolutionary Multi-Criterion Optimization. Springer, Berlin, Heidelberg, pp. 62–76. DOI: 10.1007/978-3-540-31880-4.

FAO (2011). *Crop Calendar*. URL: http://www.fao.org/agriculture/seed/cropcalendar/ (visited on 02/28/2011).

FAO, IIASA, ISRIC, ISSCAS, and JRC (2011). *The Harmonized World Soil Database*. Database 1.2. Rome: FAO and IIASA.

Farinotti, D., M. Huss, A. Bauder, and M. Funk (2009). "An Estimate of the Glacier Ice Volume in the Swiss Alps". In: *Global and Planetary Change* 68.3, pp. 225–231. DOI: 10.1016/j.gloplacha.2009.05.004.

Farinotti, D., L. Longuevergne, G. Moholdt, D. Duethmann, T. Mölg, T. Bolch, S. Vorogushyn, and A. Güntner (2015). "Substantial Glacier Mass Loss in the Tien Shan over the Past 50 Years". In: *Nature Geoscience* 8.9, pp. 716–722. DOI: 10.1038/ngeo2513.

Fatichi, S., S. Rimkus, P. Burlando, R. Bordoy, and P. Molnar (2015). "High-Resolution Distributed Analysis of Climate and Anthropogenic Changes on the Hydrology of an Alpine Catchment". In: *Journal of Hydrology* 525, pp. 362–382. DOI: 10.1016/j.jhydrol.2015.03.036.

Feike, T., Y. Mamitimin, L. Li, and R. Doluschitz (2015). "Development of Agricultural Land and Water Use and Its Driving Forces along the Aksu and Tarim River, P.R.

China". In: *Environmental Earth Sciences* 73.2, pp. 517–531. DOI: 10.1007/s12665-014-3108-x.

Ferguson, R. I. (1999). "Snowmelt Runoff Models". In: *Progress in Physical Geography* 23.2, pp. 205–227. DOI: 10.1177/030913339902300203.

Ficklin, D. L., B. L. Barnhart, J. H. Knouft, I. T. Stewart, E. P. Maurer, S. L. Letsinger, and G. W. Whittaker (2014). "Climate Change and Stream Temperature Projections in the Columbia River Basin: Habitat Implications of Spatial Variation in Hydrologic Drivers". In: *Hydrol. Earth Syst. Sci.* 18.12, pp. 4897–4912. DOI: 10.5194/hess-18-4897-2014.

Finger, D., F. Pellicciotti, M. Konz, S. Rimkus, and P. Burlando (2011). "The Value of Glacier Mass Balance, Satellite Snow Cover Images, and Hourly Discharge for Improving the Performance of a Physically Based Distributed Hydrological Model". In: *Water Resources Research* 47.7, W07519. DOI: 10.1029/2010WR009824.

Fischer, M., M. Huss, and M. Hoelzle (2015). "Surface Elevation and Mass Changes of All Swiss Glaciers 1980–2010". In: *The Cryosphere* 9.2, pp. 525–540. DOI: 10.5194/tc-9-525-2015.

Fischer, M., M. Huss, C. Barboux, and M. Hoelzle (2014). "The New Swiss Glacier Inventory SGI2010: Relevance of Using High-Resolution Source Data in Areas Dominated by Very Small Glaciers". In: *Arctic, Antarctic, and Alpine Research* 46.4, pp. 933–945. DOI: 10.1657/1938-4246-46.4.933.

Fontaine, T. A., T. S. Cruickshank, J. G. Arnold, and R. H. Hotchkiss (2002). "Development of a Snowfall–snowmelt Routine for Mountainous Terrain for the Soil Water Assessment Tool (SWAT)". In: *Journal of Hydrology* 262 (1–4), pp. 209–223. DOI: 10.1016/S0022-1694(02)00029-X.

Frey, H., H. Machguth, M. Huss, C. Huggel, S. Bajracharya, T. Bolch, A. Kulkarni, A. Linsbauer, N. Salzmann, and M. Stoffel (2014). "Estimating the Volume of Glaciers in the Himalayan–Karakoram Region Using Different Methods". In: *The Cryosphere* 8.6, pp. 2313–2333. DOI: 10.5194/tc-8-2313-2014.

Friedl, M. A., D. K. McIver, J. C. F. Hodges, X. Y. Zhang, D. Muchoney, A. H. Strahler, C. E. Woodcock, S. Gopal, A. Schneider, A. Cooper, A. Baccini, F. Gao, and C. Schaaf (2002). "Global Land Cover Mapping from MODIS: Algorithms and Early Results". In: *Remote Sensing of Environment* 83 (1-2), pp. 287–302. DOI: 10.1016/S0034-4257(02)00078-0.

Gan, R., Y. Luo, Q. Zuo, and L. Sun (2015). "Effects of Projected Climate Change on the Glacier and Runoff Generation in the Naryn River Basin, Central Asia". In: *Journal of Hydrology* 523, pp. 240–251. DOI: 10.1016/j.jhydrol.2015.01.057.

Gardelle, J., E. Berthier, Y. Arnaud, and A. Kääb (2013). "Region-Wide Glacier Mass Balances over the Pamir-Karakoram-Himalaya during 1999–2011". In: *The Cryosphere* 7.4, pp. 1263–1286. DOI: 10.5194/tc-7-1263-2013.

Gardelle, J., E. Berthier, and Y. Arnaud (2012). "Slight Mass Gain of Karakoram Glaciers in the Early Twenty-First Century". In: *Nature Geoscience* 5.5, pp. 322–325. DOI: 10.1038/ngeo1450.

Gardner, A. S., G. Moholdt, J. G. Cogley, B. Wouters, A. A. Arendt, J. Wahr, E. Berthier, R. Hock, W. T. Pfeffer, G. Kaser, S. R. M. Ligtenberg, T. Bolch, M. J. Sharp, J. O. Hagen, M. R. van den Broeke, and F. Paul (2013). "A Reconciled Estimate of Glacier Contributions to Sea Level Rise: 2003 to 2009". In: *Science* 340.6134, pp. 852–857. DOI: 10.1126/science.1234532. pmid: 23687045.

Gascoin, S., C. Kinnard, R. Ponce, S. Lhermitte, S. MacDonell, and A. Rabatel (2011). "Glacier Contribution to Streamflow in Two Headwaters of the Huasco River, Dry Andes of Chile". In: *The Cryosphere* 5.4, pp. 1099–1113. DOI: 10.5194/tc-5-1099-2011.

Gelfan, A., J. Pomeroy, and L. Kuchment (2004). "Modeling Forest Cover Influences on Snow Accumulation, Sublimation, and Melt". In: *Journal of Hydrometeorology* 5.5, pp. 785–803.

Giorgi, F. and W. J. Gutowski (2015). "Regional Dynamical Downscaling and the CORDEX Initiative". In: *Annual Review of Environment and Resources* 40.1, pp. 467–490. DOI: 10.1146/annurev-environ-102014-021217.

Glazirin, G. (2010). "A Century of Investigations on Outbursts of the Ice-Dammed Lake Merzbacher (Central Tien Shan)". In: *Austrian Journal of Earth Sciences* 103.2, pp. 171–179.

Glen, J. W. (1955). "The Creep of Polycrystalline Ice". In: *Proceedings of the Royal Society of London. Series A, Mathematical and Physical Sciences* 228.1175, pp. 519–538. JSTOR: 99642.

Glen, J. W. (1958). "The Flow Law of Ice: A Discussion of the Assumptions Made in Glacier Theory, Their Experimental Foundations and Consequences". In: *IASH Publ* 47, pp. 171–183.

Gosling, S. N., D. Bretherton, K. Haines, and N. W. Arnell (2010). "Global Hydrology Modelling and Uncertainty: Running Multiple Ensembles with a Campus Grid". In: *Philosophical Transactions of the Royal Society of London A: Mathematical, Physical and Engineering Sciences* 368.1926, pp. 4005–4021. DOI: 10.1098/rsta.2010.0164. pmid: 20679119.

GRDC (2016). *The Global Runoff Data Centre*. 56068 Koblenz, Germany: Bundesanstalt für Gewässerkunde.

Grenfell, T. C. (2011). "Albedo". In: *Encyclopedia of Snow, Ice and Glaciers*. Ed. by V. P. Singh, P. Singh, and U. K. Haritashya. Encyclopedia of Earth Sciences Series. 00003. Springer Netherlands, pp. 23–35.

Greuell, W. and C. Genthon (2004). "Modelling Land-Ice Surface Mass Balance". In: *Mass Balance of the Cryosphere: Observations and Modelling of Contemporary and Future Changes*. Ed. by J. L. Bamber and A. J. Payne. Cambridge University Press.

Gupta, H. V., K. J. Beven, and T. Wagener (2006). "Model Calibration and Uncertainty Estimation". In: *Encyclopedia of Hydrological Sciences*. John Wiley & Sons, Ltd.

Gurtz, J., M. Zappa, K. Jasper, H. Lang, M. Verbunt, A. Badoux, and T. Vitvar (2003). "A Comparative Study in Modelling Runoff and Its Components in Two Mountainous Catchments". In: *Hydrological Processes* 17.2, pp. 297–311. DOI: 10.1002/hyp.1125.

Haeberli, W and M Hoelzle (1995). "Application of Inventory Data for Estimating Characteristics of and Regional Climate-Change Effects on Mountain Glaciers: A Pilot Study from the European Alps". In: *Annals of Glaciology* 21, pp. 206–212.

Haeberli, W. and R. Hohmann (2008). "Climate, Glaciers, and Permafrost in the Swiss Alps 2050: Scenarios, Consequences, and Recommendations". In: Proceedings Ninth International Conference on Permafrost. Vol. 1. 00027, pp. 607–612.

Hagg, W., L. N. Braun, M. Kuhn, and T. I. Nesgaard (2007). "Modelling of Hydrological Response to Climate Change in Glacierized Central Asian Catchments". In: *Journal of Hydrology* 332 (1–2), pp. 40–53. DOI: 10.1016/j.jhydrol.2006.06.021.

Hagg, W., C. Mayer, A. Lambrecht, and A. Helm (2008). "Sub-Debris Melt Rates on Southern Inylchek Glacier, Central Tian Shan". In: *Geografiska Annaler: Series A, Physical Geography* 90.1, pp. 55–63. DOI: 10.1111/j.1468-0459.2008.00333.x.

Hagg, W., M. Hoelzle, S. Wagner, E. Mayr, and Z. Klose (2013). "Glacier and Runoff Changes in the Rukhk Catchment, Upper Amu-Darya Basin until 2050". In: *Global and Planetary Change*. Water in Central Asia – Perspectives under global change 110, pp. 62–73. DOI: 10.1016/j.gloplacha.2013.05.005.

Hall, D. K., G. A. Riggs, V. V. Salomonson, N. E. DiGirolamo, and K. J. Bayr (2002). "MODIS Snow-Cover Products". In: *Remote Sensing of Environment* 83 (1–2), pp. 181–194. DOI: 10.1016/S0034-4257(02)00095-0.

Hambrey, M. J., D. J. Quincey, N. F. Glasser, J. M. Reynolds, S. J. Richardson, and S. Clemmens (2008). "Sedimentological, Geomorphological and Dynamic Context of Debris-Mantled Glaciers, Mount Everest (Sagarmatha) Region, Nepal". In: *Quatern-*

ary Science Reviews 27 (25–26), pp. 2361–2389. DOI: 10.1016/j.quascirev.2008.08.010.

Hamby, D. M. (1994). "A Review of Techniques for Parameter Sensitivity Analysis of Environmental Models". In: *Environmental Monitoring and Assessment* 32.2, pp. 135–154. DOI: 10.1007/BF00547132.

Hattermann, F., V. Krysanova, F. Wechsung, and M. Wattenbach (2004). "Integrating Groundwater Dynamics in Regional Hydrological Modelling". In: *Environmental Modelling & Software* 19.11, pp. 1039–1051. DOI: 10.1016/j.envsoft.2003.11.007.

Hattermann, F. F., M. Wattenbach, V. Krysanova, and F. Wechsung (2005). "Runoff Simulations on the Macroscale with the Ecohydrological Model SWIM in the Elbe Catchment-Validation and Uncertainty Analysis". In: *Hydrological Processes* 19.3, pp. 693–714. DOI: 10.1002/hyp.5625.

Hattermann, F. F., S. Huang, O. Burghoff, W. Willems, H. Österle, M. Büchner, and Z. Kundzewicz (2014). "Modelling Flood Damages under Climate Change Conditions – a Case Study for Germany". In: *Natural Hazards and Earth System Science* 14.12, pp. 3151–3168. DOI: 10.5194/nhess-14-3151-2014.

Hattermann, F., M. Weiland, S. Huang, V. Krysanova, and Z. Kundzewicz (2011). "Model-Supported Impact Assessment for the Water Sector in Central Germany Under Climate Change—A Case Study". In: *Water Resources Management* 25.13, pp. 3113–3134. DOI: 10.1007/s11269-011-9848-4.

Hawkins, E. and R. Sutton (2009). "The Potential to Narrow Uncertainty in Regional Climate Predictions". In: *Bulletin of the American Meteorological Society* 90.8, pp. 1095–1107. DOI: 10.1175/2009BAMS2607.1.

Hazell, P. and S. Wood (2008). "Drivers of Change in Global Agriculture". In: *Philosophical Transactions of the Royal Society B: Biological Sciences* 363.1491, pp. 495–515. DOI: 10.1098/rstb.2007.2166.

Heimsath, A. M., W. E. Dietrich, K. Nishiizumi, and R. C. Finkel (1999). "Cosmogenic Nuclides, Topography, and the Spatial Variation of Soil Depth". In: *Geomorphology* 27 (1–2), pp. 151–172. DOI: 10.1016/S0169-555X(98)00095-6.

Hempel, S., K. Frieler, L. Warszawski, J. Schewe, and F. Piontek (2013). "A Trend-Preserving Bias Correction; the ISI-MIP Approach". In: *Earth System Dynamics* 4.2, pp. 219–236. DOI: 10.5194/esd-4-219-2013.

Hengeveld, H. (2006). "Climate Change – Past, Present and Future". In: *Encyclopedia of Hydrological Sciences*. John Wiley & Sons, Ltd.

Hewitt, K. (2005). "The Karakoram Anomaly? Glacier Expansion and the 'Elevation Effect,' Karakoram Himalaya". In: *Mountain Research and Development* 25.4. 00231, pp. 332–340. DOI: 10.1659/0276-4741(2005)025[0332:TKAGEA]2.0.CO;2.

Hewitt, K. (2011). "Glaciers of the Karakoram Himalaya". In: *Encyclopedia of Snow, Ice and Glaciers*. Ed. by V. P. Singh, P. Singh, and U. K. Haritashya. Encyclopedia of Earth Sciences Series. 00000. Springer Netherlands, pp. 429–436.

Hewitt, K. and J. Liu (2010). "Ice-Dammed Lakes and Outburst Floods, Karakoram Himalaya: Historical Perspectives on Emerging Threats". In: *Physical Geography* 31.6, pp. 528–551. DOI: 10.2747/0272-3646.31.6.528.

Hock, R. (2005). "Glacier Melt: A Review of Processes and Their Modelling". In: *Progress in Physical Geography* 29.3, pp. 362 –391. DOI: 10.1191/0309133305pp453ra.

Hock, R. (2003). "Temperature Index Melt Modelling in Mountain Areas". In: *Journal of Hydrology* 282 (1–4). 00406, pp. 104–115. DOI: 10.1016/S0022-1694(03)00257-9.

Hock, R. and B. Holmgren (1996). "Some Aspects of Energy Balance and Ablation of Storglaciären, Northern Sweden". In: *Geografiska Annaler. Series A, Physical Geography* 78 (2/3), pp. 121–131. DOI: 10.2307/520974. JSTOR: 520974.

Hock, R. and B. Holmgren (2005). "A Distributed Surface Energy-Balance Model for Complex Topography and Its Application to Storglaciären, Sweden". In: *Journal of Glaciology* 51.172, pp. 25–36. DOI: 10.3189/172756505781829566.

Hock, R. and R. L. Hooke (1993). "Evolution of the Internal Drainage System in the Lower Part of the Ablation Area of Storglaci?Ären, Sweden". In: *Geological Society of America Bulletin* 105.4, pp. 537–546. DOI: 10.1130/0016-7606(1993)105<0537:EOTIDS>2.3.CO;2.

Hock, R. and P. Jansson (2006). "Modeling Glacier Hydrology". In: *Encyclopedia of Hydrological Sciences*. John Wiley & Sons, Ltd.

Holzer, N., S. Vijay, T. Yao, B. Xu, M. Buchroithner, and T. Bolch (2015). "Four Decades of Glacier Variations at Muztagh Ata (Eastern Pamir): A Multi-Sensor Study Including Hexagon KH-9 and Pléiades Data". In: *The Cryosphere* 9.6, pp. 2071–2088. DOI: 10.5194/tc-9-2071-2015.

Horton, P., B. Schaefli, A. Mezghani, B. Hingray, and A. Musy (2006). "Assessment of Climate-Change Impacts on Alpine Discharge Regimes with Climate Model Uncertainty". In: *Hydrological Processes* 20.10, pp. 2091–2109. DOI: 10.1002/hyp.6197.

Houghton, J. T., G Jenkins, and J. Ephraums, eds. (1996). *Climate Change 1995: The Science of Climate Change: Contribution of Working Group I to the Second Assess-*

ment Report of the Intergovernmental Panel on Climate Change. 03253. Cambridge University Press.

Houghton, J. T., Y. Ding, D. J. Griggs, M. Noguer, P. J. van der LINDEN, X. Dai, K. Maskell, and C. Johnson (2001). *Climate Change 2001: The Scientific Basis*. Vol. 881. 07330. Cambridge University Press Cambridge.

Huang, S., V. Krysanova, and F. F. Hattermann (2013a). "Projection of Low Flow Conditions in Germany under Climate Change by Combining Three RCMs and a Regional Hydrological Model". In: *Acta Geophysica* 61.1, pp. 151–193. DOI: 10.2478/s11600-012-0065-1.

Huang, S., V. Krysanova, H. Österle, and F. F. Hattermann (2010). "Simulation of Spatiotemporal Dynamics of Water Fluxes in Germany under Climate Change". In: *Hydrological Processes* 24.23, pp. 3289–3306. DOI: 10.1002/hyp.7753.

Huang, S., F. F. Hattermann, V. Krysanova, and A. Bronstert (2013b). "Projections of Climate Change Impacts on River Flood Conditions in Germany by Combining Three Different RCMs with a Regional Eco-Hydrological Model". In: *Climatic Change* 116 (3-4), pp. 631–663. DOI: 10.1007/s10584-012-0586-2.

Hubbard, A., H. Blatter, P. Nienow, D. Mair, and B. Hubbard (1998). "Comparison of a Three-Dimensional Model for Glacier Flow with Field Data from Haut Glacier d'Arolla, Switzerland". In: *Journal of Glaciology* 44.147, pp. 368–378.

Huffman, G., E. F. Stocker, D. Bolvin, and E. Nelkin (2014). *3IMERGM Data Set*.

Huggel, C., A. Kääb, W. Haeberli, and B. Krummenacher (2003). "Regional-scale GIS-models for assessment of hazards from glacier lake outbursts: evaluation and application in the Swiss Alps". In: *Natural Hazards and Earth System Science* 3.6, pp. 647–662.

Huss, M., A. Bauder, M. Werder, M. Funk, and R. Hock (2007). "Glacier-Dammed Lake Outburst Events of Gornersee, Switzerland". In: *Journal of Glaciology* 53.181, pp. 189–200. DOI: 10.3189/172756507782202784.

Huss, M., G. Jouvet, D. Farinotti, and A. Bauder (2010a). "Future High-Mountain Hydrology: A New Parameterization of Glacier Retreat". In: *Hydrol. Earth Syst. Sci.* 14.5, pp. 815–829. DOI: 10.5194/hess-14-815-2010.

Huss, M., D. Farinotti, A. Bauder, and M. Funk (2008). "Modelling Runoff from Highly Glacierized Alpine Drainage Basins in a Changing Climate". In: *Hydrological Processes* 22.19, pp. 3888–3902. DOI: 10.1002/hyp.7055.

Huss, M., R. Hock, A. Bauder, and M. Funk (2010b). "100-Year Mass Changes in the Swiss Alps Linked to the Atlantic Multidecadal Oscillation". In: *Geophysical Research Letters* 37.10. 00077, p. L10501. DOI: 10.1029/2010GL042616.

Huss, M., S. Usselmann, D. Farinotti, and A. Bauder (2010c). "Glacier Mass Balance in the South-Eastern Swiss Alps since 1900 and Perspectives for the Future". In: *Erdkunde* 64.2. 00025, pp. 119–140. JSTOR: 20749414.

ICIMOD and UNEP (2001). *Inventory of Glaciers, Glacial Lakes and Identification of Potential Glacial Lake Outburst Floods Affected by Global Warming in the Mountains of Himalayan Region*. International Centre for Integrated Mountain Development.

Immerzeel, W. W., F. Pellicciotti, and M. F. P. Bierkens (2013). "Rising River Flows throughout the Twenty-First Century in Two Himalayan Glacierized Watersheds". In: *Nature Geoscience* 6.9, pp. 742–745. DOI: 10.1038/ngeo1896.

Immerzeel, W. W., L. Petersen, S. Ragettli, and F. Pellicciotti (2014). "The Importance of Observed Gradients of Air Temperature and Precipitation for Modeling Runoff from a Glacierized Watershed in the Nepalese Himalayas". In: *Water Resources Research* 50.3. 00005, pp. 2212–2226. DOI: 10.1002/2013WR014506.

Immerzeel, W. W., N. Wanders, A. F. Lutz, J. M. Shea, and M. F. P. Bierkens (2015). "Reconciling High-Altitude Precipitation in the Upper Indus Basin with Glacier Mass Balances and Runoff". In: *Hydrol. Earth Syst. Sci.* 19.11, pp. 4673–4687. DOI: 10.5194/hess-19-4673-2015.

Immerzeel, W. W., L. P. H. van Beek, and M. F. P. Bierkens (2010). "Climate Change Will Affect the Asian Water Towers". In: *Science* 328.5984, pp. 1382–1385. DOI: 10.1126/science.1183188. pmid: 20538947.

Immerzeel, W. W., L. P. H. van Beek, M. Konz, A. B. Shrestha, and M. F. P. Bierkens (2011). "Hydrological Response to Climate Change in a Glacierized Catchment in the Himalayas". In: *Climatic Change* 110 (3-4), pp. 721–736. DOI: 10.1007/s10584-011-0143-4.

Immerzeel, W. W., F. Pellicciotti, and A. B. Shrestha (2012). "Glaciers as a Proxy to Quantify the Spatial Distribution of Precipitation in the Hunza Basin". In: *Mountain Research and Development* 32.1. 00023, pp. 30–38. DOI: 10.1659/MRD-JOURNAL-D-11-00097.1.

IPCC (2007). *IPCC Fourth Assessment Report: Climate Change 2007 (AR4)*. 00389.

IPCC (2014a). *Climate Change 2014: Impacts, Adaptation, and Vulnerability. Part B: Regional Aspects. Contribution of Working Group II to the Fifth Assessment Report of the Intergovernmental Panel on Climate Change [Barros, V.R., C.B. Field, D.J. Dokken, M.D. Mastrandrea, K.J. Mach, T.E. Bilir, M. Chatterjee, K.L. Ebi, Y.O.*

Estrada, R.C. Genova, B. Girma, E.S. Kissel, A.N. Levy, S. MacCracken, P.R. Mastrandrea, and L.L. White (Eds.)] Cambridge, United Kingdom and New York, NY, USA: Cambridge University Press. 688 pp.

IPCC (2014b). "Summary for Policymakers". In: *Climate Change 2014: Impacts, Adaptation, and Vulnerability. Part A: Global and Sectoral Aspects. Contribution of Working Group II to the Fifth Assessment Report of the Intergovernmental Panel on Climate Change*. Ed. by C. B. Field, V. R. Barros, D. J. Dokken, K. J. Mach, M. D. Mastrandrea, T. E. Bilir, M. Chatterjee, K. L. Ebi, Y. O. Estrada, R. C. Genova, B. Girma, E. S. Kissel, A. N. Levy, S. MacCracken, P. R. Mastrandrea, and L. L. White. Cambridge, United Kingdom, and New York, NY, USA: Cambridge University Press, pp. 1–32.

Iturrizaga, L. (2011). "Glacier Lake Outburst Floods". In: *Encyclopedia of Snow, Ice and Glaciers*. Ed. by V. P. Singh, P. Singh, and U. K. Haritashya. Encyclopedia of Earth Sciences Series. 00004. Springer Netherlands, pp. 381–399.

Jain, S. K., A. K. Lohani, R. D. Singh, A. Chaudhary, and L. N. Thakural (2012). "Glacial Lakes and Glacial Lake Outburst Flood in a Himalayan Basin Using Remote Sensing and GIS". In: *Natural Hazards* 62.3, pp. 887–899. DOI: 10.1007/s11069-012-0120-x.

Jarvis, A., H. Reuter, A. Nelson, and E. Guevara (2007). *Hole-Filled Seamless SRTM Data, Version 4*. DEM. International Centre for Tropical Agriculture (CIAT).

Jiménez Cisneros, B. E., T. Oki, N. W. Arnell, G. Benito, J. G. Cogley, P. Döll, T. Jiang, and S. S. Mwakalila (2014). "Freshwater Resources". In: *Climate Change 2014: Impacts, Adaptation, and Vulnerability. Part A: Global and Sectoral Aspects. Contribution of Working Group II to the Fifth Assessment Report of the Intergovernmental Panel of Climate Change*. Ed. by C. B. Field, V. R. Barros, D. J. Dokken, K. J. Mach, M. D. Mastrandrea, T. E. Bilir, M. Chatterjee, K. L. Ebi, Y. O. Estrada, R. C. Genova, B. Girma, E. S. Kissel, A. N. Levy, S. MacCracken, P. R. Mastrandrea, and L. L. White. Cambridge, United Kingdom and New York, NY, USA: Cambridge University Press, pp. 229–269.

Jiskoot, H. (2011a). "Dynamics of Glaciers". In: *Encyclopedia of Snow, Ice and Glaciers*. Ed. by V. P. Singh, P. Singh, and U. K. Haritashya. Encyclopedia of Earth Sciences Series. 00005. Springer Netherlands, pp. 245–256.

Jiskoot, H. (2011b). "Glacier Surging". In: *Encyclopedia of Snow, Ice and Glaciers*. Ed. by V. P. Singh, P. Singh, and U. K. Haritashya. Encyclopedia of Earth Sciences Series. 00006. Springer Netherlands, pp. 415–428.

Jones, J. A. A. (1997). *Global Hydrology : Processes, Resources and Environmental Management*. Harlow [u.a.]: Longman.

Jonoski, A. (2006). "Network Distributed Decision Support Systems and the Role of Hydrological Knowledge". In: *Encyclopedia of Hydrological Sciences*. John Wiley & Sons, Ltd.

Juen, M., C. Mayer, A. Lambrecht, H. Han, and S. Liu (2014). "Impact of Varying Debris Cover Thickness on Ablation: A Case Study for Koxkar Glacier in the Tien Shan". In: *The Cryosphere* 8.2, pp. 377–386. DOI: 10.5194/tc-8-377-2014.

Kane, D. and R. Gieck (1997). "Snowmelt Modeling at Small Alaskan Arctic Watershed". In: *Journal of Hydrologic Engineering* 2.4, pp. 204–210. DOI: 10.1061/(ASCE)1084-0699(1997)2:4(204).

Kargel, J. S., G. J. Leonard, M. P. Bishop, A. Kääb, and B. H. Raup, eds. (2014). *Global Land Ice Measurements from Space*. 00007. Berlin, Heidelberg: Springer Berlin Heidelberg.

Kaser, G., M. Großhauser, and B. Marzeion (2010). "Contribution Potential of Glaciers to Water Availability in Different Climate Regimes". In: *Proceedings of the National Academy of Sciences* 107.47. 00106 PMID: 21059938, pp. 20223–20227. DOI: 10.1073/pnas.1008162107.

Keilholz, P., M. Disse, and . Halik (2015). "Effects of Land Use and Climate Change on Groundwater and Ecosystems at the Middle Reaches of the Tarim River Using the MIKE SHE Integrated Hydrological Model". In: *Water* 7.6, pp. 3040–3056. DOI: 10.3390/w7063040.

Kirchhofer, W., ed. (2000). *Klimaatlas Der Schweiz*. Wabern: Schweizerische Meteorologische Anstalt.

Kirkbride, M. P. and P. Deline (2013). "The Formation of Supraglacial Debris Covers by Primary Dispersal from Transverse Englacial Debris Bands". In: *Earth Surface Processes and Landforms* 38.15, pp. 1779–1792. DOI: 10.1002/esp.3416.

Klein, A. and B. Isacks (1998). "Alpine Glacial Geomorphological Studies in the Central Andes Using Landsat Thematic Mapper Images". In: *Glacial Geology and Geomorphology*.

Klein, A. G. and J. L. Kincaid (2006). "Retreat of Glaciers on Puncak Jaya, Irian Jaya, Determined from 2000 and 2002 IKONOS Satellite Images". In: *Journal of Glaciology* 52.176. 00019, pp. 65–79. DOI: 10.3189/172756506781828818.

Klemeš, V. (1986). "Operational Testing of Hydrological Simulation Models". In: *Hydrological Sciences Journal* 31.1, pp. 13–24. DOI: 10.1080/02626668609491024.

Klemeš, V (1990). "The Modelling of Mountain Hydrology: The Ultimate Challenge". In: *Hydrology of Mountainous Areas*. Vol. 190. IAHS, pp. 29–43.

Klok, E. L. and J. Oerlemans (2002). "Model Study of the Spatial Distribution of the Energy and Mass Balance of Morteratschgletscher, Switzerland". In: *Journal of Glaciology* 48.163, pp. 505–518. DOI: 10.3189/172756502781831133.

Koch, H., S. Liersch, and F. F. Hattermann (2013). "Integrating Water Resources Management in Eco-Hydrological Modelling". In: *Water Science & Technology* 67.7. DOI: 10.2166/wst.2013.022.

Koch, J., B. Menounos, and J. J. Clague (2009). "Glacier Change in Garibaldi Provincial Park, Southern Coast Mountains, British Columbia, since the Little Ice Age". In: *Global and Planetary Change* 66 (3–4). 00032, pp. 161–178. DOI: 10.1016/j.gloplacha.2008.11.006.

Konz, M. and J. Seibert (2010). "On the Value of Glacier Mass Balances for Hydrological Model Calibration". In: *Journal of Hydrology* 385 (1–4), pp. 238–246. DOI: 10.1016/j.jhydrol.2010.02.025.

Kotljakov, V. M. (1997). *World Atlas of Snow and Ice Resources*. 00000. Moscow: Russian Academy of Sciences, Institute of Geography.

Kotlyakov, V. M. and N. N. Dreyner (1985). "The World Atlas of Snow and Ice Resources". In: *Mapping Sciences and Remote Sensing* 22.3. 00001, pp. 249–256. DOI: 10.1080/07493878.1985.10641595.

Krause, P., D. P. Boyle, and F. Bäse (2005). "Comparison of Different Efficiency Criteria for Hydrological Model Assessment". In: *Advances in Geosciences* 5, pp. 89–97.

Krogh, S. A., J. W. Pomeroy, and J. McPhee (2014). "Physically Based Mountain Hydrological Modeling Using Reanalysis Data in Patagonia". In: *Journal of Hydrometeorology* 16.1, pp. 172–193. DOI: 10.1175/JHM-D-13-0178.1.

Krysanova, V. and F. Wechsung (2000). *SWIM Manual*.

Krysanova, V., A. Meiner, J. Roosaare, and A. Vasilyev (1989). "Simulation Modelling of the Coastal Waters Pollution from Agricultural Watershed". In: *Ecological Modelling* 49 (1-2), pp. 7–29. DOI: 10.1016/0304-3800(89)90041-0.

Krysanova, V., D. Müller-Wohlfeil, and A. Becker (1998). "Development and Test of a Spatially Distributed Hydrological/Water Quality Model for Mesoscale Watersheds". In: *Ecological Modelling* 106 (2-3). 00306, pp. 261–289. DOI: 10.1016/S0304-3800(97)00204-4.

Krysanova, V. and F. F. Hattermann (2017). "Intercomparison of Climate Change Impacts in 12 Large River Basins: Overview of Methods and Summary of Results". In: *Climatic Change* 141.3, pp. 363–379. DOI: 10.1007/s10584-017-1919-y.

Krysanova, V. and M. White (2015). "Advances in Water Resources Assessment with SWAT—an Overview". In: *Hydrological Sciences Journal* 60.5, pp. 771–783. DOI: 10.1080/02626667.2015.1029482.

Krysanova, V., F. Wechsung, A. Becker, W. Poschenrieder, and J. Gräfe (1999). "Mesoscale Ecohydrological Modelling to Analyse Regional Effects of Climate Change". In: *Environmental Modeling and Assessment* 4.4, pp. 259–271. DOI: 10.1023/A:1019020518977.

Krysanova, V., M. Wortmann, T. Bolch, B. Merz, D. Duethmann, J. Walter, S. Huang, J. Tong, S. Buda, and Z. W. Kundzewicz (2015a). "Analysis of Current Trends in Climate Parameters, River Discharge and Glaciers in the Aksu River Basin (Central Asia)". In: *Hydrological Sciences Journal* 60.4, pp. 566–590. DOI: 10.1080/02626667.2014.925559.

Krysanova, V., F. Hattermann, S. Huang, C. Hesse, T. Vetter, S. Liersch, H. Koch, and Z. W. Kundzewicz (2015b). "Modelling Climate and Land-Use Change Impacts with SWIM: Lessons Learnt from Multiple Applications". In: *Hydrological Sciences Journal* 60.4, pp. 606–635. DOI: 10.1080/02626667.2014.925560.

Kuchment, L. S. and A. N. Gelfan (1996). "The Determination of the Snowmelt Rate and the Meltwater Outflow from a Snowpack for Modelling River Runoff Generation". In: *Journal of Hydrology* 179 (1–4), pp. 23–36. DOI: 10.1016/0022-1694(95)02878-1.

Kulkarni, A. (2014). "Glaciers as Source of Water: The Himalaya". In: *Sustainable Humanity, Sustainable Nature: Our Responsibility*. Pontifical Academy of Sciences Extra Series 41. Vatican City: Pontifical Academy of Sciences.

Kumar, R. (2011). "Glacier Sliding". In: *Encyclopedia of Snow, Ice and Glaciers*. Ed. by V. P. Singh, P. Singh, and U. K. Haritashya. Encyclopedia of Earth Sciences Series. 00000. Springer Netherlands, pp. 415–415.

Kunstmann, H., J. Krause, and S. Mayr (2006). "Inverse Distributed Hydrological Modelling of Alpine Catchments". In:

Kutuzov, S. and M. Shahgedanova (2009). "Glacier Retreat and Climatic Variability in the Eastern Terskey–Alatoo, Inner Tien Shan between the Middle of the 19th Century and Beginning of the 21st Century". In: *Global and Planetary Change* 69 (1–2), pp. 59–70. DOI: 10.1016/j.gloplacha.2009.07.001.

Kääb, A., D. Treichler, C. Nuth, and E. Berthier (2015). "Brief Communication: Contending Estimates of 2003–2008 Glacier Mass Balance over the Pamir–Karakoram–Himalaya". In: *The Cryosphere* 9.2, pp. 557–564. DOI: 10.5194/tc-9-557-2015.

Lambiel, C., R. Delaloye, and I. Gärtner-Roer (2011). "Creep". In: *Encyclopedia of Snow, Ice and Glaciers*. Ed. by V. P. Singh, P. Singh, and U. K. Haritashya. Encyclopedia of Earth Sciences Series. Springer Netherlands, pp. 163–165.

Lawrence, D. M. and A. G. Slater (2009). "The Contribution of Snow Condition Trends to Future Ground Climate". In: *Climate Dynamics* 34 (7-8). 00000, pp. 969–981. DOI: 10.1007/s00382-009-0537-4.

Lawrence, D. M., A. G. Slater, R. A. Tomas, M. M. Holland, and C. Deser (2008). "Accelerated Arctic Land Warming and Permafrost Degradation during Rapid Sea Ice Loss". In: *Geophysical Research Letters* 35.11. 00173, p. L11506. DOI: 10.1029/2008GL033985.

Lee, Y, S Chung, I Bogardi, M Dahab, and S Oh (2001). "Dose-Response Assessment by a Fuzzy Linear-Regression Method". In: *Water Science & Technology* 43, pp. 133–140.

Liersch, S., J. Cools, B. Kone, H. Koch, M. Diallo, J. Reinhardt, S. Fournet, V. Aich, and F. Hattermann (2012). "Vulnerability of Rice Production in the Inner Niger Delta to Water Resources Management under Climate Variability and Change". In: *Environmental Science & Policy*. 00003. DOI: 10.1016/j.envsci.2012.10.014.

Lindström, G., B. Johansson, M. Persson, M. Gardelin, and S. Bergström (1997). "Development and Test of the Distributed HBV-96 Hydrological Model". In: *Journal of Hydrology* 201 (1–4), pp. 272–288. DOI: 10.1016/S0022-1694(97)00041-3.

Linsbauer, A., F. Paul, and W. Haeberli (2012). "Modeling Glacier Thickness Distribution and Bed Topography over Entire Mountain Ranges with GlabTop: Application of a Fast and Robust Approach". In: *Journal of Geophysical Research: Earth Surface* 117 (F3), F03007. DOI: 10.1029/2011JF002313.

Liu, J. (1992). "Jökulhlaups in the Kunmalike River, Southern Tien Shan Mountains, China". In: *Annals of Glaciology* 16, pp. 85–88.

Liu, J. and Y. Fukushima (1999). "Recent Change and Prediction of Glacier-Dammed Lake Outburst Floods from Kunmalik River in Southern Tien Shan, China". In: *Hydrological Extrmes: Understanding, Predicting, Mitigating*. IAHS Publication, pp. 99–107.

Liu, J. (2011). "Kunlun Mountains". In: *Encyclopedia of Snow, Ice and Glaciers*. Ed. by V. P. Singh, P. Singh, and U. K. Haritashya. Encyclopedia of Earth Sciences Series. 00004. Springer Netherlands, pp. 679–682.

Liu, Q. and S. Liu (2015). "Response of Glacier Mass Balance to Climate Change in the Tianshan Mountains during the Second Half of the Twentieth Century". In: *Climate Dynamics* 46 (1-2), pp. 303–316. DOI: 10.1007/s00382-015-2585-2.

Liu, S., Y. Ding, D. Shangguan, Y. Zhang, J. Li, H. Han, J. Wang, and C. Xie (2006a). "Glacier Retreat as a Result of Climate Warming and Increased Precipitation in the Tarim River Basin, Northwest China". In: *Annals of Glaciology* 43.1, pp. 91–96. DOI: 10.3189/172756406781812168.

Liu, X., Q. Yang, and Y. Liang (2006b). "Study on the change of runoff and the effect factors in the Aksu River basin in recent 40 years". In: *China Population, Resources and Environment* 16.3, pp. 83–87.

Liu, Y. and Y. Chen (2006). "Impact of Population Growth and Land-Use Change on Water Resources and Ecosystems of the Arid Tarim River Basin in Western China". In: *International Journal of Sustainable Development & World Ecology* 13.4, pp. 295–305. DOI: 10.1080/13504500609469681.

Lobanova, A., H. Koch, S. Liersch, F. F. Hattermann, and V. Krysanova (2016). "Impacts of Changing Climate on the Hydrology and Hydropower Production of the Tagus River Basin". In: *Hydrological Processes* 30.26, pp. 5039–5052. DOI: 10.1002/hyp.10966.

Lutz, A. F., W. W. Immerzeel, A. Gobiet, F. Pellicciotti, and M. F. P. Bierkens (2013). "Comparison of Climate Change Signals in CMIP3 and CMIP5 Multi-Model Ensembles and Implications for Central Asian Glaciers". In: *Hydrol. Earth Syst. Sci.* 17.9, pp. 3661–3677. DOI: 10.5194/hess-17-3661-2013.

Lutz, A. F., W. W. Immerzeel, A. B. Shrestha, and M. F. P. Bierkens (2014). "Consistent Increase in High Asia's Runoff Due to Increasing Glacier Melt and Precipitation". In: *Nature Climate Change* 4.7, pp. 587–592. DOI: 10.1038/nclimate2237.

Maidment, D. (1993). *Handbook of Hydrology*. New York: McGraw-Hill.

Major River Basins of the World / Global Runoff Data Centre (2007). In collab. with G. R.D. C. GRDC. 00000. Koblenz.

Marshall, S. J. and G. K. C. Clarke (1999). "Ice Sheet Inception: Subgrid Hypsometric Parameterization of Mass Balance in an Ice Sheet Model". In: *Climate Dynamics* 15.7. 00058, pp. 533–550. DOI: 10.1007/s003820050298.

Marshall, S. J., E. C. White, M. N. Demuth, T. Bolch, R. Wheate, B. Menounos, M. J. Beedle, and J. M. Shea (2011). "Glacier Water Resources on the Eastern Slopes of the Canadian Rocky Mountains". In: *Canadian Water Resources Journal / Revue canadienne des ressources hydriques* 36.2. 00027, pp. 109–134. DOI: 10.4296/cwrj3602823.

Mattson, L. (1993). "Ablation on Debris Covered Glaciers: An Example from the Rakhiot Glacier, Panjab, Himalaya". In: *IAHS publication* 218. 00125, pp. 289–296.

Maussion, F., D. Scherer, T. Mölg, E. Collier, J. Curio, and R. Finkelnburg (2014). "Precipitation Seasonality and Variability over the Tibetan Plateau as Resolved by the High Asia Reanalysis". In: *Journal of Climate* 27.5, pp. 1910–1927. DOI: 10.1175/JCLI-D-13-00282.1.

Mayr, E., W. Hagg, C. Mayer, and L. Braun (2013). "Calibrating a Spatially Distributed Conceptual Hydrological Model Using Runoff, Annual Mass Balance and Winter Mass Balance". In: *Journal of Hydrology* 478, pp. 40–49. DOI: 10.1016/j.jhydrol.2012.11.035.

McMichael, C. E., A. S. Hope, and H. A. Loaiciga (2006). "Distributed Hydrological Modelling in California Semi-Arid Shrublands: MIKE SHE Model Calibration and Uncertainty Estimation". In: *Journal of Hydrology* 317 (3-4), pp. 307–324. DOI: 10.1016/j.jhydrol.2005.05.023.

Meile, T., J.-L. Boillat, and A. J. Schleiss (2010). "Hydropeaking Indicators for Characterization of the Upper-Rhone River in Switzerland". In: *Aquatic Sciences* 73.1, pp. 171–182. DOI: 10.1007/s00027-010-0154-7.

Merz, R., J. Parajka, and G. Blöschl (2011). "Time Stability of Catchment Model Parameters: Implications for Climate Impact Analyses". In: *Water Resources Research* 47.2. DOI: 10.1029/2010WR009505.

Merzbacher, G. (1905). *The Central Tian-Shan Mountains 1902-1903*. London: J. Murray.

Miller, J. D., W. W. Immerzeel, and G. Rees (2012). "Climate Change Impacts on Glacier Hydrology and River Discharge in the Hindu Kush–Himalayas". In: *Mountain Research and Development* 32.4, pp. 461–467. DOI: 10.1659/MRD-JOURNAL-D-12-00027.1.

Molini, A., G. G. Katul, and A. Porporato (2011). "Maximum Discharge from Snowmelt in a Changing Climate". In: *Geophysical Research Letters* 38.5. DOI: 10.1029/2010GL046477.

Moss, R. H., J. A. Edmonds, K. A. Hibbard, M. R. Manning, S. K. Rose, D. P. van Vuuren, T. R. Carter, S. Emori, M. Kainuma, T. Kram, G. A. Meehl, J. F. B. Mitchell, N. Nakicenovic, K. Riahi, S. J. Smith, R. J. Stouffer, A. M. Thomson, J. P. Weyant, and T. J. Wilbanks (2010). "The next Generation of Scenarios for Climate Change Research and Assessment". In: *Nature* 463.7282, pp. 747–756. DOI: 10.1038/nature08823.

Moussa, R., N. Chahinian, and C. Bocquillon (2007). "Distributed Hydrological Modelling of a Mediterranean Mountainous Catchment - Model Construction and Multi-Site Validation". In: *Journal of Hydrology* 337 (1-2), pp. 35–51. DOI: 10.1016/j.jhydrol.2007.01.028.

MRIEDWWG (2015). "Elevation-Dependent Warming in Mountain Regions of the World". In: *Nature Climate Change* 5.5. Mountain Research Initiative EDW Working Group (MRIEDWWG), pp. 424–430. DOI: 10.1038/nclimate2563.

Musselman, K. N., M. P. Clark, C. Liu, K. Ikeda, and R. Rasmussen (2017). "Slower Snowmelt in a Warmer World". In: *Nature Climate Change* 7.3, pp. 214–219. DOI: 10.1038/nclimate3225.

Mölg, T., N. J. Cullen, and G. Kaser (2009). "Solar Radiation, Cloudiness and Longwave Radiation over Low-Latitude Glaciers: Implications for Mass-Balance Modelling". In: *Journal of Glaciology* 55.190, pp. 292–302. DOI: 10.3189/002214309788608822.

Nakawo, M. and B. Rana (1999). "Estimate of Ablation Rate of Glacier Ice under a Supraglacial Debris Layer". In: *Geografiska Annaler: Series A, Physical Geography* 81.4. 00079, pp. 695–701. DOI: 10.1111/1468-0459.00097.

Nash, J. and J. Sutcliffe (1970). "River Flow Forecasting through Conceptual Models Part I – A Discussion of Principles". In: *Journal of Hydrology* 10.3, pp. 282–290. DOI: 10.1016/0022-1694(70)90255-6.

Naz, B. S., C. D. Frans, G. K. C. Clarke, P. Burns, and D. P. Lettenmaier (2014). "Modeling the Effect of Glacier Recession on Streamflow Response Using a Coupled Glacio-Hydrological Model". In: *Hydrol. Earth Syst. Sci.* 18.2, pp. 787–802. DOI: 10.5194/hess-18-787-2014.

Neckel, N., J. Kropáček, T. Bolch, and V. Hochschild (2014). "Glacier Mass Changes on the Tibetan Plateau 2003–2009 Derived from ICESat Laser Altimetry Measurements". In: *Environmental Research Letters* 9.1, p. 014009. DOI: 10.1088/1748-9326/9/1/014009.

Ng, F., S. Liu, B. Mavlyudov, and Y. Wang (2007). "Climatic Control on the Peak Discharge of Glacier Outburst Floods". In: *Geophysical Research Letters* 34.21, p. L21503. DOI: 10.1029/2007GL031426.

Nicholson, L. and D. I. Benn (2006). "Calculating Ice Melt beneath a Debris Layer Using Meteorological Data". In: *Journal of Glaciology* 52.178. 00078, pp. 463–470. DOI: 10.3189/172756506781828584.

Oerlemans, J. (2000). "Analysis of a 3 Year Meteorological Record from the Ablation Zone of Morteratschgletscher, Switzerland: Energy and Mass Balance". In: *Journal of Glaciology* 46.155, pp. 571–579. DOI: 10.3189/172756500781832657.

Oerlemans, J. (2008). *Minimal Glacier Models*. 00038 Universiteit Utrecht. Igitur, Utrecht Publishing & Archiving Services.

Oesterle, H, F. Gerstengarbe, and P. Werner (2003). "Homogenisierung Und Aktualisierung Des Klimadatensatzes Des Climate Research Unit Der Universität of East Anglia". In: *Norwich: University of East Anglia*.

Ohmura, A. (2001). "Physical Basis for the Temperature-Based Melt-Index Method". In: *Journal of Applied Meteorology* 40.4, pp. 753–761. DOI: 10.1175/1520-0450(2001)040<0753:PBFTTB>2.0.CO;2.

Oki, T. (2006). "The Hydrologic Cycles and Global Circulation". In: *Encyclopedia of Hydrological Sciences*. John Wiley & Sons, Ltd.

Oki, T. and S. Kanae (2006). "Global Hydrological Cycles and World Water Resources". In: *Science* 313.5790. 00674 PMID: 16931749, pp. 1068–1072. DOI: 10.1126/science.1128845.

Osmonov, A., T. Bolch, C. Xi, A. Kurban, and W. Guo (2013). "Glacier Characteristics and Changes in the Sary-Jaz River Basin (Central Tien Shan, Kyrgyzstan) – 1990–2010". In: *Remote Sensing Letters* 4.8, pp. 725–734. DOI: 10.1080/2150704X.2013.789146.

Osti, R. and S. Egashira (2009). "Hydrodynamic Characteristics of the Tam Pokhari Glacial Lake Outburst Flood in the Mt. Everest Region, Nepal". In: *Hydrological Processes* 23.20, pp. 2943–2955. DOI: 10.1002/hyp.7405.

Osti, R., S. Egashira, and Y. Adikari (2013). "Prediction and Assessment of Multiple Glacial Lake Outburst Floods Scenario in Pho Chu River Basin, Bhutan". In: *Hydrological Processes* 27.2, pp. 262–274. DOI: 10.1002/hyp.8342.

Panitz, H.-J., A. Dosio, M. Büchner, D. Lüthi, and K. Keuler (2014). "COSMO-CLM (CCLM) Climate Simulations over CORDEX-Africa Domain: Analysis of the ERA-Interim Driven Simulations at 0.44 and 0.22 Resolution". In: *Climate Dynamics* 42 (11-12), pp. 3015–3038. DOI: 10.1007/s00382-013-1834-5.

Pattyn, F., C. Schoof, L. Perichon, R. C. A. Hindmarsh, E. Bueler, B. de Fleurian, G. Durand, O. Gagliardini, R. Gladstone, D. Goldberg, G. H. Gudmundsson, P. Huybrechts, V. Lee, F. M. Nick, A. J. Payne, D. Pollard, O. Rybak, F. Saito, and A. Vieli (2012). "Results of the Marine Ice Sheet Model Intercomparison Project, MISMIP". In: *The Cryosphere* 6.3, pp. 573–588. DOI: 10.5194/tc-6-573-2012.

Pattyn, F. (2002). "Transient Glacier Response with a Higher-Order Numerical Ice-Flow Model". In: *Journal of Glaciology* 48.162, pp. 467–477. DOI: 10.3189/172756502781831278.

Paul, F. (2003). "The new Swiss glacier inventory 2000: Application of Remote Sensing and GIS". Department of Geography, University of Zurich.

Paul, F. (2010). "The Influence of Changes in Glacier Extent and Surface Elevation on Modeled Mass Balance". In: *The Cryosphere* 4.4, pp. 569–581. DOI: 10.5194/tc-4-569-2010.

Pechlivanidis, I., B. Jackson, N. McIntyre, and H. Wheater (2011). "Catchment Scale Hydrological Modelling: A Review of Model Types, Calibration Approaches and Uncertainty Analysis Methods in the Context of Recent Developments in Technology and Applications". In: *Global NEST journal* 13.3, pp. 193–214.

Peel, M. C. and G. Blöschl (2011). "Hydrological Modelling in a Changing World". In: *Progress in Physical Geography* 35.2, pp. 249–261. DOI: 10.1177/0309133311402550.

Piao, S., P. Ciais, Y. Huang, Z. Shen, S. Peng, J. Li, L. Zhou, H. Liu, Y. Ma, Y. Ding, P. Friedlingstein, C. Liu, K. Tan, Y. Yu, T. Zhang, and J. Fang (2010). "The Impacts of Climate Change on Water Resources and Agriculture in China". In: *Nature* 467.7311. 00260, pp. 43–51. DOI: 10.1038/nature09364.

Pieczonka, T., T. Bolch, W. Junfeng, and S. Liu (2013). "Heterogeneous Mass Loss of Glaciers in the Aksu-Tarim Catchment (Central Tien Shan) Revealed by 1976 KH-9 Hexagon and 2009 SPOT-5 Stereo Imagery". In: *Remote Sensing of Environment* 130, pp. 233–244. DOI: 10.1016/j.rse.2012.11.020.

Pieczonka, T. and T. Bolch (2015). "Region-Wide Glacier Mass Budgets and Area Changes for the Central Tien Shan between ~ 1975 and 1999 Using Hexagon KH-9 Imagery". In: *Global and Planetary Change* 128, pp. 1–13. DOI: 10.1016/j.gloplacha.2014.11.014.

Pimentel, S. and G. E. Flowers (2011). "A Numerical Study of Hydrologically Driven Glacier Dynamics and Subglacial Flooding". In: *Proceedings of the Royal Society of London A: Mathematical, Physical and Engineering Sciences* 467.2126, pp. 537–558. DOI: 10.1098/rspa.2010.0211.

Praskievicz, S. and H. Chang (2009). "A Review of Hydrological Modelling of Basin-Scale Climate Change and Urban Development Impacts". In: *Progress in Physical Geography* 33.5, pp. 650–671. DOI: 10.1177/0309133309348098.

Priestley, C. H. B. and R. J. Taylor (1972). "On the Assessment of Surface Heat Flux and Evaporation Using Large-Scale Parameters". In: *Monthly Weather Review* 100.2, pp. 81–92. DOI: 10.1175/1520-0493(1972)100<0081:OTAOSH>2.3.CO;2.

Pritchard, H. D. (2017). "Asia's Glaciers Are a Regionally Important Buffer against Drought". In: *Nature* 545.7653, pp. 169–174. DOI: 10.1038/nature22062.

Quick, M. C. and A. Pipes (1977). "U.B.C. WATERSHED MODEL / Le Modèle Du Bassin Versant U.C.B". In: *Hydrological Sciences Bulletin* 22.1, pp. 153–161. DOI: 10.1080/02626667709491701.

Rabatel, A., B. Francou, A. Soruco, J. Gomez, B. Cáceres, J. L. Ceballos, R. Basantes, M. Vuille, J.-E. Sicart, C. Huggel, M. Scheel, Y. Lejeune, Y. Arnaud, M. Collet, T. Condom, G. Consoli, V. Favier, V. Jomelli, R. Galarraga, P. Ginot, L. Maisincho, J. Mendoza, M. Ménégoz, E. Ramirez, P. Ribstein, W. Suarez, M. Villacis, and P. Wagnon (2013). "Current State of Glaciers in the Tropical Andes: A Multi-Century Perspective on Glacier Evolution and Climate Change". In: *The Cryosphere* 7.1. 00072, pp. 81–102. DOI: 10.5194/tc-7-81-2013.

Radić, V. and R. Hock (2010). "Regional and Global Volumes of Glaciers Derived from Statistical Upscaling of Glacier Inventory Data". In: *Journal of Geophysical Research: Earth Surface* 115 (F1). 00126, F01010. DOI: 10.1029/2009JF001373.

Radić, V., A. Bliss, A. C. Beedlow, R. Hock, E. Miles, and J. G. Cogley (2013). "Regional and Global Projections of Twenty-First Century Glacier Mass Changes in Response to Climate Scenarios from Global Climate Models". In: *Climate Dynamics* 42 (1-2), pp. 37–58. DOI: 10.1007/s00382-013-1719-7.

Ragettli, S., F. Pellicciotti, R. Bordoy, and W. W. Immerzeel (2013). "Sources of Uncertainty in Modeling the Glaciohydrological Response of a Karakoram Watershed to Climate Change". In: *Water Resources Research* 49.9, pp. 6048–6066. DOI: 10.1002/wrcr.20450.

Rahman, K., C. Maringanti, M. Beniston, F. Widmer, K. Abbaspour, and A. Lehmann (2012). "Streamflow Modeling in a Highly Managed Mountainous Glacier Watershed Using SWAT: The Upper Rhone River Watershed Case in Switzerland". In: *Water Resources Management* 27.2, pp. 323–339. DOI: 10.1007/s11269-012-0188-9.

Rasemann, S., J. Schmidt, L. Schrott, and R. Dikau (2004). "Geomorphometry in Mountain Terrain". In: Bishop, M. and J. F. Shroder. *Geographic Information Science and Mountain Geomorphology*. Springer Science & Business Media, pp. 101–137.

Rast, M., J. Johannessen, and W. Mauser (2014). "Review of Understanding of Earth's Hydrological Cycle: Observations, Theory and Modelling". In: *Surveys in Geophysics* 35.3, pp. 491–513. DOI: 10.1007/s10712-014-9279-x.

Refsgaard, J. C., H. Madsen, V. Andréassian, K. Arnbjerg-Nielsen, T. A. Davidson, M. Drews, D. P. Hamilton, E. Jeppesen, E. Kjellström, J. E. Olesen, T. O. Sonnenborg, D. Trolle, P. Willems, and J. H. Christensen (2014). "A Framework for Testing the Ability of Models to Project Climate Change and Its Impacts". In: *Climatic Change* 122 (1-2), pp. 271–282. DOI: 10.1007/s10584-013-0990-2.

Refsgaard, J., B. Storm, and T. Clausen (2010). "Système Hydrologique Europeén (SHE): Review and Perspectives after 30 Years Development in Distributed Physically-Based Hydrological Modelling". In: *Hydrology Research* 41.5, p. 355. DOI: 10.2166/nh.2010.009.

Refsgaard, J. C. (1997). "Parameterisation, Calibration and Validation of Distributed Hydrological Models". In: *Journal of Hydrology* 198 (1-4), pp. 69–97. DOI: 10.1016/S0022-1694(96)03329-X.

Regonda, S. K., B. Rajagopalan, M. Clark, and J. Pitlick (2005). "Seasonal Cycle Shifts in Hydroclimatology over the Western United States". In: *Journal of Climate* 18.2, pp. 372–384. DOI: 10.1175/JCLI-3272.1.

Revenga, C. (2003). *Watersheds of the World*. 00035. World Resources Institute ; IUCN : IWMI : Ramsar Convention Bureau.

Ritchie, J. T. (1998). "Soil Water Balance and Plant Water Stress". In: *Understanding Options for Agricultural Production*. Ed. by G. Y. Tsuji, G. Hoogenboom, and P. K. Thornton. Systems Approaches for Sustainable Agricultural Development 7. 00220. Springer Netherlands, pp. 41–54.

Robinson, D. A. and A. Frei (2000). "Seasonal Variability of Northern Hemisphere Snow Extent Using Visible Satellite Data". In: *The Professional Geographer* 52.2. 00120, pp. 307–315. DOI: 10.1111/0033-0124.00226.

Rockel, B, A Will, and A Hense (2008). "Special Issue: Regional Climate Modelling With COSMO-CLM (CCLM), 17". In: *Meteorol. Z.*

Rosenfeld, D., S. Sherwood, R. Wood, and L. Donner (2014). "Climate Effects of Aerosol-Cloud Interactions". In: *Science* 343.6169, pp. 379–380. DOI: 10.1126/science.1247490. pmid: 24458631.

Ross, M. A. and P. D. Tara (1993). "Integrated Hydrologic Modeling with Geographic Information Systems". In: *Journal of Water Resources Planning and Management* 119.2, pp. 129–140.

Rowan, A. V., D. L. Egholm, D. J. Quincey, and N. F. Glasser (2015). "Modelling the Feedbacks between Mass Balance, Ice Flow and Debris Transport to Predict the Response to Climate Change of Debris-Covered Glaciers in the Himalaya". In: *Earth and Planetary Science Letters* 430, pp. 427–438. DOI: 10.1016/j.epsl.2015.09.004.

Rowland, J. C., C. E. Jones, G. Altmann, R. Bryan, B. T. Crosby, L. D. Hinzman, D. L. Kane, D. M. Lawrence, A. Mancino, P. Marsh, J. P. McNamara, V. E. Romanvosky, H. Toniolo, B. J. Travis, E. Trochim, C. J. Wilson, and G. L. Geernaert (2010). "Arctic Landscapes in Transition: Responses to Thawing Permafrost". In: *Eos, Transactions American Geophysical Union* 91.26. 00065, pp. 229–230. DOI: 10.1029/2010EO260001.

Rumbaur, C., N. Thevs, M. Disse, M. Ahlheim, A. Brieden, B. Cyffka, D. Duethmann, T. Feike, O. Frör, P. Gärtner, U. Halik, J. Hill, M. Hinnenthal, P. Keilholz, B. Kleinschmit, V. Krysanova, M. Kuba, S. Mader, C. Menz, H. Othmanli, S. Pelz, M. Schroeder,

T. F. Siew, V. Stender, K. Stahr, F. M. Thomas, M. Welp, M. Wortmann, X. Zhao, X. Chen, T. Jiang, J. Luo, H. Yimit, R. Yu, X. Zhang, and C. Zhao (2015). "Sustainable Management of River Oases along the Tarim River (SuMaRiO) in Northwest China under Conditions of Climate Change". In: *Earth Syst. Dynam.* 6.1, pp. 83–107. DOI: 10.5194/esd-6-83-2015.

Sakai, A., M. Nakawo, and K. Fujita (1998). "Melt Rate of Ice Cliffs on the Lirung Glacier, Nepal Himalayas, 1996". In: *Bulletin of glacier research* 16, pp. 57–66.

Sakai, A., T. Nuimura, K. Fujita, S. Takenaka, H. Nagai, and D. Lamsal (2015). "Climate Regime of Asian Glaciers Revealed by GAMDAM Glacier Inventory". In: *The Cryosphere* 9.3, pp. 865–880. DOI: 10.5194/tc-9-865-2015.

Sakai, A., N. Takeuchi, K. Fujita, and M. Nakawo (2000). "Role of Supraglacial Ponds in the Ablation Process of a Debris-Covered Glacier in the Nepal Himalayas". In: *IAHS-AISH publication*, pp. 119–130.

Sangrey, D., K. Harrop-Williams, and J. Klaiber (1984). "Predicting Groundwater Response to Precipitation". In: *Journal of Geotechnical Engineering* 110.7, pp. 957–975. DOI: 10.1061/(ASCE)0733-9410(1984)110:7(957).

Sanzana, P., S. Jankowfsky, F. Branger, I. Braud, X. Vargas, N. Hitschfeld, and J. Gironás (2013). "Computer-Assisted Mesh Generation Based on Hydrological Response Units for Distributed Hydrological Modeling". In: *Computers & Geosciences* 57, pp. 32–43. DOI: 10.1016/j.cageo.2013.02.006.

Schaefli, B., B. Hingray, M. Niggli, and A. Musy (2005). "A Conceptual Glacio-Hydrological Model for High Mountainous Catchments". In: *Hydrology and Earth System Sciences* 9, pp. 95 –109.

Schaefli, B. and H. V. Gupta (2007). "Do Nash Values Have Value?" In: *Hydrological Processes* 21.15, pp. 2075–2080. DOI: 10.1002/hyp.6825.

Scherler, D., B. Bookhagen, and M. R. Strecker (2011). "Spatially Variable Response of Himalayan Glaciers to Climate Change Affected by Debris Cover". In: *Nature Geoscience* 4.3, pp. 156–159. DOI: 10.1038/ngeo1068.

Schneider, U., Becker, Andreas, Finger, Peter, Meyer-Christoffer, Anja, Rudolf, Bruno, and Ziese, Markus (2015). *GPCC Full Data Reanalysis Version 7.0 at 0.5: Monthly Land-Surface Precipitation from Rain-Gauges Built on GTS-Based and Historic Data*.

Schoups, G., N. C. van de Giesen, and H. H. G. Savenije (2008). "Model Complexity Control for Hydrologic Prediction". In: *Water Resources Research* 44.12, W00B03. DOI: 10.1029/2008WR006836.

Schweizer, J., J. Bruce Jamieson, and M. Schneebeli (2003). "Snow Avalanche Formation". In: *Reviews of Geophysics* 41.4, p. 1016. DOI: 10.1029/2002RG000123.

Sevruk, B. (1985). "Systematischer Niederschlagsmessfehler in Der Schweiz". In: *Beiträge zur Geologie der Schweiz–Hydrologie* 31, pp. 65–75.

Sevruk, B. and K. Mieglitz (2002). "The Effect of Topography, Season and Weather Situation on Daily Precipitation Gradients in 60 Swiss Valleys". In: *Water Science and Technology*. 00016.

Shangguan, D., S. Liu, Y. Ding, L. Ding, L. Xiong, D. Cai, G. Li, A. Lu, S. Zhang, and Y. Zhang (2006). "Monitoring the Glacier Changes in the Muztag Ata and Konggur Mountains, East Pamirs, Based on Chinese Glacier Inventory and Recent Satellite Imagery". In: *Annals of Glaciology* 43.1, pp. 79–85. DOI: 10.3189/172756406781812393.

Shangguan, D., L. Shiyin, D. Yongjian, L. Jing, Z. Yong, D. Lianfu, W. Xing, X. Changwei, and L. Gang (2007). "Glacier Changes in the West Kunlun Shan from 1970 to 2001 Derived from Landsat TM/ETM+ and Chinese Glacier Inventory Data". In: *Annals of Glaciology* 46.1, pp. 204–208. DOI: 10.3189/172756407782871693.

Shen, Y., G. Wang, C. Shao, W. Mao, and S. Wang (2007). "Response of Glacier Flash Flood to Climate Warming in the Tarim River Basin". In: *Advances in Climate Change Research*.

Shen, Y., G. Wang, Y. Ding, H. Su, W. Mao, S. Wang, and M. Duishen M (2009). "Changes in Merzbacher Lake of Inylchek Glacier and Glacial Flash Floods in Aksu River Basin, Tianshan during the Period of 1903-2009". In: *Journal of Glaciology and Geocryology* 31.6. 00007, pp. 993–1002.

Shi, X. Z., D. S. Yu, E. D. Warner, X. Z. Pan, G. W. Petersen, Z. G. Gong, and D. C. Weindorf (2004). "Soil Database of 1:1,000,000 Digital Soil Survey and Reference System of the Chinese Genetic Soil Classification System". In: *Soil Horizons* 45.4, p. 129. DOI: 10.2136/sh2004.4.0129.

Shi, Y., Y. Shen, E. Kang, D. Li, Y. Ding, G. Zhang, and R. Hu (2006). "Recent and Future Climate Change in Northwest China". In: *Climatic Change* 80 (3-4), pp. 379–393. DOI: 10.1007/s10584-006-9121-7.

Shrestha, A. B. (2011). "Climate Change and Glaciers". In: *Encyclopedia of Snow, Ice and Glaciers*. Ed. by V. P. Singh, P. Singh, and U. K. Haritashya. Encyclopedia of Earth Sciences Series. 00069. Springer Netherlands, pp. 145–152.

Shur, Y., M. T. Jorgenson, and M. Z. Kanevskiy (2011). "Permafrost". In: *Encyclopedia of Snow, Ice and Glaciers*. Ed. by V. P. Singh, P. Singh, and U. K. Haritashya. Encyclopedia of Earth Sciences Series. Springer Netherlands, pp. 841–848.

Singh, P. and N. Kumar (1997). "Impact Assessment of Climate Change on the Hydrological Response of a Snow and Glacier Melt Runoff Dominated Himalayan River". In: *Journal of Hydrology* 193 (1-4), pp. 316–350. DOI: 16/S0022-1694(96)03142-3.

Singh, V. and D. K. Frevert (2002). *Mathematical Models of Large Watershed Hydrology*. Water Resources Publication. 930 pp.

Singh, V. and D. Woolhiser (2002). "Mathematical Modeling of Watershed Hydrology". In: *Journal of Hydrologic Engineering* 7.4, pp. 270–292. DOI: 10.1061/(ASCE)1084-0699(2002)7:4(270).

Sivapalan, M. (2003). "Prediction in Ungauged Basins: A Grand Challenge for Theoretical Hydrology". In: *Hydrological Processes* 17.15, pp. 3163–3170. DOI: 10.1002/hyp.5155.

Skamarock, W. C. (2004). "Evaluating Mesoscale NWP Models Using Kinetic Energy Spectra". In: *Monthly Weather Review* 132.12, pp. 3019–3032. DOI: 10.1175/MWR2830.1.

Slater, A. G. and D. M. Lawrence (2013). "Diagnosing Present and Future Permafrost from Climate Models". In: *Journal of Climate* 26.15. 00018, pp. 5608–5623. DOI: 10.1175/JCLI-D-12-00341.1.

Slaymaker, O. and R. E. J. Kelly (2007). *The Cryosphere and Global Environmental Change*. 00000. Malden, MA: Blackwell Pub.

Smedema, L. K., W. F. Vlotman, and D. W. Rycroft (2004). *Modern Land Drainage: Planning, Design and Management of Agricultural Drainage Systems*. London: Taylor & Francis. 472 pp.

Solomon, S., D. Qin, M. Manning, Z. Chen, M. Marquis, K. Averyt, M. Tignor, and H. Miller, eds. (2007). *Climate Change 2007: The Physical Science Basis. Contribution of Working Group I to the Fourth Assessment Report of the Intergovernmental Panel on Climate Change*. Cambridge: Cambridge University Press.

Sorg, A., T. Bolch, M. Stoffel, O. Solomina, and M. Beniston (2012). "Climate Change Impacts on Glaciers and Runoff in Tien Shan (Central Asia)". In: *Nature Climate Change* 2.10, pp. 725–731. DOI: 10.1038/nclimate1592.

Sorg, A., M. Huss, M. Rohrer, and M. Stoffel (2014). "The Days of Plenty Might Soon Be over in Glacierized Central Asian Catchments". In: *Environmental Research Letters* 9.10, p. 104018. DOI: 10.1088/1748-9326/9/10/104018.

Stagge, J. H. and G. E. Moglen (2014). "Evolutionary Algorithm Optimization of a Multireservoir System with Long Lag Times". In: *Journal of Hydrologic Engineering* 19.9, p. 05014011. DOI: 10.1061/(ASCE)HE.1943-5584.0000972.

Steppeler, J., G. Doms, U. Schättler, H. W. Bitzer, A. Gassmann, U. Damrath, and G. Gregoric (2003). "Meso-Gamma Scale Forecasts Using the Nonhydrostatic Model LM". In: *Meteorology and Atmospheric Physics* 82 (1-4), pp. 75–96. DOI: 10.1007/s00703-001-0592-9.

Stewart, I. T. (2009). "Changes in Snowpack and Snowmelt Runoff for Key Mountain Regions". In: *Hydrological Processes* 23.1. 00150, pp. 78–94. DOI: 10.1002/hyp.7128.

Stewart, I. T., D. R. Cayan, and M. D. Dettinger (2005). "Changes toward Earlier Streamflow Timing across Western North America". In: *Journal of Climate* 18.8, pp. 1136–1155. DOI: 10.1175/JCLI3321.1.

Stisen, S., A. L. Højberg, L. Troldborg, J. C. Refsgaard, B. S. B. Christensen, M. Olsen, and H. J. Henriksen (2012). "On the Importance of Appropriate Precipitation Gauge Catch Correction for Hydrological Modelling at Mid to High Latitudes". In: *Hydrol. Earth Syst. Sci.* 16.11. 00014, pp. 4157–4176. DOI: 10.5194/hess-16-4157-2012.

Stocker, T., D. Qin, G.-K. Plattener, M. Tignor, S. Allen, J. Boschung, A. Nauels, Y. Xia, V. Bex, and P. Midgley, eds. (2014). *Climate Change 2013: The Physical Science Basis: Working Group I Contribution to the Fifth Assessment Report of the Intergovernmental Panel on Climate Change*. 00013. Cambridge University Press. 1553 pp.

Strasser, U. and H. Kunstmann (2013). "Tackling Complexity in Modelling Mountain Hydrology: Where Do We Stand, Where Do We Go?" In: *Cold and Mountain Region Hydrological Systems under Climate Change: Towards Improved Projections*. International Association of Hydrological Sciences, pp. 3–12.

Tangborn, W. (2013). "Mass Balance, Runoff and Surges of Bering Glacier, Alaska". In: *The Cryosphere* 7.3, pp. 867–875. DOI: 10.5194/tc-7-867-2013.

Tao, H., M. Gemmer, Y. Bai, B. Su, and W. Mao (2011). "Trends of Streamflow in the Tarim River Basin during the Past 50 Years: Human Impact or Climate Change?" In: *Journal of Hydrology* 400 (1-2), pp. 1–9. DOI: 16/j.jhydrol.2011.01.016.

Taylor, K. E., R. J. Stouffer, and G. A. Meehl (2011). "An Overview of CMIP5 and the Experiment Design". In: *Bulletin of the American Meteorological Society* 93.4, pp. 485–498. DOI: 10.1175/BAMS-D-11-00094.1.

Thevs, N. (2011). "Water Scarcity and Allocation in the Tarim Basin: Decision Structures and Adaptations on the Local Level". In: *Journal of Current Chinese Affairs* 40.3. 00008, pp. 113–137.

Thomas, A. (2008). "Agricultural Irrigation Demand under Present and Future Climate Scenarios in China". In: *Global and Planetary Change* 60 (3–4), pp. 306–326. DOI: 10.1016/j.gloplacha.2007.03.009.

Thompson, J. R., A. J. Green, D. G. Kingston, and S. N. Gosling (2013). "Assessment of Uncertainty in River Flow Projections for the Mekong River Using Multiple GCMs and Hydrological Models". In: *Journal of Hydrology* 486, pp. 1–30. DOI: 10.1016/j.jhydrol.2013.01.029.

Thompson, L. G., H. H. Brecher, E. Mosley-Thompson, D. R. Hardy, and B. G. Mark (2009). "Glacier Loss on Kilimanjaro Continues Unabated". In: *Proceedings of the National Academy of Sciences* 106.47. 00060, pp. 19770–19775. DOI: 10.1073/pnas.0906029106. pmid: 19884500.

Uhlmann, B., F. Jordan, and M. Beniston (2013). "Modelling Runoff in a Swiss Glacierized Catchment—part I: Methodology and Application in the Findelen Basin under a Long-Lasting Stable Climate". In: *International Journal of Climatology* 33.5, pp. 1293–1300. DOI: 10.1002/joc.3501.

Uppala, S. M., P. W. KÅllberg, A. J. Simmons, U. Andrae, V. D. C. Bechtold, M. Fiorino, J. K. Gibson, J. Haseler, A. Hernandez, G. A. Kelly, X. Li, K. Onogi, S. Saarinen, N. Sokka, R. P. Allan, E. Andersson, K. Arpe, M. A. Balmaseda, A. C. M. Beljaars, L. V. D. Berg, J. Bidlot, N. Bormann, S. Caires, F. Chevallier, A. Dethof, M. Dragosavac, M. Fisher, M. Fuentes, S. Hagemann, E. Hólm, B. J. Hoskins, L. Isaksen, P. a.E. M. Janssen, R. Jenne, A. P. Mcnally, J.-F. Mahfouf, J.-J. Morcrette, N. A. Rayner, R. W. Saunders, P. Simon, A. Sterl, K. E. Trenberth, A. Untch, D. Vasiljevic, P. Viterbo, and J. Woollen (2005). "The ERA-40 Re-Analysis". In: *Quarterly Journal of the Royal Meteorological Society* 131.612, pp. 2961–3012. DOI: 10.1256/qj.04.176.

Vetter, T., S. Huang, T. Yang, V. Aich, X. Wang, H. Gu, V. Krysanova, and F. Hattermann (2013). "Intercomparison of Climate Impacts and Evaluation of Uncertainties from Different Sources Using Three Regional Hydrological Models for Three River Basins on Three Continents". In: *Proceedings of the IMPACTS World Conference*.

Vetter, T., S. Huang, V. Aich, T. Yang, X. Wang, V. Krysanova, and F. Hattermann (2015). "Multi-Model Climate Impact Assessment and Intercomparison for Three Large-Scale River Basins on Three Continents". In: *Earth Syst. Dynam.* 6.1, pp. 17–43. DOI: 10.5194/esd-6-17-2015.

Vieli, A. (2015). "Glacier Change: Dynamic Projections". In: *Nature Geoscience* 8.5, pp. 332–333. DOI: 10.1038/ngeo2425.

Wagener, T., H. S. Wheater, and H. Gupta (2004). *Rainfall-Runoff Modelling In Gauged And Ungauged Catchments*. London: Imperial College Press. 320 pp.

Wang, D., C. Menz, T. Simon, C. Simmer, and C. Ohlwein (2013). "Regional Dynamical Downscaling with CCLM over East Asia". In: *Meteorology and Atmospheric Physics* 121 (1-2), pp. 39–53. DOI: 10.1007/s00703-013-0250-z.

Wang, G., Y. Shen, H. Su, J. Wang, W. Mao, Q. Gao, and S. Wang (2008). "Runoff Changes in Aksu River Basin during 1956-2006 and Their Impacts on Water Availability for Tarim River". In: *Journal of Glaciology and Geocryology* 30.4, pp. 562–568.

Wang, G., Y. Shen, J. Zhang, S. Wang, and W. Mao (2010). "The Effects of Human Activities on Oasis Climate and Hydrologic Environment in the Aksu River Basin, Xinjiang, China". In: *Environmental Earth Sciences* 59.8, pp. 1759–1769. DOI: 10.1007/s12665-009-0158-6.

Wang, Y., ed. (2006). *Local records of the Aksu River basin*. Beijing, China: Fangshi Publisher.

Weedon, G. P., S. Gomes, P. Viterbo, W. J. Shuttleworth, E. Blyth, H. Oesterle, J. C. Adam, N. Bellouin, O. Boucher, and M. Best (2011). "Creation of the WATCH Forcing Data and Its Use to Assess Global and Regional Reference Crop Evaporation over Land during the Twentieth Century". In: *Journal of Hydrometeorology* 12.5. 00081, pp. 823–848. DOI: 10.1175/2011JHM1369.1.

Weertman, J. (1969). "Water Lubrication Mechanism of Glacier Surges". In: *Canadian Journal of Earth Sciences* 6.4, pp. 929–942. DOI: 10.1139/e69-097.

WGMS and UNEP (2008). *Global Glacier Changes: Facts and Figures*. Zürich: World Glacier Monitoring Service.

Willis, I. (2006). "Hydrology of Glacierized Basins". In: *Encyclopedia of Hydrological Sciences*. John Wiley & Sons, Ltd.

Willis, I. C. (2011). "Hydrological Response in Glacierized Basins". In: *Encyclopedia of Snow, Ice and Glaciers*. Ed. by V. P. Singh, P. Singh, and U. K. Haritashya. Encyclopedia of Earth Sciences Series. 00000. Springer Netherlands, pp. 541–544.

Winkler, M., I. Juen, T. Mölg, P. Wagnon, J. Gómez, and G. Kaser (2009). "Measured and Modelled Sublimation on the Tropical Glaciar Artesonraju, Perú". In: *The Cryosphere* 3.1, pp. 21–30. DOI: 10.5194/tc-3-21-2009.

Winsemius, H. C., B. Schaefli, A. Montanari, and H. H. G. Savenije (2009). "On the Calibration of Hydrological Models in Ungauged Basins: A Framework for Integrating Hard and Soft Hydrological Information". In: *Water Resources Research* 45.12, W12422. DOI: 10.1029/2009WR007706.

Woesten, J., Y. A. Pachepsky, and W. J Rawls (2001). "Pedotransfer Functions: Bridging the Gap between Available Basic Soil Data and Missing Soil Hydraulic Characteristics". In: *Journal of Hydrology* 251, pp. 123–150.

Xu, H., B. Zhou, and Y. Song (2010a). "Impacts of Climate Change on Headstream Runoff in the Tarim River Basin". In: *Hydrology Research* 42.1, p. 20. DOI: 10.2166/nh.2010.069.

Xu, J., W. Li, M. Ji, F. Lu, and S. Dong (2010b). "A Comprehensive Approach to Characterization of the Nonlinearity of Runoff in the Headwaters of the Tarim River, Western China". In: *Hydrological Processes* 24.2, pp. 136–146. DOI: 10.1002/hyp.7484.

Xu, Z., Z. Liu, G. Fu, and Y. Chen (2010c). "Trends of Major Hydroclimatic Variables in the Tarim River Basin during the Past 50 Years". In: *Journal of Arid Environments* 74.2, pp. 256–267. DOI: 16/j.jaridenv.2009.08.014.

Yao, J., L. Gu, H. Han, Y. Wang, and S. Liu (2014). "The Surface Energy Budget on the Debris-Covered Koxkar Glacier in China". In: *Environmental Earth Sciences* 72.11, pp. 4503–4510. DOI: 10.1007/s12665-014-3350-2.

Yao, T., L. Thompson, W. Yang, W. Yu, Y. Gao, X. Guo, X. Yang, K. Duan, H. Zhao, B. Xu, J. Pu, A. Lu, Y. Xiang, D. B. Kattel, and D. Joswiak (2012). "Different Glacier Status with Atmospheric Circulations in Tibetan Plateau and Surroundings". In: *Nature Climate Change* 2.9, pp. 663–667. DOI: 10.1038/nclimate1580.

Yatagai, A., K. Kamiguchi, O. Arakawa, A. Hamada, N. Yasutomi, and A. Kitoh (2012). "APHRODITE: Constructing a Long-Term Daily Gridded Precipitation Dataset for Asia Based on a Dense Network of Rain Gauges". In: *Bulletin of the American Meteorological Society* 93.9. 00128, pp. 1401–1415. DOI: 10.1175/BAMS-D-11-00122.1.

Young, P. C. (2002). "Advances in Real–time Flood Forecasting". In: *Philosophical Transactions of the Royal Society of London A: Mathematical, Physical and Engineering Sciences* 360.1796, pp. 1433–1450. DOI: 10.1098/rsta.2002.1008. pmid: 12804258.

Zemp, M., M. Hoelzle, and W. Haeberli (2009). "Six Decades of Glacier Mass-Balance Observations: A Review of the Worldwide Monitoring Network". In: *Annals of Glaciology* 50.50, pp. 101–111. DOI: 10.3189/172756409787769591.

Zemp, M., W. Haeberli, M. Hoelzle, and F. Paul (2006). "Alpine Glaciers to Disappear within Decades?" In: *Geophysical Research Letters* 33.13. 00200, p. L13504. DOI: 10.1029/2006GL026319.

Zhang, X., D. Yang, X. Xiang, and X. Huang (2012). "Impact of Agricultural Development on Variation in Surface Runoff in Arid Regions: A Case of the Aksu River Basin". In: *Journal of Arid Land* 4.4, pp. 399–410.

Zhang, X. (1992). “Investigation of Glacier Bursts of the Yarkant River in Xinjiang, China”. In: *Annals of Glaciology* 16, pp. 135–139. DOI: 10.1017/S0260305500004948.

Zhang, Y., S. Liu, and Y. Ding (2006). “Observed Degree-Day Factors and Their Spatial Variation on Glaciers in Western China”. In: *Annals of Glaciology* 43.1. 00037, pp. 301–306. DOI: 10.3189/172756406781811952.

Zhou, Y., Z. Li, and J. Li (2017). “Slight Glacier Mass Loss in the Karakoram Region during the 1970s to 2000 Revealed by KH-9 Images and SRTM DEM”. In: *Journal of Glaciology* 63.238, pp. 331–342. DOI: 10.1017/jog.2016.142.

Zhu, C. (1996). “Rates of Periglacial Processes in the Central Tianshan, China”. In: *Permafrost and Periglacial Processes* 7.1, pp. 79–94. DOI: 10.1002/(SICI)1099-1530(199601)7:1<79::AID-PPP208>3.0.CO;2-O.

Östrem, G. (1959). “Ice Melting under a Thin Layer of Moraine, and the Existence of Ice Cores in Moraine Ridges”. In: *Geografiska Annaler* 41.4, pp. 228–230. JSTOR: 4626805.

Appendix

A SWIM-G source code

A.1 Module outline

```
module glaciers
use common_par
implicit none

!!! MAIN ARRAYS !!!!!!!!!!!!!!!!!!!!!!!!!!!!!!!!!!!!!!!!!!!!!!!!!!!!!!!!
integer, dimension(:,:), allocatable :: ghyd  ! Hydrotope-glacier unit
    + mapping (same length as hydrotope arrays)
integer, dimension(:), allocatable   :: gj    ! Subbasin of glacier unit
integer, dimension(:), allocatable   :: gje   ! Hydrotope of glacier unit
integer, dimension(:), allocatable   :: nxtgu ! Downstream glacier unit
real, dimension(:), allocatable      :: gla   ! Current glacier water
    + equivalent
real, dimension(:), allocatable      :: gla0  ! Glacier water equivalent of
    + previous year
real, dimension(:), allocatable      :: glr   ! Glacier water storage after
    + melting
real, dimension(:), allocatable      :: garea ! Glacier unit area (km^2)
    + (from catchment drainage area)
integer, dimension(:,:), allocatable :: gfirn ! Hydrotope firn water
    + equivalent for accounting
real, dimension(:), allocatable      :: gsl   ! Slope of glacier unit
    + (degrees)
real, dimension(:), allocatable      :: gavp  ! Proportion of glacier unit
    + prone to avalanching (0-1)
real, dimension(:), allocatable      :: ghc   ! Glacier critical hight, mm
    + w.eq. (depending on slope)
real, dimension(:), allocatable      :: gshs  ! Hours of sun on in summer
    + (N: doy=172, S: doy=355)
real, dimension(:), allocatable      :: gshw  ! Hours of sun on in winter
    + (S: doy=172, N: doy=355)
real, dimension(:), allocatable      :: ghu   ! Glacier heat units for
    + accounting, dg C
real, dimension(:), allocatable      :: gddf  ! Degree-day factor of each
    + glacier unit, mm d^-1 per day
real, dimension(:), allocatable      :: debr  ! Debris cover (0/1 or m)
real, dimension(:), allocatable      :: gq    ! Daily glacier flux volume,
    + m3 water
```

```
real, dimension(:), allocatable      :: gqh   ! Glacier flux height, mm
    + water eq. (for accounting, accumulated until reset)
real, dimension(:), allocatable      :: gme   ! Glacier melt per unit, mm
    + water eq. (for accounting, accumulated until reset)
real, dimension(:), allocatable      :: gsn   ! Glacier snow accumulation
    + per unit, mm water eq. (for accounting, accumulated until reset)
real, dimension(:), allocatable      :: gsub  ! Glacier sublimation (and
    + evaporation), mm water eq. (for accounting, accumulated until reset)
real, dimension(:), allocatable      :: glost ! Glacier volume lost to
    + outside of glacier area/catchment, w.eq. m3
real, dimension(:), allocatable      :: gevap ! Glacier evaporation for
    + accounting, mm weq.


!!! CONSTANTS !!!!!!!!!!!!!!!!!!!!!!!!!!!!!!!!!!!!!!!!!!!!!!!!!!!!!!!
character(len=256)                   :: glacierStrPath='Input/glaciers.str'
    + ! data for each glacier unit
character(len=256)                   :: glacierBsnPath='Input/glaciers.bsn'
    + ! general glacier parameters
character(len=256),dimension(1000)   :: gcols    ! columns in glacier.str
    + file
integer                              :: maxgid=0 ! highest glacier unit ID
    + (size of arrays)
real                                 :: agla0=0  ! number of units with
    + initial glacier cover
integer                              :: ngu      ! number of glacier units
    + (nrows in file -1)
integer                              :: gmbout   ! file unit id for the
    + massbalance output file
integer                              :: gweout   ! file unit id for glacier
    + water equiv. output file
integer                              :: gqout    ! file unit id for glacier
    + water equiv. output file
integer                              :: ddfout   ! file unit id for
    + degree-day-factor output file
integer                              :: debrout  ! file unit id for glacier
    + debris cover output file
integer                              :: gvarout  ! variable output file id
    + for debugging
integer                              :: gstrout  ! file unit id of glacier
    + structure output file
real                                 :: PI=DACOS(-1.D0) ! Pi defined as a
    + constant, DACOS and D0 makes cos super compile proof
integer                              :: SSglob=100000  ! global average
    + shear stress in Pa or kg/(m s2), global is 10^5
real                                 :: rhex=1.2E-8  ! glacier flow
    + rheology, m^-4 a^-1
real                                 :: rest=2   ! glacier water storage
    + residence time, days
!    real                                 :: premb=0   ! prescribed glacier
    + mass balance for initialisation, mm w eq. (now in common.f for
    + subcatch)
real                                 :: gdc       ! debris concentration in
    + ice
integer                              :: gonly     ! switch to run snow and
    + glacier module only
real                                 :: geva      ! actual glacier
    + evaporation on given day and glacier unit, mm d^-1
```

```
real                                    :: geo       ! scaled potential
    + evapotranspiration, mm d^-1

56

CONTAINS

subroutine glacierInitialise
61 subroutine glacierReadInput
subroutine glacierAllocate
subroutine glacierOpenOutput
subroutine glacierRain(j,je)
subroutine glacierEvap(j,je)
66 subroutine glacierAblation(j, je)
subroutine glacierAccum(gu, firn)
subroutine glacierFirn(j,je, firn)
function criticalH(sl)
subroutine glacierFlow(j,je)
71 subroutine glacierRoute
subroutine glacierMassbalance(year,iday,sc)
subroutine glacierMassbalanceSubcatch(year,ix)


76 !--- HELPER FUNCTIONS/SUBROUTINES -----------------------------
subroutine getRowsCols(path,nrows,ncols,columns)
integer function openFile(fname, status)
real function warnRg(lo,up, v, var, i)

81 end module glaciers
```

A.2 Implementation in SWIM

Subroutines need to 'use' the glacier module using 'use glaciers'.

subbasin.f: Calculate all glacier processes in hydrotope loop

```
C#### GLACIER PROCESSES
      if (ghyd(j,jea)>0) then
        if (precipe > 0) call glacierRain(j,jea)
        call glacierAblation(j,jea)
360     call glacierFlow(j,jea)
      endif
C### Snow and glaciers only if switch is on
      if (gonly/=0) goto 100
```

monthly.f: Perform the glacier routing

```
      call glacierRoute
```

solt.f: Adjust snow melt by aspect and terrain shading

```
C!MW scale melt factor by sun hours, ie. aspect and terrain shading if in
    + glacier area
        gu = ghyd(j,jea)
        if (gu.gt.0) then
195         ! half range of annual amplitude
```

```
            hlfrg = (gshs(gu)-gshw(gu))/2
            ! hours of sunlight
            hrs = gshw(gu) + hlfrg + cos((ida-172)*2*PI/366)*hlfrg
            smr = hrs/12 * smr
200       endif
```

hydrotop.f: Glacier evaporation instead of soil evaporation

```
155 C#### if glacier cover, no soil evaporation
      if (ghyd(j,jea) .gt. 0) then
        if (gla(ghyd(j,jea)) > 0) then
  C#### take evaporation calculated previously in glacierAblation
            eo=geo
160         eopot=geo
            ep=0
            es=geva
            canev = 0
        else
165        call evap(j,jea,k,n)
        endif
      else
        call evap(j,jea,k,n)
      endif
```

A.3 Subroutines and functions

```
  subroutine glacierInitialise
  ! first assessing the number of glacier units and columns,
  ! then allocate all shared arrays, then reading the glacier.str file and
85 ! initialise other variables and opening output files
      implicit none
      integer nrows,ncols,i,fui
      real clck_bg, clck_end, clck_rt, dummy
      integer                          :: gid=0
90
      write(*,*) '-----------------------------------------------------'
      write(*,*) 'GLACIER MODULE ACTIVE'
      ! get nrows,ncols and report
      call getRowsCols(glacierStrPath,nrows,ncols,gcols)
95    write(*,*) nrows,'rows found in glaciers.str with these data columns:'
      do i=1,ncols
          write(*,*) i,trim(gcols(i))
      enddo
      ngu = nrows-1
100
      ! get highest glacier unit id
      fui = openFile(glacierStrPath,'r')
      read(fui,*) ! header line
      do i=1,ngu
105       read(fui,*) gid
          maxgid = max(gid,maxgid)
      enddo
      close(fui)
      write(*,*) 'Highest glacier unit ID:',maxgid
110
      ! allocate glacier parameters
      call glacierAllocate
```

```
    ! read in the actual data
    call cpu_time(clck_bg)
    call glacierReadInput
    call cpu_time(clck_end)
    write(*,*) 'Reading input took', (clck_end-clck_bg), 'seconds'

    ! Calculate constant or initial values
    do i=1,ngu
        ! critical glacier height
        ghc(i) = criticalH(gsl(i))
        ghc(i) = warnRg(1.,2e6,ghc(i),'Critical height',i)
        ! check if critical height / avalanche prop are out of bounds
        dummy = warnRg(1.,2e6,ghc(i)/(1-min(0.9,gavp(i))),  &
                       'Critical height/(1-avalanche proportion)',i)
        ! make sure debris concentration is at least gdc
        if (debr(i)<gdc) debr(i) = gdc
        ! gwe of last year
        gla0(i)  = gla(i)
        ! ice area of unit (km^2) considering avalanche area, unless all
        ! area is avalanche prone
        if (gavp(i)>0.9) then
            garea(i) = da*flu(gj(i))*frar(gj(i),gje(i))
        else
            garea(i) = da*flu(gj(i))*frar(gj(i),gje(i)) * (1-gavp(i))
        endif
        ! area of units initially with glacier water
        if (gla0(i) > 0) agla0 = agla0 + garea(i)*min(gla(i)/ghc(i), 1.)
    enddo

    ! Report on initial glacier area
    write(*,*) 'Area with glacier cover:',agla0,'km',(agla0/da)*100,'%'

    ! open output files
    call glacierOpenOutput

    write(*,*) '-------------------------------------------------------'

end subroutine glacierInitialise


subroutine glacierReadInput
! read glacier unit structure file
    implicit none
    integer i,fui
    integer             :: gid, subb, hyd, nxt
    real                :: sl, sunSum, sunWin, debris, isnow, av
    real gwe

    ! open glacier.bsn file
    fui = openFile(glacierBsnPath,'r')
    read(fui,*) ! names
    ! default basin-wide gmrate & gsubf declared in common.f90
    read(fui,*) gmrate_, gsubf_, rest, gdc
    read(fui,*) ! names
    read(fui,*) SSglob, rhex
    read(fui,*) ! names
    read(fui,*) premb_, gonly
```

```
        ! open str file
        fui = openFile(glacierStrPath,'r')

        read(fui,*) ! header line
        do i=1,ngu
        !!!!!!!!!!!!!! GLACIER UNIT DATA READ IN !!!!!!!!!!!!!!!!!!!!!!!!!!!!
            read(fui,*) gid,subb,hyd,nxt,gwe,sl,av,sunSum,sunWin,debris,isnow

            !!! Initilisation for each glacier unit
            ! subbasin/hydrotope mapping
            ghyd(subb,hyd) = gid
            ! glacier info
            gj(gid)    = subb
            gje(gid)   = hyd
            nxtgu(gid) = nxt
            ! assign and check
            gla(gid)  = warnRg(0.,2.e6,gwe,'Initial glacier height',gid)
            gsl(gid)  = warnRg(0.001,90.,sl,'Slope',gid)
            gavp(gid) = warnRg(0.,1.,av,'Avalanche proportion',gid)
            gshs(gid) = warnRg(0.,24.,sunSum,'Summer sun hours',gid)
            gshw(gid) = warnRg(0.,24.,sunWin,'Winter sun hours',gid)
            debr(gid) = warnRg(0.,1.,debris,'Initial debris concentration',gid)
            snoa(subb,hyd) = warnRg(0.,1.e6,isnow,'Initial snow cover',gid)
        enddo

    end subroutine glacierReadInput


    subroutine glacierAllocate
    ! allocate major glacier arrays after reading the input
        ! glacier ID - subbasin/hydrotope mapping
        implicit none
        allocate(ghyd(mb,meap))
        ghyd = 0

        ! glacier unit information
        allocate(gj(maxgid))
        gj = 0
        allocate(gje(maxgid))
        gje = 0
        allocate(nxtgu(maxgid))
        nxtgu = 0
        allocate(gla(maxgid))
        gla = 0
        allocate(gla0(maxgid))
        gla0 = 0
        allocate(glr(maxgid))
        glr = 0
        allocate(garea(maxgid))
        garea = 0
        allocate(gfirn(mb,meap))
        gfirn = 0
        allocate(gsl(maxgid))
        gsl=0
        allocate(gavp(maxgid))
        gavp=0
        allocate(ghc(maxgid))
        ghc=0
```

```
        allocate(gshs(maxgid))
        gshs=0
        allocate(gshw(maxgid))
        gshw=0
        allocate(gddf(maxgid))
        gddf=0
        allocate(ghu(maxgid))
        ghu=0
        allocate(debr(maxgid))
        debr=0
        allocate(gq(maxgid))
        gq=0
        allocate(gqh(maxgid))
        gqh=0
        allocate(gme(maxgid))
        gme=0
        allocate(gsn(maxgid))
        gsn=0
        allocate(gsub(maxgid))
        gsub=0
        allocate(glost(maxgid))
        glost=0
        allocate(gevap(maxgid))
        gevap=0

    end subroutine glacierAllocate


    subroutine glacierOpenOutput
    ! Open all output files and write their headers
        implicit none
        character(len=256) :: gmboutpath='Res/glacier_mb.prn'! Massbalance stats
        character(len=256) :: gweoutpath='GIS/gla-gis.out'   ! water equivalents
            + for each glacier unit
        character(len=256) :: ddfoutpath='GIS/gddf-gis.out'  ! degree-day-factor
            + for each glacier unit
        character(len=256) :: debroutpath='GIS/debr-gis.out' ! glacier debris
            + concentrations output
        character(len=256) :: gqoutpath  ='GIS/gq-gis.out'   ! glacier q for
            + each glacier unit
        character(len=256) :: gstroutpath ='Res/glaciers.str'! glacier structure
            + file at the end of simulation

        write(*,*) 'GLACIER OUTPUT:'

        ! MASSBALANCE OUTPUT
        gmbout = openFile(trim(swimPath)//gmboutpath,'w')
        write(gmbout,'(3A5,100A18)') 'year','iday', 'subc',    &
        !                       MASSBALANCES
                    'mbmean','acmean','acmax','abmean','abmax', &
        !                        MELT AND SNOW, VOLUME
                    'mddf','meltb','melt','subl','evap','snow','vol', &
        !                       AREAS
                    'agla','agu','aca','mb0a','aba', 'amelt','asnow', &
        !                       ELEVATIONS
                    'gelmean','gelmin','acelev','mb0elev','abelev', &
        !                       DEBRIS
                    'mdeb', 'mxdeb', 'adeb', &
        !                       FIRN
```

```
285                 'fir','fira', &
    !                           FLUX
                    'qh','glost'
    write(*,*) 'Mass balance components: ',trim(swimPath)//trim(gmboutpath)

290 ! GLACIER WATER EQUIVALENT GIS OUTPUT
    gweout = openFile(trim(swimPath)//gweoutpath,'w')
    write(*,*) 'Glacier water equiv.: ',trim(swimPath)//trim(gweoutpath)

    ! GLACIER DEGREE-DAY-FACTOR GIS OUTPUT
295 ddfout = openFile(trim(swimPath)//ddfoutpath,'w')
    write(*,*) 'Glacier degree-day-factor: ',trim(swimPath)//trim(ddfoutpath)

    ! GLACIER DEBRIS CONCENTRATION GIS OUTPUT
    debrout = openFile(trim(swimPath)//debroutpath,'w')
300 write(*,*) 'Glacier debris concentration:
        + ',trim(swimPath)//trim(debroutpath)

    ! GLACIER FLUX OUTPUT
    gqout = openFile(trim(swimPath)//gqoutpath,'w')
    write(*,*) 'Glacier flux: ',trim(swimPath)//trim(gqoutpath)
305
    ! GLACIER FLUX OUTPUT
    gstrout = openFile(trim(swimPath)//gstroutpath,'w')
    write(*,*) 'Glacier structure file at end of simulation: ', &
                trim(swimPath)//trim(gstroutpath)
310
    ! debugging output
    gvarout = openFile(trim(swimPath)//'glacier_var_out.prn','w')

end subroutine glacierOpenOutput
315

subroutine glacierRain(j,je)
! Add rain and snow melt to glacier water storage
    implicit none
320 integer, intent(in)                 :: j, je
    integer                             :: gu    ! glacier unit ID

    gu = ghyd(j,je)
    if (gla(gu) > 0. .and. precipe > 0) then
325     glr(gu) = glr(gu) + precipe
        precipe = 0
    endif

end subroutine glacierRain
330
subroutine glacierEvap(j,je)
! calculate evaporation from glaciers via the Priestley-Taylor ETp and
   + scaled by
! sun hours
    implicit none
335 integer, intent(in) :: j, je
! internal variables
    integer             :: gu    ! glacier unit ID
    real                :: tmitk ! Tmean in K
    real                :: hv    ! latent heat of vaporisation
340 real                :: ssvp  ! slope of sat vap pressure
    real                :: bp    ! barometric pressure
```

```
      real                  :: psych ! psychrometer constant
      real                  :: evp   ! potential evaporation of
     + Priestley-Taylor, mm d^-1
      real                  :: hlfrg ! half range of sun hrs over the year
      real                  :: hrs   ! sun hrs, h
      real                  :: aprop ! glacier area proportion for avalanche
     + area and proportional snout coverage

! ---- copy start of evap.f --------

!**** PURPOSE: THIS SUBROUTINE COMPUTES THE AMOUNT OF SOIL EVAPORATION
!             & THE POTENTIAL PLANT TRANSPIRATION USING RITCHIE'S METHOD
!**** CALLED IN:  HYDROTOP
!~~~~~~~~~~~~~~~~~~~~~~~~~~~~~~~~~~~~~~~~~~~~~~~~~~~~~~~~~~~~~~~~~~~~~~~~~~~~~~~~
!     PARAMETERS & VARIABLES
!
!      >>>>> COMMON PARAMETERS & VARIABLES
!      alai(j,je)     = leaf area index
!      canev          = canopy evaporation, mm
!      canstor(j,je)  = canopy water storage, mm
!      cva(j,je)      = vegetation cover, kg/h
!      ecal           = general potential evap calibration factor
!      eo             = potential evapotranspiration, mm
!      eopot          = potential evapotranspiration, mm
!      ep             = plant transpiration, mm
!      es             = soil evaporation, mm
!      et             = es + ep, mm
!      humi(j)        = air humidity in the subbasin, %
!      ida            = current day
!      ievap          = switch code to print from evap()
!      ievhd          = number of hydrotope to print from evap(), if ievap = 1
!      ievsb          = number of subbasin to print from evap(), if ievap = 1
!      nn             = number of soil layers
!      omega          = month factor for Turc(Ivanov) evap (Glugla 1989)
!block pit            = parameter for estimation of the day length
!      preinf(j,je)   = precipitation adjusted for canopy storage, mm
!      qd             = daily surface runoff, mm
!      ra(j)          = solar radiation, J/cm^2
!      s1(j,je)       = internal func. for Richie's method to estimate es
!      s2(j,je)       = internal func. for Richie's method to estimate es
!      salb(j)        = soil albedo
!      snoa(j,je)     = water content in snow, mm
!      snoev          = snow evaporation, mm
!      ste(j,je,l)    = water storage in a layer, , mm, calc in hydrotop &
     + purk
!      thc            = correction factor for potential evapotranspiration
!                       range for thc: (0.8-1.0), value 1. - from R. Muttiah
!      tv(j,je)       = internal func. for Richie's method to estimate es
!      tx(j)          = average daily temperatue, degree C
!      ylc(j)         = cos(ylt()/clt), ylt() - lat, clt=57.296, to calc rmx
!      yls(j)         = sin(ylt()/clt), ylt() - lat, clt=57.296, to calc rmx
!                       (convert degrees to radians (2pi/360=1/57.296) )
!      z(l,k)         = soil depth, mm

      real alb,aph,cej,ch,d,dayl,dd,eaj,eos,esx,ff,gma
      real h,hh,ho,p,rmx,rto,sb,sd,skyem,sp,suu,thrad,tk,tkk
      real u,vp,vps,xi,xx,yc,ys,yy,zz, omega

      vps = 0.0
```

```
!**** CALC albedo
      p = preinf(j,je) - qd
      eaj = exp(cej*(cva(j,je)+.1))
      tk = tmit + 273.
      tkk = tk * tk
      if (idvwk.eq.1) then
        if (tmit.ge.0.) then
          vps = 6.11 * exp((17.62*tmit)/(243.12+tmit))
          d = vps * 4284. / (243.12+tmit)**2
        else
          vps = 6.11 * exp((22.46*tmit)/(272.62+tmit))
          d = vps * 6123. / (272.62+tmit)**2
        end if
        gma = d / (d+.655)
      else
        d = exp(21.255-5304./tk) * 5304. / tkk
        gma = d / (d+.68)
      end if
      if (snoa(j,je).le.5.) then
        alb = salb(j)
        if (alai(j,je).gt.0.) alb = .23 * (1.-eaj) + salb(j) * eaj
      else
        alb = .6
        if(rsn(j,je).eq. rnew) alb = .8
      end if

!**** CALC max solar radiation rmx, coef 711 changed to 916
!                               916 (ly) ==> 3847.2 (J/cm^2)
      xi = ida
      sd = .4102 * sin((xi-80.25)/pit)
      ch = -yls(j) * tan(sd) / ylc(j)

      if (ch.le.-1.) then
        h = 3.1416
      else if (ch.lt.1.) then
        h = acos(ch)
      else
        h = 0.
      endif

      dayl = 7.72 * h
      dd = 1. + .0335 * sin((xi+88.2)/pit)
      ys = yls(j) * sin(sd)
      yc = ylc(j) * cos(sd)
      rmx = 3847.2 * (h*ys+yc*sin(h))

!**** CORRECTION of radiation on sky emissivity (Ranjan)
!     ho1 - old, ho - from Ranjan, divisor 58.3 for cal ==> 244.86 for J
!     thrad correction, thc - calib. coef.(0.8-1.)
!       ho1 = ra(j) * (1.-alb) / 58.3
!       ho = (ra(j) * (1.-alb)+thrad) / 58.3
      if (idvwk.ne.1) then
!     Idso & Jackson (1969) J. Geophys. Res. 74(23):5397--5403
        skyem = 1. - 0.261*exp(-7.77e-4*(tk-273.15)**2)
        thrad = (skyem-0.96)*4.914e-7*tk**4*(.2+.8*(ra(j)/rmx))
        ho = (ra(j) * (1.-alb)+thc(j)*thrad) / 244.86
      else
!     DVWK (1995) Merkblatt Nr. 238 / Brunt (1932)
```

```
          vp = vps * (humi(j)/100.)
          skyem = 0.34 - 0.044 * sqrt(vp)
          thrad = -5.67 * 8.64e-8 * tk**4. * skyem * (.1+.9*(ra(j)/rmx))
          ho = (ra(j) * (1.-alb) + thrad) / (249.8 - .242*tmit)
        end if
        if (ho.lt.0.) ho = 0.001

!**** CORRECTION of aph=1.28 on humidity:
!       aph = f(humidity):  aph(60) = 1.74, aph(90)=1.28
        hh = humi(j)/100.
        zz = 40. * hh - 29.
        if (zz.gt.10.) zz = 10.
        if (zz.lt.-10.) zz = -10.
        ff = hh / (hh + exp(zz))
        aph = 1.28 + 0.46 * ff

!**** CALC POTENTIAL ET

      if (idvwk.eq.1) then
        eo = ecal (j) * 1.26 * ho * gma
      else
        eo = ecal (j) * aph * ho * gma
      end if

! ---- end copy from evap.f -----

      gu = ghyd(j,je)

      ! scale eo by glacier area and sun hrs
      ! half range of annual amplitude
      hlfrg = (gshs(gu)-gshw(gu))/2
      ! hours of sunlight
      hrs = gshw(gu) + hlfrg + cos((ida-172)*2*PI/366)*hlfrg
      ! proportional area by avalanche area and proportional snout
      aprop = min(gla(gu)/ghc(gu), 1.) * (1-gavp(gu))

      ! scale eo by correction factor, sun hrs, area proportion, albedo
      geo = eo * hrs/12. * aprop
      geva = min(glr(gu), geo)


      ! take from glacier water storage
      glr(gu) = glr(gu) - geva
      gevap(gu) = gevap(gu) + geva

end subroutine

subroutine glacierAblation(j, je)
! calculate glacier melt taking subbasin j, hydrotope je as input
      implicit none
      integer, intent(in) :: j, je
! internal variables
      integer             :: gu    ! glacier unit ID
      real                :: gmr   ! glacier melt rate of current subbasin
      real                :: hlfrg ! half range of summer-winter sunshine hrs
      real                :: hrs   ! actual hours of sunshine
      real                :: of    ! water outflow from glacier water storage
      real                :: dcov  ! debris cover, mm
      real                :: fmar  ! frontal melt area, km2
```

```
      real                  :: aprop ! area proportion
      real                  :: dfac  ! debris cover factor to scale gmrate
      real                  :: hu    ! heat units of the day, dg above tmelt, dg
          + C
      real                  :: sub   ! sublimation, mm
      real                  :: subr  ! sublimation rate, mm per dg C per day
      real dummy

      gu = ghyd(j,je)

      ! Glacier present and exceeding melt temperature?
      if (snoa(j,je).eq.0 .and. tmit.gt.tmelt(j) .and. gla(gu).gt.0.) then

          !!! TODO / TOTEST calculate melting depending on radiation
          ! specific heat of ice: 2.108 J/kg per C
          ! specific heat of fusion of ice: 334 J/kg
          !!!
          ! ice or debris covered
          dcov= max(0., (debr(gu) - gdc)*ghc(gu) )
          ! ddf relation to debris cover from Hagg et al. 2008
          dfac = exp(-0.00572* dcov)

          ! half range of annual amplitude
          hlfrg = (gshs(gu)-gshw(gu))/2
          ! hours of sunlight
          hrs = gshw(gu) + hlfrg + cos((ida-172)*2*PI/366)*hlfrg

          ! proportional area if below critical hight including
          ! + constant frontal melt area proportion
          ! + minus avalanche proportion (0 if gavp=1, will be routed in next
              + timestep)
          ! ghc(gu)*1E-6 * sqrt(garea(gu)) = width * hight of front
          fmar  = ghc(gu)*1E-6 * sqrt(garea(gu))
          aprop = min(gla(gu)/ghc(gu) + fmar/garea(gu), 1.) * (1-gavp(gu))

          ! scale ddf by debris, hours of sunlight and area covered
          gmr = gmrate(j) * dfac * hrs/12. * aprop

          ! DEGREE-DAY APROACH WITH VARIABLE DDF
          hu   = tmit-tmelt(j)
          gmle = gmr*hu

          ! SUBLIMATION LINKED TO SCALED DEGREE-DAY FACTOR
          ! heat of fusion/sublimation: 0.334/2.501 MJoule per kg
          subr = (gmr * 0.334 * gsubf(j)) / ((1-gsubf(j)) * 2.501)
          sub  = subr * hu
          ! glacier is gone
          if (gmle+sub > gla(gu)) then
              sub = min(sub, gla(gu))
              gmle = gla(gu) - sub
          endif

          ! reduce glacier height by melting and sublimation
          gla(gu) = max(gla(gu) - gmle - sub, 0.)  ! 0 constrain for numerical
              + stability
          ! add melt water to glacier water storage
          glr(gu) = glr(gu) + gmle
```

```
        ! increase debris concentration through melting (gla is already new
            + height)
        if (gonly==0) then
            if (gla(gu) .eq. 0.) then
                debr(gu) = gdc
            else
                ! fraction of debris in ice (constrained to 1)
                debr(gu) = min(1., debr(gu)*(gla(gu)+gmle+sub) / gla(gu))
            endif
        endif
    else
    ! No glacier or T not high enough
        gmle = 0.
        hu   = 0.
        sub  = 0.
    end if

    ! add melt and heat hunits for accounting (ddf will be calculated via
        + melt/hu)
    gme(gu)  = gme(gu)+gmle
    ghu(gu)  = ghu(gu)+hu
    gsub(gu) = gsub(gu)+sub

    ! Calculate glacier evaporation and water outflow
    of = glr(gu)/rest
    glr(gu) = glr(gu) - of
    precipe = precipe + of
    if (glr(gu)>0) call glacierEvap(j,je)


end subroutine glacierAblation


subroutine glacierAccum(gu, firn)
! Glacier accumulation from firn
    implicit none
    integer, intent(in) :: gu      ! current glacier unit
    real, intent(in)    :: firn    ! snow (water eq.) to be turned into
        + glacier

    ! Add firn to glacier water eq.
    gla(gu) = max(0., gla(gu)+firn)  ! constraint to 0 in case positive premb

    ! Reduce debris concentration (constrained to lower limit of gdc)
    if (gonly==0) debr(gu) = max(gdc, debr(gu)*(gla(gu)-firn)/gla(gu))

    ! Add accumulated snow for accounting
    gsn(gu) = gsn(gu) + firn

end subroutine glacierAccum


subroutine glacierFirn(j,je, firn)
! Store firn in for balance calculation
    implicit none
    integer, intent(in) :: j,je    ! subbasin, hydrotope IDs
    real, intent(in)    :: firn    ! snow (water eq.) to be turned into
        + glacier
```

```
625     real                :: afirn   ! avalanched snow (water eq.) to be
            + turned into glacier
        integer             :: gu      ! glacier unit id

        ! check if in glacier area and if critical hight is exceeded
        if (ghyd(j,je) > 0) then
630         gu = ghyd(j,je)
            if (firn+gla(gu) >= ghc(gu)) then
                if (gavp(gu)>0.9) then
                    afirn = firn
                else
635                 afirn = firn/(1-gavp(gu))
                endif
                call glacierAccum(gu,afirn)
                snoa(j,je)  = 0
                rsn(j,je)   = 0
640             gfirn(j,je) = 0
            else
            ! store firn for accounting
            gfirn(j,je) = firn
            endif
645     else
        ! store firn for accounting
            gfirn(j,je) = firn
        endif

650     return

    end subroutine glacierFirn


655 function criticalH(sl)
        ! calculate critical snow/ice height for ice flow
        implicit none
        real          :: criticalH      ! critical hight of glacier
        real          :: sl             ! slope in degrees
660
        ! height = shear stress / (gla density * gravity * tan(slope))
        ! TODO: test sin(slope)!!!
        criticalH = SSglob / (917 * 9.8066 * tan(max(sl,0.01)*2*PI/360 )) ! m
        ! convert from m ice to mm w eq.
665     criticalH = criticalH * 917
        return
    end function

    subroutine glacierFlow(j,je)
670 ! calculate the amount of glacier weq. to pass to downstream glacier unit
        implicit none
        integer, intent(in) :: j,je  ! subbasin, hydrotope IDs
        integer             :: gu    ! glacier unit id
        integer             :: gunx  ! glacier unit id of next downstr
675     real                :: q     ! glacier flux in volume
        real                :: de    ! elevation difference btw this and
            + downstream gu
        real                :: grad  ! gradient, change in h over length, dh/L
        real                :: mass  ! ice+snow

680     gu = ghyd(j,je)
```

```
    ! cause avalanche, if slope is too steep, ie. all glacier height removed
    if (gla(gu) > 0 .and. gavp(gu)>0.9) then
        gq(gu)  =   garea(gu)*1E6 * gla(gu)*1E-3
    ! only flow if height above critical height
    else if (gla(gu) > ghc(gu)) then
        ! ice and snow column
        mass = gla(gu) + snoa(j,je)
        ! Calculate gradient
        grad = tan(max(gsl(gu),0.01)*2*PI/360)
        ! other method would be to estimate length and calculate gradient
        ! via elevation difference
        ! l = (garea(gu)*1E6)**0.5 ! m
        ! elevation difference btw this and next gu but at ice surface
        ! de = (elevh( gj(gu), gje(gu) )+gla(gu)*1E-3) - (elevh( gj(gunx), &
        !         gje(gunx) ) + (gla(gunx)*1E-3))
        ! if (de.lt.0) write(*,*) 'Elevation',gunx, 'higher than',gu,'by',de
        ! grad = de/l

        ! calculate flux according to Glen's law and Marshall et al. 2011
            + adaptation
        ! flux = X (rheology term) * area * glacier height**5 * elevation
            + difference**3

        q =  1./365  *  garea(gu)*1E6  *  rhex  *  (mass*1E-3)**5  *
            + grad**3   ! m^3 water

        ! constrain so that critical height of glacier is maintained
        gq(gu)  =   min(q, garea(gu)*1E6 * (gla(gu) - ghc(gu))*1E-3)

    else
        ! no flux
        gq(gu)    = 0
    endif


end subroutine glacierFlow


subroutine glacierRoute
! loop over all glacier units and add glacier flux to next downstream unit
    implicit none
    integer  :: gunx      ! glacier unit id of next downstr
    real     :: accfrac   ! fraction of accumulation of existing gla height
    real     :: ush, dsh  ! transfered volume in upstream and downstream
       + glacier height, w.eq.
    integer i


    ! loop over each glacier unit adding flux to next unit downstream
    do i=1,maxgid
        if (gq(i) > 0) then
            gunx = nxtgu(i)
            ! calculate heights (convert from volume m3 to mm w eq.)
            ush = gq(i)/(garea(i)*1000)
            dsh = gq(i)/(garea(gunx)*1000)

            ! apply flux
```

```
            gla(i)     = max(gla(i)     - ush, 0.)  ! 0 constrain for
                + numerical stability
            ! only move down if i/=gunx or 0, i.e. outside of glacier area
            if (i /= gunx .and. gunx /= 0) then
                gla(gunx) = gla(gunx) + dsh
            else
            ! volume of glacier water lost outside of glacier area/catchment
                glost(i) = glost(i) + gq(i)
            endif

            ! accumulate lost height for accouting
            gqh(i)     = gqh(i) + ush

            ! if all-unit avalanche, add to snow accumulation
            if (gavp(i)>0.9) gsn(gunx) = gsn(gunx) + dsh

            ! debris flow, 0 constraint for numerical stability
            if (gonly==0) debr(gunx) = max(gdc, (debr(gunx) * &
                (gla(gunx)-dsh) + max(0., debr(i)-gdc )*dsh) / gla(gunx))

        endif
    enddo

end subroutine glacierRoute


subroutine glacierMassbalance(year,iday,sc)
! calculate the mass balance, areas and elevations for the accumulation,
! ablation and equilibrium zones by subtracting the last gla0 values from
    + the current
! gla water equivalent and resetting the gla0 to the current
    implicit none
    integer, intent(in)  :: year, iday, sc       ! current year and day of
        + year, subcatchment id (if 0, take all)
    real                 :: mbmean               ! glabal mass balance (mm
        + weq.)
    real                 :: gelmean, gelmin      ! mean and min glacier
        + elevation (m asl.)
    real                 :: agla, alla           ! current total glacier
        + area, total glacier unit area
    real                 :: aba, mb0a, aca       ! area of massbalance
        + negative, 0, positive (km^2)
    real                 :: abmean, abmax        ! mean, max ablation (mm
        + weq.)
    real                 :: acmean, acmax        ! mean, max accumulation
        + (mm weq.)
    real                 :: acelev , mb0elev , abelev   ! mean elevations of
        + accum, equil., ablat. zones (m asl)
    real                 :: thresh0 = 100.       ! absolute
        + accumulation/ablation threshold (mm weq.)
    real                 :: fir , fira           ! accumulated firn and firn
        + area
    real                 :: qh                   ! height lost to flux (mm
        + weq.)
    real                 :: mddf                 ! Mean degree day factor,
        + mm per deg per day
    real                 :: me, su, sn, meb      ! glacier melt, sublimation
        + and glacier snow and balance (mm w eq.) for entire catchment
```

```
780     real                    :: ame , asn, ameb      ! areas of snow melt and
            + snow
        real                    :: vol                  ! total glacier volume,
            + km^3 w.eq.
        real                    :: mdeb, mxdeb, adeb    ! Mean, max [mm] and area
            + of debris cover
        real                    :: glo                  ! Lost glacier volume, m^3
            + weq.
        real                    :: meva                 ! mean evaporation, mm
785     real                    :: tmba                 ! total rea for mb
            + accounting, should be the mean area of last and this times step
        integer i, j, je
        real gmb, guel, ga, ga0, gam, gmp,dummy

        ! initialise (doesnt work in declarations)
790     mbmean= 0
        gelmean=0
        gelmin= 8848 ! Mt. Everest
        agla  = 0
        alla  = 0
795     aba   = 0
        mb0a  = 0
        aca   = 0
        abmean= 0
        abmax = 0
800     acmean= 0
        acmax = 0
        acelev= 0
        mb0elev=0
        abelev= 0
805     qh    = 0
        mddf  = 0
        gddf  = 0
        me    = 0
        su    = 0
810     sn    = 0
        meb   = 0
        ame   = 0
        asn   = 0
        ameb  = 0
815     vol   = 0
        fir   = 0
        fira  = 0
        mdeb  = 0
        mxdeb = 0
820     adeb  = 0
        glo   = 0
        meva  = 0
        tmba  = 0

825     ! loop over each glacier unit
        do i=1,maxgid
            ! dont take those that have a different subcatch
            if(subcatch_id(gj(i)).ne.sc.and.sc.ne.0) cycle

830         ! check if is or used to be glacier covered
            if (((gla(i) > 0) .OR. (gla0(i) > 0)) .AND. gavp(i)<=0.9 ) then
                ! warn if gla or gl0 is below 0
```

```
            dummy = warnRg(0.,2e6,gla(i),'Glacier height in MB
                + calculation',i)
            dummy = warnRg(0.,2e6,gla0(i),'Glacier height of previous &
                                          timestep in MB calculation',i)

            ! proportional or all (1) glacier area, minus avalanche area
            ga  = min(gla(i)/ghc(i), 1.)  * garea(i)
            ga0 = min(gla0(i)/ghc(i), 1.) * garea(i)
            ! area for weightings and massbalance
            if (gla(i)>0) then
                gam = ga
            else
                gam = ga0
            endif

            ! local massbalance (glacier unit) in mm over the mean area
            gmb = (gla(i)*ga - gla0(i)*ga0)/gam

            ! sum for later mean calculation (weighted by area)
            mbmean = mbmean + gmb * gam

            ! elevations
            guel    = elevh( gj(i), gje(i) )

            ! only if glacier still exists
            if (gla(i) > 0) then
                ! current glacier area accouting for proportional coverage
                agla = agla + ga
                alla = alla + garea(i)
                ! volume, km3
                vol = vol + gla(i)*1E-6 * garea(i)
                ! mean and min glacier elevation
                gelmean = gelmean + guel * ga
                gelmin  = min(gelmin, guel )
            endif

            ! ACCUMULATION ZONE
            if (gmb > thresh0) then
                aca    = aca + gam
                acmax  = max(acmax, gmb )
                acmean = acmean + gmb * gam
                acelev = acelev + guel * gam
            ! ABLATION ZONE
            elseif (gmb < -thresh0) then
                aba    = aba + gam
                abmax  = min(abmax, gmb )
                abmean = abmean + gmb*gam
                abelev = abelev + guel*gam
            ! EQUILIBRIUM ZONE
            else
                mb0a    = mb0a + gam
                mb0elev = mb0elev + guel*gam
            endif

            ! FLUX
            qh = qh + gqh(i) *  gam
            ! warn if glacier lost outside of glacier area
            if (glost(i)>0) then
                ! Fail on volume lost
```

```
                ! dummy = warnRg(0.,0.,glost(i),'Glacier domain',i)
                if (sc.eq.0) write(*,*) 'Glacier volume lost (ID,
                    + m**3):',i,glost(i)
                glo = glo+glost(i)
            endif

            ! GLACIER MELT, DDF, SUBLIMATION AND SNOW AND THEIR BALANCE
            if (gme(i) > 0) then
                me      = me + gme(i)* garea(i)
                su      = su + gsub(i)* garea(i)
                ame     = ame + gam
                gddf(i) = gme(i)/ghu(i)
                mddf    = mddf + gddf(i) * garea(i)
            endif
            if (gsn(i) > 0) then
                sn = sn + gsn(i)* garea(i)
                asn= asn + gam
            endif
            if (gme(i) > 0 .or. gsn(i) > 0) then
                meb = meb + (gsn(i) - gme(i) - gsub(i)) * garea(i)
            endif

            ! evaporation
            meva = meva + gevap(i) * garea(i)

            ! DEBRIS ACCOUNTING
            ! check if out of range
            dummy = warnRg(0.,1., debr(i),'Debris concentration in &
                                          massbalance calculation',i)
            if (debr(i)>gdc) then
                adeb = adeb + gam
                mdeb = mdeb + (debr(i)-gdc)*ghc(i) * garea(i)
                mxdeb= max(mxdeb, (debr(i)-gdc)*ghc(i))
            endif
        endif
    enddo

    ! calculate mass balance/elevation means
    ! if areas are = 0, sums must be 0 as well
    tmba = (aca+mb0a+aba)
    if (tmba>0) then
        mbmean = mbmean/tmba
        qh     = qh/tmba
        if (agla>0) gelmean= gelmean/agla
        if (aca>0) acelev = acelev/aca
        if (aca>0) acmean = acmean/tmba
        if (aba>0) abmean = abmean/tmba
        if (aba>0) abelev = abelev/aba
        if (mb0a>0) mb0elev= mb0elev/mb0a
        if (ame>0) then
            me   = me/tmba
            mddf = mddf/ame
            su   = su/tmba
        endif
        if (asn>0) sn = sn/tmba
        meb = meb/tmba
        if (adeb>0) mdeb = mdeb/adeb
        meva = meva/tmba
    endif
```

```
    ! firn accounting
    do j=1,mb
        ! dont take those that have a different subcatch
        if(subcatch_id(j).ne.sc.and.sc.ne.0) cycle

        do je=1,meap
            if (gfirn(j,je) > 0) then
                ! hydrotope area
                fira= fira + da*flu(j)*frar(j,je)
                ! accumulate weighted firn
                fir = fir + gfirn(j,je) * (da*flu(j)*frar(j,je))
            endif
        enddo
    enddo

    ! make mean
    if (fira>0) fir = fir/fira

    ! WRITE TO OUTPUT FILE
    write(gmbout, '(3i5,99f18.2)') year,iday, sc,   &
    !                       MASSBALANCES
                            mbmean,acmean,acmax,abmean,abmax,   &
    !                       MELT, SUBLIMATION AND SNOW, VOLUME
                            mddf,meb,me,su,meva, sn,vol,   &
    !                       AREAS
                            agla,alla,aca,mb0a,aba, ame, asn, &
    !                       ELEVATIONS
                            gelmean,gelmin,acelev,mb0elev,abelev, &
    !                       DEBRIS
                            mdeb, mxdeb, adeb, &
    !                       FIRN
                            fir, fira, &
    !                       FLUX
                            qh, glo

    ! WRITE OUT GLACIER THICKNESS AND FLUX (only if sc=0 and every decade or
        + the last year)
    if (sc.eq.0.and.(mod(iyr,10).eq.0.or.iy.eq.nbyr)) then
        write(gweout,'(2i8,999999f12.0)') year,iday, (gla(i),i=1,maxgid)
         ! debris concentration
        write(debrout,'(2i8,999999f12.6)') year,iday, (debr(i),i=1,maxgid)
        write(ddfout,'(2i8,999999f12.3)') year,iday,  (gddf(i),i=1,maxgid)
        write(gqout,'(2i8,999999f12.1)') year,iday,  (gqh(i),i=1,maxgid)
    endif


end subroutine glacierMassbalance

subroutine glacierMassbalanceSubcatch(year,ix)
! subcatch wrapper for glacierMassbalance
    implicit none
    ! current year and date index (month, doy), subcatchment id (if 0, take
        + all)
    integer, intent(in)          :: year, ix
    integer i

    ! loop over all subcatchments, 0 means take all and writes gunit output
    do i=0,n_subcatch
```

```
            call glacierMassbalance(year,ix,i)
        enddo
        ! reset initial glacier weq. to current and reset counters
        gla0 = gla
        gme  = 0
        gsn  = 0
        gqh  = 0
        ghu  = 0
        gevap = 0
        gsub = 0
        glost = 0

        !!! ADD/REMOVE PRESCRIBED MASS BALANCE FOR INITIALISATION AT YEAR END
        if (gonly==1 .and. ix==12) then
            do i=1,maxgid
                ! parse negative mass balance scaled by area to glacier
                    + accumulation
                if (gla(i)>0) call glacierAccum(i,
                    + -premb(gj(i))*min(gla(i)/ghc(i), 1.))
            enddo
        endif

        ! Write out glacier.str again at the end of the simulation
        if (ix==12 .and. iy==nbyr) then
            write(gstrout,'(100A50)') (gcols(i),i=1,11)
            do i=1,ngu
                write(gstrout,'(4i20,100f22.12)')
                    + i,gj(i),gje(i),nxtgu(i),gla(i), &
                        gsl(i),gavp(i),gshs(i),gshw(i),debr(i),snoa(gj(i),gje(i))
            enddo
        endif


    end subroutine glacierMassbalanceSubcatch


    !-------------------------------------------------------------------------------
    !--- HELPER FUNCTIONS/SUBROUTINES
        + -----------------------------------------

    subroutine getRowsCols(path,nrows,ncols,columns)
    !-------------------------------------------------------------------------------
    ! Routine to read a text file and return the number of columns,
    ! the names of columns and the number of rows.
    ! Limits: - max. 10000 columns, columns need to be declared with len=256
    !         - path not longer than 1024 characters
    !         - column name max. 256 characters
    !-------------------------------------------------------------------------------
        implicit none
    ! I/O variables
        character(len=*)                                :: path
        character(len=256), dimension(1000),intent(out) :: columns
        integer, intent(out)                            :: nrows, ncols
    ! Internal variables
        integer w,l,a,fui
        integer ccount
        character(len=2570000)                          :: header
        ! open file
        fui = openFile(path,'r')
```

```
      ! read header
      read(fui,'(10000a)') header
      ! loop over each header character and detect non-whitespace
      l=1
      ccount = 0
      do a=1,len(header)
          if (header(a:a).ne.' ') then ! there is a word here
               if (w.eq.0) l=a
               w = 1
          else
              ! either word end or more whitespace
              if (w.eq.1) then ! word complete, save
                  ccount = ccount+1
                  ! write word into columns array
                  read(header(l:a-1),*) columns(ccount)
              endif
           w = 0
          endif
      enddo
      ! column count to pass on
      ncols = ccount

      ! count rows
      nrows = 1
      do
          read(fui,*,END=10)
          nrows = nrows+1
      enddo
   10 close(fui)

end subroutine getRowsCols

integer function openFile(fname, status)
! This function opens a file and returns the unit id (a free unit number
    + between 21-1000,
! if file open was successful. The file status remains open!
! If file opening was not successful, the functions stops the programme and
    + closes the file.
    implicit none
    character(len=*)               :: fname
    character(len=1)               :: status   ! r for reading, w for writing
    integer                        :: opensucc
    integer ui, iostat
    logical opened

    ! get free unit id
    do ui = 21,1000
        inquire(unit=ui, opened=opened, iostat=iostat)
        if (iostat.ne.0) cycle
        if (.not.opened) exit
    end do
    openFile = ui
    ! open file
    if (status=='r') then
         open(ui,file=trim(fname),status='OLD',IOSTAT=opensucc)
    else
         open(ui,file=trim(fname),IOSTAT=opensucc)
    endif
    if ( opensucc /= 0 ) then
```

```
        write(*,*) "ERROR while opening file: ", trim(fname), " does it exist?"
        write(*,*) "Terminating!!!"
        close(ui)
        STOP -1
    end if

end function openFile

real function warnRg(lo,up, v, var, i)
! Check if the the value v is within range lo - up and exit
! with name in var and array index i if not, if yes return v again
    implicit none
    real lo,up,v
    integer i
    character(len=*) var

    if (v < lo .or. v > up) then
        write(0,*) '!!! ',trim(var),' is out of range (',lo,'-',up,'):'
        write(0,*) 'ID=',i,'value=', v
        stop -1
    endif
    warnRg = v
    return
end function warnRg
```